Technical Report Documentation Page

1. Report No.	2. Government Accession No.	3. Recipient's Catalog No.
FHWA/TX-03/1741-2		

4. Title and Subtitle	5. Report Date
Analysis, Testing, and Load Rating of Historic Steel Truss Bridge Decks	**May 2003**
	6. Performing Organization Code

7. Author(s)	8. Performing Organization Report No.
C. M. Bowen and M. D. Engelhardt	Research Report 1741-2

9. Performing Organization Name and Address	10. Work Unit No. (TRAIS)
Center for Transportation Research The University of Texas at Austin 3208 Red River, Suite 200 Austin, TX 78705-2650	11. Contract or Grant No. Research Study 0-1741

12. Sponsoring Agency Name and Address	13. Type of Report and Period Covered
Texas Department of Transportation Research and Technology Implementation Office P.O. Box 5080 Austin, TX 78763-5080	Research Report (9/96-8/00)
	14. Sponsoring Agency Code

15. Supplementary Notes

Project conducted in cooperation with the U.S. Department of Transportation

16. Abstract

This report documents the results of a study of on-system historic metal truss bridges in Texas. On-system bridges are those located on the state highway system, and the surviving on-system historic trusses in Texas were typically constructed in the 1920s and 1930s. The primary objective of this study was to investigate methods that can be used to develop an accurate and realistic load rating for an older on-system truss bridge.

In order to examine issues involved in the structural evaluation of older on-system truss bridges, two case study bridges were investigated in detail. In addition, a full-scale laboratory experimental investigation was conducted on a single bay of a typical truss bridge floor system.

Evaluation of the case study bridges indicated that the primary structural deficiency in these bridges was inadequate capacity of the steel floor beams and stringers, based on conventional load rating techniques. The analysis and field load testing conducted on the case study bridges and the laboratory investigation therefore focused primarily on the bridge floor systems.

The results of this study indicate that the use of standard AASHTO load rating techniques can substantially underestimate the strength of the floor beams and stringers. A significantly more accurate prediction of the structural response of the floor members to truck live loads can be achieved by conducting an elastic finite element analysis of the bridge floor system. Comparison with extensive field load test results and with laboratory test results shows that finite element analysis provides a more realistic but still somewhat conservative prediction of floor member response. Analysis of the floor system using a finite element model can be used to support a significantly improved load rating for historic on-system truss bridges.

17. Key Words	18. Distribution Statement
preservation, field load testing, finite element analysis, composite action, evaluation, strengthening, material sampling and testing, load distribution	No restrictions. This document is available to the public through the National Technical Information Service, Springfield, Virginia 22161.

19. Security Classif. (of report)	20. Security Classif. (of this page)	21. No. of pages	22. Price
Unclassified	Unclassified	254	

Form DOT F 1700.7 (8-72) Reproduction of completed page authorized

ANALYSIS, TESTING, AND LOAD RATING OF HISTORIC STEEL TRUSS BRIDGE DECKS

by

C. M. Bowen and M. D. Engelhardt

Research Report 1741-2

Research Project 0-1741

PRESERVATION ALTERNATIVES
FOR HISTORIC TRUSS BRIDGES

conducted for the

Texas Department of Transportation

in cooperation with the

U.S. Department of Transportation
Federal Highway Administration

by the

CENTER FOR TRANSPORTATION RESEARCH
BUREAU OF ENGINEERING RESEARCH
THE UNIVERSITY OF TEXAS AT AUSTIN

May 2003

Research performed in cooperation with the Texas Department of Transportation and the U.S. Department of Transportation, Federal Highway Administration.

ACKNOWLEDGEMENTS

The authors gratefully acknowledge the financial support provided for this project by the Texas Department of Transportation (TxDOT). The support of the individuals that have served as Project Directors at TxDOT is appreciated, including Barbara Stocklin, Steve Sadowsky, Cherise Bell, and Charles Walker. The continuing support for this project provided by the Project Coordinator, Dianna Noble, is also appreciated. Assistance and support from Lisa Hart of TxDOT is appreciated. Special thanks are extended to Charles Walker for his support and guidance throughout this project. Thanks are also extended to Dilip Maniar, Dan Leary, Mathew Haberling, Karl Frank and Joe Yura of the University of Texas at Austin for their assistance with this project. Finally, the authors thanks Mr. Abba Lichtenstein for advice provided on this project.

DISCLAIMER

M. D. Engelhardt, P.E., TX # 88934

Research Supervisor

TABLE OF CONTENTS

LIST OF FIGURES

LIST OF TABLES

SUMMARY

This report documents the results of a study of on-system historic metal truss bridges in Texas. This study was conducted as part of a larger research project on *Preservation Alternatives for Historic Metal Truss Bridges*. The overall objective of this larger project was to develop information and tools to aid engineers and decision-makers in addressing problems with historic metal truss bridges in Texas, with a goal of maintaining these bridges in vehicular service.

This report specifically addresses "on-system" metal truss bridges in Texas. On-system bridges are those on the state highway system, and are found on state highways, US highways, farm-to-market routes, ranch-to-market routes, interstate frontage roads, etc. The surviving on-system historic trusses in Texas were typically constructed in the 1920s and 1930s, and were designed by the Texas Department of Transportation for H10 to H15 truck loads.

The primary objective of this study was to investigate methods that can be used to develop an accurate and realistic load rating for an older on-system truss bridge. Based on commonly used evaluation procedures, many of these older truss bridges may show deficient load ratings based on current standards. This study examined if such low load ratings accurately reflect the true load carrying capacity of these bridges, and whether more realistic load ratings can be achieved through the use of more accurate structural analysis methods and field load testing.

In order to examine issues involved in the structural evaluation of older on-system truss bridges, two case study bridges were investigated in detail. The first case study bridge was located in Llano, Texas, and the second in Goliad, Texas. These bridges, typical of the circa 1930 on-system truss bridges in Texas, featured Parker trusses and non-composite slab on steel girder floor systems. Each bridge was studied through the use of conventional load rating techniques, through the use of more advanced structural analysis models, and through extensive field load testing. In addition to the two detailed case studies, a full scale laboratory experimental investigation was conducted on a single bay of a typical slab on steel girder truss bridge floor system in order to examine the structural response of the floor system in greater detail.

An initial evaluation of the case study bridges indicated that the truss members themselves did not pose a problem with respect to inadequate load ratings. Rather, the primary structural deficiency in these bridges was inadequate capacity of the steel floor beams and stringers, based on conventional load rating techniques. The analysis and field load testing conducted on the case study bridges and the laboratory investigation therefore focused primarily on the bridge floor systems.

The first case study bridge studied in detail was located in Llano, Texas. Known as the Roy Inks Bridge, the main structure spans approximately 800 ft. over the Llano River, and was constructed in 1936. The bridge consists of four main spans, each approximately 200 ft. in length. Each span is a Parker through-truss, with a non-composite slab on steel beam and stringer floor system. The yield strength of the steel was not specified on the available drawings for the Llano bridge. Given unknown material properties, the American Association of State Highway and Transportation Officials (AASHTO) provides guidelines for values to use based on the date of construction. For the Llano bridge, this resulted in an estimate of yield strength of steel equal to 30 ksi. This value was used in the initial load rating, which showed inventory ratings below HS20 for the steel beams and stringers in the bridge floor system, using standard AASHTO load-rating techniques.

The original mill certificates for the steel used in the Llano bridge were subsequently located. These mill certificates indicated that the yield stress of the beams and stringers was at least 36 ksi, a substantial increase over the initially assumed value of 30 ksi. Tensile tests conducted on steel samples

removed from the floor beams confirmed the higher yield stress values indicated on the mill certificates. Using a yield stress of 36 ksi, longitudinal stringers rated above HS20. Transverse beams, while still rating under HS20, had their load deficiency reduced to approximately 10 percent. Obtaining more accurate estimates of steel material properties by recovering mill certificates and by removing and testing samples of steel from the bridge proved to be a useful and economical measure to develop an improved load rating.

As the next step in the investigation of the Llano bridge, an elastic finite element model was developed for the bridge floor system to determine if a higher load rating could be justified by using analysis methods that are more advanced and more exact than used in conventional load rating. The model was constructed using commercially available finite element analysis software. The model was constructed to represent a floor system with no composite action between the steel members and the concrete slab. AASHTO HS20 truck loads were applied in positions on the model to produce maximum flexural response for both stringers and beams. The maximum moments due to live load effects were computed and used to load rate the members.

The finite element analysis showed significantly lower moments in the stringers and beams than conventional AASHTO calculations. This reduction in moment was attributed to two factors. One factor was that the finite element analysis predicted that the reinforced concrete slab resists substantial moment, thereby reducing the moment that must be carried by the steel beams and stringers. Thus, even without composite action, the finite element analysis showed that the slab provides a significant contribution to the load carrying capacity of the bridge deck. A second factor was that the finite element analysis predicted a different and more advantageous distribution of load among the steel members than obtained from AASHTO calculations.

The critical members controlling the load rating of the Llano bridge were the transverse floor beams. With the reduction in live load moment predicted by finite element analysis combined with a yield stress based on measured values, it was possible to demonstrate an inventory load rating for the transverse beams, and therefore for the entire bridge, in excess of HS20. Consequently, the use of simple finite element analysis for the bridge floor system proved to be a valuable tool for developing an improved load rating.

Field load tests were subsequently conducted on the Llano Bridge to obtain the most accurate assessment of live load effects on the floor system, and to assess the accuracy of the finite element model. In these tests, selected portions of the floor system were instrumented with strain gages. Trucks of known weight and geometry were then driven slowly over the bridge, and the response of the instrumented members was measured.

The field test data showed live load stresses in the floor beams and stringers that were significantly lower than predicted by the standard AASHTO load rating. In many cases, the field test data showed stresses that were less than half of those predicted by standard AASHTO calculations. This confirmed that the bridge floor system was significantly stronger than indicated by the standard load rating, and that an increased load rating for the bridge floor members is justified.

The field test data also showed live load stresses smaller than predicted by the finite element model of the bridge floor system. However, the difference between the field test data and the finite element model predictions were much smaller than the difference with the standard load rating calculations. Thus, the finite element model, although predicting much smaller stresses than standard load rating calculations, still provided conservative predictions compared to field test data.

Subsequent to the Llano field tests, an opportunity arose to investigate a similar truss bridge located on US 183, crossing the San Antonio River in Goliad, Texas. The Goliad bridge was very similar to the Llano bridge, except that it was slightly smaller, and consisted of only one span, as compared to the

four spans at Llano. The floor system of the Goliad bridge was also very similar to that of the Llano bridge, consisting of a non-composite slab over steel beams and stringers.

Similar to the Llano bridge case study, the floor system of the Goliad bridge was evaluated three ways: by conventional AASHTO load rating calculations, by elastic finite element analysis, and by field load testing. The Goliad bridge was scheduled for replacement and demolition, and the bridge was load tested just prior to demolition. Consequently, the testing was performed to a much higher load, since a limited amount of yielding could be tolerated. The highest loading used in the Goliad test was approximately a 57 kip axle load, almost 80 percent higher than an HS20 axle.

The overall trend in results for the Goliad bridge was quite similar to the Llano bridge. Stresses in the floor members predicted by the AASHTO calculations were significantly higher than the stresses predicted by finite element analysis. The stresses predicted by finite element analysis, in turn, were somewhat higher than those measured in the field test. The Goliad field load test confirmed that the finite element model of the bridge deck provided a significantly more accurate prediction of member response than that obtained from conventional AASHTO calculations. The stresses measured in the floor beams and stringers were significantly lower than predicted by the AASHTO calculations, indicating that the conventional AASHTO calculations significantly underestimated bridge deck capacity. The stresses predicted by the finite element analysis were much closer, although still somewhat higher, compared to those measured in the field test. Thus, as was the conclusion from the Llano test, the Goliad test indicated that the finite element analysis provides a very useful tool for load rating. The finite element analysis provides a more realistic, but still somewhat conservative prediction of the response of the bridge floor members to truck loading.

As with the Llano bridge, the deck of the Goliad truss bridge did not have shear connectors for the development of composite action. The field test data for the Goliad bridge showed the development of some composite action, primarily in the longitudinal stringers. A similar observation was made in the Llano field tests. Other researchers have observed such unintended composite action in other field tests on bridges without mechanical shear connectors. The question arises as to whether this additional strength can be utilized in the evaluation and load rating of the bridge deck. Data collected in the Goliad field test showed that at higher load levels slip occurred between the steel and concrete, and that most of the unintended composite action was lost. Based on the data collected in the Goliad field test, it appears that such unintended composite action may not be sufficiently reliable for use in capacity determinations.

The final task of this research study was an experimental investigation of a full-scale portion of a non-composite slab on steel girder bridge deck. The laboratory model was similar in member sizes and geometry to the bridge decks on the Llano and Goliad truss bridges. The primary goal of the experimental study was to provide further data on the distribution of forces and stresses within the beams and stringers of the floor system and to corroborate the field test data and finite element analysis. The laboratory bridge deck model was also subsequently used for preliminary evaluation of a potential strengthening scheme for the bridge deck.

Loads were applied to the laboratory model at a variety of locations and with varying magnitudes. For each load case, the stresses measured in the beams and stringers were compared to the stresses predicted using conventional AASHTO load rating calculations and using an elastic finite element model. The same trends seen in the case study bridges were also seen in the laboratory experimental investigation. The stresses measured in the transverse beams and longitudinal stringers of the laboratory bridge deck model were significantly less than the stresses predicted using calculation methods typically used for AASHTO load rating. Simple finite element modeling of the laboratory bridge deck specimen predicted stresses much closer to the measured values. However, the stresses predicted by the finite element model were still somewhat higher than the measured values. The laboratory model confirmed

that a simple finite element analysis of the bridge deck can provide a significantly improved prediction of stresses as compared to conventional AASHTO based calculations, while still providing overall conservative results.

Overall, the results of this study have shown that the use of standard AASHTO load rating techniques substantially underestimates the strength of the floor beams and stringers. A significantly more accurate prediction of the structural response of the floor members to truck live loads can be achieved by conducting an elastic finite element analysis of the bridge floor system. Comparison with extensive field load test results and with laboratory test results shows that finite element analysis provides a more realistic but still somewhat conservative prediction of floor member response. Analysis of the floor system using a finite element model can be used to support a significantly improved load rating for historic on-system truss bridges.

Chapter 1:
Introduction

1.1 BACKGROUND

There are several hundred older metal truss bridges that remain in vehicular service in the state of Texas, many in the range of 70 to over 100 years in age. A number of these bridges are of historical interest due to their age or other unique features, and are either listed or eligible for the National Register of Historic Places. Considerable interest exists in maintaining historic metal truss bridges in continued vehicular service. However, achieving this goal is often problematic due to structural and functional deficiencies found in these bridges. The structural load rating can often be low due to the initial low design loads used for the bridge combined with damage and deterioration that has occurred over the long service life of the bridge. In addition to structural problems, historic metal truss bridges also frequently have functional deficiencies due to narrow widths and constricted vertical clearances. An examination of issues associated with the structural capacity of historic metal truss bridges is the primary focus of this report.

The work reported herein is part of a larger project conducted for the Texas Department of Transportation (TxDOT) entitled: "Preservation Alternatives for Historic Metal Truss Bridges." (TxDOT Project 0-1741). The overall objectives of this larger project were to develop information and tools to aid engineers and decision-makers involved with historic metal truss bridges and to help maintain these bridges in vehicular service.

Historic metal truss bridges in Texas can be divided into two broad categories: "on-system" bridges and "off-system" bridges. On-system bridges are those on the state highway system, and are found on state highways, US highways, farm-to-market routes, ranch-to-market routes, interstate frontage roads, etc. The surviving on-system historic trusses in Texas were typically constructed in the 1920s and 1930s, and were designed by TxDOT for H10 to H15 loads. On-system historic metal truss bridges are the subject of this report.

"Off-system" bridges are those not on the state highway system, and are typically found on county roads or city streets. Many of the off-system historic truss bridges in Texas were constructed in the late 1800's or early 1900's. These bridges were often designed and erected by private bridge companies. The off-system bridges are typically constructed of light steel, wrought iron or cast iron components and frequently have timber decks. Many of the off-system trusses pre-date the automobile, and originally carried horse traffic and livestock.

Research for Project 0-1741 was organized into the following tasks:

1. Conduct a survey of literature and of the practices of other Departments of Transportation (DOTs) on metal truss bridge evaluation and rehabilitation.
2. Conduct a case study of an off-system historic metal truss bridge.
3. Conduct a case study of an on-system historic metal truss bridge.
4. Conduct laboratory studies on floor systems representative of on-system historic truss bridges in Texas.
5. Conduct studies on the application of historic preservation principles to projects involving historic metal truss bridges.

This report addresses Tasks 3 and 4 of the overall project. Tasks 1 and 2 have been completed previously, and results are reported elsewhere. An extensive literature survey on the evaluation and

rehabilitation of metal truss bridges was conducted under Task 1, and is reported by Thiel, et al (2002). This document includes an annotated bibliography of literature on historic metal truss bridges, a survey of practices of other state DOTs in addressing problems with historic metal truss bridges, and a discussion and synthesis of the literature and the DOT survey. The interested reader is referred to Thiel, et al (2002) for an extensive review and discussion of the literature on historic metal truss bridges.

Task 2 of Project 0-1741 was a case study of an off-system historic metal truss bridge in Texas. Results of this Task are reported by Maniar, et al (2003). The primary objective of Task 2 was to address structural issues involved with off-system truss bridges. More specifically, Task 2 examined methods that can be used to develop an accurate and realistic load rating for a historic off-system metal truss bridge, and methods that can be used to strengthen the bridge, if needed. The case study bridge for Task 2 was located in Shackelford County, Texas and was constructed in 1885. For this case study bridge, Maniar, et al (2003) describes collection of data, evaluation of materials, structural analysis and load rating, field load testing, and development of rehabilitation options.

1.2 PROJECT OBJECTIVES AND SCOPE

As described above, this report addresses Tasks 3 and 4 of the overall project on Preservation Alternatives for Historic Metal Truss Bridges. More specifically, this report is concerned with addressing structural issues involved with on-system historic metal truss bridges in Texas. The primary objective of this study is to investigate methods that can be used to develop an accurate and realistic load rating for an older on-system truss bridge. Based on commonly used evaluation procedures, many of these older truss bridges may show deficient load ratings based on current standards. This study will examine if such low load ratings accurately reflect the true load carrying capacity of these bridges, and whether more realistic load ratings can be achieved through the use of more accurate structural analysis methods and field load testing. This study will also briefly examine a potential technique for strengthening floor systems on older truss bridges.

To investigate structural issues involved with on-system historic metal truss bridges, two case study bridges were chosen as a central focus of this study. The primary case study bridge is located in Llano, Texas. Constructed in 1936, the Llano case study bridge features Parker trusses and a floor system consisting of a noncomposite concrete slab on steel beams and stringers. Additional investigation was also conducted on a second case truss bridge located in Goliad, Texas in order to augment information collected on the Llano bridge. The Llano and Goliad case study bridges were chosen as typical examples of surviving on-system historic metal truss bridges in Texas.

The investigation of the case study bridges included the development of standard load ratings, more advanced structural analysis of the bridges using finite element analysis, and extensive field load testing. An initial evaluation of the case study bridges indicated that the truss members themselves did not pose a problem with respect to inadequate load ratings. Rather, the primary structural deficiency in these bridges was inadequate capacity of the steel floor beams and stringers, based on conventional load rating techniques. The analysis and field load testing conducted on the case study bridges therefore focused primarily on the bridge floor systems. In addition to the two detailed case studies, a full scale laboratory experimental investigation was conducted on a single bay of a typical slab on steel girder truss bridge floor system in order to examine the structural response of the floor system in greater detail.

Chapter 2 of this report provides an overview of the Llano case study bridge, including the results of material tests conducted on samples of steel removed from the bridge. Chapter 2 also presents the results of a conventional load rating for the bridge. As noted above, the steel floor beams and stringers controlled the load rating of the bridge.

In Chapter 3, a detailed elastic finite element analysis is conducted on the floor system of the Llano bridge. The response and load rating of the floor beams and stringers based on the finite element analyses are compared with those based on conventional load rating calculations.

Chapter 4 presents the results of field load tests conducted on the floor system of the Llano bridge. In these field tests, trucks with known axle weights are driven over the bridge, and the actual stresses in the floor beams and stringers are measured. These measured stresses are then compared with the stresses predicted both by conventional load rating calculations and by finite element analysis, in order to assess the accuracy of the stress predictions.

Chapter 5 describes additional load testing conducted on the second case study truss bridge located in Goliad, Texas. The Goliad bridge was scheduled for demolition. Consequently, the bridge could be tested at much higher loads than were possible at Llano, since was there less concern about potential yielding and damage of the bridge during load testing. The Goliad bridge therefore provided a unique opportunity for testing well beyond normal design loads. Stresses measured in the floor beams and stringers of the Goliad bridge were also compared to stresses predicted by finite element analysis to provide further assessment of the accuracy of the predicted stresses.

Chapter 6 of this report describes laboratory tests on a full-scale portion of a slab on steel girder bridge deck typical of those found in on-system truss bridges. The laboratory tests were conducted to provide further insight into the actual stresses developed in the floor beams and stringers, and to further assess the accuracy of finite element model predictions. The laboratory model was also used to provide a preliminary assessment of a potential technique for strengthening the floor system.

Finally, Chapter 7 presents a summary of the key findings of this study and describes implications for load rating of on-system historic metal truss bridges.

Chapter 2:
Llano Bridge Case Study Overview

2.1 INTRODUCTION

As a part of this research, two case study bridges were selected to examine approaches for evaluating historic truss bridges. This chapter focuses on one of those case studies, the Roy Inks Bridge in Llano, Texas. Presented in this chapter are the background and description of the structure, along with results of American Association of State Highway and Transportation Officials (AASHTO) load ratings of the members. Comparisons between the Allowable Stress and Load Factor ratings are given, as well as the results of material tests to determine the yield stress of the steel.

2.2 OVERVIEW AND DESCRIPTION OF THE LLANO BRIDGE

2.2.1 Introduction

The first of the bridges selected as a case study is a four span bridge in Llano, Texas. Formally known as the Roy Inks Bridge, the main structure spans approximately 800 feet crossing the Llano River. Located near the center of town, it is the main entryway from the north to the downtown area. Figure 2.1 shows an aerial view of the bridge. The location of the bridge is highlighted on the map in Figure 2.2. The 1991 TxDOT estimate of the Average Daily Traffic (ADT) was 9,100 vehicles per day.

Figure 2.1 Aerial photo of Roy Inks Bridge
(photo courtesy of Texas Department of Transportation)

The bridge was completed in September of 1936 and was built to replace an 1892 structure that was destroyed in a 1935 flood. The bridge was nominated in 1988 for the United States Department of Interior National Register of Historic Places.

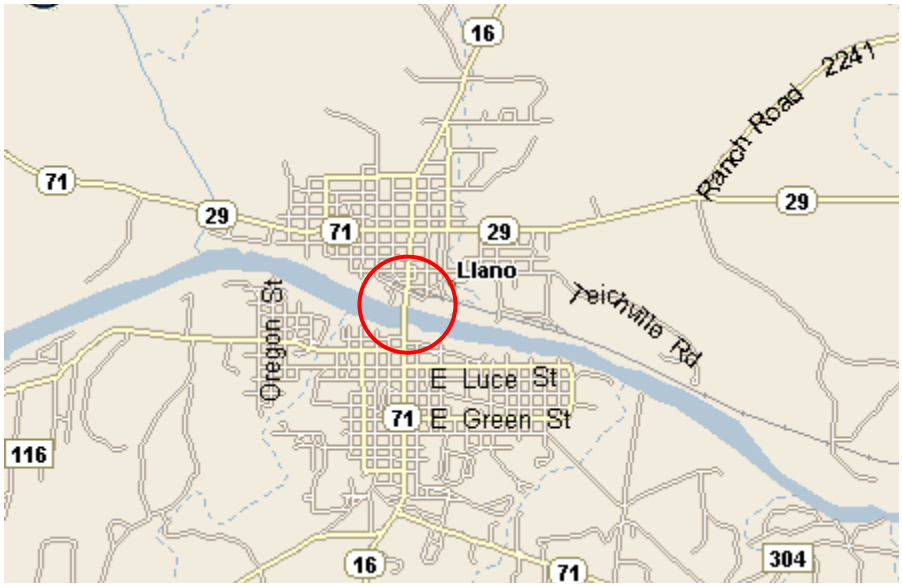

Figure 2.2 Location of Llano case study bridge

2.2.2 Bridge Details

The overall shape can identify a particular truss. The Llano Bridge is known as a Parker truss. The Parker is basically a Pratt truss with a polygonal top chord, and is distinguished by having diagonal members in tension and vertical members in compression under dead loads. Three of the four spans of the Llano Bridge may be seen in Figure 2.3, and a schematic with dimensions for one span can be seen in Figure 2.4. The Llano configuration is on occasion referred to as a Camelback truss, which is simply a specific type of Parker characterized by exactly five pairs of equal slopes on the top chord.

Figure 2.3 Three of the four spans of the Llano Bridge

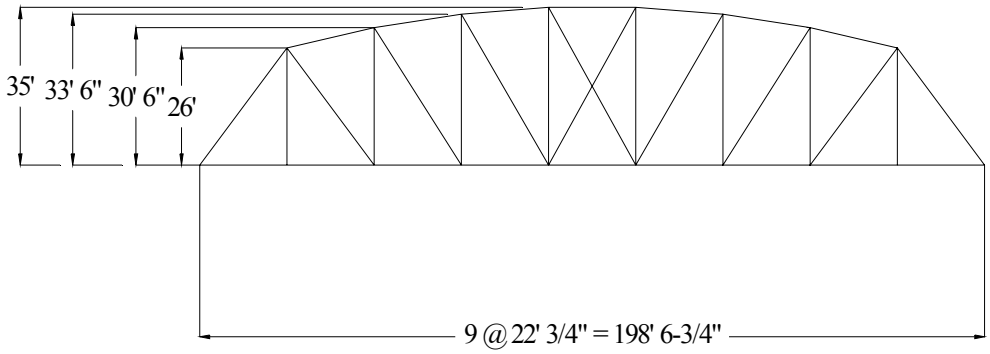

Figure 2.4 Llano bridge profile with dimensions

The details of the bridge were obtained from copies of Texas State Highway Department (TxDOT) drawings dated October 1935. Details were subsequently verified by field measurements. The truss is constructed of rolled W8x40 sections, (diagonals and the outer most verticals) and built up members (verticals and both top and bottom chords). The built up sections are typically double channels with riveted lacings and/or cover plates. Member details were compiled from either the AISC Manual of Steel Construction (AISC 1994), or for the obsolete truss members, from Structural Data, (Mosher 1923) or from an AISC manual listing of obsolete sections (AISC 1990).

The bridge deck is a reinforced concrete slab on steel beams and stringers as depicted in Figures 2.5 through 2.8. The slab is 6-½ inches thick with both longitudinal and transverse #5 reinforcement bars. Longitudinal reinforcement was placed approximately 13 in. on center between longitudinal steel members, and transverse reinforcement was spaced approximately 6 in. on center. Transverse reinforcement was bent to accommodate both positive negative moments in the slab (see Figures 2.6 and 2.7).

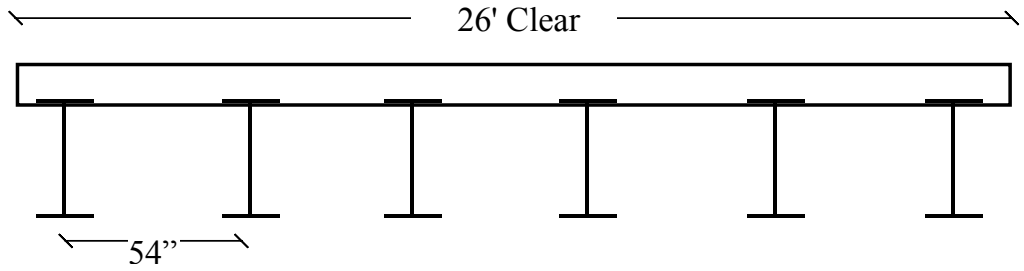

Figure 2.5 Deck longitudinal stringers and slab

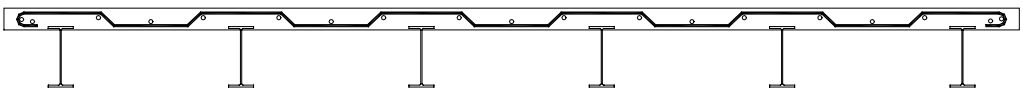

Figure 2.6 Longitudinal and transverse reinforcement in the bridge deck

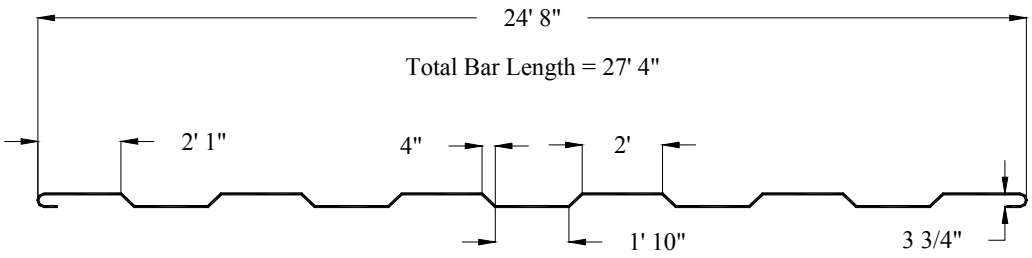

Figure 2.7 Bent configuration of transverse reinforcement

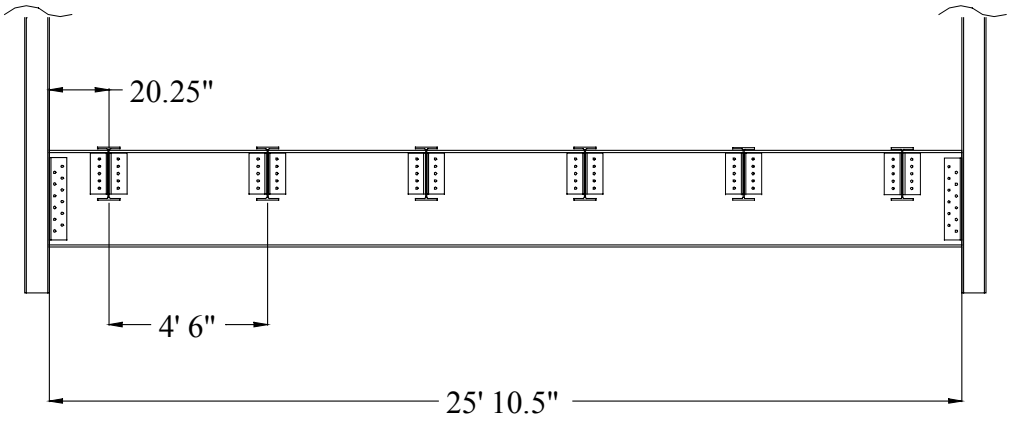

Figure 2.8 Transverse beam attached to the truss verticals, with connecting longitudinal stringers

Each deck slab segment is approximately 22 ft. in length and extends from panel point to panel point of the lower chord. Longitudinal reinforcing steel is not continuous across segments, and there are construction joints at the end of each of the deck segments. Longitudinal stringers are W18x50 sections, 21 ft. - 1l in. long. Transverse beams, located at each of the panel points of the bottom chord, are W33x132 sections, 25 ft. - 10-½ in. long. Longitudinal members are riveted to the transverse members with double clip angles (L6x4x 3/8), and transverse members are riveted directly to vertical members of the truss with double clip angles (L6x4x 7/16). There are no mechanical shear connectors between the slab and the steel sections. Consequently, the deck was originally designed non-compositely. The yield stress of the reinforcing steel, as well as the design compressive strength of the concrete was not reported on the available drawings. The yield stress of the truss and deck-framing members also was not reported on the drawings. For unknown steel, AASHTO requires the use of a yield stress based on the construction date (AASHTO, 1994). In the Llano Bridge, the yield stress for structural steel specified by AASHTO based on year built was 30 ksi.

One feature found in this bridge was that the longitudinal stringers were attached in such a manner that their top flanges were higher than the top flange of the transverse beam. This distance varied with each member due to the camber of the transverse member, but is on the order of 1 inch. The effect of this connection was that the slab rested directly on top of the transverse beams, but the longitudinal stringers were embedded approximately 1 in. into the bottom of the slab. This detail is shown in Figure 2.9. It is not known why this detail was incorporated, but one possible explanation may have been to ensure full lateral stability of the top flange under positive moment.

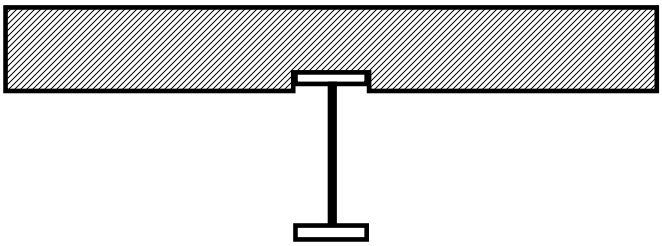

Figure 2.9 Detail of longitudinal stringer embedment

The railing of the bridge consisted of channel sections directly connected to the vertical and diagonal members of the truss, as shown in Figure 2.10. In between the verticals and diagonals, rails are attached to the outermost stringers with angles, as shown in Figure 2.11. Because of the relatively small size and relatively flexible connections to the deck, the railing was not considered structurally significant, and not included in the analysis.

Figure 2.10 Railing attached to vertical and diagonal truss members

Figure 2.11 Angle attachments of railing to longitudinal stringers

2.2.3 Material Mill Certificates and Sampling

In order to accurately determine the capacity of a structure, the material properties must be known. As mentioned previously, these properties were unknown in the initial stages of this investigation. Because of this, a conservative estimate of material yield stress as specified by AASHTO must be used. If the true material strength can be established at a higher level, the rated capacity of the structure can be increased.

Subsequent to the initial load rating, the original mill certificates for the Llano Bridge steel were found on microfilm. These documents indicated that the steel used had a yield stress between 36 and 47 ksi. The Pittsburgh Testing Company and Southwestern Laboratories of Dallas, Texas tested the majority of the truss steel. A typical mill certificate from microfilm is shown in Figure 2.12.

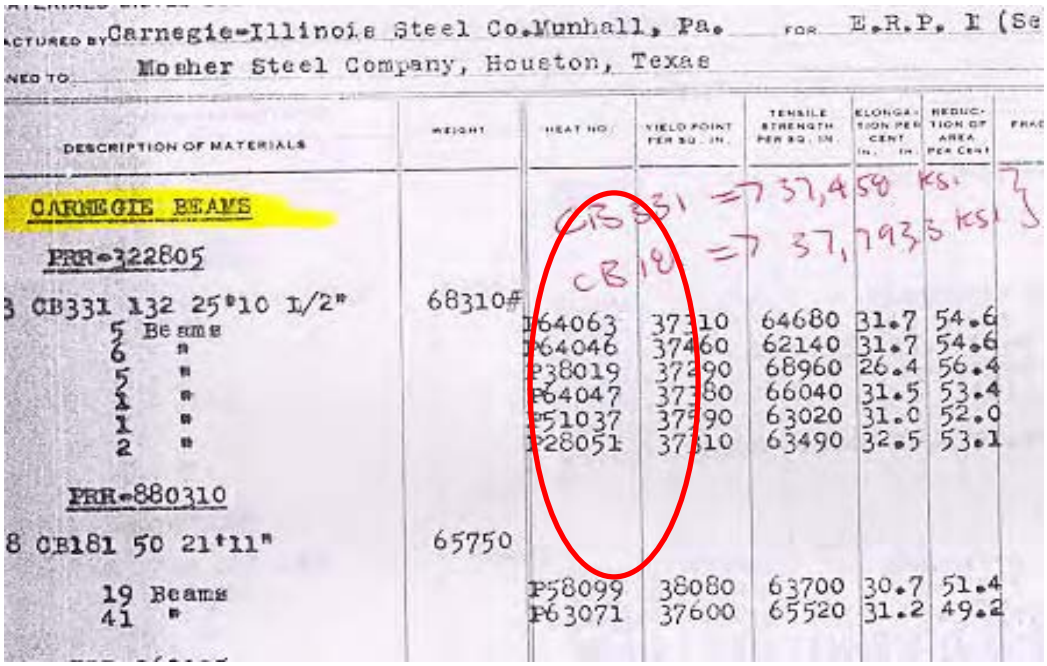

ACTURED BY Carnegie-Illinois Steel Co. Munhall, Pa. FOR E.R.P. I (Se
NED TO Mosher Steel Company, Houston, Texas

DESCRIPTION OF MATERIALS	WEIGHT	HEAT NO.	YIELD POINT PER SQ. IN.	TENSILE STRENGTH PER SQ. IN.	ELONGATION PER CENT IN. IN.	REDUCTION OF AREA PER CENT	FRAC
CARNEGIE BEAMS			CB331 => 37,458 KSI				
PRR-322805			CB181 => 37,793 KSI				
3 CB331 132 25'10 1/2"	68310#						
5 Beams		P64063	37310	64680	31.7	54.6	
6 "		P64046	37460	62140	31.7	54.6	
5 "		P38019	37290	68960	26.4	56.4	
1 "		P64047	37380	66040	31.5	53.4	
1 "		P51037	37590	63020	31.0	52.0	
2 "		P28051	37310	63490	32.5	53.1	
PRR-880310							
8 CB181 50 21'11"	65750						
19 Beams		P58099	38080	63700	30.7	51.4	
41 "		P63071	37600	65520	31.2	49.2	

Figure 2.12 Microfilm of one of the original mill certificates

To verify the accuracy of these mill certificates, the decision was made to conduct material tests on two samples of steel removed from the bridge. To reduce the possibility of selecting samples from the same heat of steel, the specimens were taken from transverse floor beams at opposite ends of the bridge as shown in Figure 2.13. Figure 2.14 shows the sampling size and location. The samples were taken from areas of the beam subject to very low stress. The samples were cut from the flanges with a torch, and subsequently the area was painted to protect the bare steel (see Figures 2.15 and 2.16).

The samples were machined to ASTM specifications for standard 0.5 inch round tensile specimens. (ASTM A370) The samples were tested in a universal test machine at the University of Texas at a crosshead rate of 0.02 inches per minute up to yield, and a rate of 0.2 inches per minute post yield. Test results are summarized below in Table 2.1.

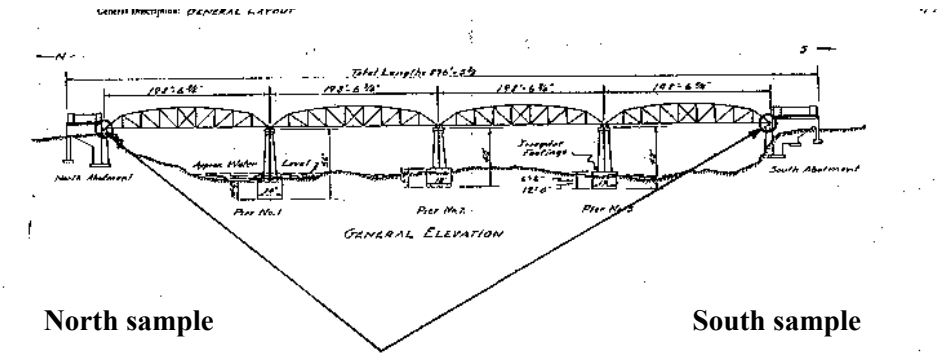

Figure 2.13 Steel sampling locations

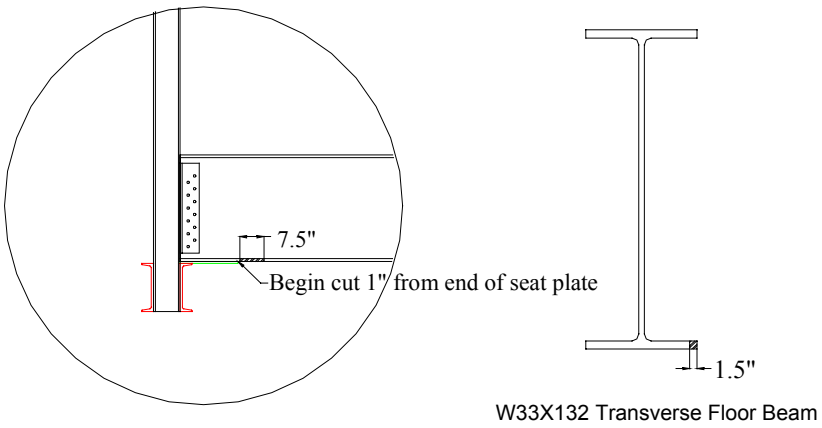

Figure 2.14 Steel sample details

Figure 2.15 Removing the steel sample

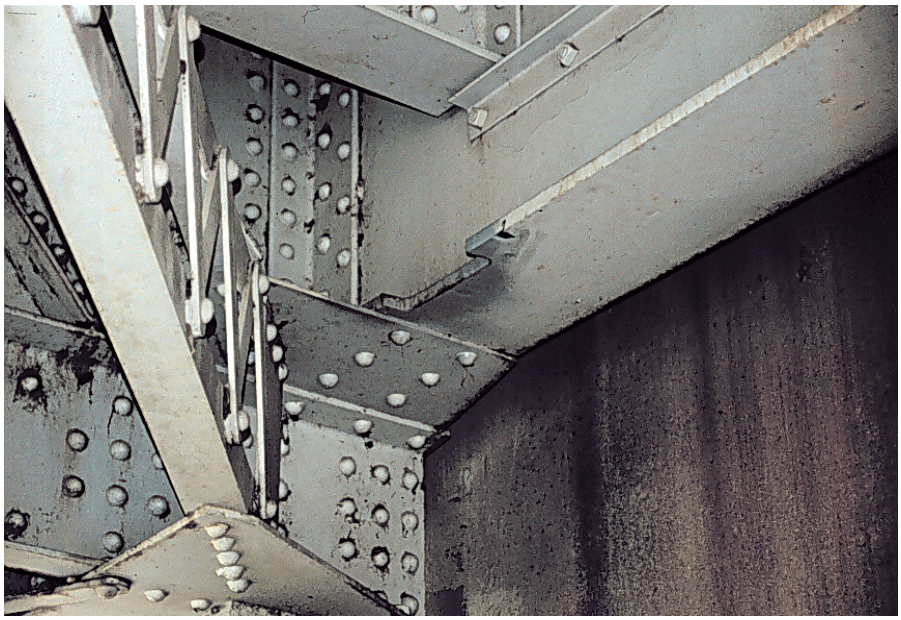

Figure 2.16 Location after steel sample removal

Table 2.1 Tensile test results

	North Sample	South Sample
Area	0.197 in^2	0.197 in^2
Gage length	2 in	2 in
Yield Stress	36.2 ksi	37.1 ksi
Ultimate Stress	60.2 ksi	61.5 ksi
Percent Elongation	42%	41%

The results of the two tension tests conducted on the beam flange samples supported the data reported on the mill certificates. Considering the data from the mill certificates and from the tension tests, the yield stress was taken as 36 ksi for the subsequent analysis and load ratings.

2.3 AASHTO LOAD RATINGS

2.3.1 Introduction

After establishing the actual member sizes and material characteristics, the next step in evaluating the Llano Bridge was load capacity analysis. Two of the methods utilized by bridge engineers are the Allowable Stress method and the Load Factor method. Another newer method, the Load and Resistance Factor Design (LRFD) method is still under development and was not used to remain consistent with the procedures most commonly utilized by TxDOT.

2.3.2 ASD and LFD Load Rating Systems

To provide a standard procedure to determine the load capacity of an existing bridge, AASHTO publishes the "Manual for Condition Evaluation of Bridges". (AASHTO 1994) This manual offers two methods for load rating bridges, the Allowable Stress (AS) method and the Load Factor (LF) method.

The Allowable Stress method uses unfactored loads for the demand coupled with a maximum allowable working stress capacity. The working stress is determined using a factor of safety. Alternatively, the Load Factor method employs factored loads and capacities determined by AASHTO load factor design specifications. (AASHTO 1996)

In order to load rate a bridge, AASHTO utilizes a rating factor. The rating factor (RF) is a scaling number used as a multiplier on the loading used in determining the live load effects. For example, if an HS 20 load vehicle was used in determining the live load effect (L), and the rating factor was calculated to be 0.87, the bridge rating would be 0.87 x 20 = HS 17.4.

AASHTO (1994) specifies two rating levels: inventory and operating. The inventory rating level corresponds to the live load that can be safely utilized on an existing structure for an indefinite period of time. The second level of rating is the operating level. Load ratings based on the operating level generally describe the maximum permissible live load to which the structure may be subjected. Allowing unlimited numbers of vehicles to use the bridge at the operating level may shorten the life of the bridge. (AASHTO 1994)

Essentially, the inventory level represents the capacity of a bridge for normal traffic, whereas the operating level corresponds to an occasional oversized load. Each member of the Llano Bridge was load rated for both levels of use, utilizing both the Allowable Stress and Load Factor methods. The bridge was rated using two yield stress levels: 30 ksi which represents the yield stress required by AASHTO for unknown steel, and 36 ksi which represents the actual yield stress measured.

Both rating methods (AS and LF) use the same general expression in determining the load rating of a structure;

$$RF = \frac{C - A_1 D}{A_2 L(1+I)} \tag{2.1}$$

The terms and values of equation 2.1 are defined Tables 2.2 and 2.3.

Table 2.2 Terms used in load rating equation

Term	Definition	Term	Definition
RF	Rating Factor	A_1	Dead load factor
C	Member Capacity	A_2	Live load factor
D	Dead load effect	I	Impact factor
L	Live load effect		

The impact factor is a multiplier on live load intended to account for the dynamic effects of vehicles. This factor may be calculated by the equation (AASHTO 94);

$$I = \frac{50}{L+125} \leq 0.3 \tag{2.2}$$

where L is the member length in feet. For the Llano Bridge, the upper limit of 0.3 governed in all cases. Table 2.3 lists the values used for the various terms in the rating factor equation, as specified in the Manual for Condition Evaluation of Bridges (AASHTO 94).

Table 2.3 Values used in AASHTO load ratings

Item	Allowable Stress	Load Factor
A_1 (Inventory - Operating)	1.0 - 1.0	1.3 – 1.3
A_2 (Inventory - Operating)	1.0 - 1.0	2.7 – 1.3
Allowable Stress in Tension (Inventory)	0.55 F_y	F_y
Allowable Stress in Tension (Operating)	0.75 F_y	F_y
Allowable Stress in Compression members (Inventory)	$F_{cr}/2.12$	0.85 F_{cr}
Allowable Stress in Compression members (Operating)	$F_{cr}/1.7$	0.85 F_{cr}

Although the allowable stress for tension (inventory level) is given by AASHTO (1994) as 0.55 times the yield stress, the tabulated values listed in AASHTO (1994) for inventory levels are rounded down for 30 ksi steel. Therefore, the inventory allowable stress is rounded down from $0.55 \cdot 30 = 16.5$ ksi to 16.0 ksi. For 36 ksi steel, however, the allowable inventory stress is rounded up from $0.55 \cdot 36 = 19.8$ to 20 ksi. Although this may seem to be a minor issue, the final load rating of a member can vary by several percent, depending on whether the computed or tabulated (and rounded) values of allowable stress are used. In the case of the Llano Bridge, if the computed values of 0.55 Fy are used, the member capacity is increased by 20% in going from 30 to 36 ksi (36/30=1.2). However, if the tabulated values of allowable stress are used, the member capacity is increased 25% (20/16=1.25). For load rating of the Llano Bridge, the tabulated values for allowable stress were used.

2.3.3 AASHTO Load Rating Vehicles

To represent the various loadings that bridges are subjected to, AASHTO has devised a series of trucks to use in design and analysis. The heaviest truck load used in design is known as an HS 20-44. (The 20 refers to the weight of the combined first and second wheel line loads in tons, and the 44 refers to 1944, the year this loading was incorporated. For brevity, the 44 will be dropped in further references). An HS 20 loading consists of a three-axle configuration with a total weight of 72 kips. The front axle is 8 kips, the second axle is 32 kips, and the rear axle is 32 kips. The spacing from the front to second axle is 14 ft., and the spacing from the second to third axle may vary from 14 ft. to 30 ft. to obtain the maximum response. Because of the short spans of the Llano deck, a 14 ft. rear axle spacing governed in all cases. Figure 2.17 illustrates the HS 20 loading.

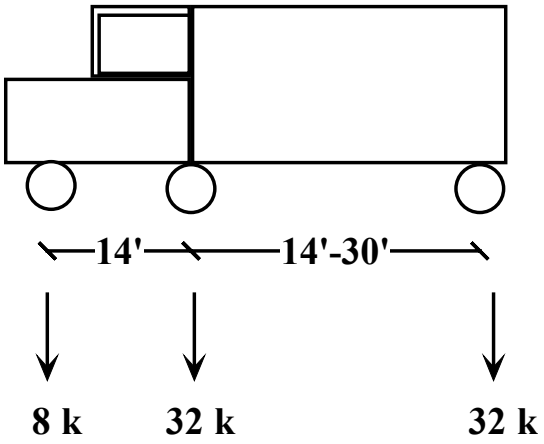

Figure 2.17 HS 20-44 truck

In addition to considering bridge response under HS 20 point loading, AASHTO also requires the bridge to be evaluated under a distributed load, known as lane loading. However, because of the relatively short spans of the Llano Bridge, the truck loadings controlled the response in all cases.

2.3.4 Llano Load Rating Results – Truss Members

The truss was rated using an HS 20 live load with both 30 ksi and 36 ksi yield stress steel. A dead load of 2.7 kips per linear foot of truss was taken from the original TxDOT drawings and applied. Because of its small size and weight, the sidewalk was not initially considered in the calculations. All members were assumed to be pin connected.

Tension member capacities were calculated using gross section properties, and compression member capacities were calculated using an effective length of 0.75 L as per AASHTO specifications for riveted end connections. (AASHTO 1994) Detailed connection analysis was not performed. Structural analysis was performed using a standard commercial finite element software package, Visual Analysis. (Integrated Engineering Software, V3.50) For reference, panel point numbering is shown in Figure 2.18.

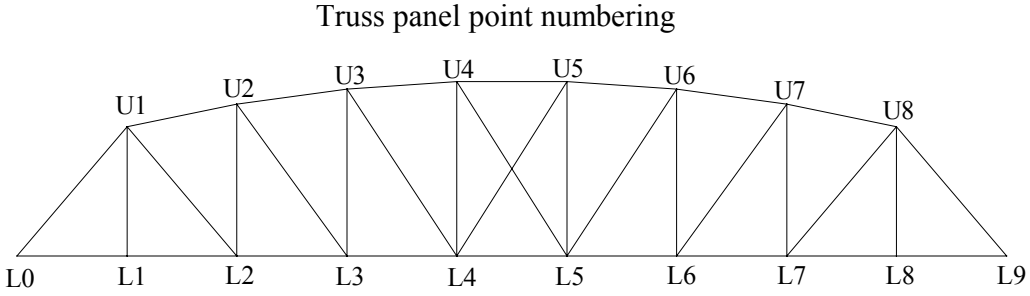

Figure 2.18 Panel point numbering for truss analysis

The center diagonal members (L4-U5 and L5-U4) were relatively small; twin angles 3 ½ x 3 x 5/16 and consequently for analysis purposes it was assumed they were incapable of resisting compressive forces. Hence, if during any load case these members were found to be in compression, they were removed from the model.

Results of the truss load ratings are shown in Figures 2.19 to 2.26. Since the truss is symmetrical, ratings are shown for only one-half of the truss. Allowable Stress results are shown in Figures 2.19 through 2.22, and Load Factor results follow in Figures 2.23 through 2.26.

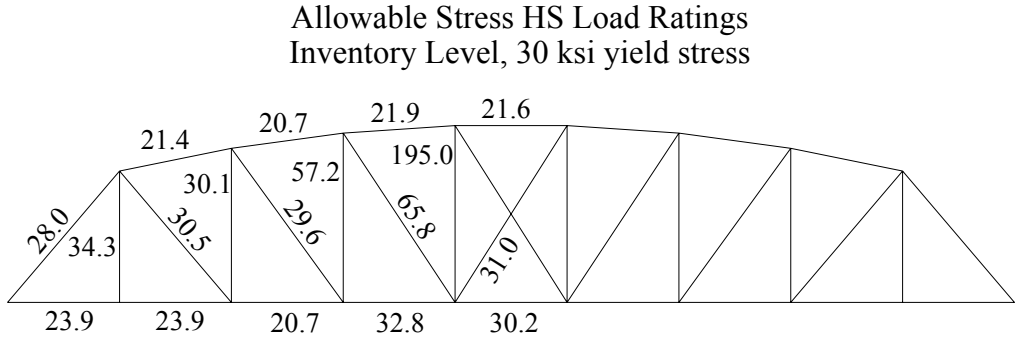

Figure 2.19 Allowable stress HS inventory level load rating results based on 30 ksi yield stress

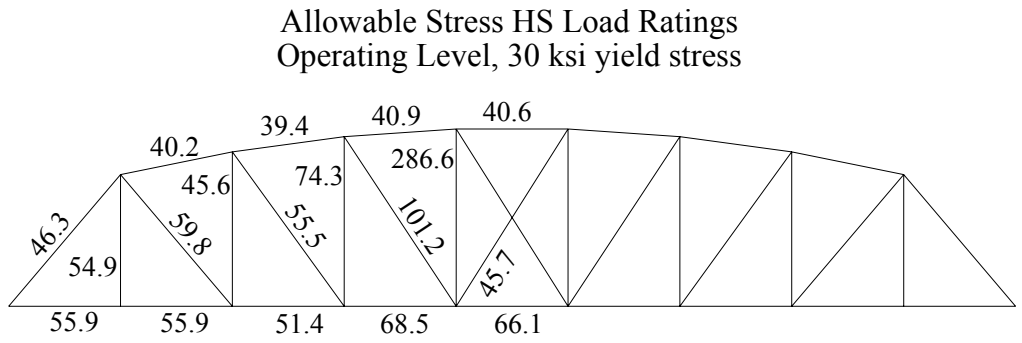

Figure 2.20 Allowable stress HS operating level load rating results based on 30 ksi yield stress

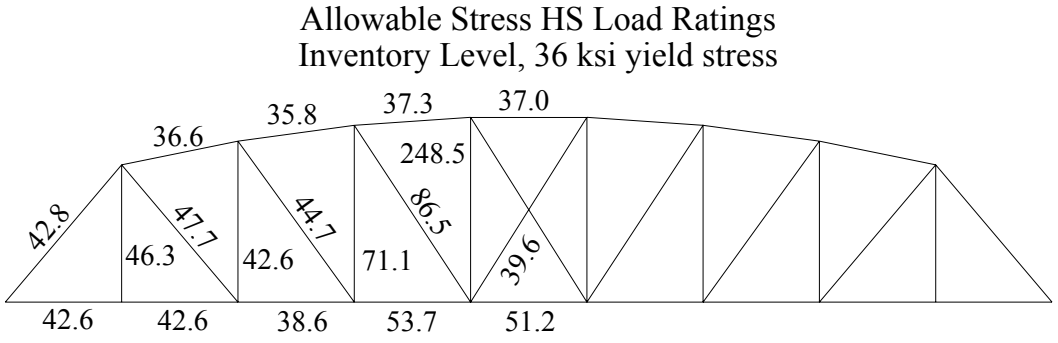

Figure 2.21 Allowable stress HS inventory level load rating results based on 36 ksi yield stress

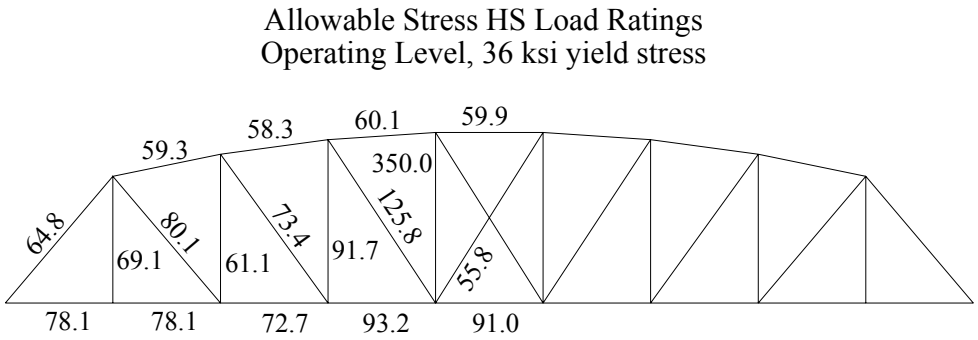

Figure 2.22 Allowable stress HS operating level load rating results based on 36 ksi yield stress

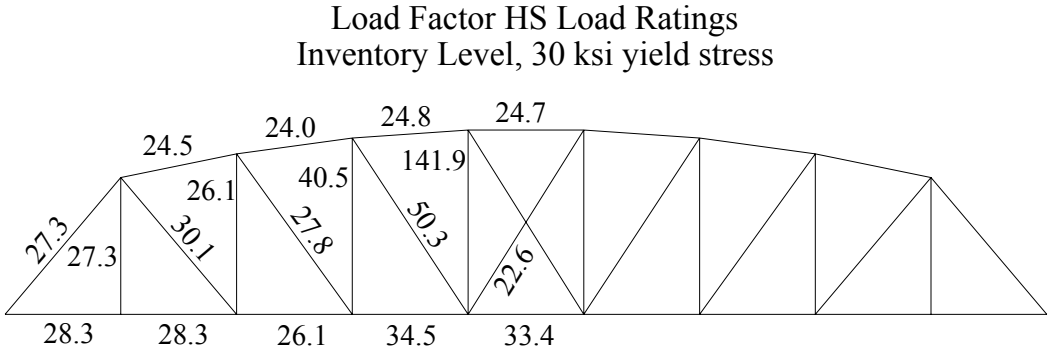

Figure 2.23 Load factor HS inventory level load rating results based on 30 ksi yield stress

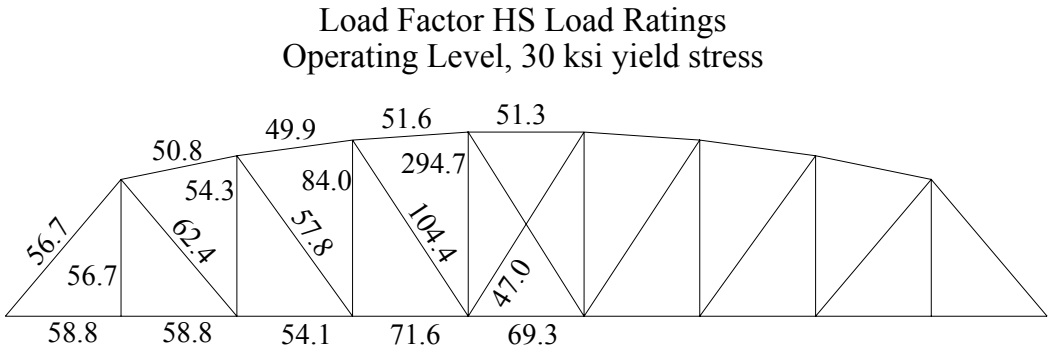

Figure 2.24 Load factor HS operating level load rating result based on 30 ksi yield stress

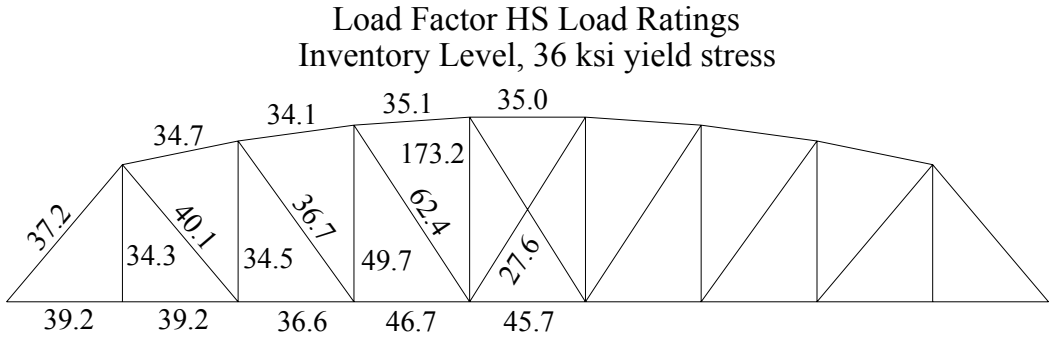

Figure 2.25 Load factor HS inventory level load rating results based on 36 ksi yield stress

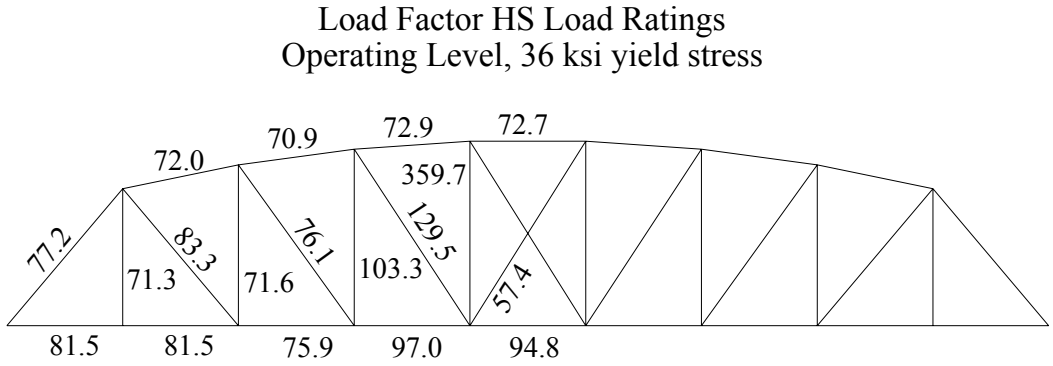

Figure 2.26 Load factor HS operating level load rating results based on 36 ksi yield stress

Figures 2.27 through 2.30 below show comparisons between the Allowable Stress and the Load Factor methods for both 30 and 36 ksi steel. Each figure shows the ratio of the Allowable Stress rating to the Load Factor rating, expressed as a percent. Depending on the member, rating level (inventory or operating), and assumed yield stress, significant differences can be seen between Allowable Stress ratings and Load Factor based ratings. In some cases the Allowable Stress rating is higher, however in other cases the load factor rating is higher.

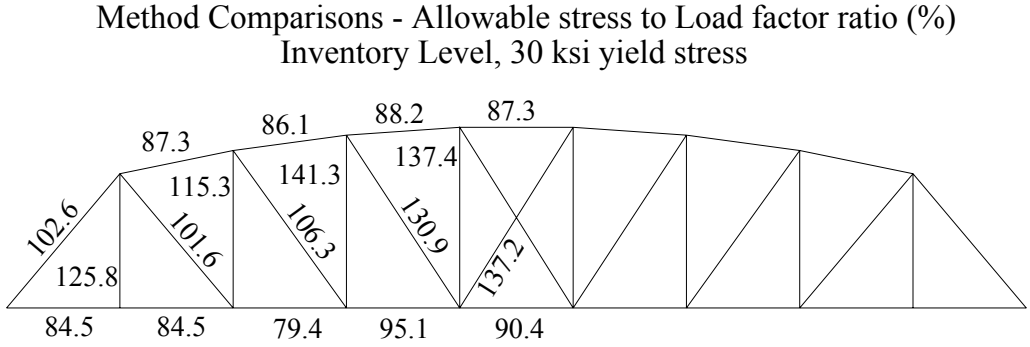

Figure 2.27 Comparisons between AS and LF inventory ratings for 30 ksi yield stress

Method Comparisons - Allowable stress to Load factor ratio (%)
Operating Level, 30 ksi yield stress

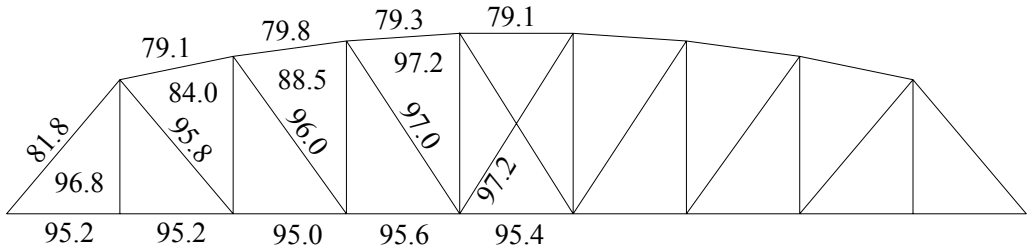

Figure 2.28 Comparisons between AS and LF operating ratings for 30 ksi yield stress

Method Comparisons - Allowable stress to Load factor ratio (%)
Inventory Level, 36 ksi yield stress

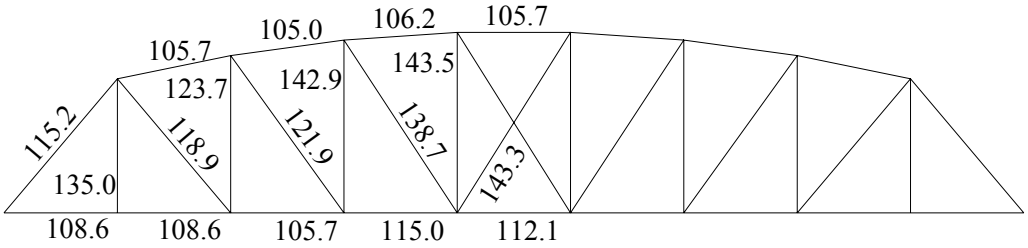

Figure 2.29 Comparisons between AS and LF inventory ratings for 36 ksi yield stress

Method Comparisons - Allowable stress to Load factor ratio (%)
Operating Level, 36 ksi yield stress

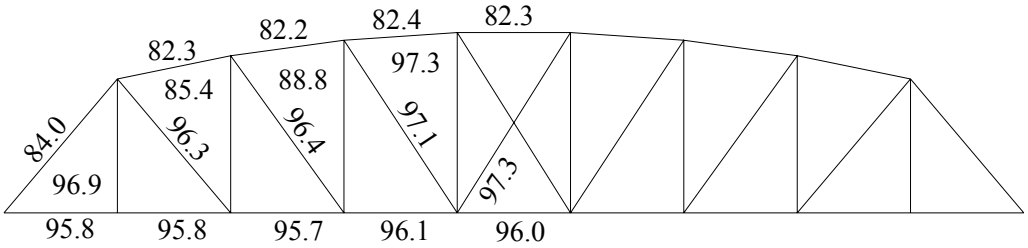

Figure 2.30 Comparisons between AS and LF operating ratings for 36 ksi yield stress

2.3.5 Llano Load Rating Results – Floor Deck Beams and Stringers

In a similar fashion to the truss, the floor beams and stringers were load rated using an HS 20 live load, assuming both 30 and 36 ksi yield strength. Dead loads consisted of self-weight of the steel, plus 6-½ in. of reinforced concrete plus an assumed 1-½ in. of asphalt overlay. Both the concrete and the overlay were assumed to weigh 150 lbs. per ft.[3.] Member lengths were conservatively rounded to 26 ft. for the transverse beams and 22 ft. for the longitudinal stringers.

Transverse beams had an assumed unbraced length of 4.5 ft. Due to the top flange embedment into the slab, the longitudinal stringers were considered to be fully laterally supported.

Both transverse beams and longitudinal stringers were considered to have pinned ends for the analysis. This assumption was based on the flexibility of the connections as well as the flexibility of the members to which they were connected. Longitudinal members framed into the web of the transverse members, and transverse members framed into the truss verticals. Neither the webs of the transverse members or the truss verticals provide significant rotational stiffness. Table 2.4 gives results for dead and live load moments based on AASHTO calculations, including impact (I) and distribution factors (DF).

Table 2.4 AASHTO calculations for deck member moments

Member	M_{DL} (k-ft)	M_{LL} (k-ft)	DF	I	$M_{LL\ (tot)}$ (k-ft)
Longitudinal	30.3	88	0.82	0.3	93.8
Transverse	219	398	1.0	0.3	518

To load rate a longitudinal stringer with the allowable stress or load factor method, a wheel line is placed directly over a member in the location to produce the maximum response. A wheel line is a series of point loads equal in magnitude to one half the axle loads placed at the spacing indicated in Figure 2.17. Essentially, wheel line loading is placing half (longitudinally) of the truck directly over the stringer. Because of the short span length for longitudinal members (22 ft.) the maximum loading position for those members was simply a single HS 20 wheel load (16 kips) located at midspan.

To account for distribution of the load to adjacent stringers by the slab, AASHTO uses what is known as a distribution factor (DF). A simple equation is used to calculate the DF, based on the spacing of the stringers. For a slab on girder bridge;

$$DF = \frac{S}{5.5} \tag{2.3}$$

With a spacing of 4.5 ft., the DF for the Llano deck was 0.82. AASHTO specifications however, allow no load distribution for transverse members.

Members were also Load Factor rated with what is referred by AASHTO as a serviceability criterion. The Load Factor method contains a provision (section 10.57.1, (AASHTO 96)) referred to as overload. Section 10.43.3 describes overloads as live loads that can be allowed on a structure on infrequent occasions without causing permanent damage. For non-composite beams and girders, the maximum flange stress caused by the dead load plus 5/3 times the live load plus impact must not exceed 0.8 times the yield stress of the flange. This provision in equation form in terms of stress is as follows:

$$\sigma_D + \tfrac{5}{3}\sigma_{L+I} \le 0.8\,F_{yf} \tag{2.4}$$

Figure 2.31 shows the position of loads to produce the maximum moment in the transverse members. Each concentrated load consisted of the resultant of an HS 20 wheel line with the second axle directly on top of the transverse member. From statics, the resultant of the three wheel loads is 23.3 kips. Figure 2.32 illustrates the three wheel loads longitudinally resulting in a single 23.3 kip point load on the center transverse member.

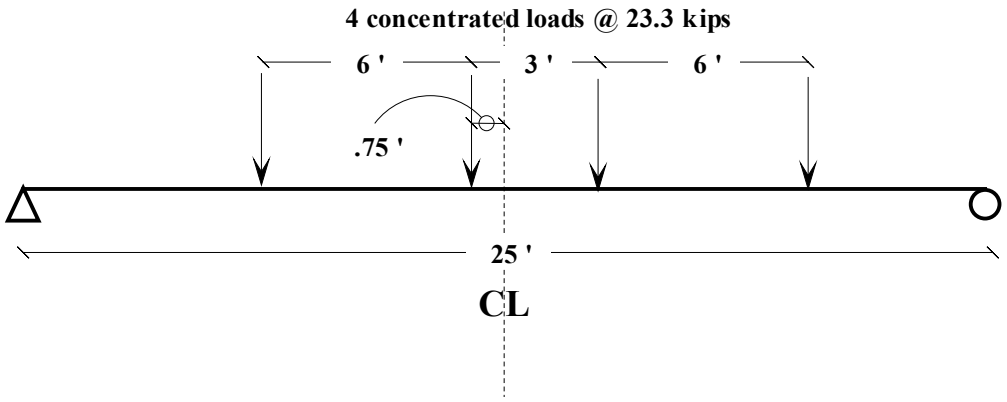

Figure 2.31 Point load locations for maximum flexural response of transverse beams

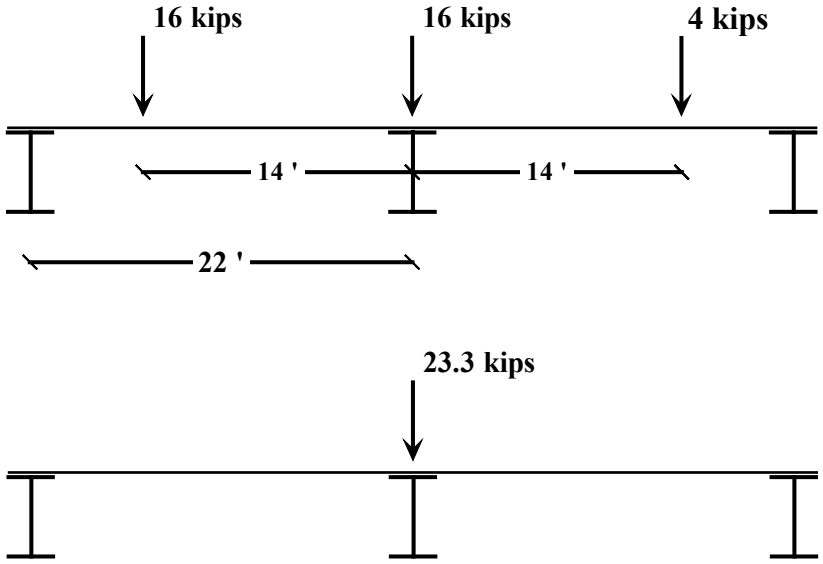

Figure 2.32 Decomposition of three wheel loads into equivalent single point load

Results of the ratings are summarized in Tables 2.5 and 2.6. Table 2.5 shows that for the 30 ksi yield stress assumption, the stringers fail to achieve an HS 20 inventory rating for both AS and LF methods. The transverse beams also failed to achieve an HS 20 inventory load ratings for both AS and LF methods. As indicated in Table 2.6, with the 36 ksi yield stress assumption, the longitudinal stringers meet HS 20 inventory load ratings for both AS and LF methods. However, the transverse members still fail to achieve an HS 20 inventory rating for both AS and LF ratings. Note that in all cases for the load factor method, the overload serviceability criteria (equation 2.4) governed.

Table 2.5 HS Load rating results for bridge deck beams and stringers based on 30 ksi yield stress

30 ksi yield stress			
Longitudinal Stringers			
Method	**Inventory**	**Operating**	**Overload**
AS	18.9	29.1	N/A
LF	20.9	35.0	18.9
Transverse Beams			
Method	**Inventory**	**Operating**	**Overload**
AS	12.9	21.5	N/A
LF	15.7	26.3	14.1

Table 2.6 HS Load rating results for bridge deck beams and stringers based on 36 ksi yield stress

36 ksi yield stress			
Longitudinal Stringers			
Method	Inventory	Operating	Overload
AS	24.9	36.2	N/A
LF	25.9	43.2	23.5
Transverse Beams			
Method	Inventory	Operating	Overload
AS	18.2	27.5	N/A
LF	19.9	33.2	18.0

2.4 SUMMARY

The Roy Inks Bridge in Llano, Texas was chosen as the subject for a detailed structural investigation. This chapter outlined the details of the bridge and the AASHTO load rating analysis. The following summarizes the key findings:

1. Accurate determination of member properties and material strengths can greatly improve a bridge load rating. Based on year built, AASHTO specifies a yield stress of 30 ksi for use in load rating of the Llano bridge. However, based on examination of mill certificates and tension testing of steel samples removed from the bridge, a yield stress of 36 ksi can be justified. As shown in Figures 2.19 through 2.26, and Tables 2.5 and 2.6, an increase in the load rating of anywhere from 20 to over 100 per cent is possible in going from 30 ksi to 36 ksi yield stress, depending on the member and dead to live load ratio.
2. Although usually not as significant as an increase in material properties, utilizing a different load rating method can increase the bridge capacity. Generally the difference between

Allowable Stress and Load Factor ratings was between 5 and 20 per cent for the Llano Bridge. However, the method providing the higher load rating was not consistent between members or rating levels.

3. AASHTO load rating showed a large reserve capacity in the truss members of the Llano Bridge, often over 200% above an HS 20 inventory rating. Thus, the truss members of the Llano Bridge pose no problems with respect to load rating.
4. Load ratings for the beams and stringers in the deck of the Llano Bridge showed inadequate capacity for both transverse and longitudinal members using HS 20 loading and 30 ksi yield stress.
5. Using a more realistic yield stress of 36 ksi, the longitudinal members surpass HS 20 loading, but the transverse members are still approximately 20% deficient.

Chapter 3:
Finite Element Analysis Of Llano Bridge Deck

3.1 INTRODUCTION

The previous chapter presented results of a load rating of the Llano truss case study bridge based on AASHTO standards and simplified hand methods of structural analysis. As indicated in Chapter 2, the truss members of this bridge demonstrated load ratings well above HS 20, whereas the floor beams and stringers rated below HS 20. Thus, the floor system controlled the overall load rating for this bridge.

In this chapter, the floor system of the Llano Bridge is analyzed in further detail using elastic finite element analysis (FEA) techniques. The purpose of this analysis is to determine if a higher load rating can be justified by using analysis methods that are more advanced and more exact than typical hand methods of analysis used in standard load ratings.

3.2 ANALYSIS OBJECTIVES

Previous researchers have shown through both field tests (Saraf and Nowak 1998), finite element analysis (Mabsout et al 1997, Hays et al 1998), or both (Chajes et al 1997), that the stresses in slab on girder bridges can be significantly less than an typical AASHTO load rating would indicate. The objective of this portion of the project is to create a simple finite element (FE) model of the Llano bridge deck to compare to field measurements and AASHTO code.

A standard commercially available structural analysis computer program, SAP 2000 Non-Linear (SAP) was chosen to perform the analysis. SAP is readily available, relatively inexpensive, and utilizes a graphical user interface for ease of use. Although the program has non-linear capabilities, only linear elastic analyses were conducted for this study.

3.3 MODEL DESCRIPTION

Standard finite element beam and shell elements were used to create a model of two spans of the Llano bridge deck. Two node beam elements were used for the steel members, and isotropic four node shell elements for the slab. Figure 3.1 shows the model used in analysis.

Longitudinal steel members were 22 ft. in length, and were modeled with beam elements 12 inches in length. Transverse steel beams were 26 ft. in length, and were modeled with beam elements that were typically 6 or 12 inches in length. All steel members had moment releases at each end to model simply supported ends.

The majority of shell elements were either 12"x12" or 6"x12". Variations in the size of elements were needed to ensure enough element nodes to accommodate the many loading cases that were evaluated. Shell element thickness matched the slab thickness of 6.5 in. This thickness reflects only the thickness of the concrete, as it was believed that the asphalt overlay was not stiff enough to provide significant structural response. As per American Concrete Institute (ACI 1999) specifications, the elastic modulus of concrete was taken as $57,000 \cdot \sqrt{f'c}$. Since the concrete compressive strength was not specified on the available drawings, AASHTO requires an estimate based on the date built. This estimate was 2,500 psi, resulting in a modulus of 2850 ksi. The contribution of the steel reinforcement to the stiffness of the slab was conservatively neglected in the model.

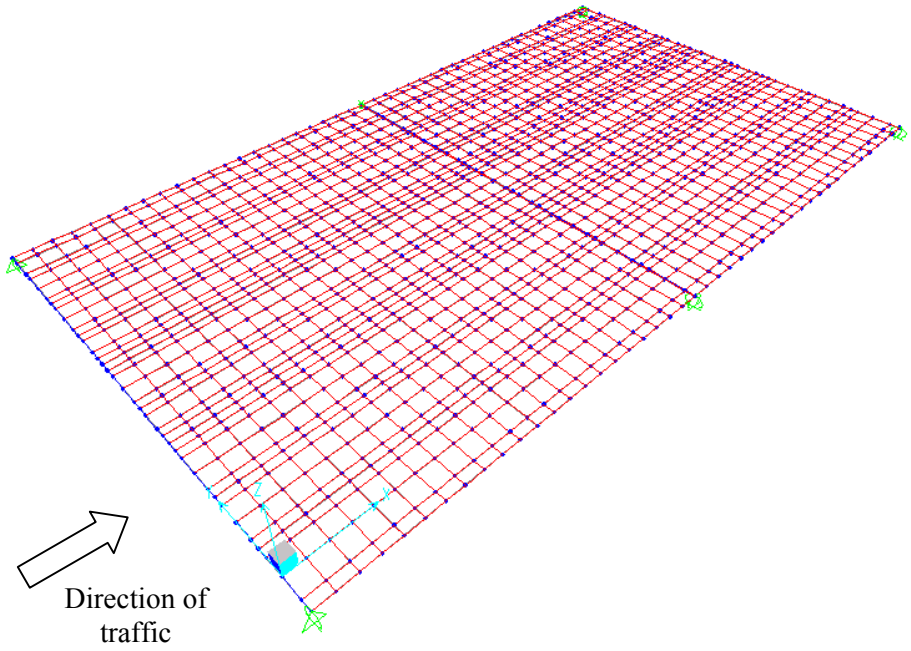

Figure 3.1 Finite element model of Llano Bridge deck

Curbs were modeled by increasing the size of the outermost shell elements to 7 inches wide by 18.5 inches high. Six supports were used at the locations where each transverse beam connected to the trusses. These supports were restrained translationally in all three directions. Although the actual supports were not likely to restrain movement other than vertically, the additional restraints introduced in the FE model did not affect the results since the model used linear geometry. The additional restraints were introduced simply to reduce the number of degrees of freedom, and remove any possible singularities from the stiffness matrix. Since in the actual bridge the slab was not continuous longitudinally and the longitudinal steel members were simply connected, the deck did not have the capacity to transfer moment across deck segments. To enforce this behavior in the model, a one-inch separation was created in the shell elements between the deck segments, as shown in Figure 3.2. The size of the separation was somewhat arbitrarily chosen, but there was no significant response difference with either smaller or larger separations. Separations were varied from 0.1 inch to 2 inches in magnitude.

To enforce vertical displacement compatibility between the edge of the shell elements and the center transverse beam, adjacent beam and shell members were constrained to identical vertical displacements.

Because of the longitudinal discontinuity, the behavior of the floor system could be adequately captured using only two segments. Figure 3.3 shows the model with the elements extruded, emphasizing the steel framework, slab, and curb. The longitudinal stringers were labeled Stringers 1 through 6 (S1-S6), and the transverse beams labeled Beams 1 through 3 (B1-B3).

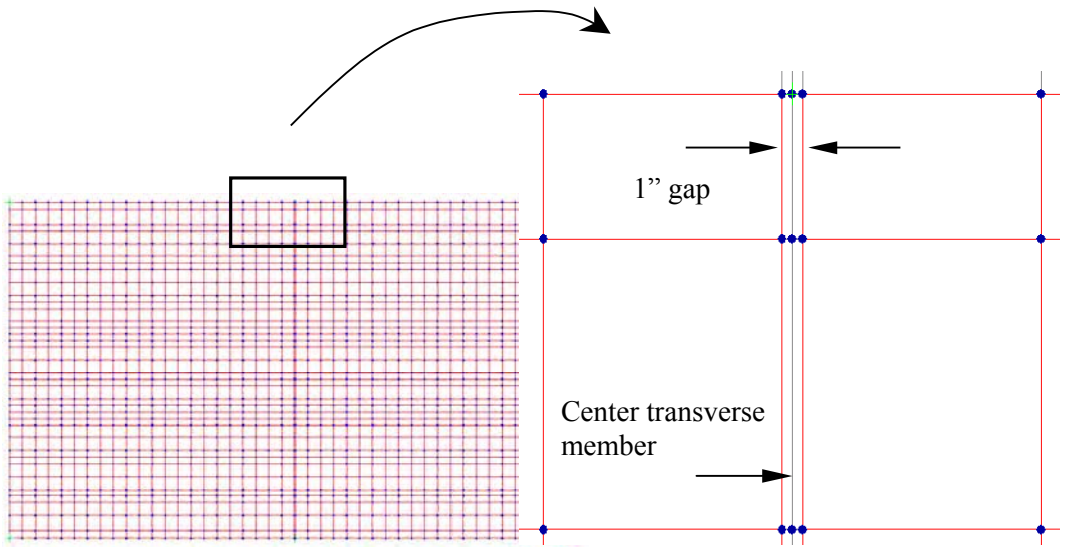

Figure 3.2 Plan view of deck model, with cut out of 1” gap in slab

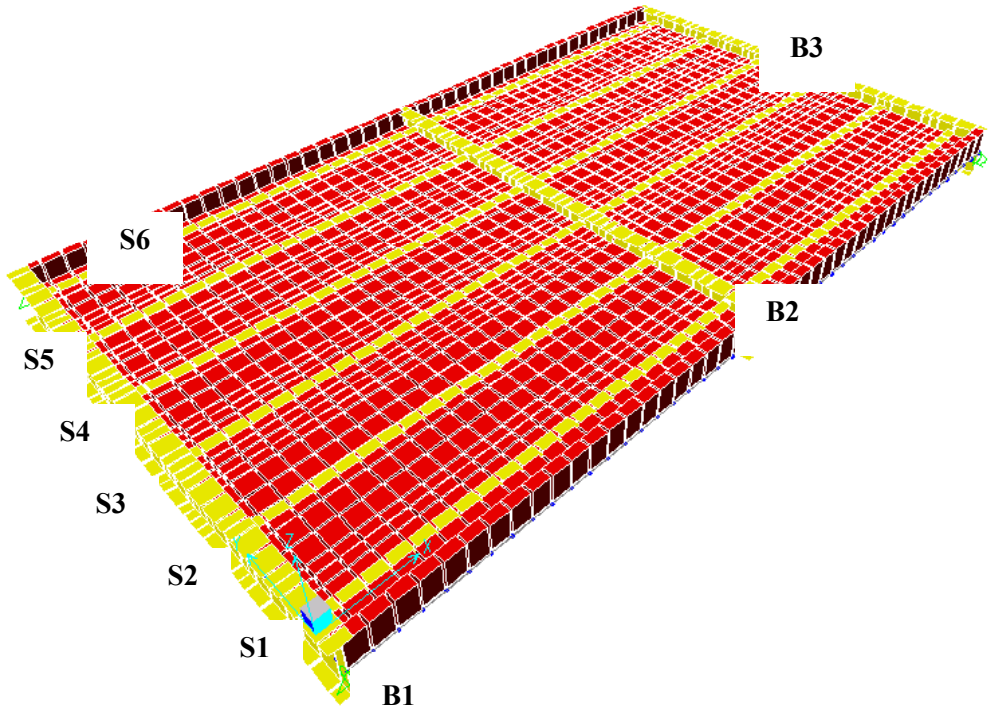

Figure 3.3 SAP model with elements extruded

The actual bridge deck structure was designed non-compositely, and no mechanical shear connectors were provided between the steel members and the slab. In the SAP finite element model, shell elements were placed at the same level as the beam elements, modeling a non-composite system. Previous researchers (Saraf and Nowak 1998, Juaregi 2000, Pennings, 2001, Chajes et al 1997) have shown evidence of composite behavior in bridge structures designed non-compositely, largely due to friction or adhesion between the steel and concrete. Consequently, even though the Llano bridge deck

was not designed or constructed to provide composite action, some degree of unintended composite action may in fact develop in the actual deck system. However, as described above, the SAP finite element model of the deck represents a non-composite system, and therefore conservatively neglects any beneficial effects of unintended composite action. The development of unintended composite action in the Llano bridge deck will be examined in more detail in the field load tests described later in Chapter 4.

3.4 LOAD CASES

3.4.1 Introduction

Due to the short spans, truck loading (as opposed to lane loading) governed all load cases for the deck. Because of the large number of nodes (approximately 1,700), most conceivable load cases could be easily applied to the model using concentrated loads at the nodes. Transverse wheel spacing was typically 6 feet. However, to avoid an extremely fine and cumbersome mesh, occasionally a 6.5 foot spacing was used. Results indicated that there was less than a 1% difference in maximum moment in the loaded beam members when using the two different spacings. Hence, these minor variations in spacing were not considered significant.

Load cases where created to simulate HS loading, and subsequently the loadings used in the field and laboratory tests. HS loading results will be discussed in this chapter; while results of the field load test and laboratory loading tests will be discussed later in Chapters 4 and 6.

3.4.2 Transverse Beam Loading

Figure 3.4 shows twin HS 20 load trucks positioned for the maximum flexural response at midpoint of the center transverse beam.

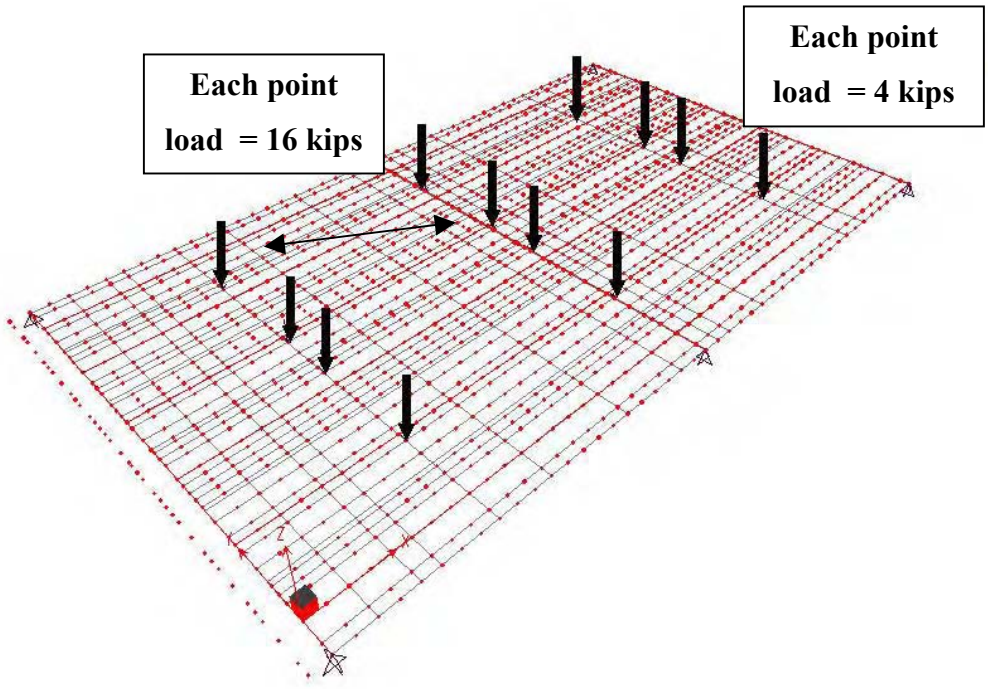

Figure 3.4 Twin HS20 truck loadings on finite element model for maximum beam response

Each of the four point loads on the first deck segment and the four loads directly over of the center transverse beam are 16 kips, while the four point loads on the forward deck segment are 4 kips. The longitudinal spacing between the first and second axles, as per AASHTO specifications, is 14 ft. AASHTO requires the third axle to be spaced from 14 to 30 feet based on the spacing that would result in the maximum response. Because of the relatively short distance between the transverse beams (approximately 21 feet) in the Llano Bridge, the axle spacing was taken as 14 feet.

Additionally, analysis was performed with a total of four point loads of 23.3 kips placed directly on the transverse member, as shown in Figure 3.5. This was done to simulate the load case used for the hand calculations utilized in the normal AASHTO load rating as discussed in the previous chapter. Note, however, the truck positioning transversely is slightly different than the hand calculations due to the node locations. Recall that the absolute maximum moment is obtained by offsetting the 23.3 kip loads a distance of 0.75 feet from the member centerline, as shown in Figure 2.31, and as used in the AASHTO hand calculations. In the finite element model, the 23.3 kip loads were offset 1.0 ft. from the member centerline, rather than 0.75 ft. The difference in moment between the two positions when performing hand calculations is less than 0.5 percent. Hence, no additional nodes were placed in the model to accommodate the offset truck locations.

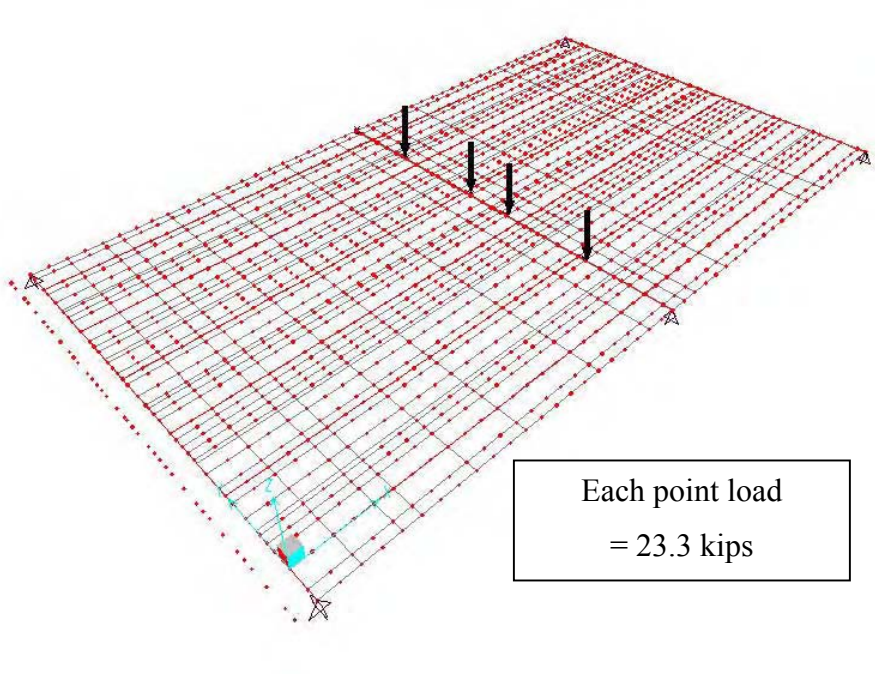

Figure 3.5 Loading used to simulate AASHTO load rating for transverse beam

3.4.3 Longitudinal Stringer Loading

AASHTO truck loads were applied in positions to produce maximum flexural response for the longitudinal stringers. Figures 3.6 through 3.8 illustrate these positions. Because of the symmetry of the structure, only three of the six stringers required analysis (S1, S2 and S3).

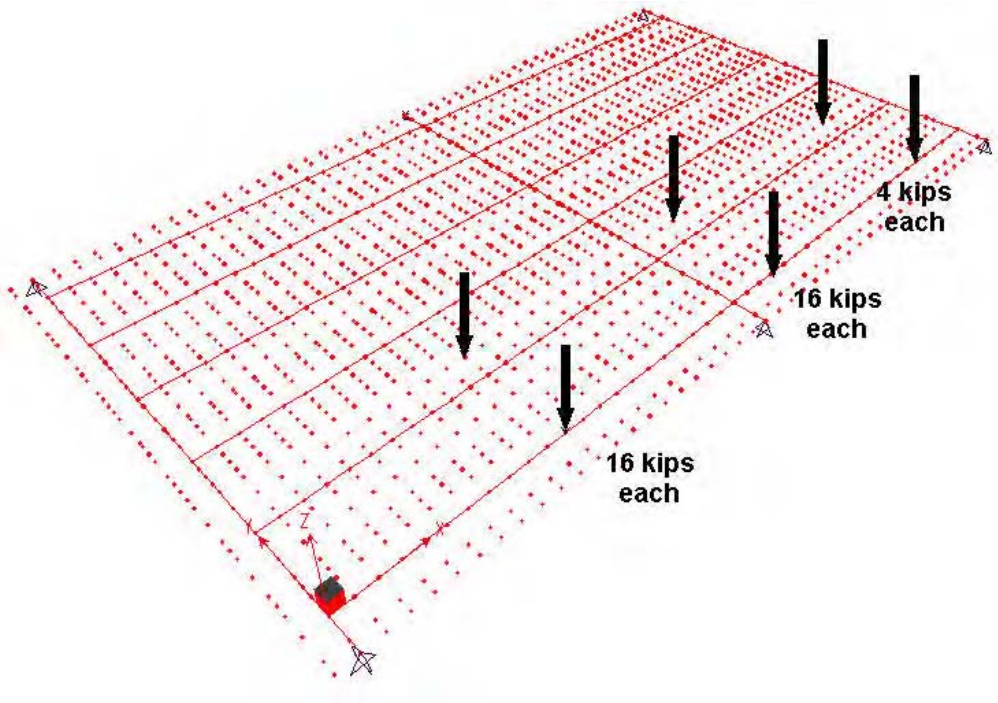

Figure 3.6 HS 20 loading position for maximum response in the first stringer

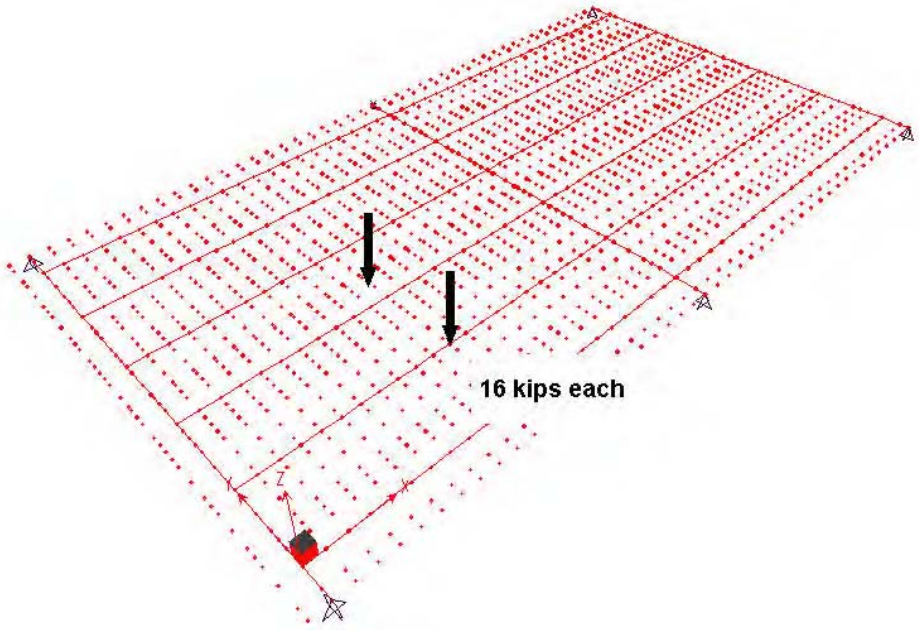

Figure 3.7 HS 20 loading position for maximum response in the second stringer

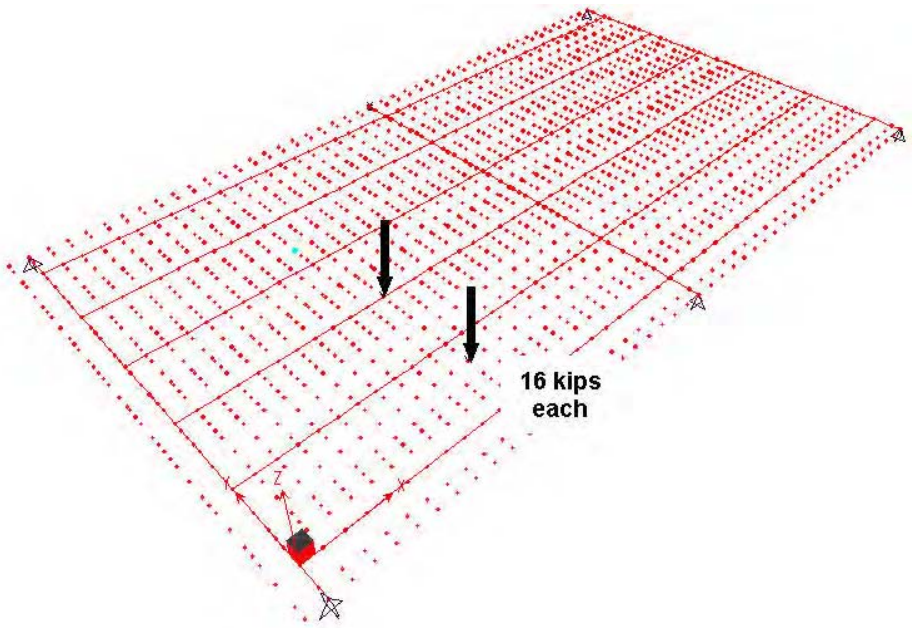

Figure 3.8 HS 20 loading position for maximum response in the third longitudinal member

Note that for stringers 2 and 3, truck loads were reduced to only one axle. Loadings on the far deck segment induced small negative moments in longitudinal members on the near deck segment, except the outermost stringers (S1 and S6). This phenomenon is cause by the sharing of nodes in the slab and the transverse steel beams. The node sharing forces the steel beams and slab to deflect equally at each shared node. As the center transverse beam deflects due to loading on one of the segments, it induces curvature and moment in the slab in the adjacent segment. Since the longitudinal members in the opposite segment are simply connected to the transverse members, the steel members transfer no moment from one segment to the next. If there were not a slab attached, the steel on the adjacent segments would simply deflect in a rigid body mode. The displacement constraints imposed by the shared nodes force an interaction between the different moments and curvatures between the steel and slab in the non-loaded segments. The result is a small negative moment (less than 1% of the positive moment) being induced into the steel in the non-loaded segments. Since the actual structure does not have this displacement constraint between the steel and slab, no negative moment is induced. Hence the nodal loadings that caused this unrealistic (although small) response were conservatively neglected in determining the maximum response in the longitudinal members.

3.5 FINITE ELEMENT RESULTS

Maximum moments from the finite element analysis of the steel members for AASHTO HS 20 loadings are summarized in Table 3.1. The table gives the maximum moment in the member, the total moment on the entire section, (including adjacent members and the slab; often referred to as the *line moment*), the percent of the total moment carried by the member, and the percent of the total moment carried by the slab.

For stringer S1, the critical loading case is shown in Figure 3.6. The total line moment generated by this loading case is 176 k-ft. This line moment is computed as the maximum moment on a simply supported span with a concentrated load at mid span (M_{max} = PL/4 = 32 kips × 22 ft. / 4 = 176 k-ft.). The 176 k-ft. line moment must be resisted by the combination of the six stringers and the concrete slab. The data in Table 3.1 indicates that stringer S1 resists 29-percent of the 176 k-ft. line moment. The concrete

slab resists 26-percent of the line moment. The remaining 45-percent is carried by the remaining five stringers. The finite element analysis shows that the slab resists a substantial portion of the total moment, even though no composite action is considered.

For stringer S2, the critical loading case is shown in Figure 3.7. The total line moment generated by this loading case, as before, is 176 k-ft. The data in Table 3.1 indicates that stringer S2 resists 24-percent of the 176 k-ft. line moment. The concrete slab resists 20-percent of the line moment. The remaining 56-percent is carried by the remaining five stringers.

Finally, for stringer S3, the critical loading case is shown in Figure 3.8. The total line moment generated by this loading case, as before, is 176 k-ft. The data in Table 3.1 indicates that stringer S3 resists 23-percent of the 176 k-ft. line moment. The concrete slab resists 22-percent of the line moment. The remaining 55-percent of the 176 k-ft. line moment is carried by the remaining five stringers.

For each of the stringers in the bridge deck system, the finite element analysis shows that even without composite action, the reinforced concrete slab resists a substantial moment, thereby relieving the moment that must be carried by the stringers.

For the center transverse beam, the critical loading case used in the finite element analysis is shown in Figure 3.5. The total line moment generated by the four 23.2 kip loads, based on statics, is 398 k-ft. The three transverse beams together with the reinforced concrete slab must resist this total line moment. The data in Table 3.1 indicates that the center transverse member resists 88-percent of the total line moment, and the slab resists 8-percent of the total line moment. The remaining 4-percent of the total line moment is resisted by the other two transverse beams.

Table 3.1 Finite element results for Llano bridge deck members

Member	Member moment (k-ft)	Total moment (k-ft)	Member % of M_{TOT}	Slab % of M_{TOT}
Stringer S1	51.0	176	29 %	26 %
Stringer S2	41.5	176	24 %	20 %
Stringer S3	40.8	176	23 %	22 %
Transverse Beam B2	349	398	88 %	8 %

Table 3.2 shows a comparison between moments predicted by the finite element analysis with moments predicted by AASHTO calculations. The AASHTO moments reported in Table 3.2 are taken from Table 2.4, except that the impact factor was not included. (no impact factor was included in the finite element analysis). As shown in Table 3.2, the moments in the stringers based on finite element analysis ranges from 57 to 71 percent of the values predicted by AASHTO calculations. Consequently, the finite element analysis is predicting substantially lower moments in the stringers. In the transverse beam, the finite element analysis predicts a moment that is 88-percent of the value predicted by AASHTO. Consequently, the reduction in moment in the transverse beam in going from the finite element analysis to the AASHTO calculation is not as dramatic as for the stringers, but still significant.

Table 3.2 Comparison of moments from finite element analysis with AASHTO

Member	FEA moment (k-ft)	AASHTO moment (k-ft)	Ratio of moments: FEA / AASHTO
Stringer S1	51	72	71 %
Stringer S2	41.5	72	58 %
Stringer S3	40.8	72	57 %
Transverse Beam B2	349	398	88 %

The smaller moments predicted by the finite element analysis appear to be due to two factors. One factor is that the finite element analysis predicts that the slab resists substantial moment, thereby reducing the moment that must be carried by the steel beams and stringers. As indicated by Table 3.1, the contribution of the slab is quite large for the stringers, with the slab resisting on the order of about 20 to 25-percent of the total moment. Since AASHTO does not regard the slab as a load carrying part of the deck system, a considerable amount of capacity is ignored. The slab contribution for the transverse beam, based on finite element analysis is less significant, with the slab resisting 8 percent of the total moment. Nonetheless, since the transverse beams are more critical than the longitudinal stringers from a load rating perspective (Table 2.6), the slab's contribution in reducing moments in the transverse beams is still quite important. Recall that the slab was modeled as a homogeneous shell member, assuming an uncracked section. This assumption is valid as long as the moment in the slab produces a tensile stress lower than the cracking stress. For all values of slab moment predicted by the finite element analysis, the tensile stress in the slab was less than the cracking stress.

Besides the slab contribution, a second factor also contributes to a reduction in beam and stringer moments in the finite element analysis as compared to the AASHTO calculation. The finite element analysis predicts a different and more advantageous distribution of moments among the steel members than obtained from the AASHTO calculations. For example, Table 3.2 shows that the transverse beam moment in the finite element analysis is 88 percent of the moment predicted by AASHTO. Of the 12-percent reduction in moment predicted by the finite element analysis, 8-percent is attributable to the slab contribution (Table 3.1). The remaining 4-percent is carried by the adjoining transverse beams. The AASHTO calculation permits no distribution of moment among transverse members, and therefore neglects this beneficial effect. The same is true for the stringers. The reduction in moment in going from the AASHTO calculations to the finite element analysis cannot be attributed solely to the slab contribution. There is an additional reduction in stringer moment due to a more advantageous distribution of moments among the six stringers than considered in the AASHTO calculations.

3.6 LOAD RATINGS BASED ON FINITE ELEMENT ANALYSIS

New load ratings were determined based on the live load moments generated by finite element analyses. Tables 3.3 and 3.4 shows the resulting load ratings based on yield stresses of 30 ksi and 36 ksi, respectively. Load ratings for the stringers, based on finite element analysis, show an increase of over 70 percent, as compared to the AASHTO load ratings developed in Chapter 2 (Tables 2.5 and 2.6). This large increase in load rating for the stringers reflects the large decrease in live load moment predicted by the finite element analysis as compared to the AASHTO calculations. The resulting FEA based load ratings for the stringers are well above an HS 20 inventory level, both for 30 ksi and 36 ksi yield stress assumptions.

Table 3.3 Llano HS load ratings for beams and stringers based on FEA and based on 30 ksi yield stress

30 ksi yield stress			
Longitudinal Stringers			
Method	**Inventory**	**Operating**	**Overload**
ASD	32.6	50.4	N/A
LF	36.3	60.6	32.7
Transverse Beams			
Method	**Inventory**	**Operating**	**Overload**
ASD	14.9	24.8	N/A
LF	18.1	30.1	16.2

Table 3.4 Llano HS load ratings for beams and stringers based on FEA and based on 36 ksi yield stress

36 ksi yield stress			
Longitudinal Stringers			
Method	Inventory	Operating	Overload
ASD	43.6	62.7	N/A
LF	44.9	75.8	40.6
Transverse Beams			
Method	Inventory	Operating	Overload
ASD	21.0	31.6	N/A
LF	22.8	38.1	20.6

As would be expected from the less significant decrease in maximum moment in the transverse members from the finite element analysis, the increase in load ratings was not as notable. Increases in load ratings for the transverse members were on the order of 15%. However, combining the use of 36 ksi for yield stress with the results of the finite element analysis shows that all floor members, both longitudinal stringers and transverse beams rate above HS 20 inventory level.

For both a conventional AASHTO load rating as well as a load rating based on finite element analysis, the transverse floor beams are the critical members controlling the load rating for the entire bridge. All truss members and longitudinal stringers load rate at a higher level than the transverse floor beams. Considering the AS method of analysis as a point of comparison, the transverse floor beams have an HS 12.9 inventory rating using conventional AASHTO procedures and without material testing. With yield stress values based on material testing combined with finite element analysis, the floor beams have an HS 21 inventory load rating, representing more than a 60 percent increase in load rating. Consequently, by using a more realistic value of yield stress based on testing material samples from the bridge combined with more advanced structural analysis in the form of a finite element analysis, it was possible to demonstrate that the Llano case study bridge satisfies an HS 20 inventory level load rating.

3.7 SUMMARY

This chapter described and provided results of a more refined analysis of the Llano bridge deck. A standard, commercially available structural analysis program, SAP 2000, was used to construct an elastic finite element model of the bridge deck and to evaluate the live load response to HS 20 loading.

Standard two node beam elements were used to model the steel members, and isotropic, four node shell elements were used to model the slab. The actual bridge deck was originally designed and constructed as a noncomposite system, as no mechanical shear connectors are present. Consequently, in the finite element model, the shell elements were connected to the beam elements in a manner that precluded composite action. That is, the finite element model was representative of a noncomposite system. Curbs were modeled by increasing the thickness of the shell elements along the outside of the slab. Because of the construction joint in the slab located above each transverse member, a one-inch separation between adjacent shell elements was introduced at that location in the model. The longitudinal reinforcement in the bridge deck was not continuous across the transverse members, and hence no moment was transferred from one deck segment to the next. This enabled the deck behavior to be adequately captured with only two segments.

HS 20 truck loadings were applied to the finite element model of the bridge deck, and maximum moments were determined in the longitudinal stringers and transverse beams. The moments predicted by the finite element analysis were significantly smaller than the moments calculated from the conventional AASHTO load rating described in Chapter 2.

Longitudinal stringers showed reductions in moment in going from the AASHTO calculation to the finite element analysis on the order of 30 to 40 percent. The decrease in response for the transverse beams was not as dramatic, but still significant. Moments in the transverse beams from the finite element analysis were approximately 12 percent lower than those predicted by AASHTO calculations.

The finite element analysis showed significantly lower moments in the stringers and beams than conventional AASHTO calculations. This reduction in moment can be largely attributed to two factors. One factor is that the finite element analysis predicts that the reinforced concrete slab resists substantial moment, thereby reducing the moment that must be carried by the steel beams and stringers. Thus, even without composite action, the finite element analysis shows that the slab provides a significant contribution to the load carrying capacity of the bridge deck. Conventional AASHTO load rating procedures do not regard a noncomposite slab as a load carrying part of the deck system. Besides the slab contribution, a second factor also contributes to a reduction in beam and stringer moments in the finite element analysis as compared to AASHTO calculations. The finite element analysis predicts a different and more advantageous distribution of moments among the steel members than obtained from the AASHTO calculations.

The critical members controlling the load rating of the Llano case study bridge are the transverse floor beams. With the reduction in live load moment predicted by finite element analysis combined with a yield stress based on measured values, it was possible to demonstrate an inventory load rating for the transverse beams, and therefore for the entire bridge, in excess of HS 20. Consequently, it appears that finite element analysis can be a valuable tool for developing improved load ratings of the deck systems of historic metal truss bridges similar to the Llano case study bridge.

As described above, finite element analysis predicts smaller live load moments in bridge floor members than obtained from conventional AASHTO load rating procedures. However, it is unclear whether the finite element model accurately captures the true structural response of the bridge deck system, and whether the results of a finite element analysis can be confidently used as a basis of load rating. To more closely examine the validity of the finite element analysis of the Llano bridge deck system, the actual response of the deck system to live load was measured in a series of field load tests. These load tests are described in the next chapter.

Chapter 4:
Llano Field Load Test

4.1 INTRODUCTION

As part of the Llano Bridge case study, two field load tests were conducted. In these load tests, selected portions of the deck system were instrumented with strain gages. Trucks of known weight and geometry were then driven slowly over the bridge, and the response of the instrumented members was measured. This chapter discusses the purpose and objectives of these tests, instrumentation, data acquisition, loading, and the results of the tests.

4.2 BACKGROUND AND PURPOSE

A standard AASHTO based load rating of the Llano truss bridge, as described in Chapter 2, showed that the truss members rated well above HS 20. The same load rating showed that the bridge floor stringers and beams were more problematic with respect to load rating. Based on an AASHTO load rating, the steel floor members controlled the load rating of this bridge at a level below HS 20. The finite element analysis, as described in Chapter 3, indicated that the actual forces developed in the floor members under truck loading are significantly less than predicted by a standard AASHTO load rating, and that a higher load rating for the floor members may be justified.

While the finite element analysis may provide a more accurate prediction of the structural response of the deck system than a standard load rating, the finite element analysis is still based on a number of simplifying assumptions and idealizations. Many of the assumptions made in constructing the finite element model of the bridge deck were chosen to provide a conservative prediction of response. For example the model was constructed assuming no composite action between the steel members and the concrete slab, and assuming no rotational fixity at the ends of the beams and stringers. Nonetheless, it is unclear how accurately the finite element model actually captures the true response of the bridge deck system.

To provide further insight into the structural behavior of the bridge deck system, and to evaluate the accuracy of the finite element model of the deck system, field load tests were conducted on the Llano bridge to measure the actual response of the deck system to known truck loads. More specific objectives of the load tests were:

1. Evaluate realistic load distribution.

   AASHTO Allowable Stress and Load Factor methods provide a simplified method to account for distribution of wheel loads to the stringers. Although this approach is easy to utilize, it is likely conservative in nature. In a similar fashion, the approximations inherent in the finite element method raise the issue as to the accuracy of load distribution predicted by this approach. By gaging each stringer in a load test, the actual distribution can be obtained. Furthermore, AASHTO does not allow any load distribution for transverse members. The accuracy of this assumption is unclear. A field load test can provide a more realistic estimate of load distribution.

2. Determine the degree of unintended composite action.

   The deck system for the Llano bridge did not have mechanical shear connectors between the slab and supporting steel, and hence the bridge was not designed compositely. However, even in the absence of mechanical shear connectors, many other investigators have observed some evidence of at least partial composite action in field tests (Bakht 1988, Jauregui 1999, Saraf and Nowak 1998). This unintended interaction has often been attributed to factors such

as friction, mechanical interlock, and chemical bond between the steel and concrete. The load test on the Llano bridge was designed to provide data and insight into this phenomenon.

3. Compare field measurements with standard load ratings and finite element analysis.

   Previous investigations (Mabsout et al 1997, Hays et al 1998, Chajes et al 1997) have provided evidence of much smaller structural responses than either standard load rating or finite element analysis would predict. The load tests can provide insight into these differences.

4.3 INSTRUMENTATION AND DATA ACQUISITION

Two load tests were conducted on the Llano bridge. The first test was on February 2, 1999, and the second on April 15, 1999. The second test was conducted to investigate different strain gage locations than used for the first test, and to augment the data collected in the first test.

The first two deck segments of the first truss (starting from the north end of the bridge) were instrumented. Figure 4.1 shows the plan view of the tested segments with stringer (S1 through S7) and beam numbering (B1 and B2). Figure 4.2 shows the strain gage layout for the first load test, and Table 4.1 lists the strain gage layout for the first test.

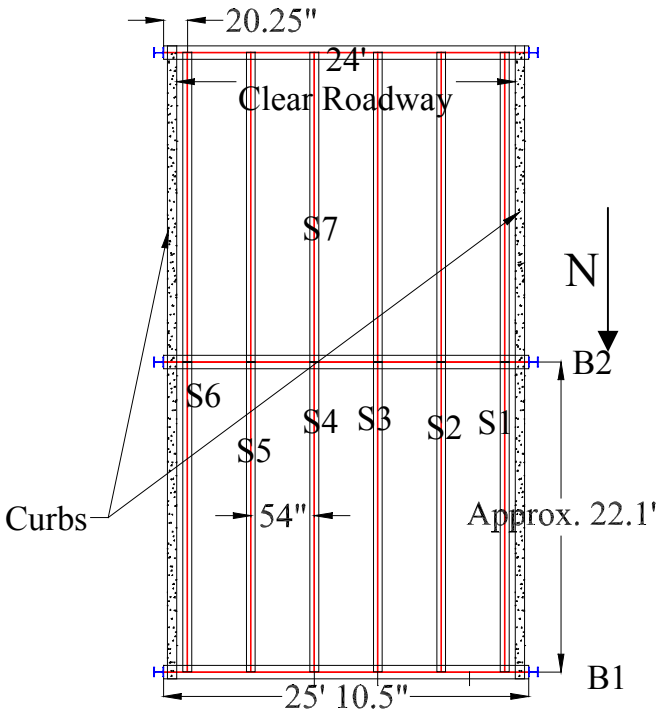

Figure 4.1 Plan view of deck area tested

Strain gages were either placed on the steel (ST) or the bottom side of the concrete slab (C), as indicated in Figure 4.2. The steel gages typically were placed on the inside top flange, inside bottom flange, and mid-height of the web. At two of the locations (midspan of stringer 7 and beam 2) an additional gage was placed on the opposite side top flange for a total of 4 strain gages. Figure 4.3 shows location of gages on the cross-section of steel members for layouts with either 3 or 4 gages. On longitudinal stringers, gages were located at either midspan, quarter points, or member ends. The

transverse beams were gaged at midspan. The first transverse beam (B1) was also gaged at the midpoint between the east side adjacent pair of longitudinal stringers (S4 and S5).

The second load test had a similar gaging pattern, but with more emphasis on the second transverse beam (B2). Additionally, some of the longitudinal stringers were gaged only at the top side of bottom flanges. Figure 4.4 shows the pattern used, with the number of gages on each member in parenthesis. For members with three or four gages, the layout of the gages on the member cross-section was identical to the first test. The midpoint of the second transverse member (B2) was gaged with 6 strain gages.

The data acquisition system used was an upgraded model of one developed earlier at the University of Texas at Austin (Jauregui 1999). The core of the system is a Campbell Scientific CR9000 data logger. The logger has a capacity of 55 channels for real time data acquisition. Shunt calibration circuitry is built into the completion boxes for each strain gage. Figure 4.5 shows the CR 9000 data logger.

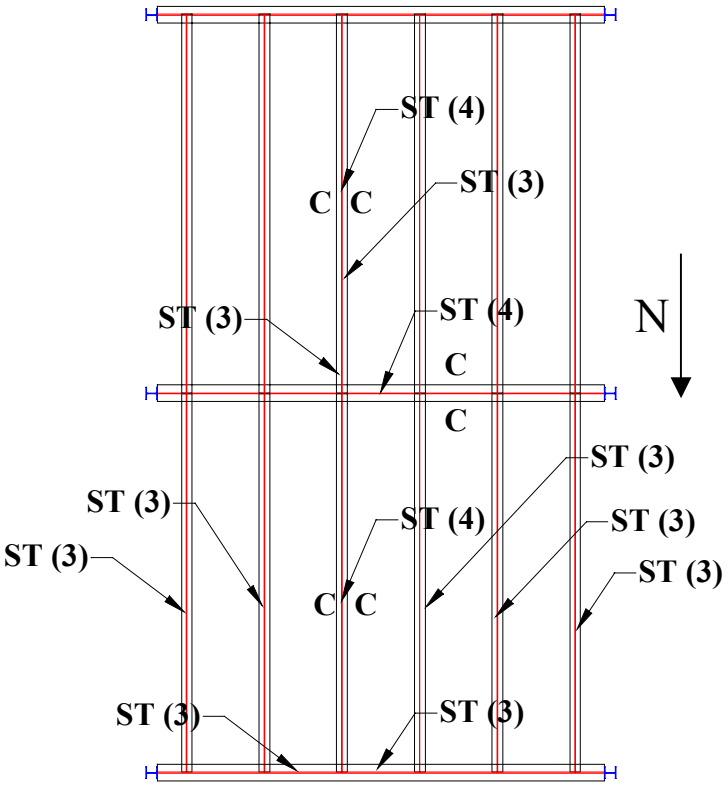

Figure 4.2 Strain gage placement for first load test

Table 4.1 Gage layout for first load test

Type	Member	Location	Type	Member	Location
ST	B1	midspan, top flange	C	S4	midspan, opposite side
ST	B1	midspan, web	ST	S6	midspan, top flange
ST	B1	midspan, bottom flange	ST	S6	midspan, web
ST	B1	1/4 span, top flange	ST	S6	midspan, bottom flange
ST	B1	1/4 span, web	ST	B2	1/4 span, top flange
ST	B1	1/4 span, bottom flange	ST	B2	1/4 span, web
ST	S4	midspan, top flange	ST	B2	1/4 span, bottom flange
ST	S4	midspan, top flange	C	B2	midspan, abutment side
ST	S4	midspan, web	ST	B2	midspan, top flange
ST	S4	midspan, bottom flange	ST	B2	midspan, top flange
ST	S1	midspan, top flange	ST	B2	midspan, web
ST	S1	midspan, web	ST	B2	midspan, bottom flange
ST	S1	midspan, bottom flange	SC	B2	midspan, opposite side
ST	S2	midspan, top flange	ST	S7	end, top flange
ST	S2	midspan, web	ST	S7	end, web
ST	S2	midspan, bottom flange	ST	S7	end, bottom flange
ST	S3	midspan, top flange	C	S7	midspan, sidewalk side
ST	S3	midspan, web	C	S7	midspan, opposite side
ST	S3	midspan, bottom flange	ST	S7	midspan, top flange
C	S4	midspan, sidewalk side	ST	S7	midspan, top flange
ST	S5	midspan, top flange	ST	S7	midspan, web
ST	S5	midspan, web	ST	S7	midspan, bottom flange
ST	S5	midspan, bottom flange			

3 Gage Layout 4 Gage Layout

Figure 4.3 Strain gage placement on stringers and beams

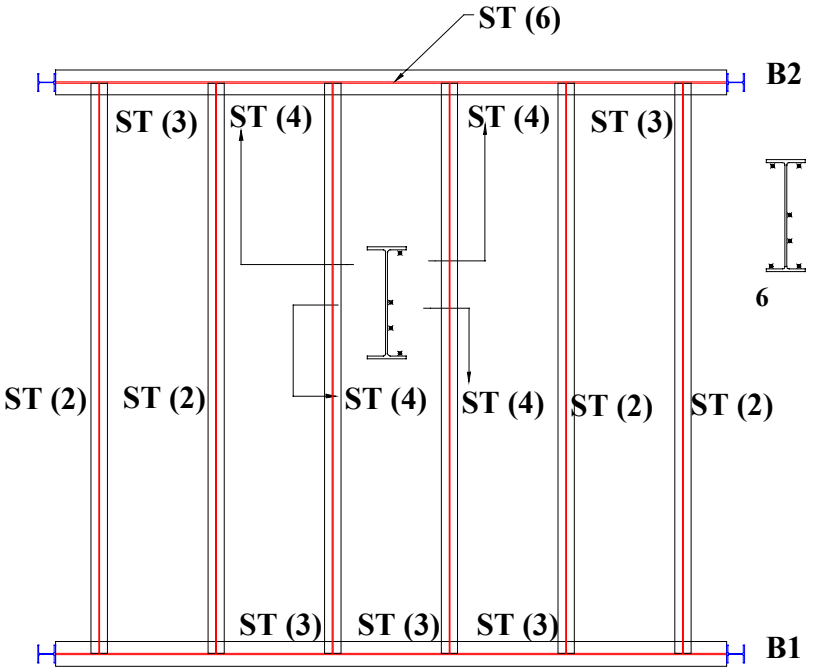

Figure 4.4 Strain gage placement for second load test

Figure 4.5 CR 9000 data logger

The data logger is controlled by instructions from code written by the user in CRBASIC language (A simple programming language based on BASIC). In the code are assignments of the parameters used in each test. The number of channels being used, excitation voltage, and sampling frequency are typical input variables. The instruction code is downloaded into the CR9000 and stored in internal memory. A test is performed, and then the data is retrieved from the CR9000 by means of a laptop computer. All load tests for this project were sampled at a rate of 10 HZ, meaning each strain gage measurement was recorded every 1/10 of a second. Since the truck loading was slow (truck speed was approximately 5 mph), this sampling rate was adequate to accurately capture the response of the instrumented members.

4.4 LOAD TEST TRUCKS

Two identical tandem dump trucks provided by TxDOT, arbitrarily labeled Truck A and Truck B, were used to load the bridge for each test. The trucks were loaded with gravel, and the front and tandem axles were weighed with portable scales prior to testing. Figure 4.6 shows a photograph of a truck used for the tests

Since the bridge had a high daily traffic, (1991 TxDOT estimate of 9,100 vehicles per day) all testing began at 10:00 pm to minimize disruptions to traffic.

Figure 4.6 Tandem truck used for Llano load tests

Figure 4.8 shows the configuration and weights of the truck used for the first test, and Figure 4.9 shows the same for the second test. The trucks used for the test were approximately equal in size and weight to an AASHTO H20 truck. The AASHTO designation for an H20 truck is essentially an HS20 truck (3 axles as shown in Figure 2.17) with the last axle removed. Figure 4.7 compares the average load test truck to an AASHTO H20 truck.

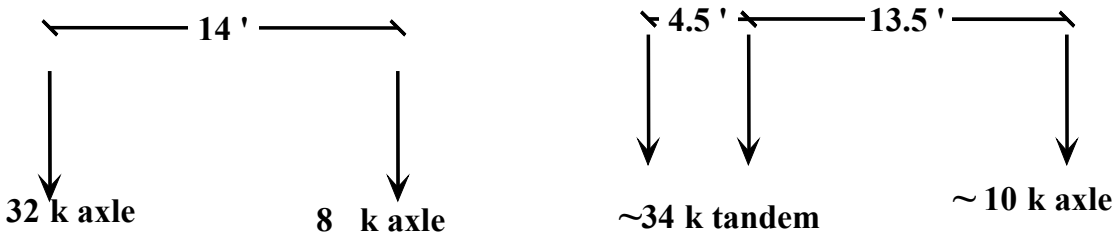

Figure 4.7 Comparisons of an H20 truck (left) and the average load test truck (right)

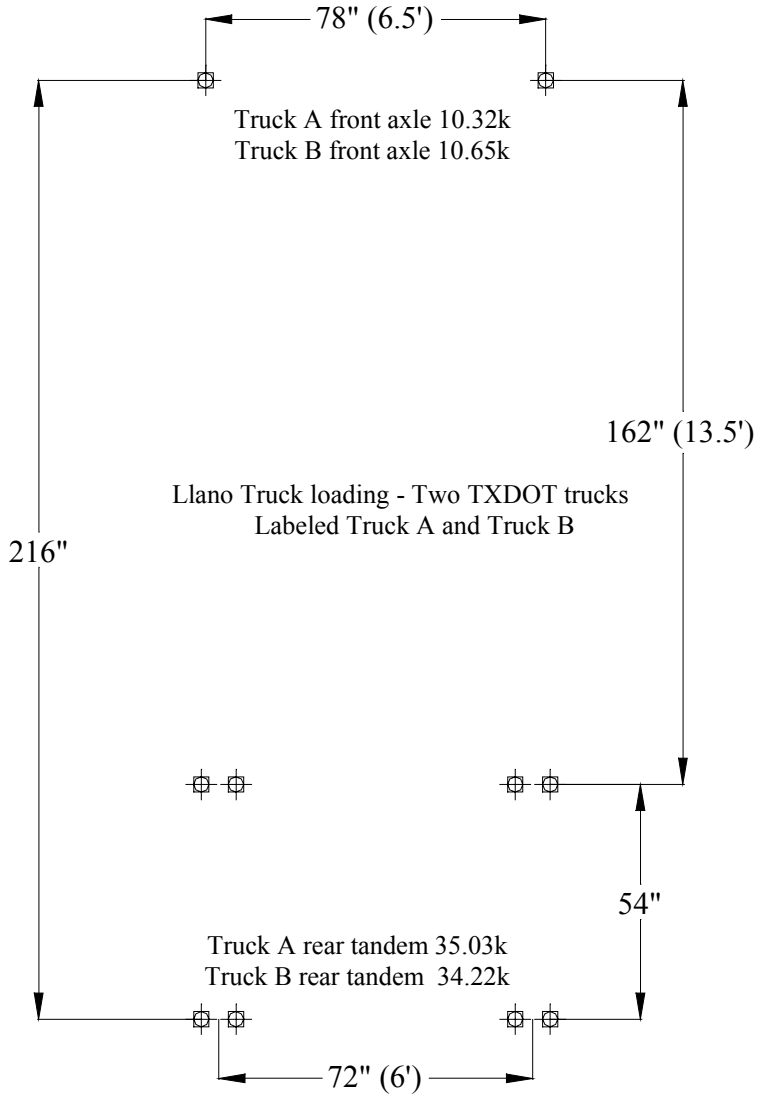

Figure 4.8 Dimensions and weights of test trucks for the first Llano load test

For each of the two load tests, runs were made in which the test trucks traveled slowly along the bridge and instrument readings were taken. The truck positions were changed from one run to the next. For some test runs, both trucks traveled along the bridge together, oriented either side by side, in line front to back, or in line back to back. For some test runs, only a single truck was used.

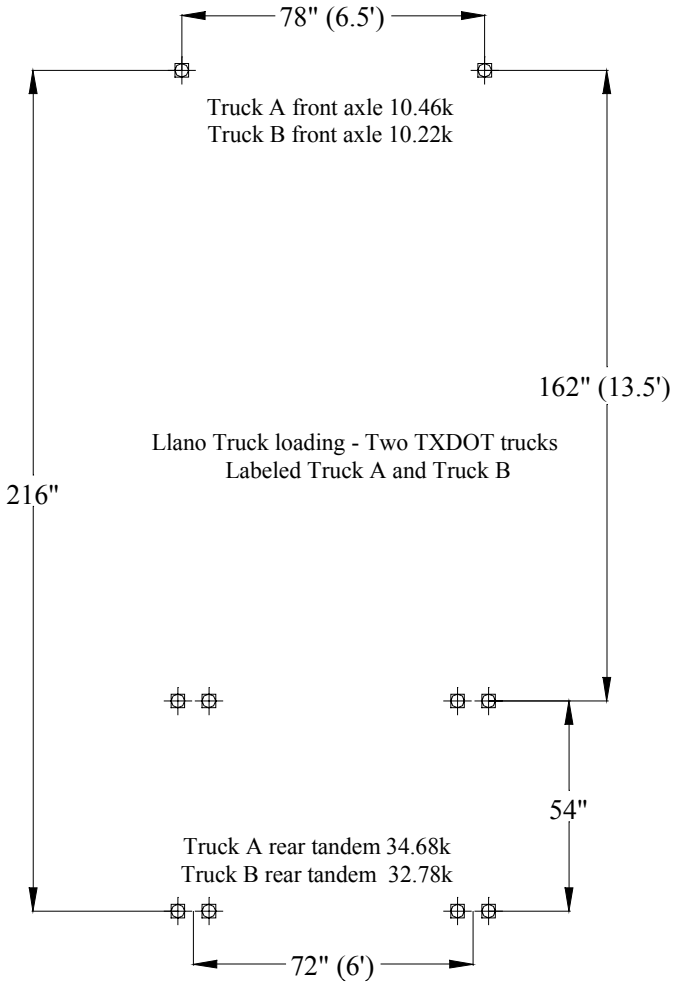

Figure 4.9 Dimensions and weights of test trucks for the second Llano load test

Among the various test runs, truck positions were varied along the width of the roadway. Test runs were conducted with the trucks positioned in the roadway center, as well as with wheel lines directly over stringers two through five. No test runs could be conducted with the truck wheel lines directly over the outside stringers (one and six) due to narrow clearances between the truss and the roadway. For each test run, the bridge was closed to all other traffic, so that the test trucks were the only vehicles on the bridge.

Each run was normally performed twice, with a total of 22 runs for the first test, and 21 runs for the second test. Table 4.2 and Table 4.3 list the runs executed for test one and two, respectively. Under the location heading, the first letter (L or R) refers to which wheel line was positioned, and the second letter and number combination refers to which stringer was underneath that wheel line. For example, L-S4 indicates the truck's left wheel line was positioned on top of stringer number four.

Table 4.2 Load runs for the first load test

Run	Truck	Location (L, R indicates left or right wheel line alignment, S refers to stringer)
1	A & B	Twin Trucks, Side by Side
1B	A & B	Twin Trucks, Side by Side
2	A & B	Twin Trucks, Side by Side
3	A & B	Twin Trucks, In Line, Front to Back
4	A & B	Twin Trucks, In Line, Front to Back
5	A	Center Run
6	B	Center Run
7	A	R, S4
8	B	R, S4
9	A	L, S5
10	B	L, S5
11	A	L, S4
12	B	L, S4
13	A	L, S3
14	B	L, S3
15	A	R, S2
16	B	R, S2
17	A	R, S3
18	B	R, S3
19	A & B	Twin Trucks, In Line, Back to Back
20	A & B	Twin Trucks, In Line, Back to Back
21	A & B	Twin Trucks, In Line, Back to Back

Table 4.3 Load runs for the second load test

Run	Truck	Location (L, R indicates left or right front wheel alignment, S refers to stringer number loaded)
1	A & B	Twin Trucks, Side by Side
2	A & B	Twin Trucks, Side by Side
3	A & B	Twin Trucks, In Line, Front to Back
4	A & B	Twin Trucks, In Line, Front to Back
5	A	Center Run
6	B	Center Run
7	A	R, S4
8	B	R, S4
9	A	L, S5
10	B	L, S5
11	A	L, S4
12	B	L, S4
13	A	L, S3
14	B	L, S3
15	A	R, S2
16	B	R, S2
17	A	R, S3
18	B	R, S3
19	A & B	Twin Trucks, In Line, Back to Back
20	A & B	Twin Trucks, In Line, Back to Back
21	A & B	Twin Trucks, In Line, Back to Back

4.5 TEST RESULTS

Strain data was collected for both load tests, and the results were converted to stress. The stresses at each gage location were then plotted as a function of truck position as it traveled across the bridge. Essentially, the plots can be viewed as influence lines for multiple axle loads. Plots of stress versus truck position for the two Llano field tests are provided in Appendices A and B. Figures 4.10 through 4.14 show typical test results. The truck position is plotted as the location of the front wheels measured from the north end of the bridge, i.e. from beam B1. The values of stress in the top and bottom flanges shown in these figures, as well as in subsequent figures and tables in this chapter, represent the extreme fiber stress. Gages were mounted on the inside face of the flanges (Figures 4.3 and 4.4). The measurements at the inside face of the flanges were then projected to the outer face of the top and bottom flange, based on an assumed linear stress distribution over the depth of the member.

The results from the first and second test were fairly consistent in stress values, as may be seen in Figures 4.10 and 4.11. These figures show stresses in stringer S4. The maximum bottom flange stress is approximately 5 ksi, and the maximum top flange stress is 4.1 ksi for the nearly equal truck loads in the two different tests. Superimposing both test results in one plot is shown in Figure 4.12.

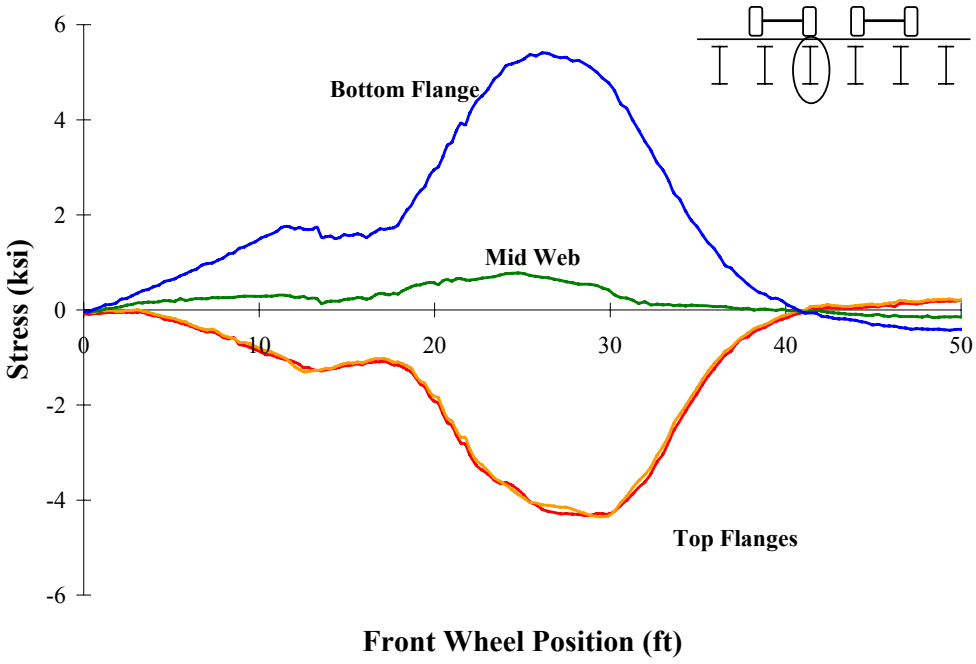

Figure 4.10 Stresses for stringer S4 in first Llano test (run number 2)

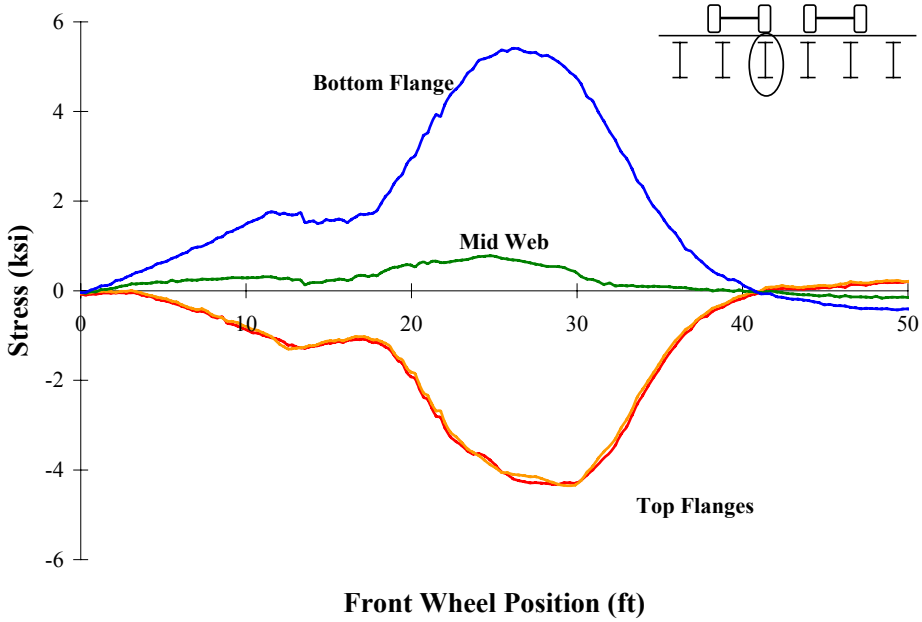

Figure 4.11 Stresses for stringer S4 in second Llano test

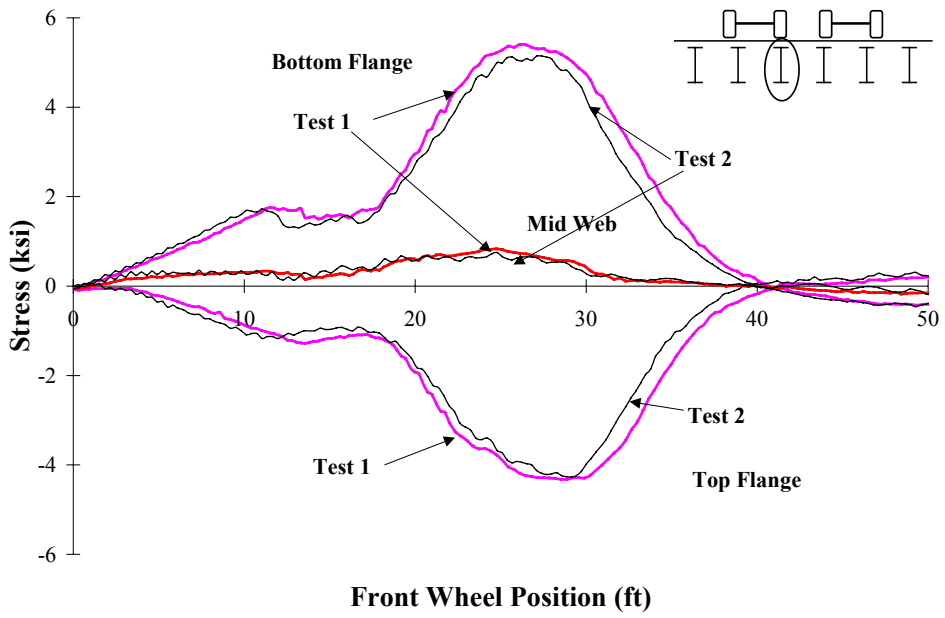

Figure 4.12 Comparisons between Llano tests 1 and 2 for stresses in stringer 4

This consistency in data between the two load tests may be seen in the transverse beams as well, as shown in Figures 4.13 and 4.14. For this particular loading on the first beam, the maximum top and bottom stress is about 1.5 ksi. These particular results (Figures 4.10 through 4.14) were chosen to illustrate typical test results, and reflect the trend for other members and loading cases.

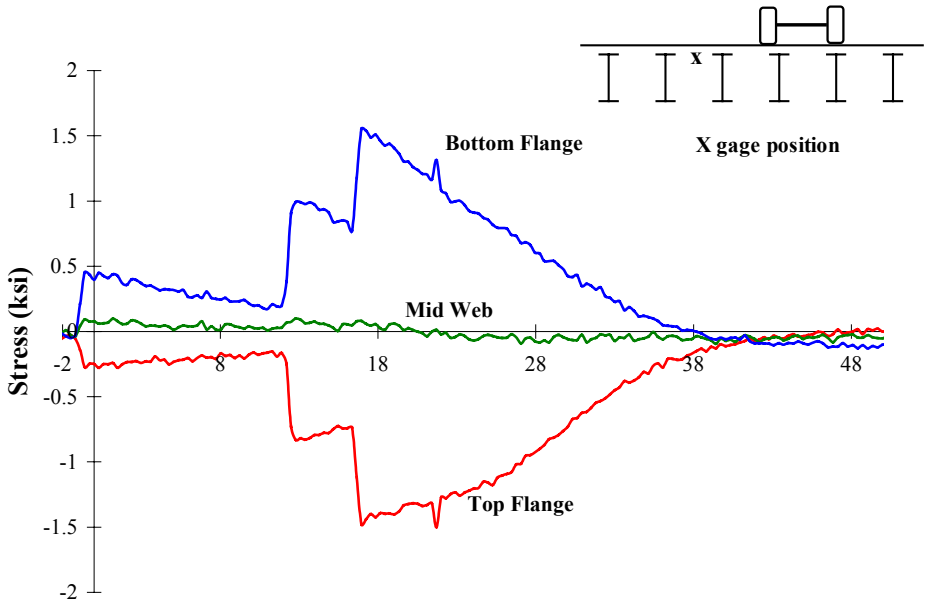

Figure 4.13 Stresses for Beam B1 for first Llano test

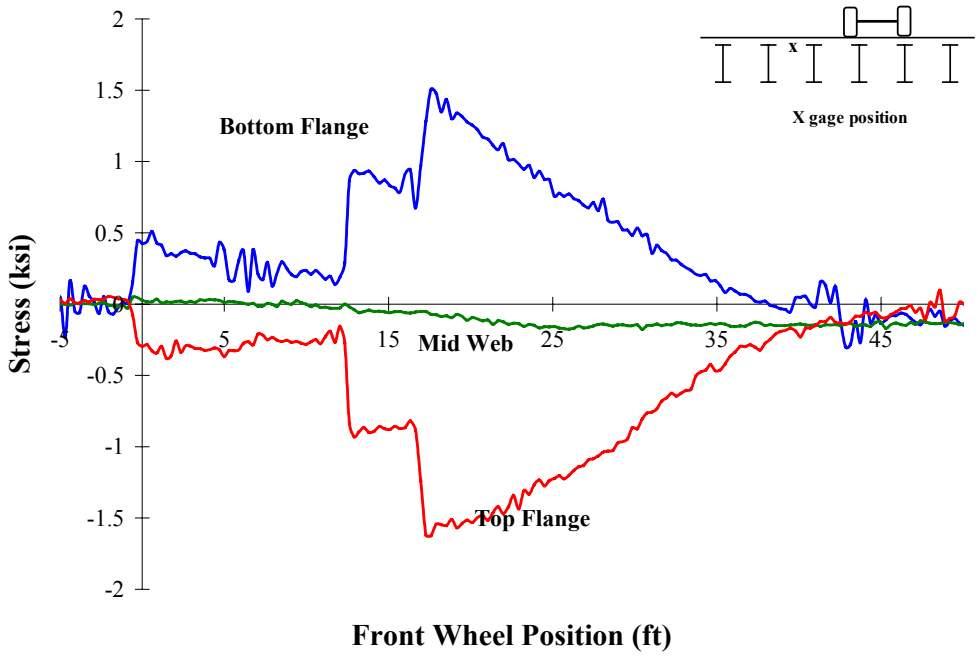

Figure 4.14 Stresses for Beam B1 for second Llano test

4.6 DISCUSSION OF RESULTS

4.6.1 Characterizing Response of Floor Members

In order to evaluate the results of the field tests (strain measurements) in comparison with the results of the finite element analysis and standard AASHTO load rating calculations, it is necessary to compare structural response quantities in a consistent manner. To load rate a structural member, the quantities most often used are moment and stress. For comparison purposes, the field strain measurements can therefore be evaluated in terms of moment or stress in the transverse beams and longitudinal stringers.

Since the beams and stringers remained elastic in the load tests, stress in the steel can be computed simply as the measured strain multiplied by the elastic modulus of steel. Moment can be more difficult to compute, however, because of the influence of unintended partial composite action exhibited in some of the members in the Llano load tests. This partial composite action was observed in some of the test data, and will be discussed in greater detail later.

For steel floor members that showed no composite action, the conversion from strain to moment is straightforward, since all members remained elastic in the load tests. For elastic behavior, strain is linearly related to stress through Young's modulus (E), and stress is linearly related to moment by the member's section modulus (S_x). Combining these relationships gives:

$$M = \varepsilon \cdot E \cdot S_x \tag{4.1}$$

Equation (4.1) is based on several assumptions, such as no out of plane bending, no torsion, and no localized web or flange distortion affecting the strain gage readings. In examining the data, these assumptions appear to be valid.

For members that demonstrated partial composite action in the load tests, the conversion from strain to moment is not as straightforward. Because of the interaction between the slab and the steel member, an axial force is induced in both the steel beam and in the concrete slab. In each component, there are two different strains at the top and bottom fibers, hence two different stresses. Since the section is not acting in a fully composite manner however, there is slip at the steel-concrete interface, and a discontinuity in the strain diagram, as shown in Figure 4.15.

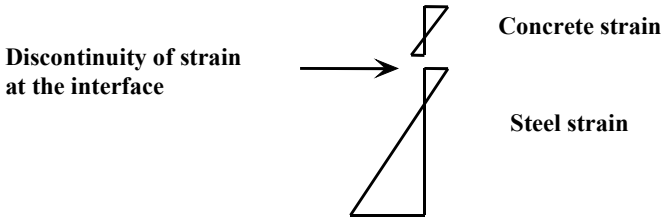

Figure 4.15 Strain distribution with partial composite action

The strain distribution for a partial composite cross-section in Figure 4.15 will result in the stress distribution shown in Figure 4.16, assuming linear elastic response of the steel and concrete. Other researchers (Baldwin 1965, Bakht 1988, Jauregui 1999) have decomposed the unsymmetrical stress distribution in the steel member into an equivalent symmetrical stress distribution (producing only moment about the centroid of the steel section) and a constant axial stress (producing only an axial force "F" at the centroid of the steel section). A similar decomposition can be made for the stresses on the concrete section.

The total moment in the combined steel-concrete cross-section (M_{total}) can then be decomposed into a moment in the steel section based on the symmetric stress distribution in the steel (M_{steel}), plus a moment in the concrete based on the symmetric stress distribution in the concrete ($M_{concrete}$), plus a moment due to the constant axial force multiplied by the distance between the centroids of the steel and concrete sections (Figure 4.16). That is:

$$M_{total} = M_{steel} + M_{concrete} + F \times e \tag{4.2}$$

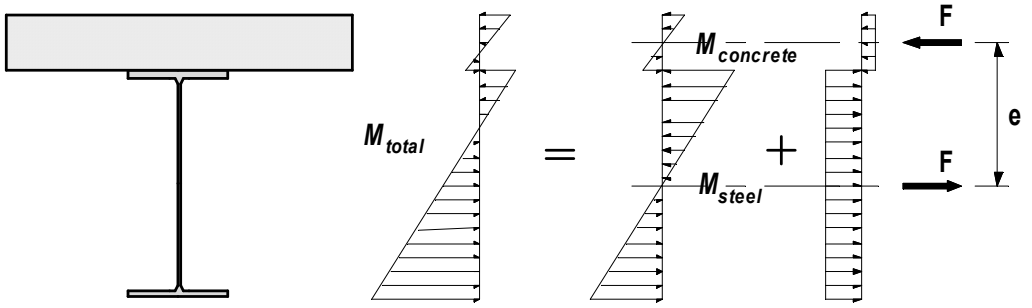

Figure 4.16 Total moment in partial composite section decomposed into components

For typical field test results, stresses are measured at the top and bottom of the steel section. The symmetrical stress in the steel is simply the average of the measured top and bottom flange stresses while the induced axial stress is half the difference between the measured top and bottom stresses. The symmetrical strain distribution results in a moment M_{steel} based on Equation (4.1). The axial force "F" in the steel section is simply the axial stress multiplied by the member area.

The question arises as to exactly what quantity should be used to characterize the live load effect in the steel for purposes of comparing field test data with the results of analysis and for purposes of load rating. The load ratings of the bridge floor members developed in Chapters 2 and 3 were based on the bending moment in the steel members computed assuming no composite action. However, the actual bridge floor system exhibited some partial composite action. Determining moment carried by the components of the actual bridge floor system (i.e., the steel and the concrete) individually in the presence of partial composite action is not straightforward. Calculating the moment in the steel member based only on the symmetrical stress (i.e., M_{steel} in Figure 4.16) would be unconservative, since the maximum symmetrical stress is lower than the maximum measured stress in the member. To account for the partial composite action exhibited, the assumed moment carried by the steel should include some effect of the axial force couple. Other researchers (Baldwin 1965, Bakht 1988, Jauregui 1999, BDI, 1999) have used differing approaches to this problem. Nonetheless, characterizing the moment carried by the steel member alone in a partially composite system can lead to some ambiguity.

Rather than interpreting the results of the field tests in the context of bending moment, an alternative and more straightforward approach is to compare the maximum stresses measured in the field tests to the maximum stresses predicted by analysis. These results are summarized in Table 4.4. Recall the first letter (L or R) in the load case designation refers to which wheel line was positioned, and the second letter and number combination refers to which stringer was underneath that wheel line. For example, L-S4 indicates that the truck's left wheel line was positioned on top of stringer number four.

The outside stringers (S1 and S6) did not have direct wheel line loading because of lack of clearance between the truss and the trucks. Hence, maximum values for those stringers were from loading on adjacent members.

Table 4.4 gives the maximum stresses for the longitudinal members for all load cases. Of interest is that the maximum recorded stress for the center stringers (S3 and S4) was not from a wheel line directly over the member. Instead, the maximum response was obtained when the load truck partially straddled the member. (This was actually a wheel line load on the adjacent member). Figure 4.17 depicts this load position.

The maximum stresses measured in the field tests will be used in the following sections for further evaluation of the behavior of the bridge floor system.

Table 4.4 Maximum stresses from the Llano load tests

Member	Load Test	Load Case	Maximum midspan stress (ksi)
B2	Llano 1	Trucks side-by-side	4.9
B2	Llano 2	Trucks side-by-side	4.6
B1	Llano 1	Trucks side-by-side	3.6
B1	Llano 2	Trucks side-by-side	3.4
S1	Llano 1	R-S2	1.8
S1	Llano 2	R-S2	1.9
S2	Llano 1	R-S2	3.7
S2	Llano 2	L-S3	3.6
S3	Llano 1	L-S4	4.3
S3	Llano 2	L-S4	3.7
S4	Llano 1	R-S3	4.2
S4	Llano 2	R-S3	4.0
S5	Llano 1	L-S5	3.4
S5	Llano 2	L-S5	3.5
S6	Llano 1	R-S4	2.2
S6	Llano 2	R-S4	2.1
S7	Llano 1	L-S4	3.6
S7	Llano 2	Not gaged	Not gaged

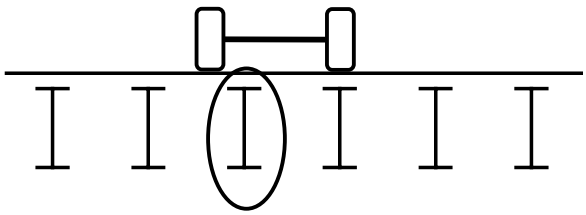

Figure 4.17 Maximum stringer response load position

4.6.2 Load Distribution

A distribution factor for a member is the fraction of the total moment on the system that is carried by that member. For example, if the total moment carried by the system is 100, and the portion carried by the individual member is 78.2, the distribution factor is 0.782. However, interpreting the field test results in the context of distribution factors leads to some ambiguity because the moment carried by a single member is not uniquely defined due to partial composite action. An alternate approach is again to use the maximum stresses obtained in the members. The distribution factor for an individual member can be

defined as the maximum stress in the member divided by the summation of maximum stresses of all the members. Hence, for the i[th] member, the distribution factor (D.F.) is:

$$D.F. = \frac{(\sigma_{\max})_i}{\sum_i \sigma_{\max}} \tag{4.3}$$

Since the finite element results are given in terms of moments, it is possible to obtain a DF by dividing the moment in an individual member by the total applied moment. This approach results however, in a DF for the steel members that does not sum to unity because the slab carries a portion of the load. An alternate approach is to calculate a distribution factor by dividing the moment in the individual member by the sum of the moments in all of the steel members. The sum of the distribution factors would then sum to unity, but this approach does not include the effect of the slab carrying a portion of the total moment. However, it was felt this method would more accurately compare with the method used to calculate the distribution factors in the field load test (Equation 4.3).

Using average weight values for the load trucks, the maximum moment carried by a longitudinal member and a transverse member was calculated. For longitudinal members, only a tandem axle was placed at midspan, since due to the short spans, the front axle was off the span when the rear tandem reached midspan. AASHTO Allowable Stress and Load Factor ratings use distribution factors based on a wheel line load. A wheel line is half the axle load – essentially the loading that would be applied as a vehicle traveled along the span with one side directly over a member, as shown in Figure 4.18. Hence, an AASHTO distribution factor is based on half the load used in a load test or the finite element analysis. Recall the AASHTO distribution factor for the Llano deck longitudinal stringers was $s/5.5 = 0.82$. To compare this AASHTO distribution factor to distribution factors obtained from the full axle loads in the field tests, it is necessary to use one half of that, or 0.41. This distribution factor was compared to the distribution factor based on field test data for stringer S4, the controlling member in the load rating for the stringers in the deck. Table 4.5 gives these results. Also shown in this Table are distribution factors based on finite element analysis, described in Section 4.7 below. As can be seen, the distribution factors derived from field load testing are much lower than values assumed in a standard load rating.

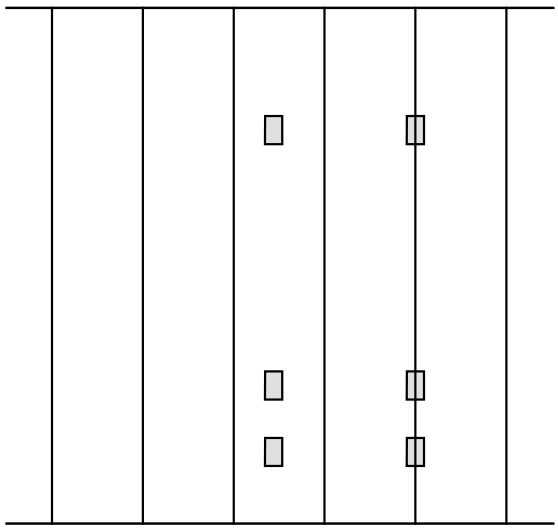

Figure 4.18 Plan view of deck showing a wheel line load on the second stringer from the right

Table 4.5 Comparison of distribution factors

Member	Load position	DF (AASHTO)	DF (FEA)	DF (Llano 1 load test)	DF (Llano2 load test)
S4	L-S4	0.41	0.29	0.29	0.28
S4	R-S3	0.41	0.28	0.28	0.30

4.6.3 Unintended Composite Action

No shear connectors are provided between the concrete slab and the steel floor beams and stringers in the Llano Bridge. Consequently, the bridge floor system was not originally designed for composite action. Although composite action was not considered in the design, some degree of composite action may develop in the actual bridge due to friction or chemical bond between the slab and steel members. Such unintended composite action may be beneficial for the load capacity of the bridge floor system.

From the field test data, composite action is evident from unequal top and bottom flange stresses in a steel member. Figures 4.19 and 4.20 show typical test results for stringers, which exhibited such unequal stresses. Figure 4.19 shows a top flange stress of approximately 82% of the bottom flange, while Figure 4.20 shows a top flange stress of approximately 63% of the bottom flange stress.

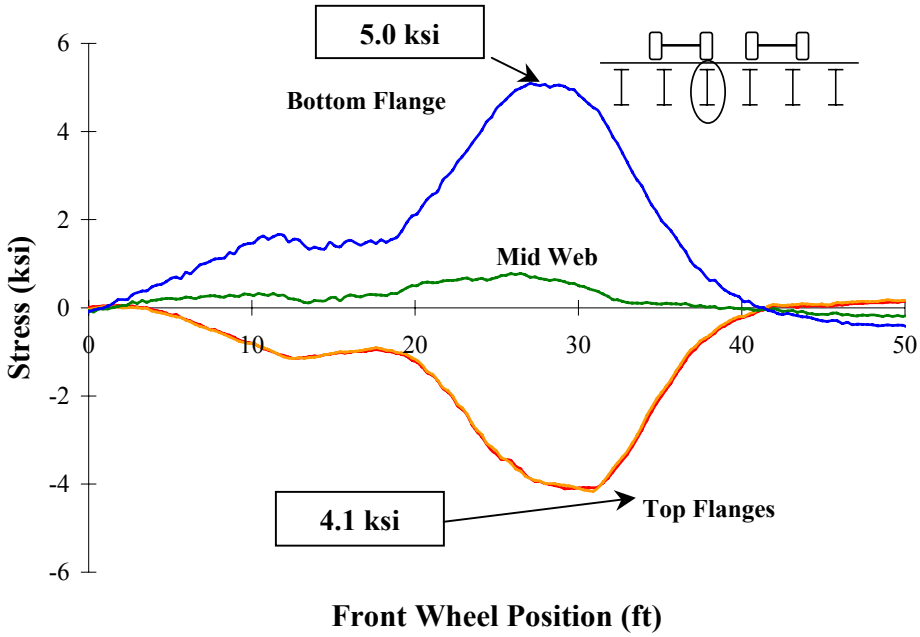

Figure 4.19 Measured stresses in stringer 4 in the first Llano test

Composite action raises the neutral axis and lowers the top flange stress relative to the bottom flange. The measured stresses at mid-height of the steel section shown Figures 4.19 and 4.20 reflect the rise in the neutral axis and further confirm the presence of partial composite action. In general, the degree of unintended composite action was not consistent in different members in the same test. An exception was the center stringers, which under the highest loads did show a consistent degree of composite action, with approximately a 20 to 30 percent increase in bottom flange stress as compared to the top flange.

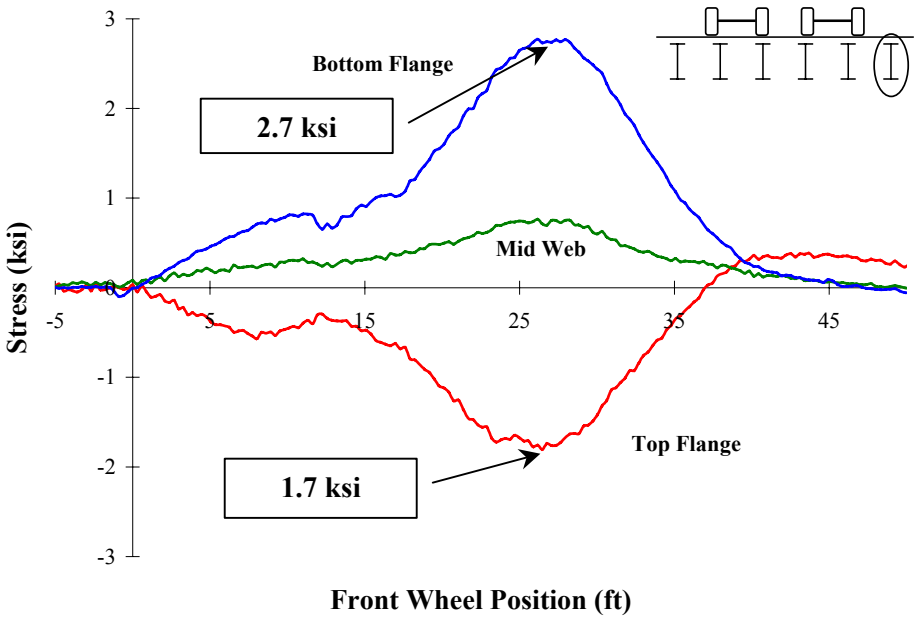

Figure 4.20 Measured stresses in stringer 1 in the first Llano test

To assess the degree of composite action present, a comparison of elastic stress distributions is plotted for a stringer. Figure 4.21 shows the stress profile of both a non-composite and fully composite stringer cross-section, with a unit bottom flange stress, corresponding to an applied moment on the non-composite section of 7.4 k-ft. Also plotted are the results presented from Figure 4.20, normalized by the maximum (bottom flange) stress. Non-composite behavior has equal top and bottom flange stresses, and the fully composite section has an elevated neutral axis, and a small top flange stress as expected. Calculations show the fully composite elastic neutral axis is 16.83 inches, measured up from the bottom side of the bottom flange. (Recall the depth of this section is 18 inches). A unit bottom flange stress would result in a 0.0695 top flange stress for a fully composite section.

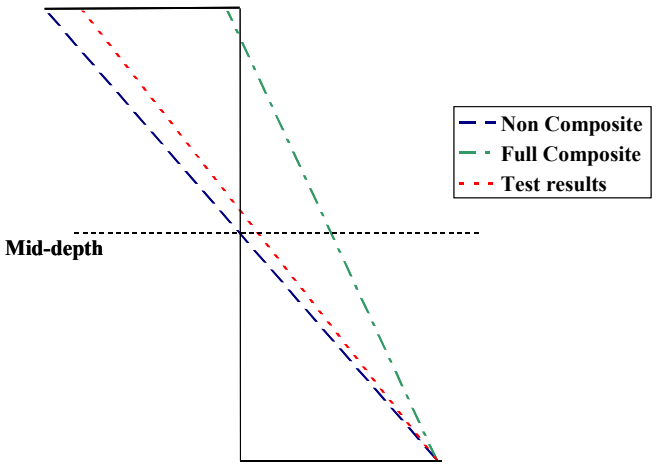

Figure 4.21 Comparison of stress profiles for stringer

Figure 4.22 shows the location of the neutral axis for full, partial (test results) and non-composite action for the same data.

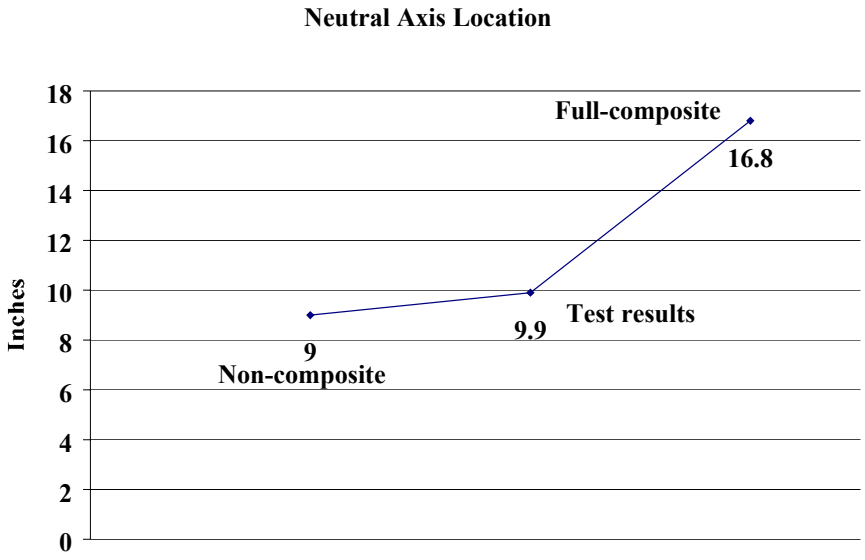

Figure 4.22 Neutral axis location in stringer

These results indicate that although the stringers are exhibiting some unintended composite action, the degree of composite action is rather small compared to what would be expected for full composite action. For a unit bottom stress, the top flange stress is approximately 0.812. No composite action would have resulted in equal flange stresses.

Composite action was seen to a greater extent in longitudinal stringers than in transverse beams. Stress plots for beams B1 and B2, shown in Figures 4.23 and 4.24, suggest very little composite action in these members.

Transverse beams showed some composite behavior, but not in all tests and typically the stress difference between top and bottom flanges was less than 0.4 ksi. In some of the tests, the transverse beams showed practically no composite behavior, while the longitudinal members showed some composite behavior in nearly every test. The reason for the difference in the degree of unintended composite action between the longitudinal stringers and transverse beams is unclear, but may be due to the details of the deck construction. As described in Chapter 2, the longitudinal stringers are embedded into the slab approximately 1 inch, whereas the transverse beams have no such embedment. Further, above each transverse beam is a slab construction joint, and the longitudinal slab reinforcement is not continuous over the transverse beams. Figure 4.25 shows the construction detail above the beams.

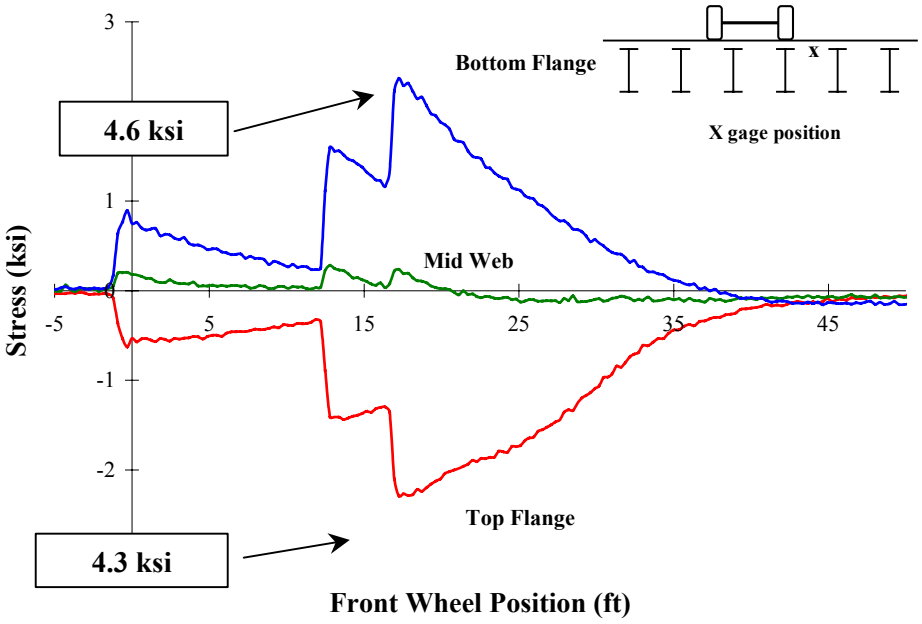

Figure 4.23 Measured stresses in beam B1 in the first Llano test

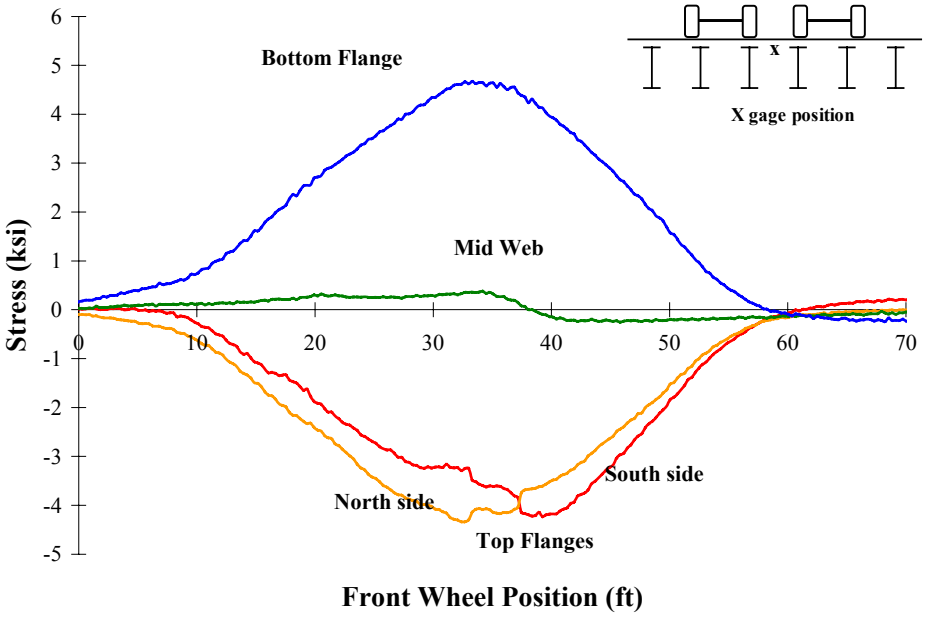

Figure 4.24 Measured stresses in beam B2 in the first Llano test

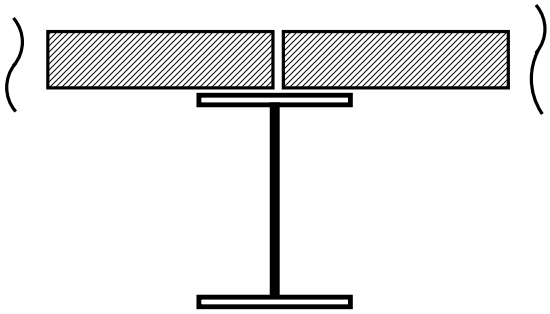

Figure 4.25 Gap in slab above each transverse beam

4.6.4 Beam End Fixity

An assumption made in the finite element analysis as well as in the AASHTO load rating was that all floor members were simply supported at their ends. This was considered to be a conservative assumption, since any degree of end fixity would reduce maximum moments in the members. The Llano field test data was therefore examined to discern whether a significant degree of fixity might actually be present at the ends of floor members.

To evaluate the possibility of beam end fixity, the stresses measured at discrete points along the length of the beam were plotted, and then extrapolated to the ends of the member. Data was used from the second Llano load test, in which gages were placed at 5 locations along the length of the second transverse beam (member B2). Figure 4.26 shows the extrapolation of flange stress data to the ends of the member. The extrapolation is based on the moment diagram expected with two point loads (corresponding to the two wheel loads) acting on the member. This results in a region of constant moment (and therefore constant stress) between the point loads, and a linear variation between the point loads and the member ends. Although there is some uncertainty associated with the data extrapolation, the plot in Figure 4.26 suggest the transverse beams of the Llano bridge deck did not exhibit significant end fixity.

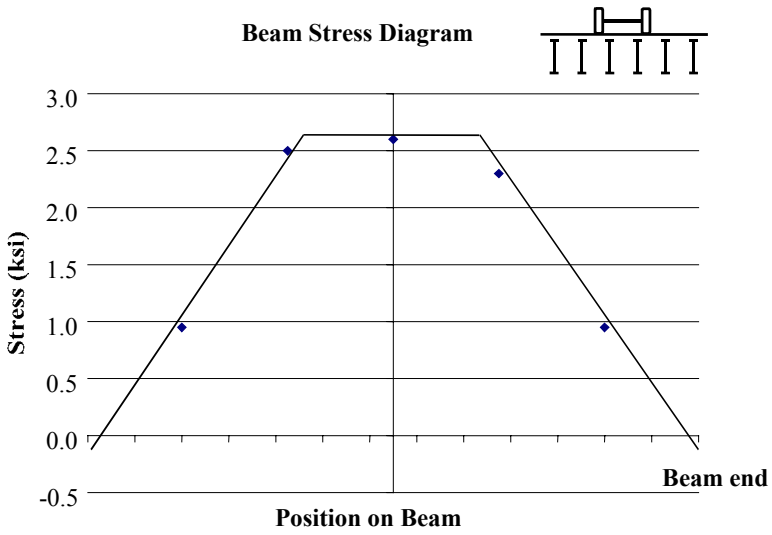

Figure 4.26 Stress along length of Beam B2 with single truck loading

Results from the first Llano test also suggest there was little restraint at the ends of the longitudinal stringers. Stringer S7 was gaged approximately 18" in from the connection and also at midspan. Figure 4.27 shows a plot of the stresses for a load test with the wheel line directly above the member and for a wheel line directly above the adjacent member. Modeling the tandem acting as two point loads centered around the midpoint of the stringer, the expected moment diagram along the length of the stringer would be as shown in the dashed lines in Figure 4.27. Again, the extrapolated stresses at the ends of the member suggest little if any fixity at the connections.

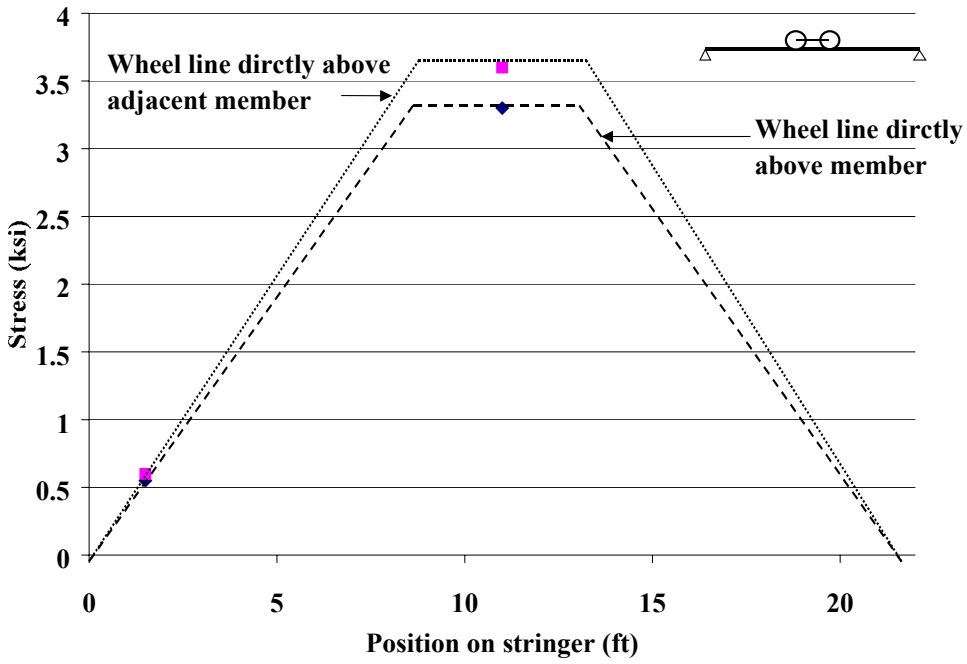

Figure 4.27 Stress along length of stringer S7

4.7 COMPARISONS WITH FINITE ELEMENT ANALYSIS

The finite element model described in Chapter 3 was used to analyze the bridge deck system with loading representing the trucks used for the field tests. As in Chapter 3, for the longitudinal stringers, the front axles were truncated because the front axle on the adjacent span lowered the moment slightly, and average axle weights were used. Figures 4.28 through 4.30 show the loadings. To more accurately depict the tandem axle, the loads were broken up into four point loads instead of two. The tandem wheel spacing was approximated at 4 feet (instead of 4.5 feet) because of the longitudinal spacing of the nodes in the deck model. In a similar fashion, the distance to the front axle was rounded down to 13 feet (instead of 13.5 feet) for the transverse beam loading. Since the outermost stringers were not tested in the field, no finite element analysis was done with field loads for these stringers.

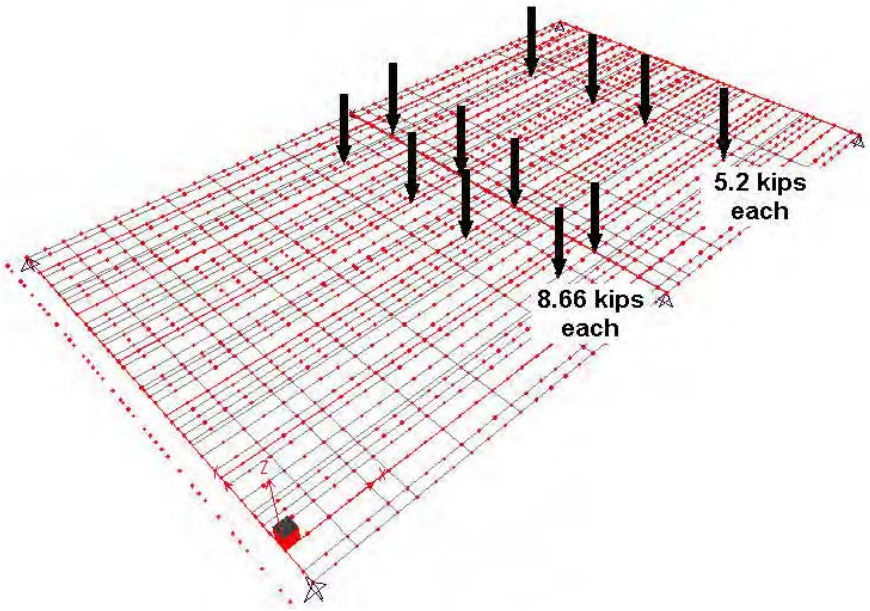

Figure 4.28 Loading for field test in transverse beam

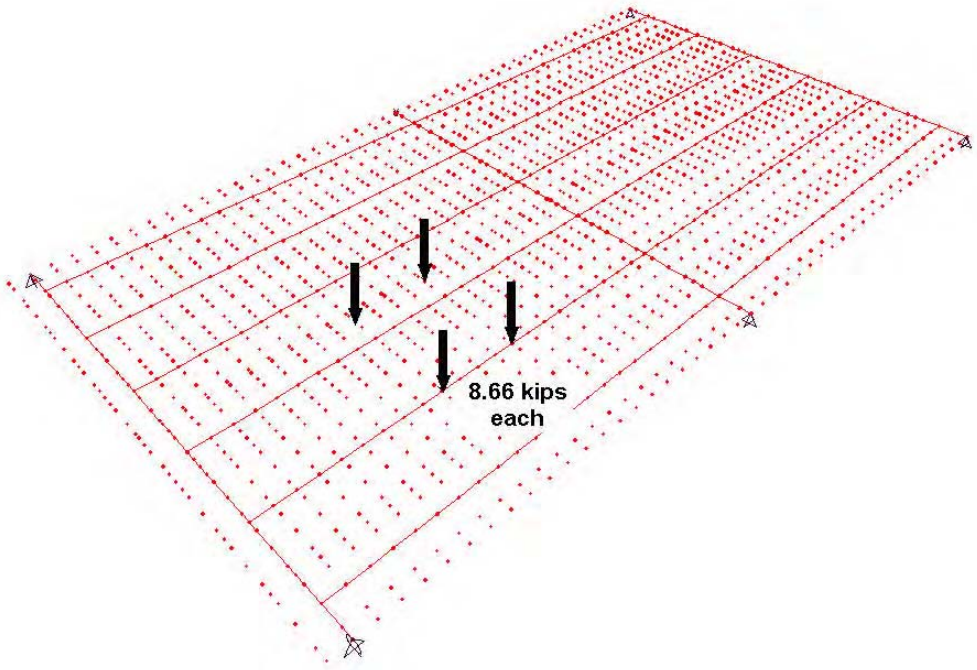

Figure 4.29 Loading for field test in stringer 2

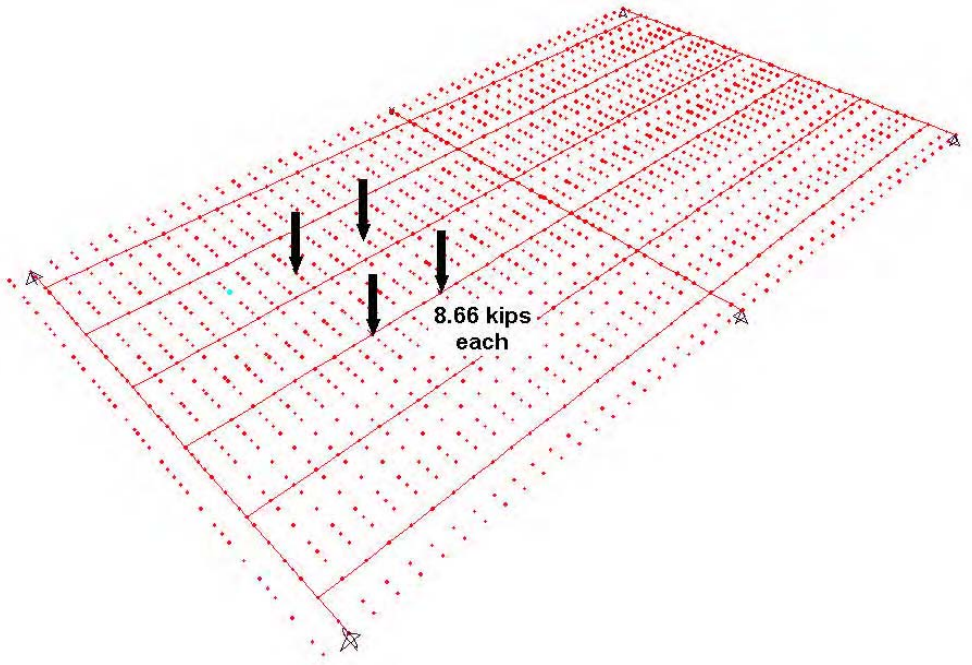

Figure 4.30 Loading for field test in stringer 3

The bending stresses obtained using average truck load values in the two stringers and the beam computed using finite element analysis are listed in Table 4.6.

Table 4.6 Finite element stress predictions with field test loads

Member	Stress (ksi)
Stringers S2, S5	4.5
Stringers S3, S4	4.3
Beam B2	6.8

Table 4.7 shows the stresses obtained from AASHTO calculations, from finite element analysis, and the average of the maximum stresses obtained from the field load tests. Figures 4.31 and 4.32 show these same comparisons graphically.

Table 4.7 Stress comparisons

Member	AASHTO	FEA	Field test	FEA/AASHTO	Field/AASHTO
S2, S5	8.4 ksi	4.5 ksi	3.6 ksi	53.6%	42.9%
S3, S4	8.4 ksi	4.3 ksi	4.1 ksi	51.2%	48.8%
B2	8.4 ksi	6.8 ksi	5.1 ksi	80.9%	60.7%

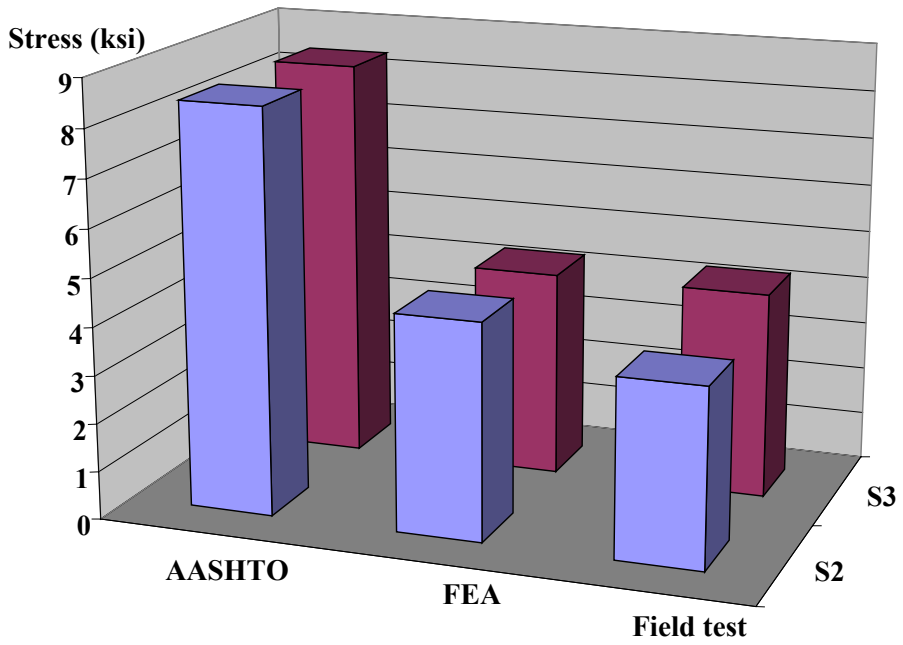

Figure 4.31 Stress comparisons for longitudinal stringers S2 and S3

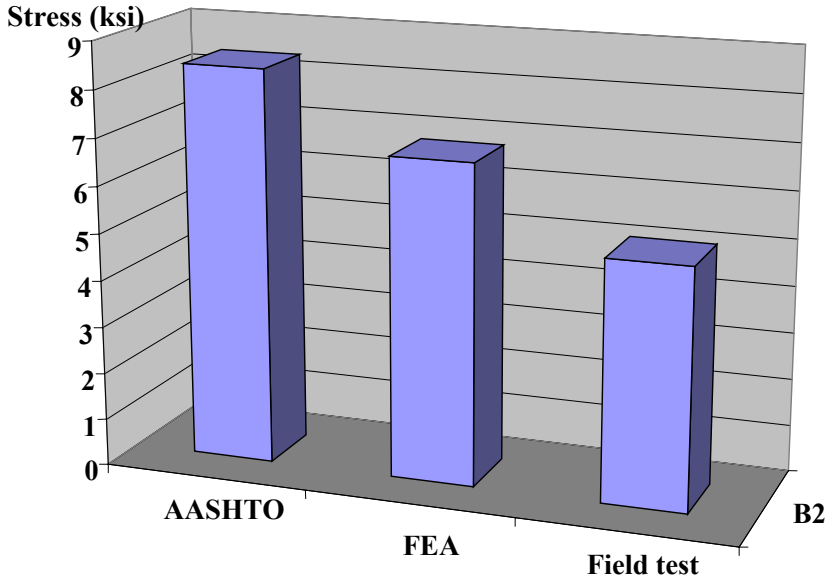

Figure 4.32 Stress comparisons for transverse beam B2

These results show that the maximum stresses measured in the stringers and beam were significantly lower than the stresses predicted using standard AASHTO load rating calculation methods. In the stringers, the measured stresses were less than half of those predicted using AASHTO calculations. In the case of the transverse beam, the measured stress was approximately 60-percent of the value based on AASHTO. The measured stresses were much closer to the stress values predicted by FEA, although

the measured stresses were still somewhat lower. This suggests that the FEA model does not completely capture the actual response of the deck members. However, the field test data suggests the error in the finite element model is on the conservative side. That is, the finite element model predicts stresses that are somewhat higher than the measured values.

4.8 SUMMARY

Two field load tests were conducted on the floor system of the Llano Bridge. Both tests utilized trucks that approximated an H20 load vehicle. Strain gage data was taken using a portable data acquisition system, and this data was converted into stress in the steel beams and stringers.

The field test data showed live load moments in the floor beams and stringers that were significantly lower than predicted by the standard AASHTO load rating presented in Chapter 2. In many cases, the field test data showed stresses that were less than half of those predicted by standard AASHTO calculations. This suggests that the bridge floor system is significantly stronger than indicated by the standard load rating, and that an increased load rating for the bridge floor members is likely justified.

The field test data also showed live load stresses smaller than predicted by the finite element model of the bridge floor system. However, the difference between the field test data and the finite element model predictions were much smaller than the difference with the standard load rating calculations. The field test data showed stresses that were at most case 5 percent smaller than predicted by the FEA for the stringers, and 25 percent smaller for the transverse beams. Thus, the finite element model, although predicting much smaller stresses than standard load rating calculations, still provided conservative predictions compared to field test data.

The field data showed that some of the floor members exhibited a small degree of unintended composite action with the concrete slab. Where composite action was measured, it most frequently occurred in the longitudinal stringers rather than the transverse beams. The composite action, however, was not consistent in all loading positions nor was it necessarily constant long the length of the member. Based on the field test data, it appears that composite action cannot be relied upon as a consistent source of additional strength in the bridge floor system.

Even without composite action, the field test data and the finite element model suggest that the concrete slab is acting as a significant structural element in the bridge floor system. The slab provides benefits to the floor system by resisting a significant amount of bending moment, thereby reducing the stress carried by the stringers, and also by providing improved distribution of loads to the floor stringers and beams. These very important benefits of the slab are not considered in the standard load rating calculations that assume the slab carries no moment and which assume very conservative load distribution factors. The beneficial effects of the concrete floor slab appear to be a key reason why the field-measured stresses as well as the stresses predicted by finite element analysis are so much smaller that the stress predicted by the standard load rating calculations.

Finally, extrapolation of field test data suggest that the bending stresses near the ends of the transverse beams are very low, and consequently that little or no fixity is present at the beam ends.

The field load tests on the Llano bridge deck have provided significant insights into the structural response of the deck system. In the following chapter, additional field test data will be examined for the deck of another truss bridge for further insight into the behavior of the system.

Chapter 5:
Goliad Field Load Test

5.1 INTRODUCTION

Subsequent to the Llano field tests described in Chapter 4, additional field tests were conducted on a similar bridge located in Goliad, Texas (Figure 5.1). This bridge was scheduled for replacement and demolition, and field load testing was conducted just prior to demolition. Consequently, this bridge was tested at a much higher load than was used for Llano, since a limited amount of yielding could be tolerated.

Figure 5.1 Parker truss bridge in Goliad, Texas

The Goliad bridge was very similar to the Llano bridge, except that it was somewhat smaller, and consisted of only one span as opposed to four. This chapter discusses the purpose and objectives, instrumentation, data acquisition, loading, and the results of the Goliad Bridge test.

5.2 BRIDGE REPLACEMENT AND DEMOLITION SEQUENCE

The Goliad truss bridge is located on US Highway 183 and crosses the San Antonio River. The truss bridge was replaced and demolished in August of 1999. In the sequence of replacement and demolition, new single lane prestressed concrete bridges were first constructed on both sides of the truss bridge, while the truss bridge remained in service. Traffic was then diverted to the new single lane bridges, and the old truss bridge was demolished. Subsequently, an additional prestressed concrete bridge was constructed in between the new outer lanes to complete the new bridge. Field load tests were conducted after traffic was diverted off the old truss bridge, just prior to demolition.

Figures 5.2 and 5.3 show the new bridge during construction and after completion. Reinforcement steel can be seen protruding from the side lanes, ready to tie the future center lanes together. Figures 5.4 and 5.5 show the replacement bridge after completion.

Figure 5.2 Lanes built around the original bridge

Figure 5.3 Detail showing connecting rebar

Figure 5.4 View to the north of finished replacement bridge

Figure 5.5 South view of finished replacement bridge

5.3 BACKGROUND

5.3.1 Bridge Description

The Goliad truss was a Parker configuration as the Llano Bridge, except that Goliad had only 6 deck segments as compared to 9 for Llano, and each segment had a length of approximately 20 feet, as compared to 22 feet for Llano. Figure 5.6 shows the Goliad truss elevation with dimensions. Plans indicate an age similar to the Llano Bridge – construction in mid 1930's.

The truss was similar in design to the Llano truss; built up sections for the top and bottom chords, as well as for most of the verticals. Diagonal members were either built up sections or I beams, as shown in Figure 5.7.

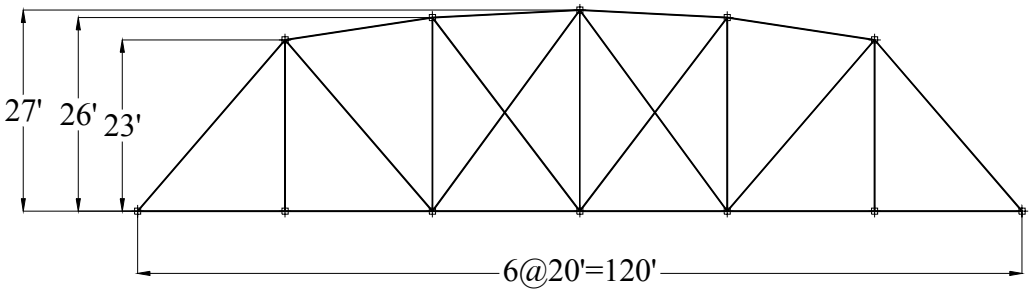

Figure 5.6 Goliad truss elevation

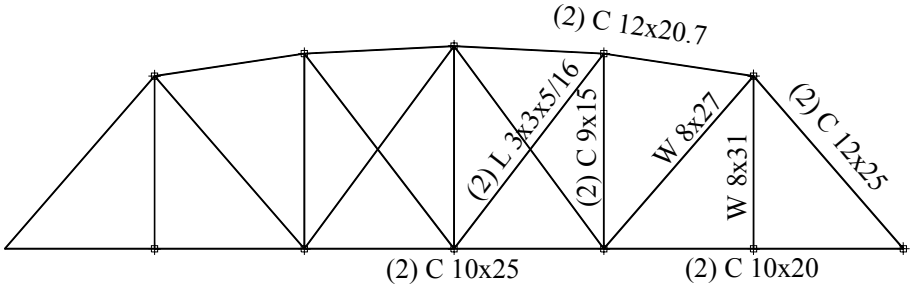

Figure 5.7 Individual members of Goliad truss

The deck consisted of transverse beams (W33x125), 25 ft.-10.5 in. long, located at the lower panel points of the truss, connected with angles to the truss verticals as in the Llano bridge. Six longitudinal stringers (W18x47) 20 ft. in length, framed into the transverse members connected with angles. Longitudinal members were embedded approximately 1 inch into the concrete slab, as in the Llano deck. Figure 5.8 is a section view of the deck. Since the yield stress of the steel was unknown, for analysis purposes, the yield stress was assumed to be 30 ksi as per AASHTO specifications for unknown steel based on date of construction.

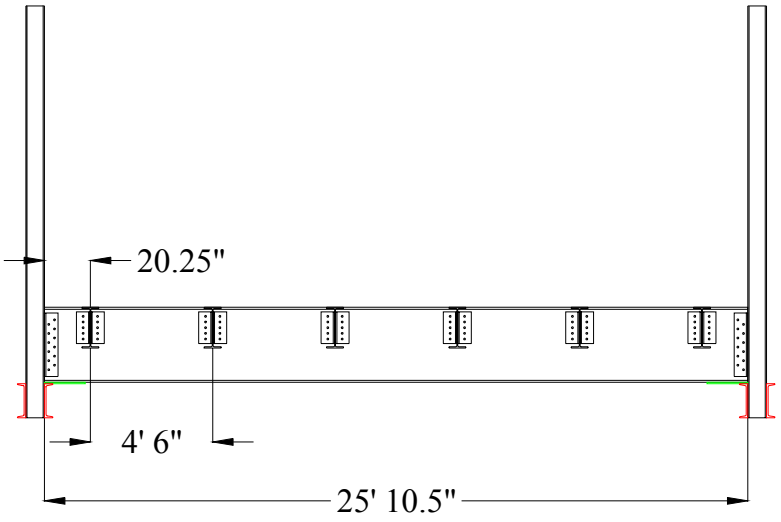

Figure 5.8 Goliad steel deck member framing

The reinforced concrete slab was very similar to the Llano slab, with a small increase in longitudinal reinforcement. The slab thickness was 6.5 inches, and all reinforcement consisted of #5 bars. Longitudinal bars were spaced at approximately 10 inches. Transverse reinforcement was estimated to be spaced at approximately 5 to 6 inches. Transverse reinforcement was bent into the same "crank bar" configuration as the Llano deck, as shown in Figure 2.7. Slab details for Goliad are shown in Figure 5.9.

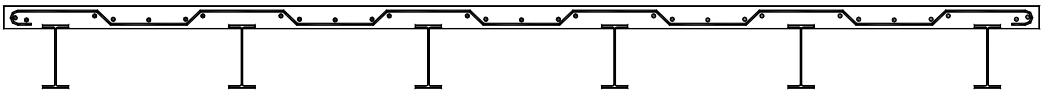

Figure 5.9 Goliad slab and reinforcement details

5.3.2 Test Objectives

The testing in Llano was limited in the magnitude of the applied loads since the bridge was still in service. Very high loads could not be placed on the structure to avoid any possibility of damage. This was not the case with the Goliad bridge. This structure was designated for demolition, and therefore some overload could be tolerated.

The Llano test results showed significant reserve capacity over the normal hand calculations performed in an AASHTO load rating. The Goliad bridge offered an opportunity to confirm these findings, and to test to a higher load than the Llano test. Hence, the goals of the Goliad test were similar to the Llano test and meant to corroborate and extend results from Llano.

5.4 INITIAL ANALYSIS

5.4.1 Introduction

As a first step in preparing to test the Goliad Bridge, a conventional AASHTO bridge load rating was done, as well as an analysis with a proposed pair of load vehicles. At the time of initial planning for the load test, the availability of loading vehicles was not known. However, an initial structural analysis was conducted to assure that the bridge could safely accommodate very heavy test vehicles. Consequently, structural analysis was conducted for an assumed pair of tandem axle concrete ready-mix trucks as a first estimate of heavy load test vehicles. Dimensions and weights were obtained for typical fully loaded trucks from a local concrete ready-mix supply company, and then conservatively the wheelbases where shortened, the tandem collapsed to a single axle, and loads increased. The fictitious truck used to evaluate the bridge is pictured in Figure 5.10.

This loading was assumed to conservatively approximate the highest possible load that would be used in a load test. Although the wheelbase is 2 ft. longer than H20 loading, the front axle is 37.5% heavier, and the rear axle is 81% heavier, making this loading much more severe than H20. Additionally, because of the short deck spans, this assumed loading is also more severe than HS20.

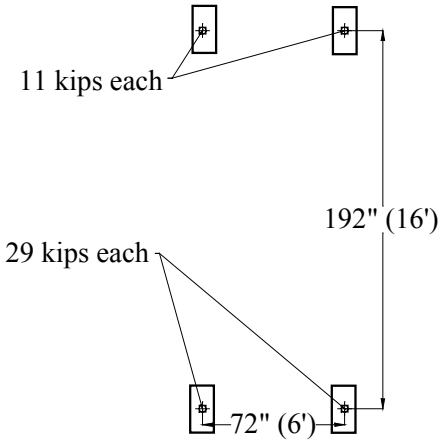

Figure 5.10 Assumed truck loading

5.4.2 Analysis Results

5.4.2.1 Assumed Truck Loading

Using the fictitious trucks in a side-by-side configuration, the unfactored results for the truss members are shown in Figure 5.11. The truck axles were placed longitudinally at different panel points to obtain the largest response in each of the members. The results are given as a ratio of the capacity of the member to the largest response from any load position. Unfactored loads and capacities were used since the loading was assumed to be larger than any actual test loading, and the yield strength was conservatively assumed to be 30 ksi based on date built. Since the results showed significant reserve capacity, the truss was deemed safe under the assumed load test vehicles.

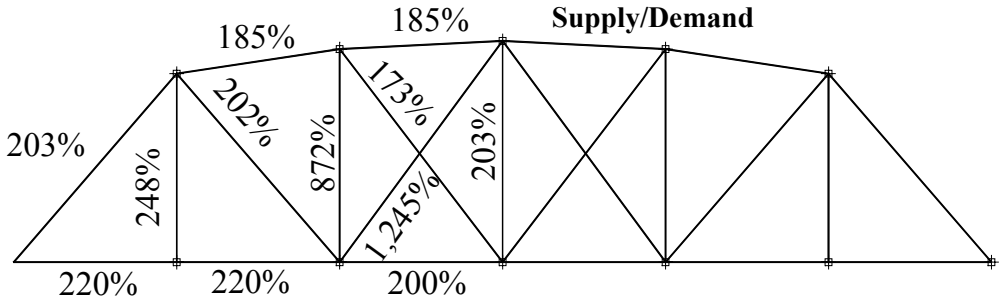

Figure 5.11 Analysis results for side-by-side truck loading

In addition to evaluating the safety of the truss members, the floor members were also evaluated for safety under the assumed load test vehicles. Placing the assumed wheel load of 29 kips at midspan of a longitudinal stringer, and *not* using any distribution factors results in a live load stress of 21.1 ksi. Superimposing a dead load stress of 3.6 ksi results in a maximum unfactored stress of 24.7 ksi. This would allow an approximate factor of safety of 18% against yield. The fact that limited yield was acceptable, plus other conservative assumptions such as no distribution factor, led to the conclusion that the stringers were safe to test to this load level.

Transverse floor beams were analyzed with trucks positioned side-by-side, three feet apart, centered transversely. This loading results in a live load stress of 16.8 ksi. Adding a 6.2 ksi dead load stress results in a total stress of approximately 23 ksi. This gives a factor of safety against first yield of over 23%, which given the conservative nature of the analysis, was deemed satisfactory. Table 5.1 summarizes the analysis results for deck members for the fictitious load test vehicles.

Table 5.1 Analysis results of assumed truck loading

Member	Live load stress	Dead load stress	Total Stress	Ratio σ_{tot}/σ_y
Stringer	21.1	3.6	24.8	82.6%
Beam	16.8	6.2	23.0	76.6%

These results are not intended to be an exact representation of bridge deck response, but an initial conservative appraisal of capacity. As can be seen in Table 5.1, the structure appears to have a significant reserve capacity to safely accommodate very heavy load test vehicles.

5.4.2.2 AASHTO Load Rating

In a similar fashion to the Llano bridge, a conventional AASHTO bridge load rating was performed on the steel deck members of the Goliad bridge. Because of the large capacity results of the truss analysis of the Llano Bridge, as well as the previous analysis for the assumed truck loadings, a load rating of the Goliad truss members was not done. Load ratings were determined only for the longitudinal stringers and transverse floor beams.

Load ratings were determined for the floor beams and stringers of the Goliad bridge, in a manner similar to Llano bridge as described in Chapter 2 (see Section 2.3.5). As in the Llano Bridge, the inventory ratings for the stringers are quite close to HS20, whereas the transverse members rate significantly below HS 20. Table 5.2 gives the rating results.

Table 5.2 AASHTO HS load rating of Goliad bridge deck

30 ksi yield stress			
Stringers			
Method	**Inventory**	**Operating**	**Overload**
AS	19.9	30.3	N/A
LF	21.5	36.0	19.7
Beams			
Method	**Inventory**	**Operating**	**Overload**
AS	12.9	21.5	N/A
LF	15.8	26.4	14.1

5.5 LOAD TEST

5.5.1 Instrumentation

As in the Llano test, the floor beams and stringers at Goliad were instrumented with strain gages. The height and location of the bridge above the San Antonio River made instrumentation somewhat more difficult than in Llano, as the members could not be reached via ladders. However, due to the

construction of the new bridge outside the truss bridge, instrumentation was possible using those lanes as a platform. TxDOT supplied a "snooper" truck to allow access to the underside of the bridge. Figures 5.12 through 5.14 show the truck and instrumentation access.

Because of the access provided by the snooper truck, it was possible to instrument a center section of the deck. The fourth deck segment from the north abutment was chosen because construction blocked other areas. Figure 5.15 shows the deck area instrumented. All instrumentation consisted of strain gages located on steel members, inside top and bottom flanges, as well as mid-depth of the web. Figure 5.16 shows the number and gage locations, while Figure 5.17 shows gage placement on the members.

The gages were placed while traffic was still on the truss bridge. Testing occurred over a month later, when traffic was diverted to the outside lanes, and the truss was closed to traffic.

Figure 5.12 TxDOT snooper truck

Figure 5.13 Access to bridge deck

Figure 5.14 Platform extension used to instrument deck

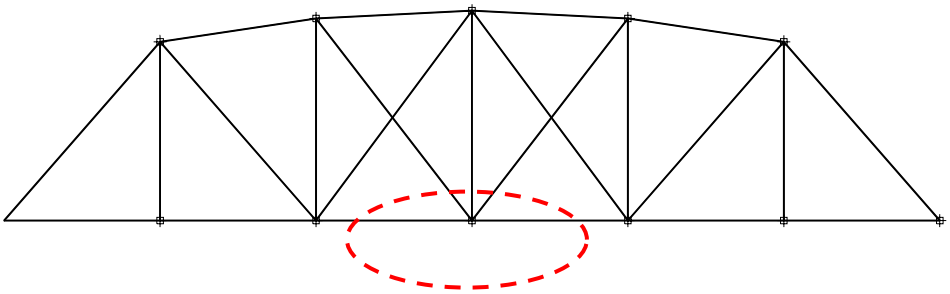

Figure 5.15 Deck segment instrumented

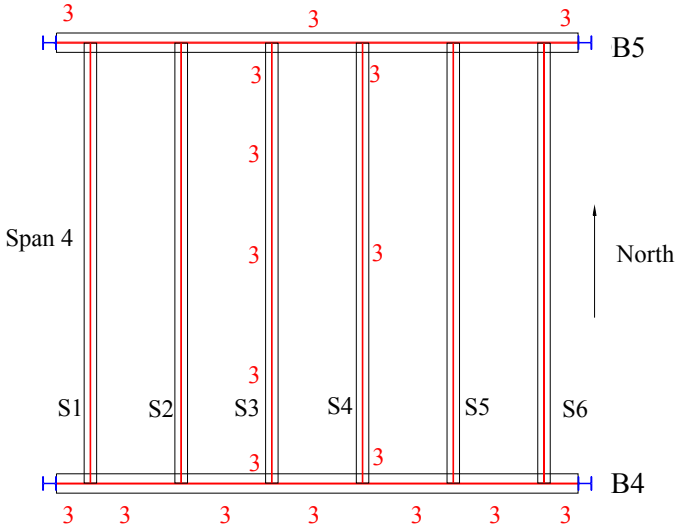

Figure 5.16 Gage locations and number of gages at each location

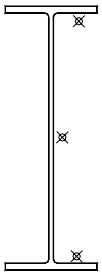

Figure 5.17 Strain gage locations on cross-section

5.5.2 Loading

Based on availability, the load test vehicle was a "low boy" tractor-trailer loaded with concrete lane dividers. Figure 5.18 shows the tractor-trailer during a load test, and Figure 5.19 shows the truck dimensions.

The number of concrete barriers placed on the truck was varied to permit testing at different load levels. Test runs were made with an empty truck, and with two, three, and finally five barriers loaded onto the truck. Portable scales provided by the Texas Department of Public Safety were used to measure each axle for all load cases. Table 5.3 lists the loadings. In this table, Axle 1 refers to the front axle, Axle 2 to the front tandem, and Axle 3 to the rear tandem. Figure 5.20 shows the loading process, and Figure 5.21 shows the portable scales weighing the trucks.

Figure 5.18 Goliad load test truck

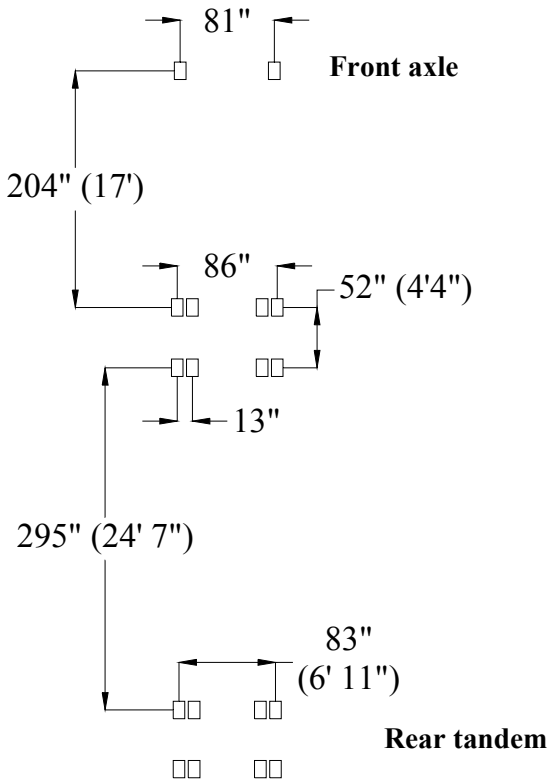

Figure 5.19 Dimensions of test vehicle

Table 5.3 Axle weights for Goliad load test truck (pounds)

Empty truck				
	Axle 1	**Axle 2**	**Axle 3**	**Total**
Axle	11,020	17,100	7,960	36,080
Wheel	5,510	8,550	3,980	18,040
1 barrier				
Axle	10,980	23,000	28,660	62,640
Wheel	5,490	11,500	14,330	31,320
2 barriers				
Axle	11,120	25,860	37,900	74,880
Wheel	5,560	12,930	18,950	37,440
3 barriers				
Axle	10,920	29,900	57,260	98,080
Wheel	5,460	14,950	28,630	49,040

Figure 5.20 Barrier loading to increase axle weight

Figure 5.21 Portable scales used to weigh truck

Multiple runs were made with different loadings and transverse positions. Test runs were made with the truck positioned with the left wheel line above the second stringer, with the truck centered on the bridge, and lastly with the right wheel line above the fifth stringer. These positions are shown in Figure 5.22. Each run was normally done twice (the empty truck was done only once in each position) with a total of 21 runs. Table 5.4 gives the run list with the barrier loadings.

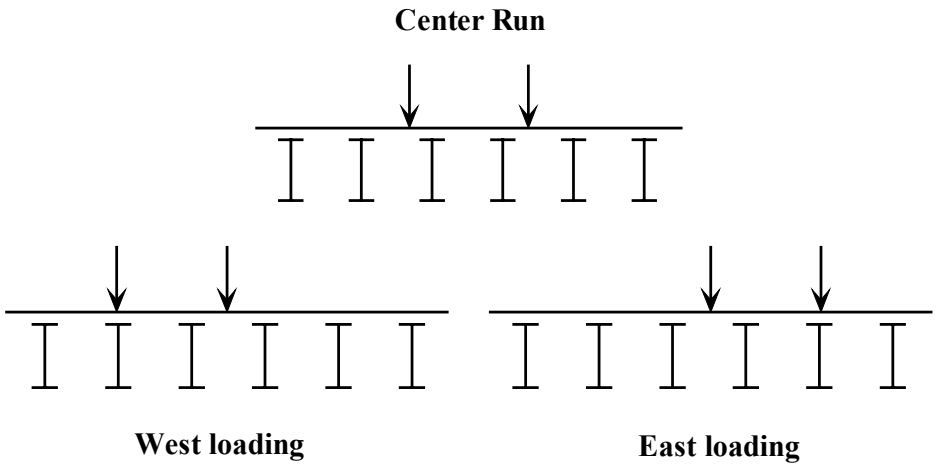

Figure 5.22 Transverse truck positioning for Goliad field load test

Table 5.4 Load runs for Goliad test

Run	Location	Load	Run	Location	Load
1	West	Empty	12	C	3 barriers
2	C	Empty	13	C	3 barriers
3	East	Empty	14	East	3 barriers
4	C	Empty	15	East	3 barriers
5	West	2 barriers	16	West	5 barriers
6	C	2 barriers	17	West	5 barriers
7	C	2 barriers	18	C	5 barriers
8	East	2 barriers	19	C	5 barriers
9	East	2 barriers	20	East	5 barriers
10	West	3 barriers	21	East	5 barriers
11	West	3 barriers			

5.5.3 Finite Element Analysis of the Goliad Bridge Deck

5.5.3.1 Finite Element Model

In a similar fashion to the Llano structure, an elastic finite element model of the Goliad bridge deck was created using SAP 2000. Standard two node beam elements were used for the steel members, and four node isotropic shell elements were used for the slab. Two deck sections were modeled, and a 1-inch gap in the shell elements was introduced to represent the construction joint between deck segments, as in the Llano model. Thick shell elements represented the curbs along the longitudinal edges. Figure 5.23 shows the model. Load cases were used to mimic the test load trucks.

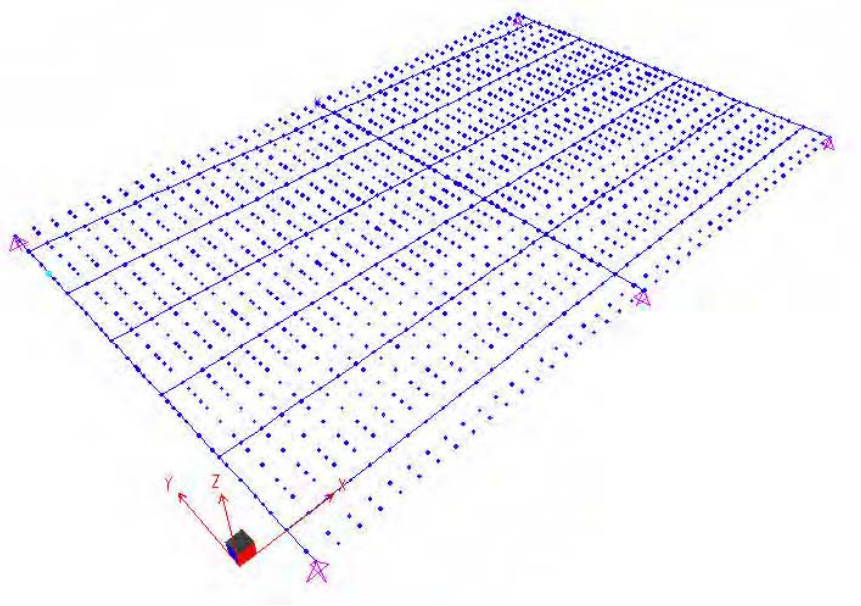

Figure 5.23 Finite element model of Goliad deck (shell elements hidden)

To obtain the maximum response, only the rear tandem was placed on the structure. The rear tandem was the most heavily loaded portion of the truck, and because of the large distance to the next axle (over 26 ft.), any other axles would be well off the span. The rear tandem was approximated with four equal concentrated loads spaced 6-1/2 feet apart transversely and 4 feet longitudinally. Figure 5.24 depicts the tandem loading on the center transverse beam.

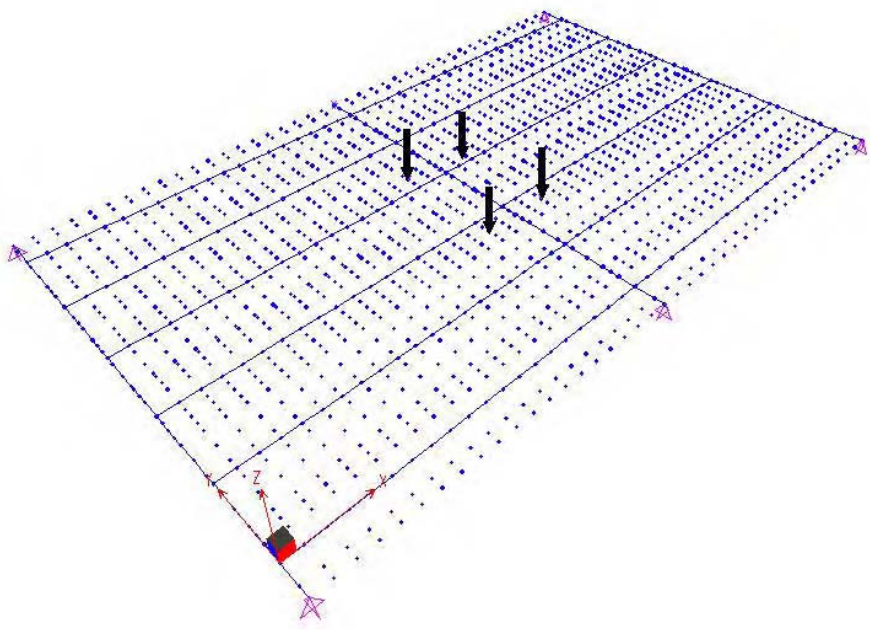

Figure 5.24 Tandem loading on center beam for Goliad deck

5.5.3.2 Finite Element Analysis Results

The finite element results are presented in Table 5.5. Results are for the center stringers (S3 and S4) loaded with a center run, second stringer (S2) loaded with an east run (wheel line over S2), and the center transverse beam loaded with a center run. For comparison, stresses were computed in these members for the same load cases using conventional AASHTO calculation methods.

Table 5.5 Finite element results for Goliad deck members

		Member stresses (ksi)		
Load	**Tandem weight (kips)**	**Beam**	**S3, S4**	**S2**
Unit axle load	1.0	0.12	0.13	0.13
Empty	7.96	0.96	1.0	1.0
2 barriers	28.7	3.4	3.6	3.7
3 barriers	37.9	4.4	4.8	4.9
5 barriers	57.3	6.7	7.3	7.4

Table 5.6 compares AASHTO calculations to the finite element predictions for a unit axle weight. AASHTO calculations for the longitudinal members used a distribution factor of $S/5.5 \cdot 1/2 = 0.41$. The distribution factor is halved because a unit axle load was used instead of a unit wheel line load. The stresses predicted by finite element analysis are significantly lower than what AASHTO calculations would predict, with a more prominent difference in longitudinal members than transverse. In the stringers, the FEA stresses are approximately 50 percent of the stresses predicted by AASHTO calculations. For the beam, the FEA stress is about 75 percent of the AASHTO calculated stress.

Table 5.6 Stress comparisons between AASHTO calculations and FEA

	Member stresses (ksi)		
Member	**Beam**	**S3, S4**	**S2**
FEA	0.12	0.13	0.13
AASHTO	0.16	0.24	0.24
	Ratio – FEA/AASHTO		
	Beam	**S3, S4**	**S2**
	75.2%	53.0%	54.3%

5.6 LOAD TEST RESULTS

Similar to the Llano field test, strain data was taken in the Goliad field test and converted to stress. The stresses where then plotted against the truck longitudinal position. Plots of stress versus truck position for the Goliad field test are provided in Appendix C. Unfortunately, apparently due to the long time gap between gaging and testing, there were a larger number of defective gages in the Goliad test. Because of the inaccessibility of the members in Goliad, gages could not be replaced prior to the test. There were, however, enough gages still functioning to obtain a satisfactory amount of data.

Representative plots of field test data for transverse beams are shown in Figures 5.25 through 5.28. Compared to the Llano field tests, the Goliad tests showed virtually no unintended composite action in the beams. Although not consistent, the Llano Bridge did show some partial composite action in the transverse beams, (Figure 4.24). Goliad test results showed little if any difference in top and bottom flange stresses in the transverse beams, indicating non-composite behavior. Although it is difficult to compare exactly the Llano and Goliad tests because of different member sizes, spans, loads and load spacing, approximate comparisons show reasonable similarity in the overall behavior of the two bridge deck systems. For example, Figure 5.28 shows the Goliad test results for a transverse beam with a maximum axle loading of approximately 37.9 kips. The maximum induced stress at midspan is approximately 3.9 ksi. Figure 5.29 shows a similar result for the Llano test, with a maximum induced stress of a transverse member at midspan to be approximately 3.3 ksi. Both members are the same length, and the higher stress associated with the Goliad test may be attributed to a smaller section modulus (385 in^3 vs. 414 in^3) and a higher axle weight (approximately 38 kips vs. 34 kips).

Representative plots for the longitudinal stringers are shown in Figures 5.30 and 5.31. As with the Llano test, longitudinal stringers showed some degree of unintended composite action. Figure 5.30 clearly indicates some degree of composite action with a larger peak stress in the bottom flange than in the top flange (1.8 ksi in the bottom vs. 1.4 ksi in the top), and an elevated mid-web stress. Similar tendencies are shown in Figure 5.31, i.e., a non-symmetrical stress distribution (3.2 ksi bottom flange and 2.6 ksi top flange stress), and a non-zero mid-depth stress.

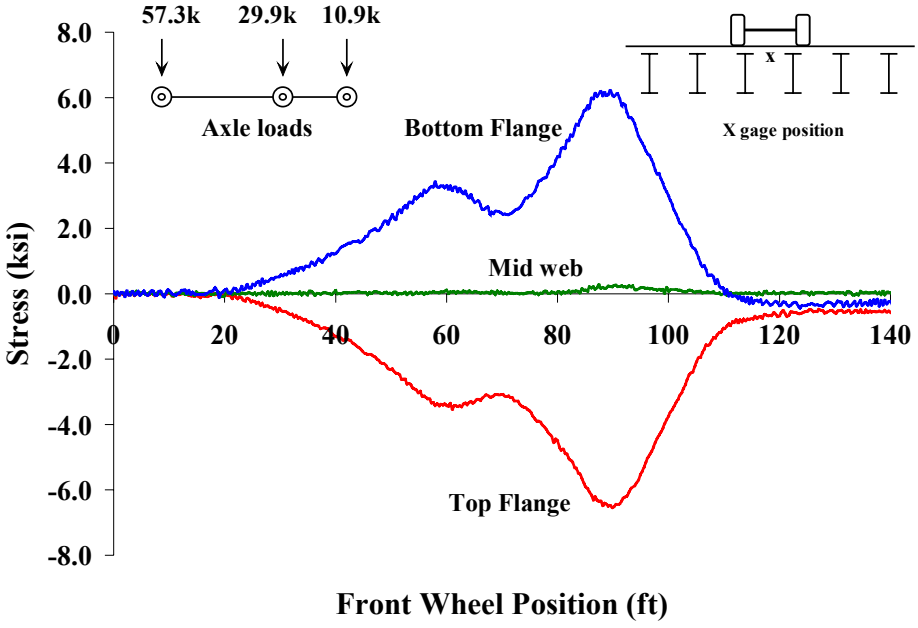

Figure 5.25 Goliad test results for midspan of transverse beam B4

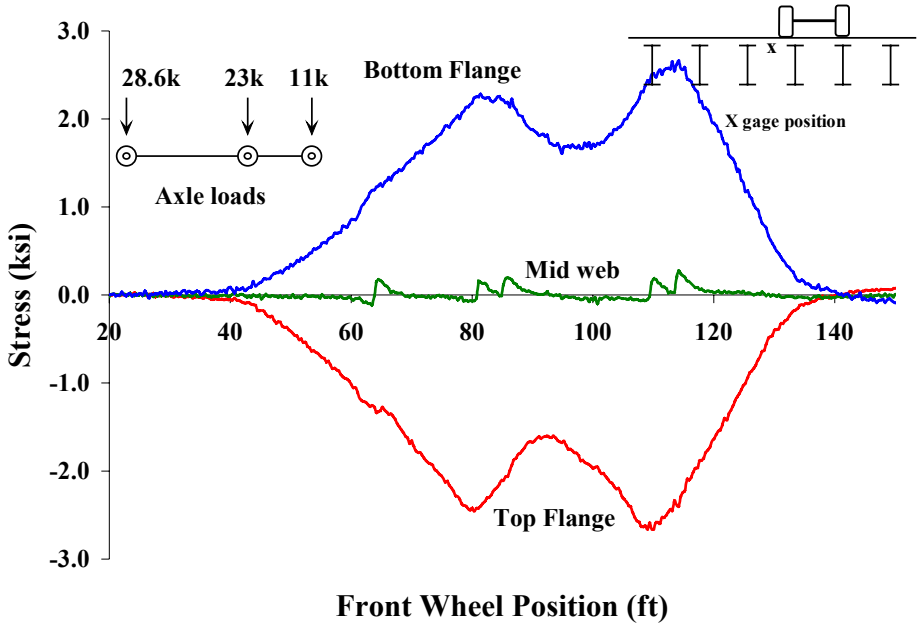

Figure 5.26 Goliad test results for midspan of transverse beam B5

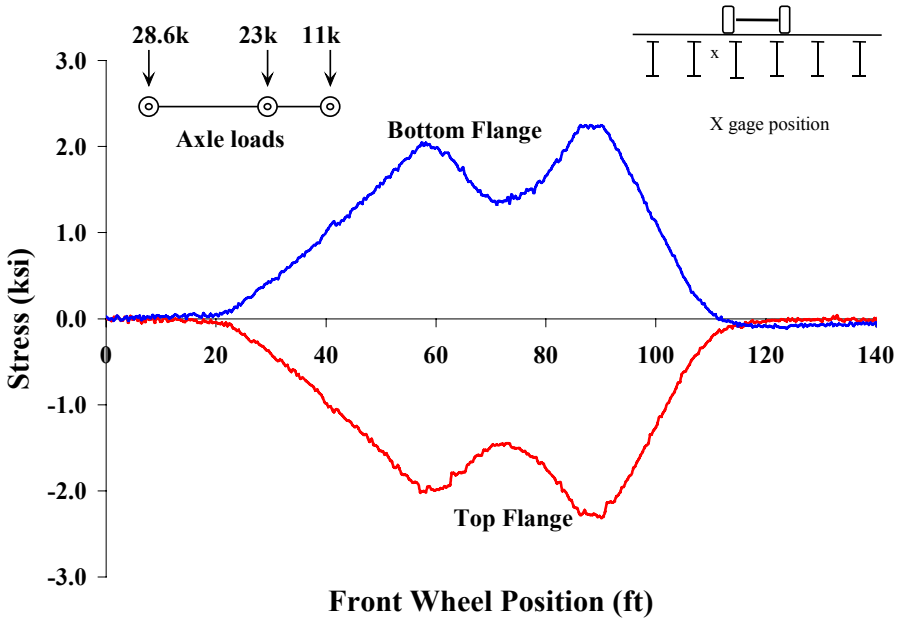

Figure 5.27 Goliad test result for quarter point transverse beam B4

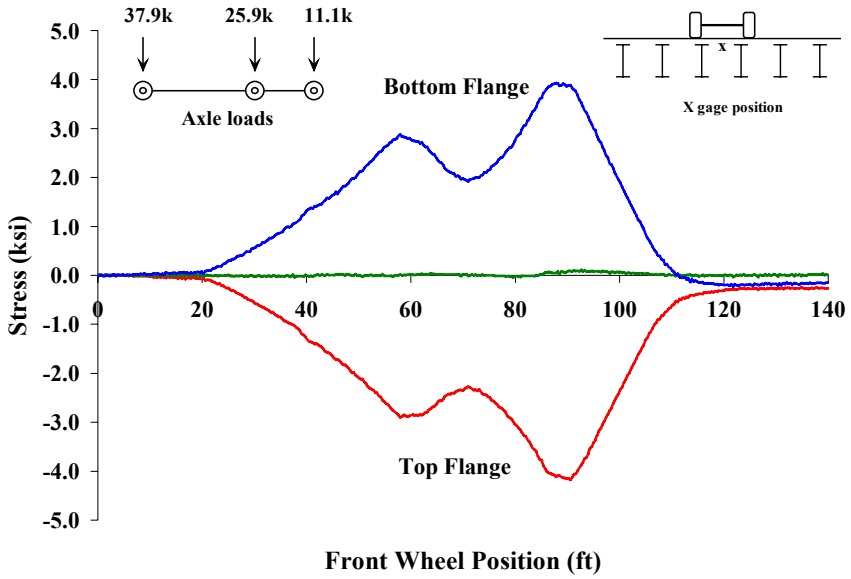

Figure 5.28 Test results for transverse beam in the Goliad test

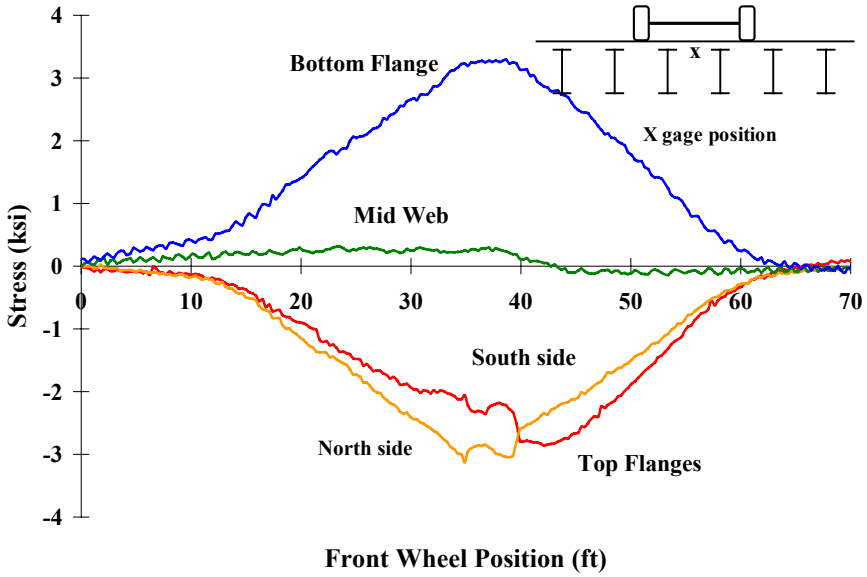

Figure 5.29 Test results for a transverse beam in the Llano test

Comparisons to the Llano test may be seen in Figures 5.32 and 5.33, although a direct comparison between Llano and Goliad is difficult because of the potentially different degrees of composite action. Additionally, the Llano stringer was longer (22' compared to 20' in Goliad), the axle weight was higher in the Goliad test, the wheel line positioning was slightly different, and the Goliad member has a smaller section modulus (82 in^3 vs. 89 in^3). Examining the average extreme fiber stress shows between 3.7 and 4.1 ksi in the Llano test, and between approximately 4.3 and 4.5 ksi in the Goliad

test. The difference is reasonable given the different parameters involved in the comparison. These comparisons indicate that the Goliad bridge deck members responded in a similar manner to the Llano bridge deck members.

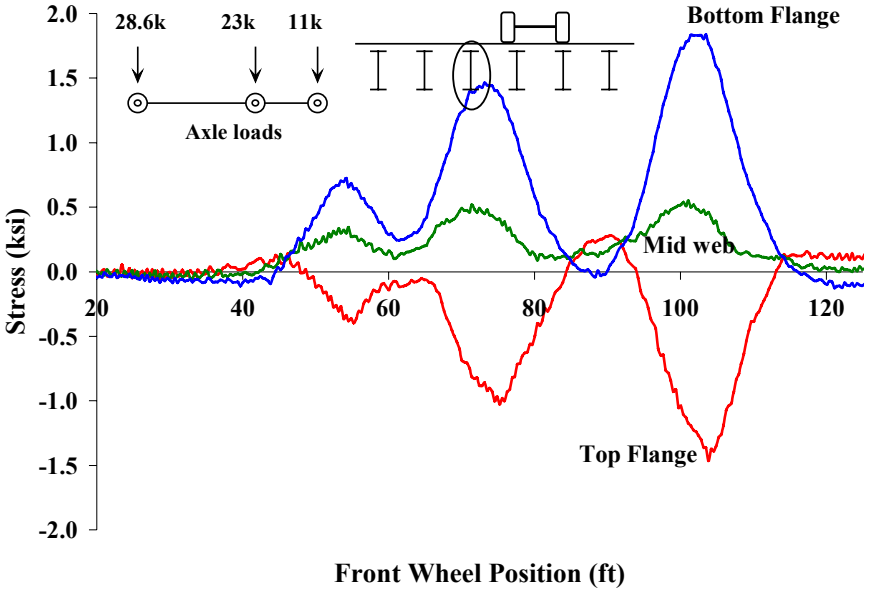

Figure 5.30 Goliad test results for longitudinal stringer S3

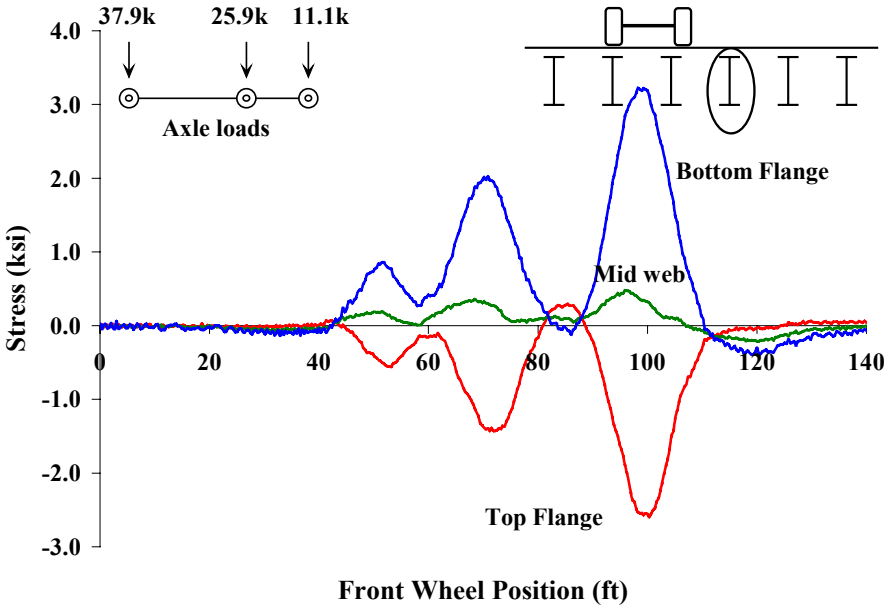

Figure 5.31 Goliad test results for longitudinal stringer S4

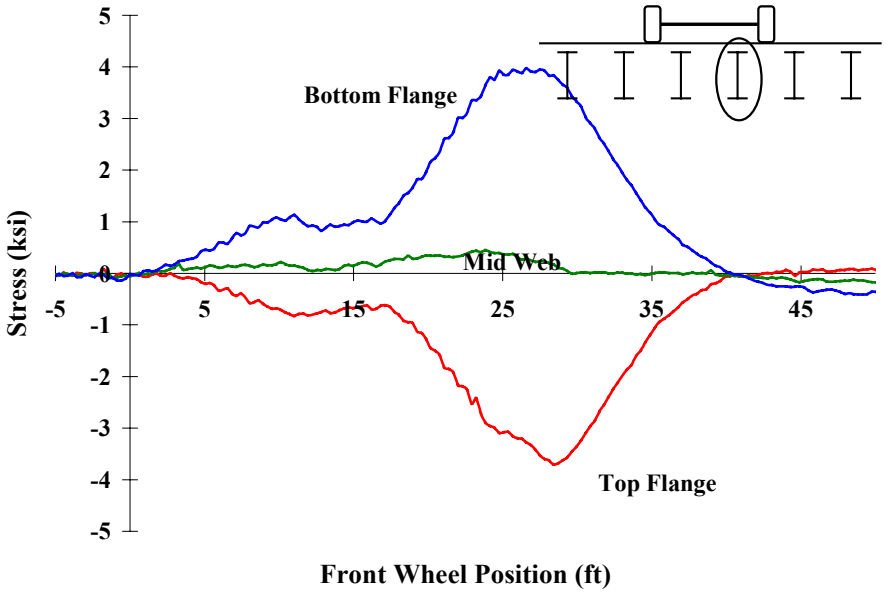

Figure 5.32 Llano midspan stress plot for longitudinal stringer

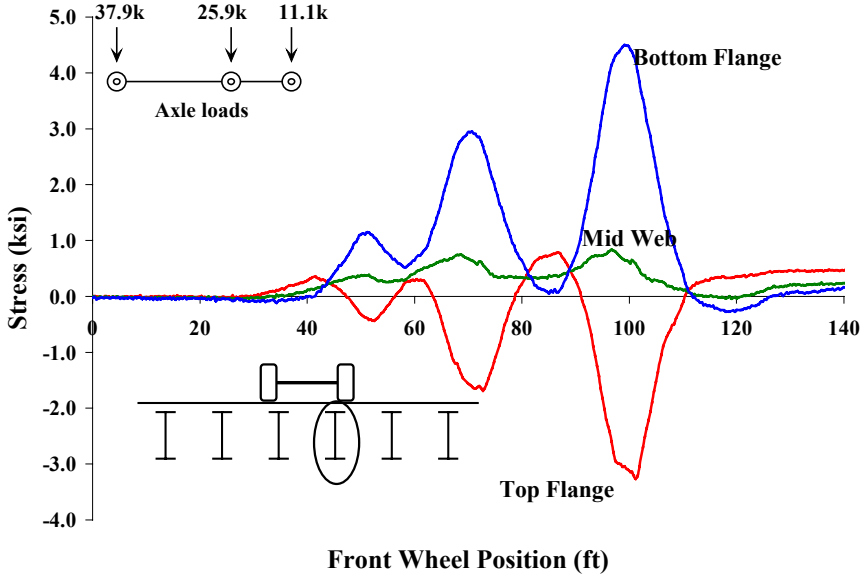

Figure 5.33 Goliad midspan stress plot for longitudinal stringer

5.7 LOAD TEST COMPARISONS TO FINITE ELEMENT ANALYSIS AND AASHTO CALCULATIONS

Tables 5.7 and 5.8 compare the maximum stresses measured in the field tests with those predicted by finite element analysis and by AASHTO calculations. Table 5.7 shows results for transverse beams, and Table 5.8 shows results for longitudinal stringers. The maximum stresses in each of the members resulted from center run load tests.

Table 5.7 Stress comparisons for transverse beams

Transverse beam B5					
	Stress (ksi)			Ratio	
Load (k)	Field Test	FEA	AASHTO	FEA/AASHTO	Field test/ AASHTO
7.96	0.7	0.9	1.2	75.2%	59.3%
28.6	3.0	3.4	4.5	75.2%	67.6%
37.9	4.1	4.4	5.9	75.2%	70.1%
57.26	6.6	6.7	8.9	75.2%	74.2%
Transverse beam B4					
	Stress (ksi)			Ratio	
Load (k)	Field Test	FEA	AASHTO	FEA/AASHTO	Field test/ AASHTO
7.96	0.8	0.9	1.2	75.2%	67.7%
28.6	3.0	3.4	4.5	75.2%	67.4%
37.9	4.2	4.4	5.9	75.2%	70.3%
57.26	6.5	6.7	8.9	75.2%	72.4%

Table 5.8 Stress comparisons for longitudinal stringers

Longitudinal stringer S3					
	Stress (ksi)			Ratio	
Load (k)	Field Test	FEA	AASHTO	FEA/AASHTO	Field test/ AASHTO
7.96	0.7	1.0	1.9	53.0%	36.3%
28.6	3.1	3.6	6.9	53.0%	45.7%
37.9	4.5	4.8	9.1	53.0%	49.4%
57.26	7.0	7.3	13.7	53.0%	51.9%
Longitudinal stringer S4					
	Stress (ksi)			Ratio	
Load (k)	Field Test	FEA	AASHTO	FEA/AASHTO	Field test/ AASHTO
7.96	0.7	1.0	1.9	53.0%	36.3%
28.6	3.0	3.6	6.9	53.0%	43.3%
37.9	4.3	4.8	9.1	53.0%	46.9%
57.26	7.1	7.3	13.7	53.0%	51.9%

Since the second and fifth longitudinal stringers (S2, S5) were not instrumented, no field test results and comparisons were possible. Also, since there was not a direct wheel line loading of stringers S3 and S4 in the field tests, the AASHTO analysis is based on slightly different load positions than the field test. However, a direct wheel line loading would move the loads only 15 inches. Finite element analysis shows only a 1-percent change in predicted stress in the stringer when the wheel line is moved 15 inches. Consequently, the differences in wheel line location between the field test and the AASHTO calculation is not considered significant.

The comparisons in Tables 5.7 and 5.8 reflect the same trend found in the Llano analysis, i.e., that conventional AASHTO calculations are conservative compared both to finite element analysis as well as to field test results. The largest differences occur in the longitudinal stringers, where the field measured stresses are typically less than half of those predicted by AASHTO. For the transverse beams, the field measured stresses range from 60 to 75 percent of the stresses predicted by AASHTO calculations. For both the transverse beams and longitudinal stringers, the stresses predicted by finite element analysis are much closer to the field measured values, but somewhat higher. Consequently, as was the case in Llano, the finite element analysis is providing a significantly more accurate, although still somewhat conservative, estimate of field measured response.

An additional observation from the Goliad test is that the ratio of the maximum stress to the load was not constant, i.e., the load – stress relationship is nonlinear. Since there was likely no inelastic material response, the stress should theoretically increase proportionately with the load. However, as shown in Figure 5.33, the ratio of maximum stress to load increases with increasing load. This phenomenon occurs with both the transverse and longitudinal members, but is most pronounced in the longitudinal members. A possible reason for this phenomenon may be that the degree of unintended composite action reduces at higher load levels, as discussed in the following section.

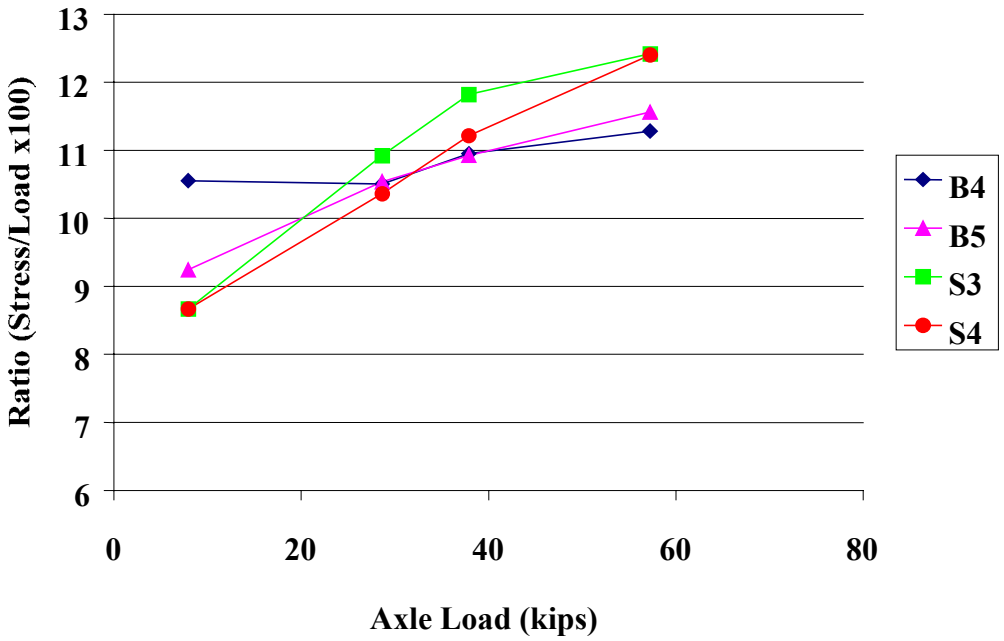

Figure 5.34 Axle Load versus Stress/Load Ratio

5.8 SLIP PHENOMENA

As described above, field load test data for longitudinal stringers often exhibited some degree of unintended composite action. This was observed in both the Llano tests (Figures 4.19 and 4.20), as well as the Goliad test (Figures 5.30 and 5.31). As discussed in chapter 4, many other researchers have observed unintended composite action in other field tests on bridges without mechanical shear connectors. The question then arises as to whether this additional strength can be utilized in the evaluation and load rating of an existing structure.

As illustrated by the data in Figure 5.35, results of the Goliad field test suggest that this unintended composite action may not be a reliable source of additional strength. The points marked by the ovals indicate a sudden shift in stress. This occurrence was repeated in both of the instrumented stringers for different loads and load positions, as seen in Figures 5.36 and 5.37. All plots indicate the same sudden jump in stress at the maximum loadings.

The loading was pseudo-static, (the truck speed was less than 5 mph); hence there was likely no sudden increase in load due to impact effects. The stress is related to the moment through the section modulus. Given that the moment is relatively constant, the jump in stress is likely caused by a sudden decrease in section modulus. Since the section modulus of a partially composite member is higher than a non-composite one, it appears that the jump in stress is caused by the sudden loss of the unintended composite action. The unintended composite action is believed to be caused by friction. At the instant of the stress jump, the shear force at the interface likely overcomes the frictional resistance.

In data taken from the graph depicted in Figure 5.36, a stress distribution over section depth is plotted in Figure 5.38 for the condition prior to slip.

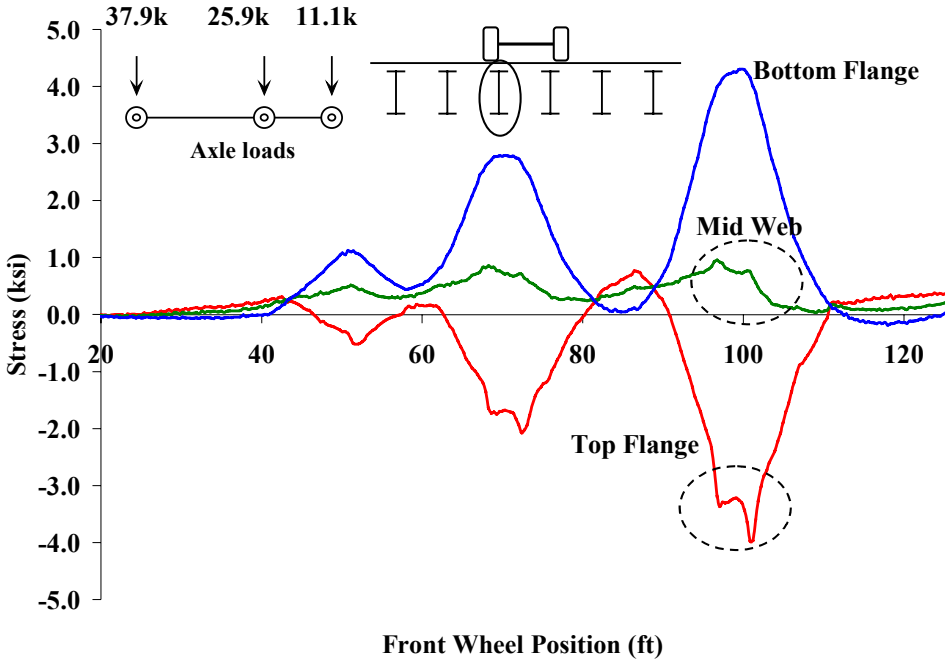

Figure 5.35 Midspan stress in stringer S3: truck loaded with two barriers

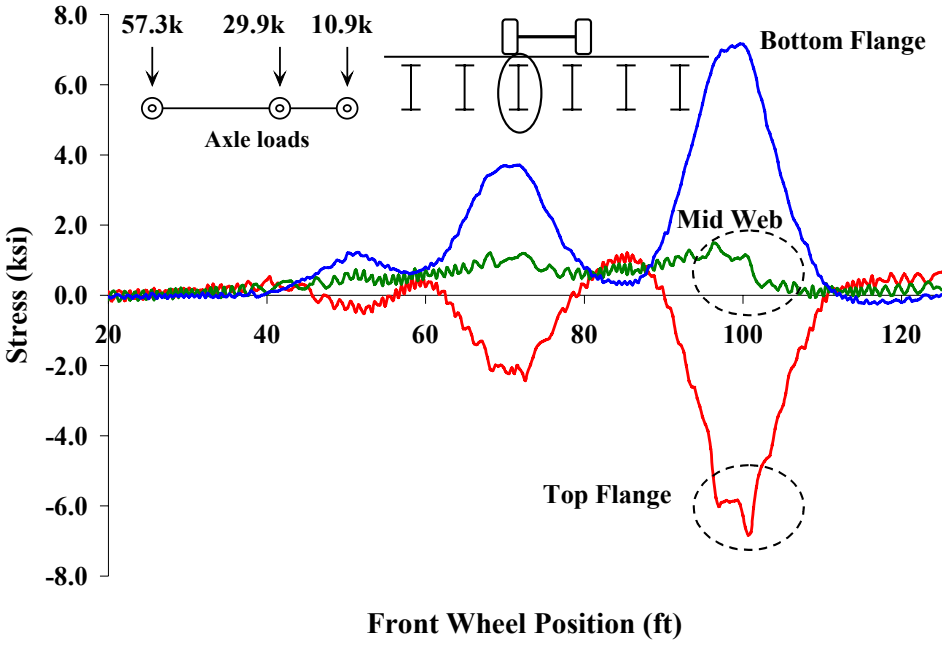

Figure 5.36 Midspan stress in stringer S3: truck loaded with three barriers

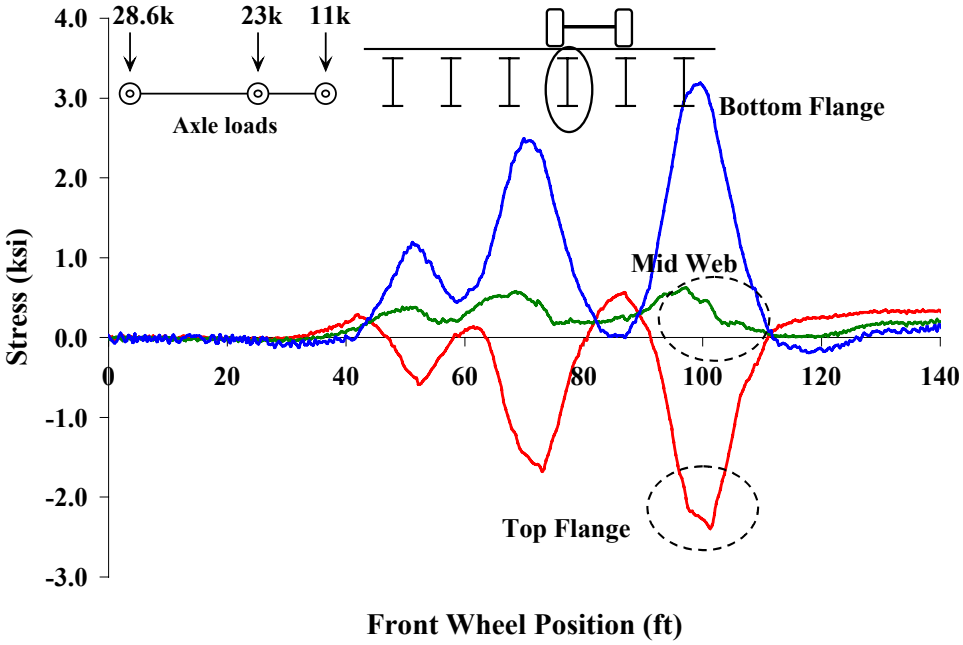

Figure 5.37 Midspan stress in stringer S4: truck loaded one barrier

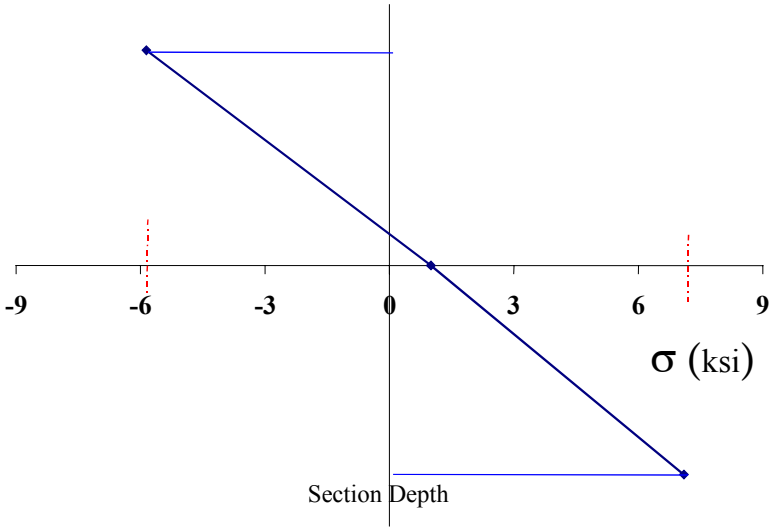

Figure 5.38 Pre-slip stress profile over depth of stringer

The figure shows the unsymmetrical stress distribution associated with composite action. Bottom flange stress is approximately 7.1 ksi, while top flange stress is approximately 5.9 ksi. The neutral axis is located approximately 2-1/2 inches above mid-depth. As the loading increases, the stress distribution suddenly changes, and the neutral axis drops as shown in Figure 5.39 for the same stringer after slip.

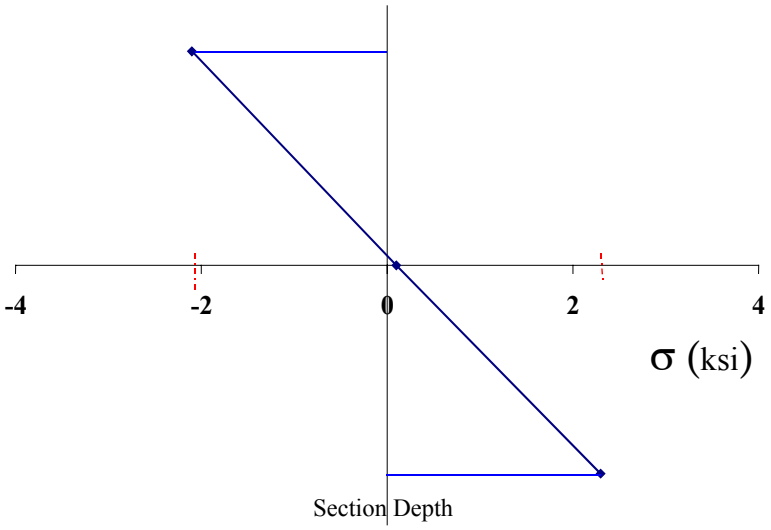

Figure 5.39 Post-slip stress profile over depth of stringer

The post-slip stress profile shows near equal stresses in the top and bottom flanges (2.1 and 2.3 ksi, respectively), and a neutral axis near mid-depth. This indicates a predominantly non-composite response. Figure 5.40 shows the drop in neutral axis associated with the loss of composite action as slip occurs.

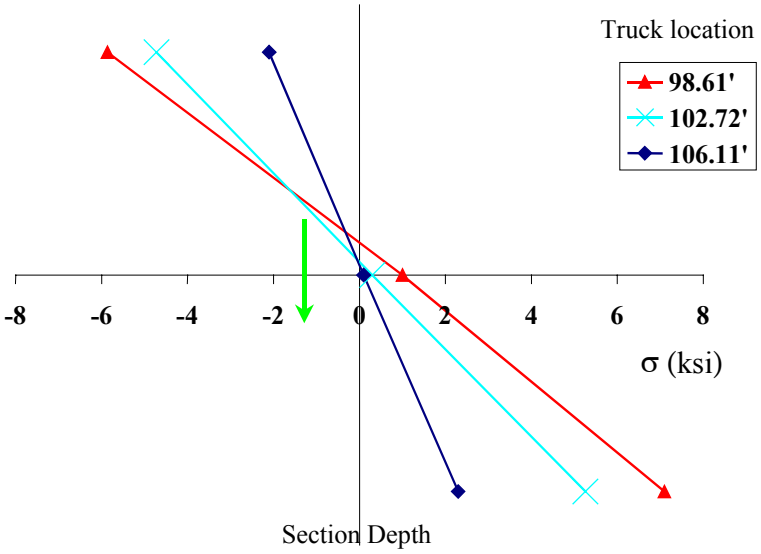

Figure 5.40 Change in neutral axis location as slip occurs in the member

This loss of composite action did not occur in every load case, and was more prominent in the stringer S3 than in S4. However, based on these results, it appears that composite action is not a reliable source of reserve strength.

The slip phenomenon was not as clearly observed in the Llano load test, and it is felt that the difference in the load vehicles may be the reason. The Llano test trucks had much shorter longitudinal wheelbases than the Goliad test truck. Other researchers, (Chajes et al 1997, Saraf and Nowak 1998), have observed partial composite action in load tests on bridges without mechanical shear connectors, and their results do not reflect any slip. However, Chajes et al (1997) used a load vehicle similar to the Llano test vehicle, and Saraf and Nowak (1998) used military tanks. It is conjectured that the much larger spacing between axles in the Goliad test contributed to the slip. Further, the conditions at the interface between the steel beams and concrete floor slab may have been different among these various cases.

5.9 SUMMARY

A bridge located in Goliad, Texas was selected as another case study for this project. Although very similar to the Llano Bridge, the Goliad structure was demolished and subsequently replaced. Because of this, the Goliad Bridge was tested prior to demolition to a much higher level than the Llano Bridge. In a similar fashion to the Llano case study, a finite element analysis was performed as well for the Goliad bridge deck system, and compared to both the field tests and conventional AASHTO calculations of stress.

The overall trend in results for Goliad was quite similar to the Llano load test. Stresses predicted by the AASHTO calculations were significantly higher than the stresses predicted by finite element analysis. The stresses predicted by finite element analysis, in turn, were somewhat higher than those measured in the field test. The highest loading used in the Goliad test was approximately a 57.3 kip axle load. Even at this high of a load (almost 80% higher than an HS20 axle), the maximum live load response was well under yielding, less than 8 ksi for both longitudinal and transverse members. (Dead load stresses were estimated to be approximately 3.6 ksi for longitudinal members, and 6.2 ksi for transverse members). The magnitude of the test loading was limited by the capacity of the load vehicle.

An additional finding in the Goliad test was the rather clear loss of unintended partial composite action in the longitudinal members during many of the load runs. A sudden jump in stress was noticed

during high moment response in the members. The test data showed both a sudden increase in stress and a simultaneous drop in the neutral axis. Stresses before the jump were found to be unsymmetrical, and subsequent to the jump, nearly symmetrical. It is believed that the shear stresses at the concrete-steel interface overcame the frictional resistance and allowed slip. This slip caused loss of the partial composite action that had been observed in other load cases, as well as in the Llano test. Because of the loss of the composite action, it appears that the additional strength associated with a composite structure cannot be relied upon for capacity determination.

The Goliad load test also confirmed that the finite element model of the bridge deck provided a significantly more accurate prediction of member response than obtained from conventional AASHTO calculations. The stresses measured in the floor beams and stringers were significantly lower than predicted by the AASHTO calculations, indicating that the conventional AASHTO calculations significantly underestimate bridge deck capacity. The stresses predicted by the finite element analysis are much closer, although still somewhat higher, compared to those measured in the field test. Thus, as was the conclusion from the Llano test, the Goliad test indicates that the finite element analysis provides a very useful tool for load rating the bridge deck members. The finite element analysis provides a more realistic, but still somewhat conservative prediction of the response of the bridge deck members to truck loading.

Chapter 6:
Laboratory Investigation

6.1 INTRODUCTION

The final portion of this research study was an experimental investigation of a full-scale portion of a non-composite slab on steel girder bridge deck. The laboratory model was similar in member sizes and geometry to the bridge decks on the Llano and Goliad truss bridges. Figure 6.1 shows the laboratory model.

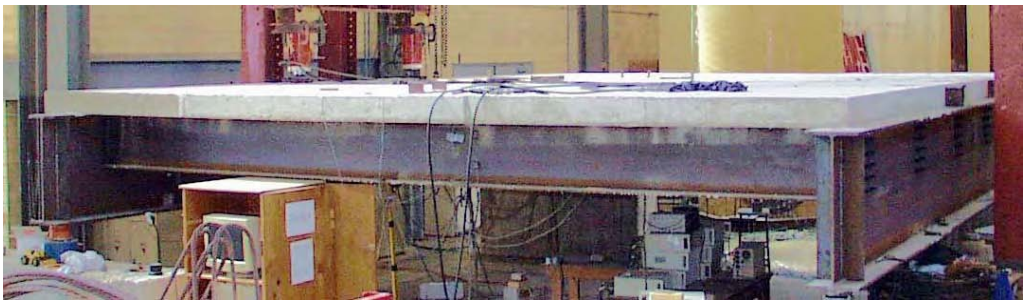

Figure 6.1 Laboratory model of single deck segment

The primary goal of the experimental study was to provide further data on the distribution of forces and stresses within the transverse and longitudinal members of the deck system under vertical loading. This data was intended to provide additional insights into the behavior of the floor system and to further corroborate the field test data and finite element analysis. The laboratory model of the floor system provided the opportunity to conduct more extensive testing than possible in the field and permitted the use of simpler and better defined boundary conditions for comparison with finite element models. The laboratory model, like the actual Llano and Goliad bridge decks, was constructed without shear connectors for composite action. An important issue considered in the bridge field tests that is examined in greater detailed in the laboratory model is the degree of unintended composite action that can be developed in the absence of shear studs. The laboratory model was also used for further study of the distribution of wheel loads to the steel beams and stringers in the deck, as well as contribution of the concrete slab to resisting load when acting non-compositely. Finally, the laboratory bridge deck model was used for preliminary evaluation of a potential strengthening scheme for the bridge deck.

This chapter describes the laboratory bridge deck model, the load testing and results, comparisons to finite element analysis, and the implementation and results of the structural retrofit.

6.2 MODEL DESCRIPTION

The laboratory model closely resembled the two case study bridge decks. The intent was not to construct an exact replica of either bridge deck, but to capture the fundamental properties of these types of deck systems. Furthermore, since the particular wide flange sections used for the transverse and longitudinal members in the actual bridge decks and the rivets used to connect them are now obsolete, neither structure could be duplicated exactly in the laboratory.

The laboratory model represented a single segment of a bridge deck at full-scale. The decision was made to construct a full-scale bridge deck model to avoid any potential uncertainties in behavior associated with reduced scale testing. The use of a full-scale model, however, precluded testing the model

to failure in the laboratory. Nonetheless, it was possible to load the model with axle loads well in excess of an HS20 truck.

In the laboratory model, the transverse beams were W33x130 sections 27 ft. long, with simple supports spaced 26 ft. apart. Longitudinal stringers were W18x50 sections 19 ft - 10.5 in. long. The slab was 6-1/2 in. thick, and 26 ft. x 21 ft. in plan. Figure 6.2 shows a section view, and Figure 6.3 shows a plan view.

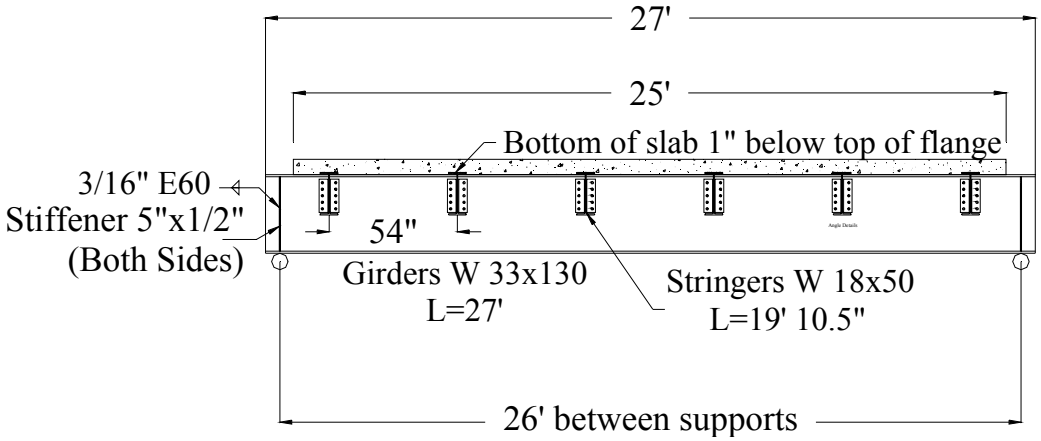

Figure 6.2 End view of laboratory model

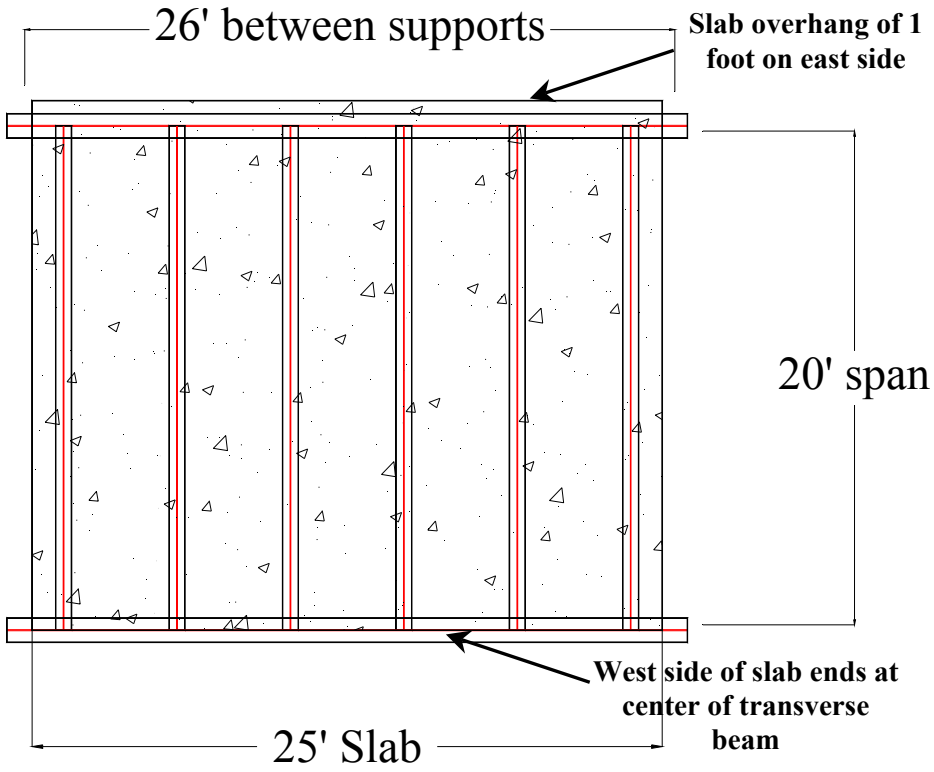

Figure 6.3 Plan view of laboratory model

Note that the east side of the slab overhangs the transverse beam by 1 ft. (see top of Figure 6.3). This was done to approximate the condition of the first deck segment that was field tested in the Llano Bridge. The Llano bridge deck had an identical 1 ft. overhang on the abutment side of the first deck segment. The west side of the slab in the laboratory model ended at the center of the transverse member, as did the slabs in both the Llano and Goliad bridges.

Longitudinal stringers were bolted to transverse beams with double angles (L6x4x3/8). Bolts were used for the connections in the laboratory model, as compared to the rivets used in the actual bridges. The degree of pretension present in the rivets in the actual bridges is unknown. In the laboratory model, the bolts were only snug tightened to simulate the condition of little or no pretension in the rivets.

The W33x130 transverse beams of the laboratory model were placed on spherical bearing base plates to allow end rotation. The base plate was then placed on a load cell, and then, on leveling plates, as shown in Figure 6.4.

The steel was fabricated off site and erected in the laboratory. Steel erection is shown in Figure 6.5 and the finished steel is shown in Figure 6.6 prior to the construction of the reinforced concrete slab.

Figure 6.4 Transverse beam placed on (top to bottom) a swivel plate, a load cell, and leveling plates

Figure 6.5 Connecting of longitudinal stringer to transverse beam

Figure 6.6 Transverse and longitudinal steel beams in laboratory model

The longitudinal stringers were coped at the ends to fit around the top flange of the transverse beams, and positioned to be 1 in. higher to enable embedment into the slab, similar to the condition found in the actual bridges. Figure 6.7 shows the connection between a stringer and beam.

Figure 6.7 Cope detail showing elevated top flange of longitudinal stringer

Concrete design strength was 2.5 ksi, and both longitudinal and transverse reinforcement used #5 bars. 28-day cylinder tests showed compressive strength between 2.3 and 2.5 ksi. Transverse reinforcement was not bent into the "crank bar" configuration used in the actual bridge decks (Figure 2.7). Instead, reinforcement bars were placed at both top and bottom, at the same spacing (approximately 5 in.). Details of transverse reinforcement are shown in Figure 6.8. Longitudinal reinforcing bars were placed as in the Llano Bridge, approximately 13 in, apart, as shown in Figures 6.9 and 6.10.

Photographs of the reinforcing bar placement and concrete pour are shown in Figures 6.11, 6.12, and 6.13.

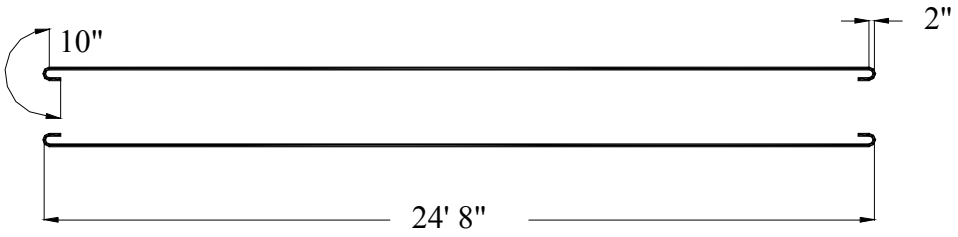

Total Bar Length = 26'

Straight Portion = 24' 4"

(2) 10" Length Hooks

Figure 6.8 Transverse reinforcement

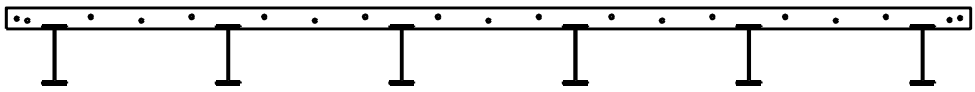

Figure 6.9 Longitudinal reinforcement

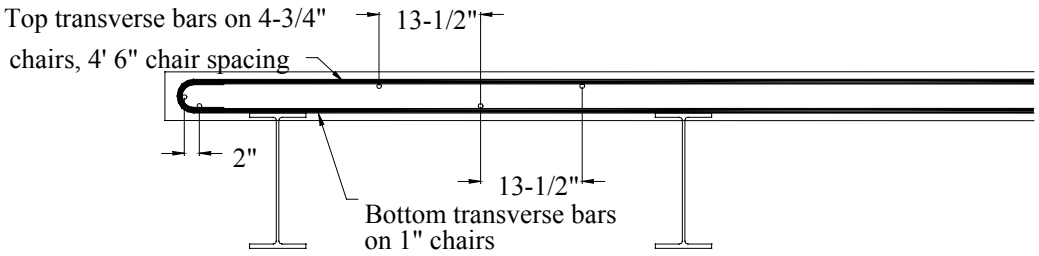

Figure 6.10 Reinforcement details

Figure 6.11 Reinforcing bar placement in slab

Figure 6.12 Concrete pour and finishing

Figure 6.13 Slab construction

Two deep W sections were bolted to four columns anchored to the floor to serve as a loading frame. These large members were positioned longitudinally in the same direction as the longitudinal stringers of the deck model, as shown in Figure 6.14. A smaller W section (labeled A in Figures 6.15 and 6.16) was placed perpendicular to the deep frame members to support two 200 kip hydraulic actuators spaced 6.5 feet apart transversely.

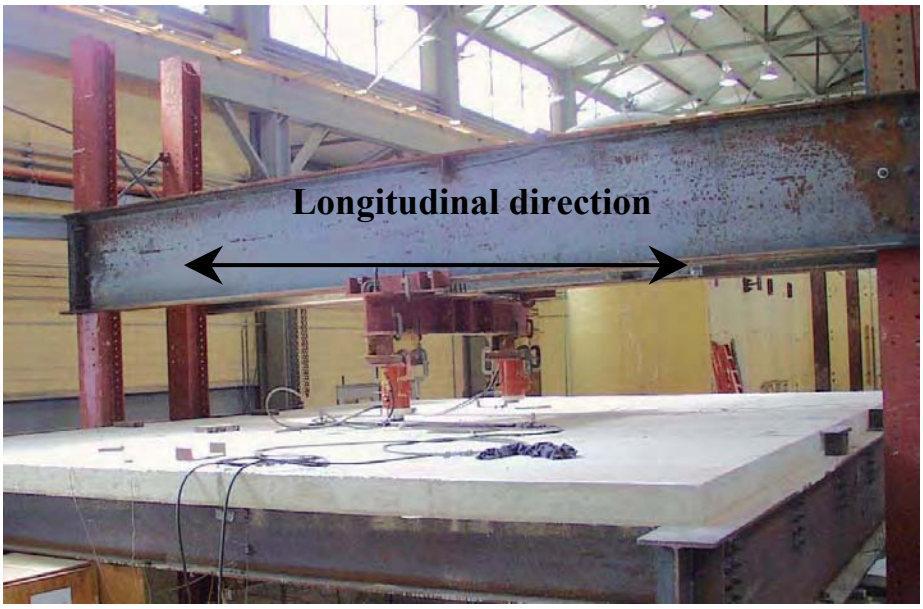

Figure 6.14 Specimen and loading frame

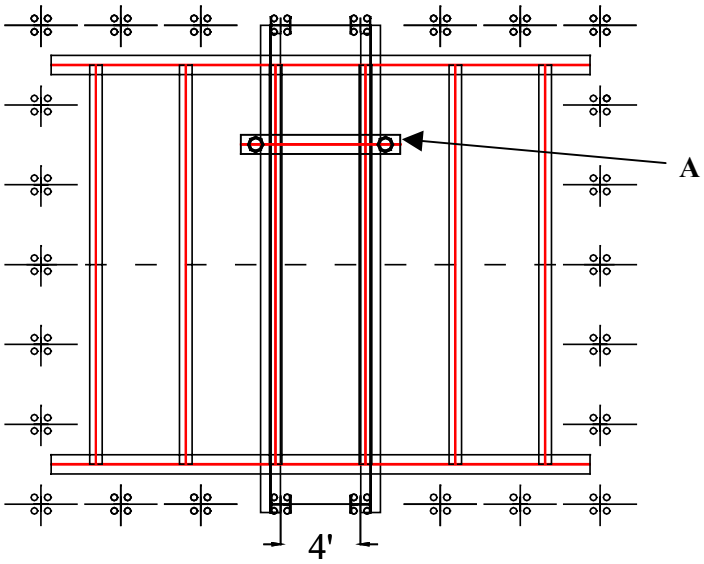

Figure 6.15 Plan view of specimen, loading frame, and surrounding tie down bolt groups

The smaller transverse member on the loading frame was placed on rollers to allow the actuators to travel longitudinally along the frame and hence load at any desired longitudinal position (Figures 6.16 and 6.17). To approximate the double axle configuration (4 rear wheels) of the load truck tandem, two structural tubes were used to spread the load to four rubber pads. The rubber pads, which are shown in Figure 6.18, were 9 in. wide by 12 in. long and 3 in. thick and were spaced 4 ft. apart longitudinally.

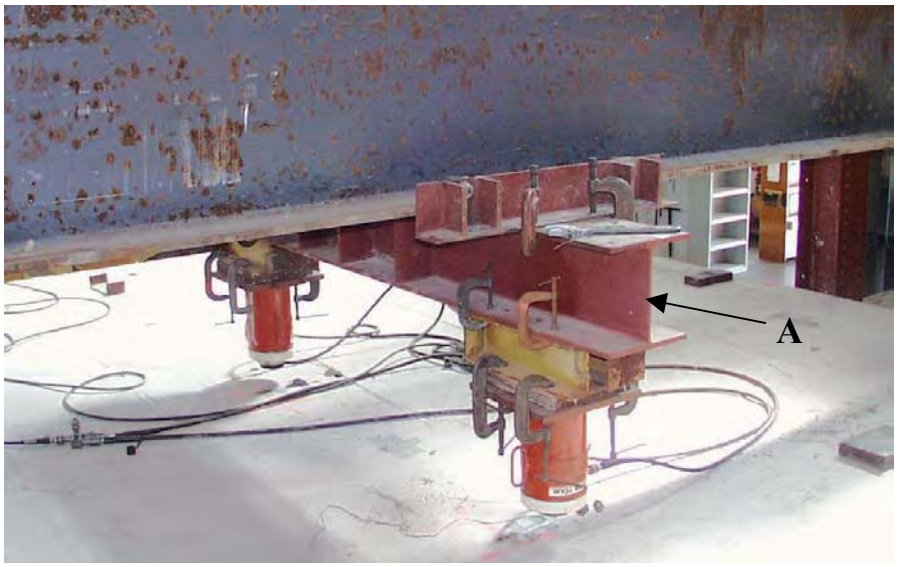

Figure 6.16 Attachment of actuators to load frame

Figure 6.17 Roller attachment of actuators to load frame

Figure 6.18 Approximation of tandem axle with structural tubing and rubber pads

6.3 INSTRUMENTATION

Because of the ease of access to the members and a larger capacity data acquisition system, the model could be instrumented to a much larger degree than possible in the field tests. Strain gages were placed on the inside face of both the top and bottom flanges. Typically, flanges were gaged on both sides of the web for a total of four gages per location. Some of the longitudinal stringers were gaged at the quarter points and midspan, and the transverse beams were gaged at the midpoint between longitudinal member attachments. Figure 6.19 shows the gage layout. Additionally, vertical deflections were measured at the midpoint of each member and vertical reactions were measured at the four supports of the laboratory model (Figure 6.4).

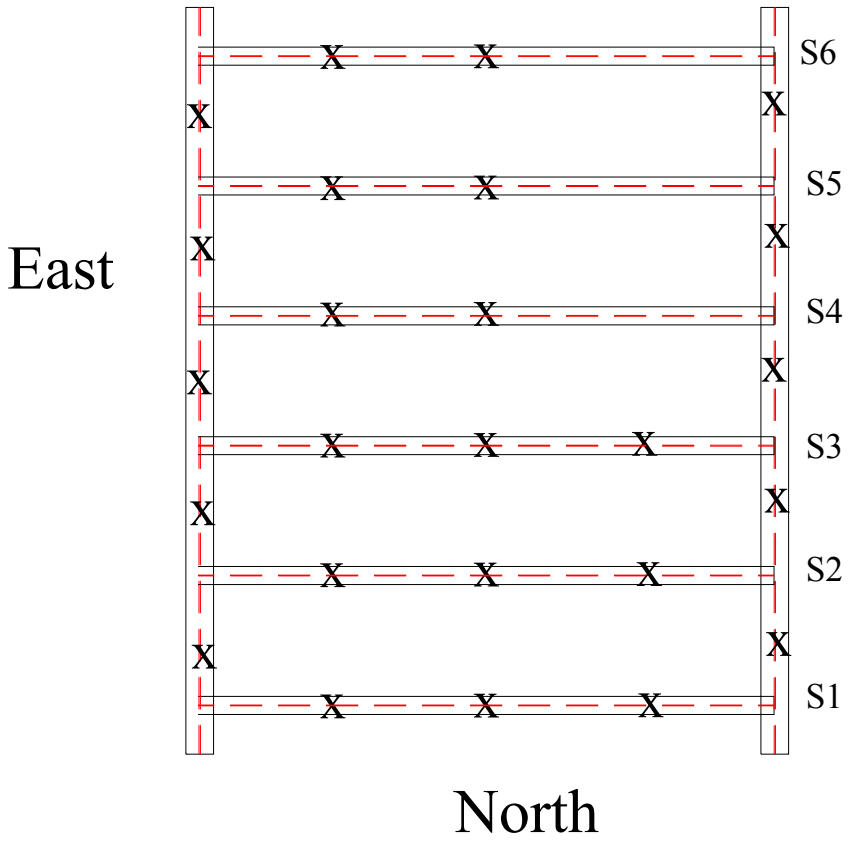

Figure 6.19 Member cross-section locations provided with strain gages

6.3.1 Testing Procedures

East and west transverse beams, and longitudinal stringers S1, S2, and S3 were loaded. Because of symmetry, members S4, S5, and S6 were not directly loaded.

Longitudinal members were loaded with the double axle configuration shown in Figure 6.18. The load of each of the two actuators was split into two loads, 4 ft. apart so as to approximate a tandem axle loading. This produced four equal point loads on the structure. To reproduce the loading in the field tests and in the finite element analysis, each stringer was loaded with one actuator directly on top of the member, and the second 6.5 ft. towards the center of the deck. Longitudinal stringers were tested with actuators positioned at midspan and quarter-span points. Figure 6.20 shows the positioning for centerline loading of the second longitudinal stringer. Transverse beams were loaded with the actuators located as shown in Figure 6.21.

Each of the loaded members (S1, S2, S3, and both the east and west transverse beams) were loaded with hydraulic actuators. The gages were zeroed under dead load only and then loaded in approximately 20 kip increments up to loads ranging between 60 and 100 kips. The deck was then unloaded in one step, and then reloaded in 20 kip increments again. The loading was manually controlled; hence it was not possible to load the structure with exactly the same load each test. Each member was tested twice in this manner.

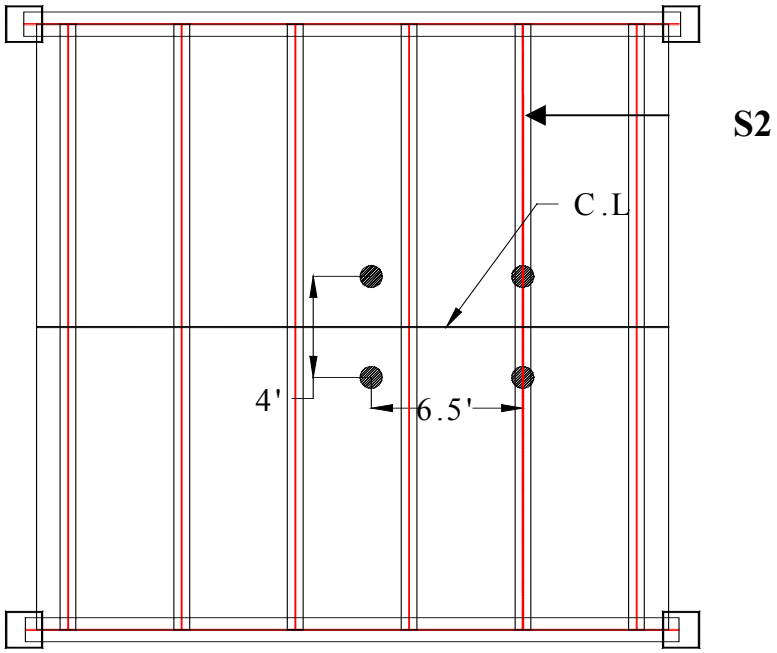

Figure 6.20 Load position for centerline testing of stringer S2

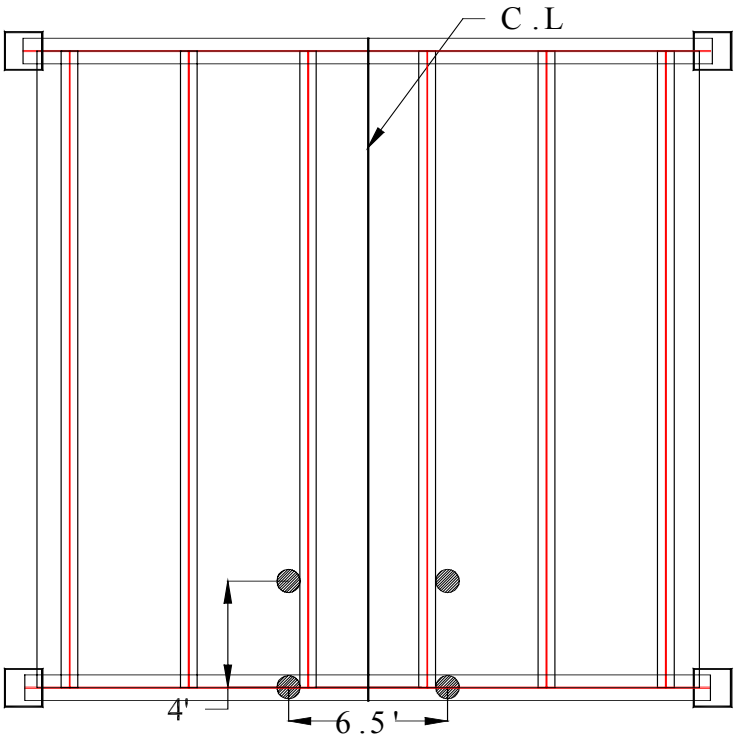

Figure 6.21 Load position for testing of transverse beam

Prior to testing, a finite element model of the laboratory specimen was developed to evaluate the expected response of the specimen. The following section describes the finite element model. This is followed by a description of the test results, and comparison with the predictions of the finite element model.

6.4 FINITE ELEMENT ANALYSIS OF LABORATORY MODEL

6.4.1 Model Definition

The finite element model used in analysis of the laboratory model was very similar to previous models used for analysis of the Goliad and Llano bridge decks. SAP2000 was again employed as the analysis software. Standard two node beam elements were used for the steel members, and four node isotropic shell elements were used to represent the slab. Only a single deck segment was modeled on SAP2000, since only a single deck segment was represented in the laboratory model. Figure 6.22 shows the finite element model.

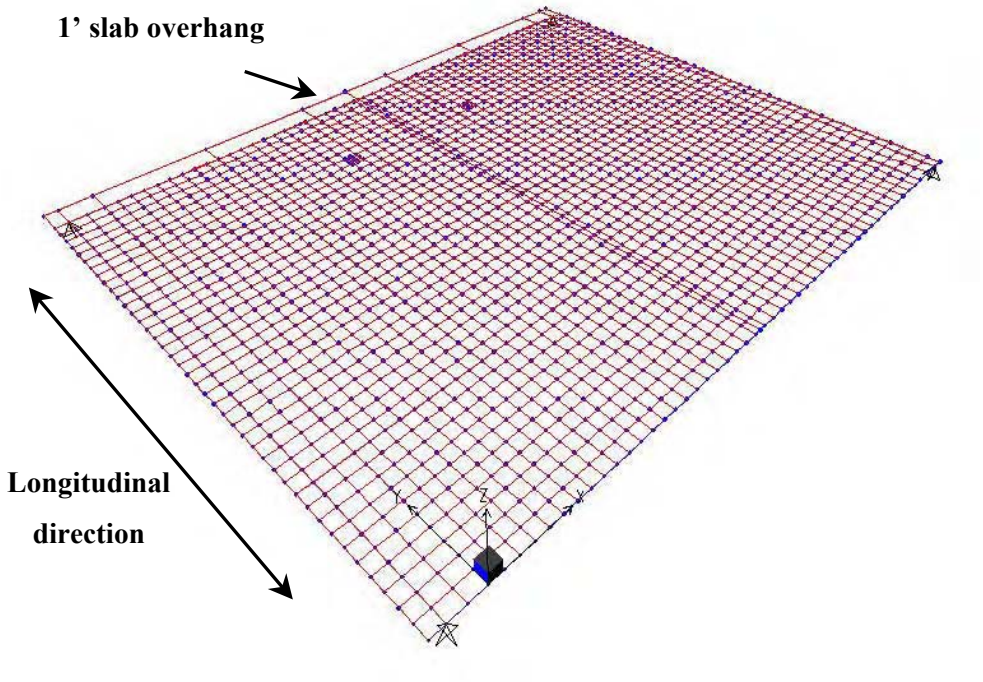

Figure 6.22 Finite element model used for analyzing the laboratory specimen

Load cases were constructed to approximate the loading used in the laboratory testing. A single tandem axle was represented with four nodal point loads, and placed on the center of both longitudinal and transverse members. Nodal loads were spaced 6.5 ft. apart transversely and 4 ft. apart longitudinally. Because of symmetry, only three of the longitudinal members were loaded in the finite element model as well as in the actual laboratory tests. Figures 6.23 and 6.24 show typical load positions for transverse beams and longitudinal stringers.

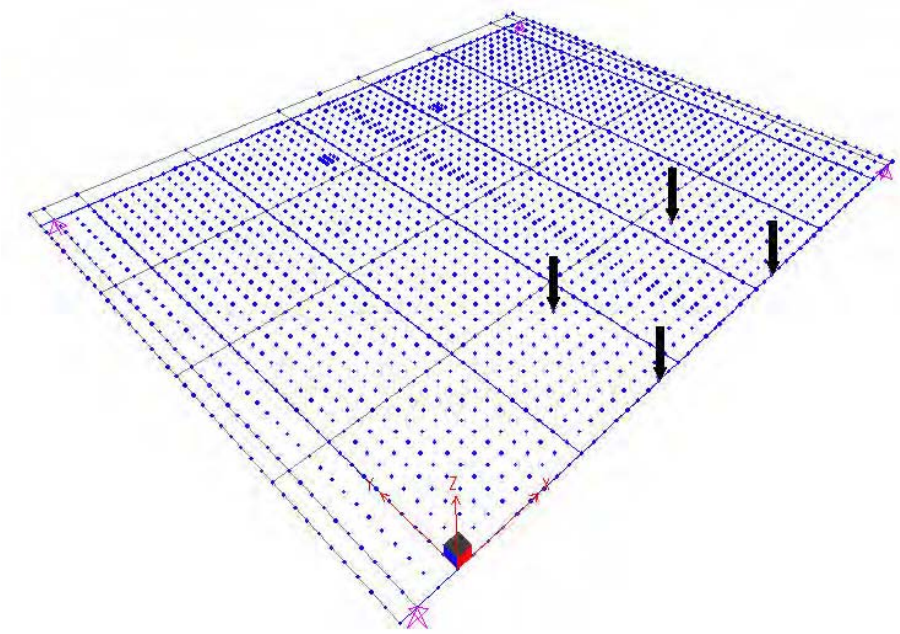

Figure 6.23 Point load position for west transverse beam loading

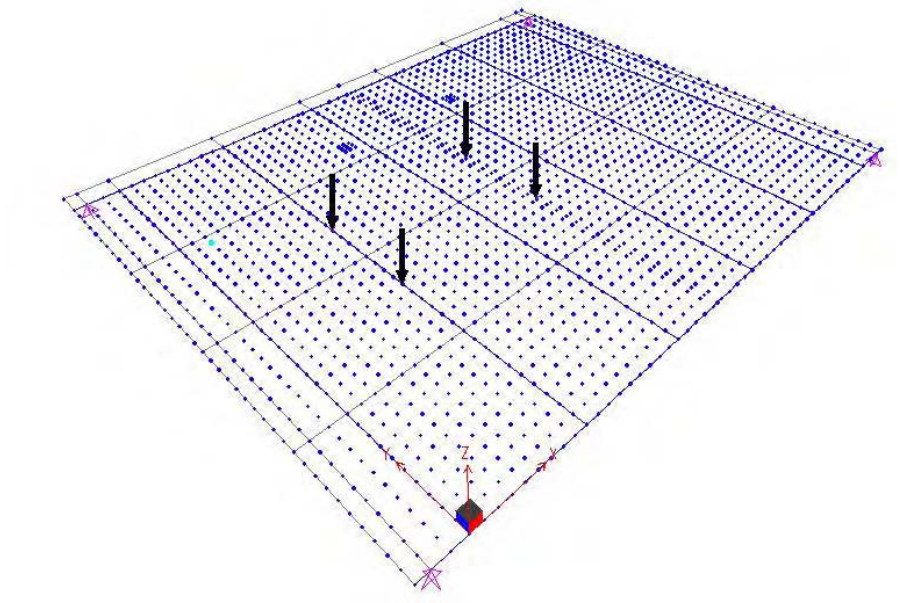

Figure 6.24 Point load position for longitudinal stringer S2 loading

6.4.2 Finite Element Analysis Results

Bending moments and stresses were computed using both conventional AASHTO load rating calculations and using the finite element model. The magnitude of the loading used for the analysis corresponds to a rear axle of an HS20 load vehicle (32 kips). Bending moments predicted by the finite element analysis are listed in Table 6.1. This table includes the maximum moment in each member, the total moment on the entire section, the percent of the total moment carried by the member, the percent of

the total moment carried by the slab, and the distribution factor for each member. The distribution factor was calculated by dividing the moment in the member by the sum of the moments in the members at a cross section, as described in Section 4.6.2.

Table 6.1 Finite element analysis results for laboratory model

Member	Member moment (kip-ft)	Total moment (kip-ft)	Member % of M_{TOT}	Slab % of M_{TOT}	Distribution Factor
S1	47.7	128.0	37.3%	10.9%	0.23
S2	30.1	128.0	23.5%	12.1%	0.18
S3	29.1	128.0	22.7%	12.3%	0.26
East beam	126.7	156.0	81.2%	4.9%	0.90
West beam	126.4	156.0	81.0%	4.6%	0.90

Table 6.2 gives results of the AASHTO and finite element calculations in terms of stresses. The AASHTO calculations for the stringers used the standard AASHTO specified distribution factor of *s*/5.5. The AASHTO calculations assumed no load distribution for the transverse beams, and no load carrying contribution of the slab.

The results in Table 6.2 show a 30 percent to almost 60 percent lower stress for longitudinal stringers when using finite element analysis as opposed to AASHTO calculations. The differences in transverse beam results are not as large, but still approximately 20 percent.

Table 6.2 Comparisons of stress results for finite element and AASHTO calculations

Member	FEA (ksi)	AASHTO (ksi)	Ratio – FEA/AASHTO
S1	6.4	8.9	72 %
S2	4.1	8.9	46 %
S3	3.9	8.9	44 %
East beam	3.7	4.6	80 %
West beam	3.7	4.6	80 %

Despite the different size and length of members in the Llano deck and in the laboratory model, the comparison between finite element analysis and AASHTO calculations for the two cases are quite consistent. Although the percentage of total moment carried by an individual longitudinal stringer compared well in the two cases (approximately 20 to 30 percent), the portion of the moment carried by the slab was on the order of 10 percent less in the finite element analysis of the laboratory model. The ratio between the finite element predicted stresses and the AASHTO predicted stresses was also fairly consistent for the longitudinal stringers, approximately 70 percent for the first stringer, and from 40 to 60 percent for the second and third stringers.

Analysis results for transverse beams were also consistent between the Llano bridge deck and the laboratory model. The beams carried over 80 percent of the total moment, and the slab in both models carried less than 10-percent of the total moment. The ratio of finite element predicted stresses to AASHTO predicted stresses was in the range of 80 percent for both cases as well.

In summary, the trends seen in comparing stress predictions of finite element analysis with conventional AASHTO calculations are very similar between the Llano bridge deck and the laboratory model. For a given loading, the finite element analysis predicts substantially lower stresses in the beams and stringers than AASHTO calculations, with the largest differences occurring in the stringers. The same trends were also seen in the finite element analysis of the Goliad bridge deck.

6.5 LABORATORY TEST RESULTS

6.5.1 General

This section presents results of loading tests conducted on the laboratory model. Results for longitudinal stringers are presented in Section 6.5.2, and results for transverse beams in Section 6.5.3. This is followed by a comparison between laboratory test results and finite element analysis. A large amount of data was collected in the laboratory tests. The following sections do not present all the data, but rather present typical results.

6.5.2 Test results for Longitudinal Stringers

Loading cases for the stringers in the laboratory model were described in Section 6.3.1. Data from strain gages was collected for the tests, and the results were converted to stress. Midspan deflection for all members was recorded as well. Typical results are shown in Figures 6.25 to 6.40. For presentation purposes, both tensile and compressive stresses are shown as positive values. All load cases produced positive bending moment, hence all bottom flange stresses are tensile, and all top flange stresses are compressive. Data showed a near linear response in both stress and deflection as can be seen in Figures 6.25 and 6.26, although a minor degree of nonlinearity can be observed in these plots. To further examine this nonlinearity, Figure 6.27 shows a plot of load versus the ratio of maximum flange stress to load. For linear behavior this ratio should be constant. The plot, however, shows a small increase in stress to load ratio as load increases. The source of this minor nonlinearity is not likely related to yielding in the stringers. Maximum flange stresses are only on the order of 15 ksi (Figure 6.25). Further, if yielding were occurring, the ratio of stress to load would be deceasing at higher loads, rather than increasing, as indicated by the data in Figure 6.27. Minor non-linear response can also be seen in the plot of load versus the ratio of midspan deflection to load in Figure 6.28. This figure shows that the ratio of deflection to load increases slightly as load increases. This indicates that the stringers are becoming more flexible, i.e., their stiffness is reducing at higher load levels. However, as noted above, this small reduction in stiffness does not appear to be due to yielding.

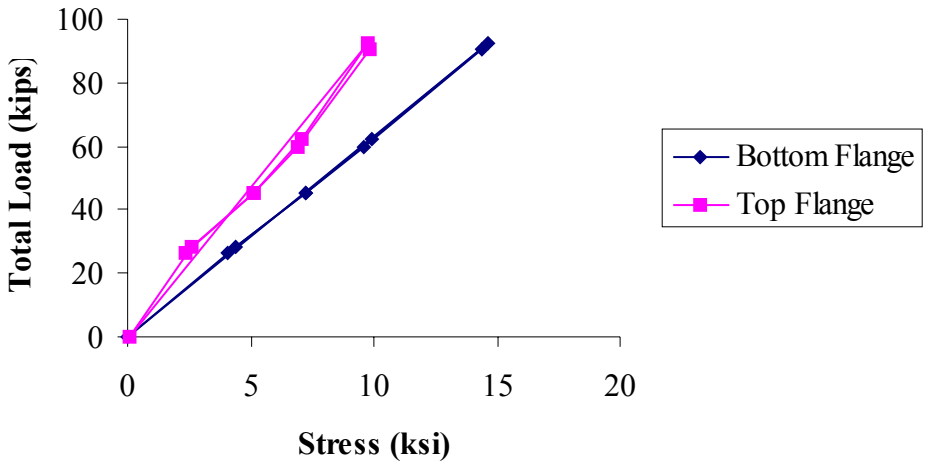

Figure 6.25 Stringer S1: load vs. midspan stress

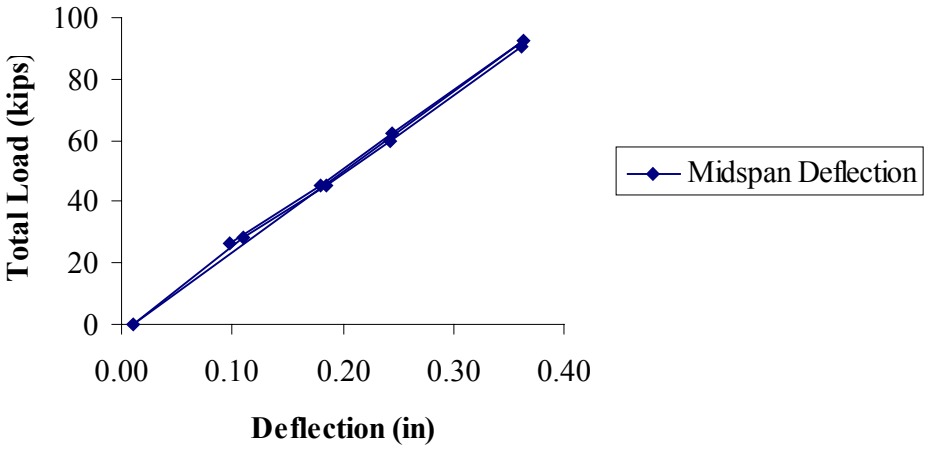

Figure 6.26 Stringer S3: load vs. midspan deflection

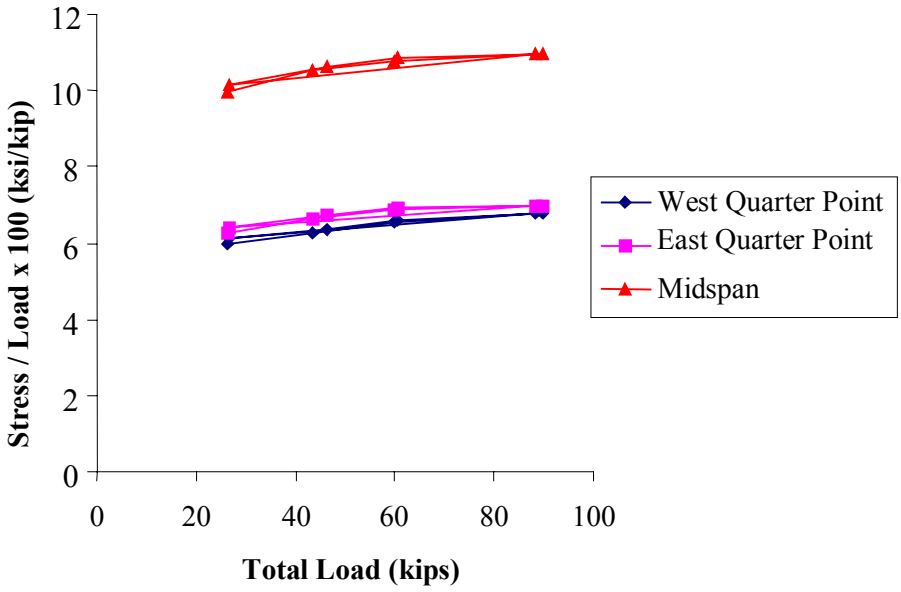

Figure 6.27 Stringer S3: load vs. stress to load ratio

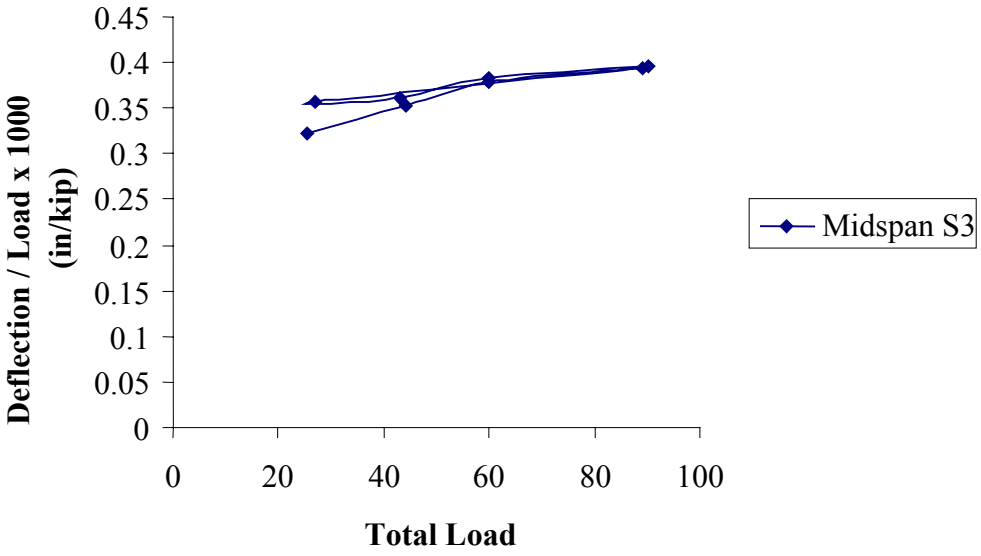

Figure 6.28 Stringer S3: load versus deflection to load ratio

Data from the field tests at Llano and Goliad typically showed the presence of unintended composite action for the stringers. Similar to Llano and Goliad, the stringers of the test specimen also exhibited unintended composite action. The presence of unintended composite behavior for the stringers can be seen in Figures 6.29 and 6.30. Figure 6.29 shows that for any given load, the stress is lower in the

top flange than in the bottom flange for stringer S3. The same phenomenon is also apparent in Figure 6.25 for stringer S1. This same pattern was evident in all instrumented stringers in the test specimen. Figure 6.30 shows the elevation of the neutral axis as load increases for stringer S2. For all load levels, the neutral axis is above mid-depth of the section, indicating the presence of composite action. However, with increasing load, the neutral axis moves closer to mid-depth, suggesting a reduction in the degree of composite action with higher loads. This reduction in composite action can account for the nonlinearity in the load-stress and load-deflection plots described earlier. As the degree of composite action is reduced, the magnitude of of the maximum flange stress for a given load as well as the deflection for a given load would increase. Reduction in composite action is therefore likely responsible for the trends seen earlier in Figures 6.27 and 6.28, which showed an increase in the stress to load ratio and an increase in the deflection to load ratio as load on the stringer increased.

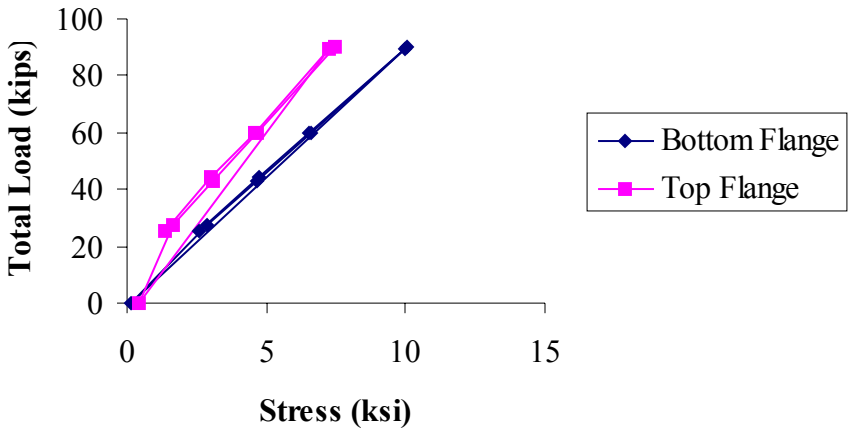

Figure 6.29 Stringer S3: load vs. midspan stress

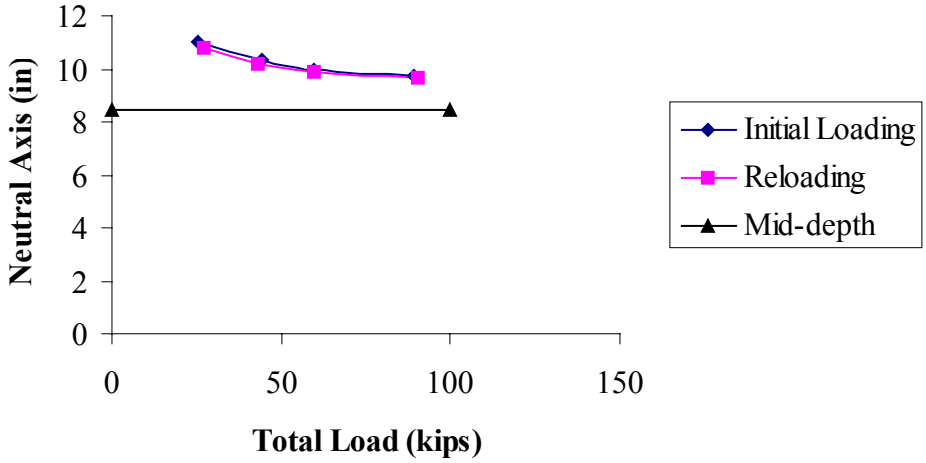

Figure 6.30 Stringer S2: load vs. neutral axis location

Tests were normally each run twice, as described in Section 6.3.1, to evaluate repeatability in the results. Test results were typically very consistent between tests, as indicated by the load versus deflection

and load versus stress plots in Figures 6.31 and 6.32. Results from flange gages on opposite sides of the web were very consistent as well, as can be seen in Figures 6.33 and 6.34.

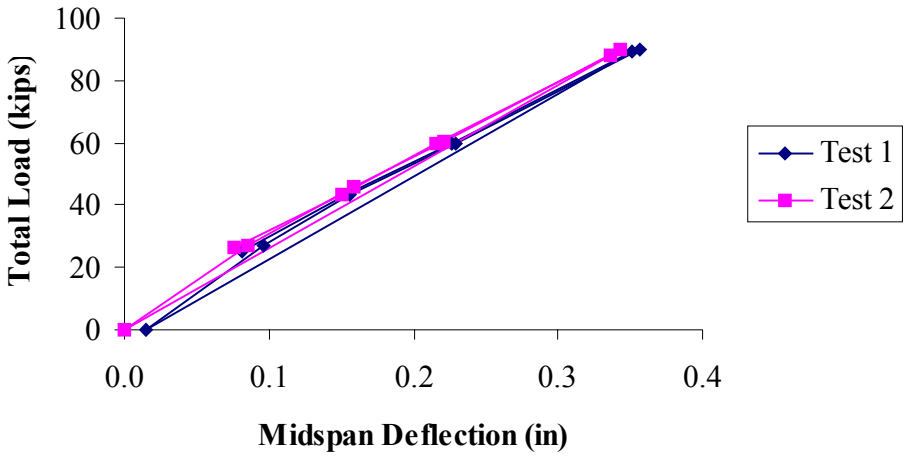

Figure 6.31 Stringer S3: load vs. midspan deflection for tests one and two

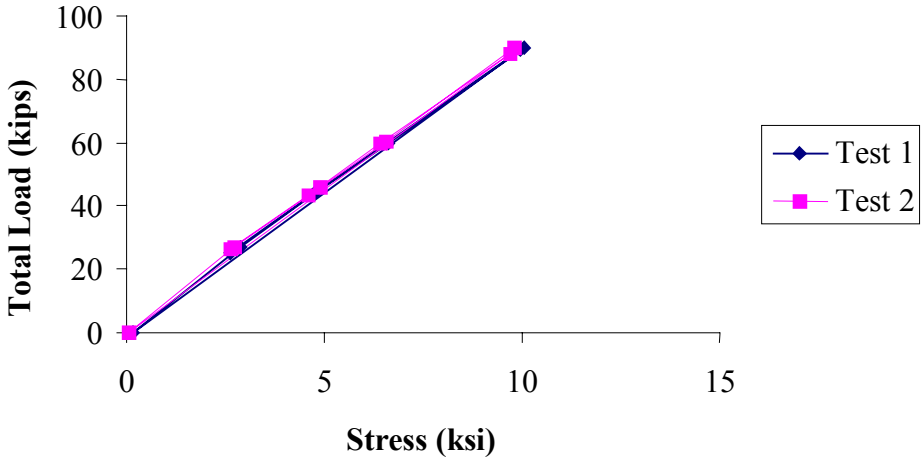

Figure 6.32 Stringer S3: load vs. bottom flange stress for tests one and two

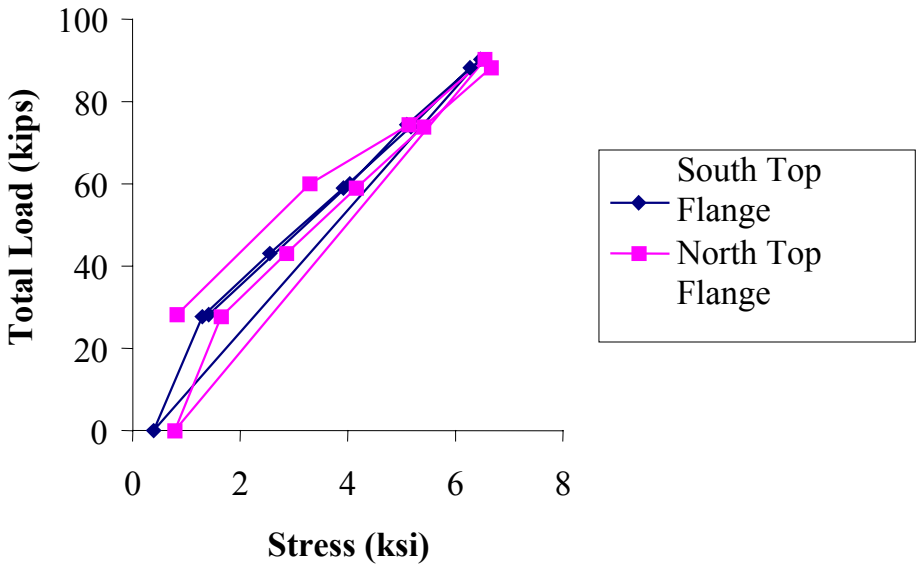

Figure 6.33 Stringer S2: load vs. north and south side top flange stresses

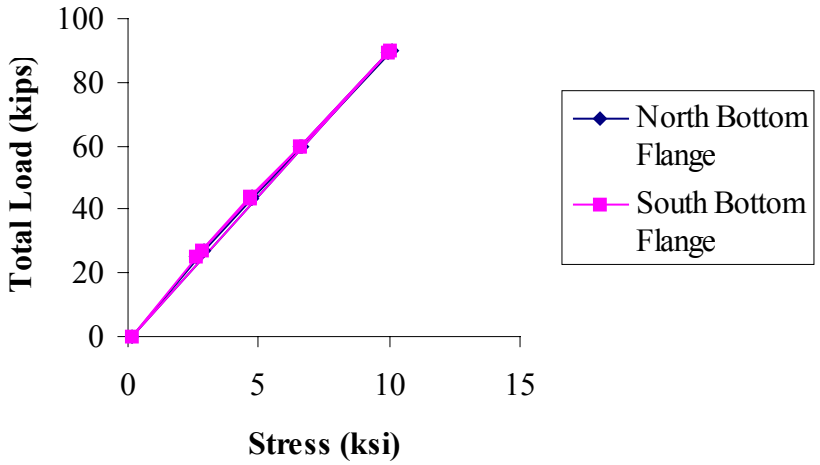

Figure 6.34 Stringer S3: load vs. north and south side bottom flange stresses

Plots of load versus stress for stringers S1 to S3, are shown together in Figure 6.35. The second and third stringers had similar maximum stresses for a given load, while the first stringer (S1) had approximately a 50% higher stress response for similar loads. Recall S1 is the member closest to the edge of the slab and likely benefited less from slab contribution due to the smaller effective width of the slab, as well as having only one adjacent longitudinal member to distribute load to.

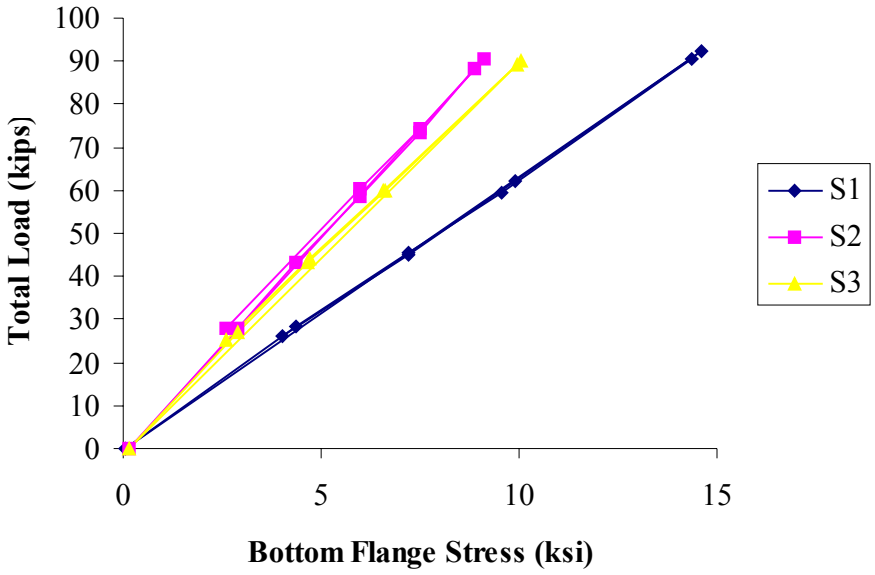

Figure 6.35 Stringers S1 to S3: load vs. stress

Figures 6.36 to 6.38 show the relationship between load and flange stress at the quarter point locations along the length of stringer S3. The same trends are exhibited by the quarter point stresses as for the mid-span stresses. The response between load and stress was mostly linear. However, as with the midspan results, there is a slight increase in stress per unit load as load increases. The quarter point locations along the stringers also exhibited some unintended composite action. This is apparent in Figure 6.38, which shows a higher bottom flange stress than top flange stress.

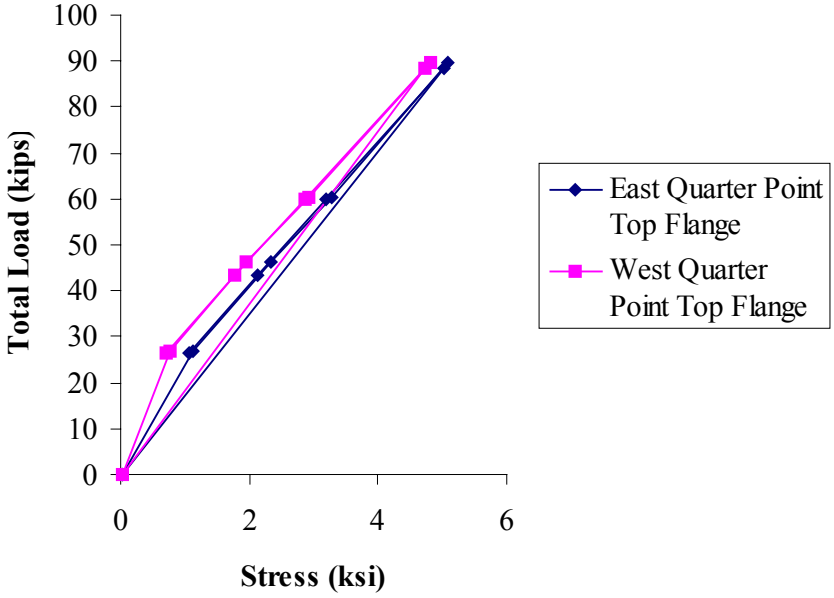

Figure 6.36 Stringer S3: load vs. quarter point top flange stress

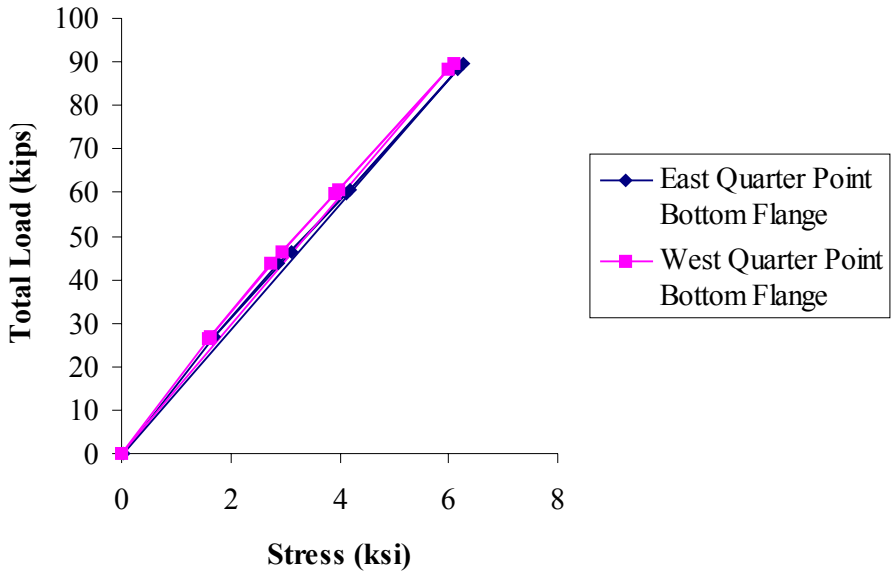

Figure 6.37 Stringer S3: load vs. quarter point bottom flange stress

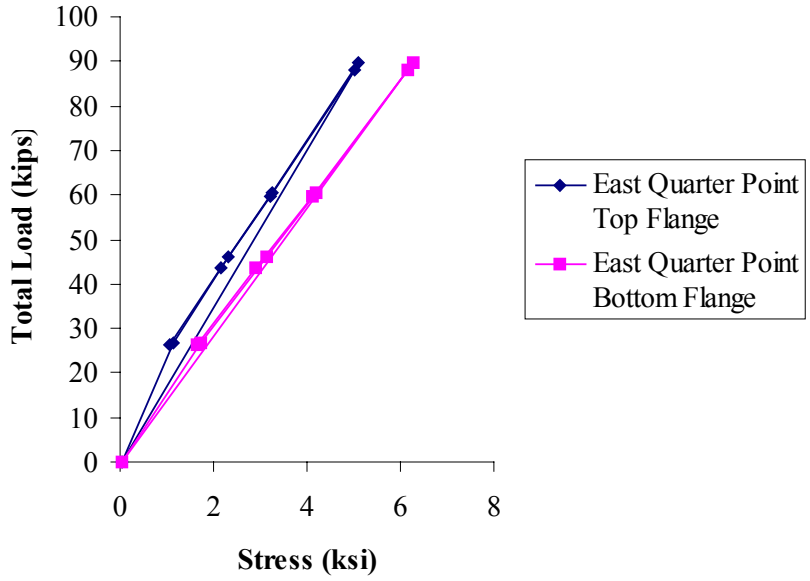

Figure 6.38 Stringer S3: load vs. top and bottom quarter point flange stresses

To examine the degree of composite action present in the stringers, Figures 6.39 and 6.40 show plots of the ratio of bottom flange stress to top flange stress versus load.

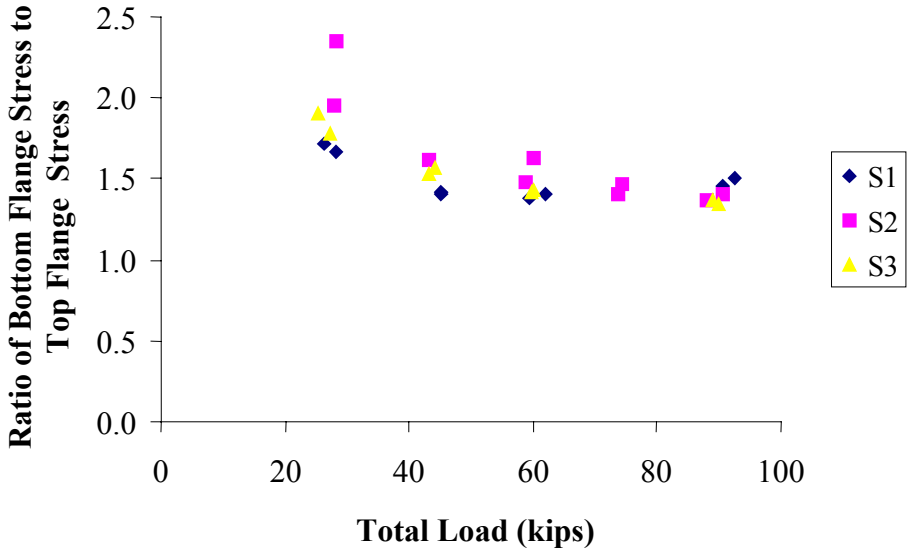

Figure 6.39 Stringers S1 to S3: load vs. bottom to top flange stress ratio

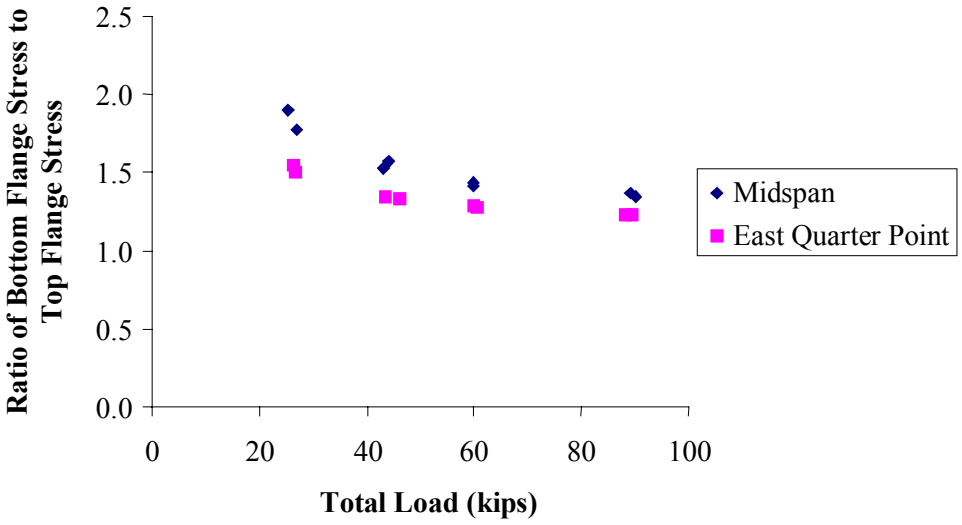

Figure 6.40 Stringer S3: load vs. midspan and quarter point bottom to top flange stress ratios

Figure 6.39 shows results for the midspan stresses of stringers S1 through S3. Figure 6.40 shows a comparison between the stress ratios for the east quarter point and midspan in S3. Both figures show a decrease in the ratio of bottom to top flange stress with increasing load, indicating a reduction in composite action with increasing load.

In a manner similar to Figure 4.22, Figure 6.41 provides an indication of the degree of composite action present in the stringers at maximum load by showing the stress profile over the cross section for the average experimental results compared to both a fully composite stress distribution as well as a non-composite stress distribution.

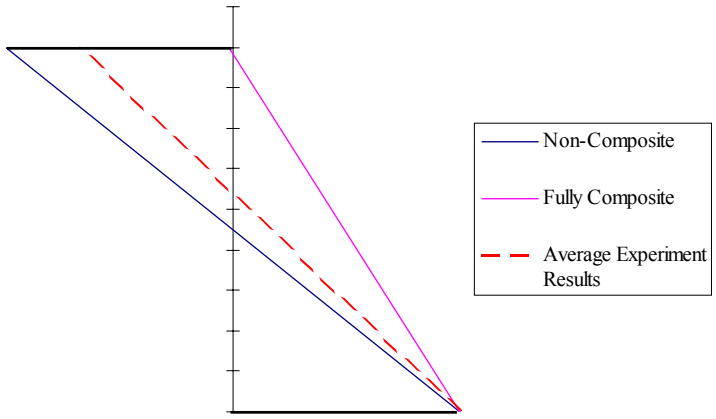

Figure 6.41 Stress profile over section depth

The plot shows the stress distribution over the depth for each case of degree of composite action with a unit bottom stress. As in the field tests, the degree of composite action exhibited by the stringers in the test specimens is relatively small compared to the fully composite case.

6.5.3 Test results for transverse beams

Strain and midspan deflection data were recorded for both the east and west transverse beams under centerline loading, as illustrated in Figure 6.21. As with the longitudinal stringers, each test was run twice. Typical results are shown in Figures 6.42 through 6.49.

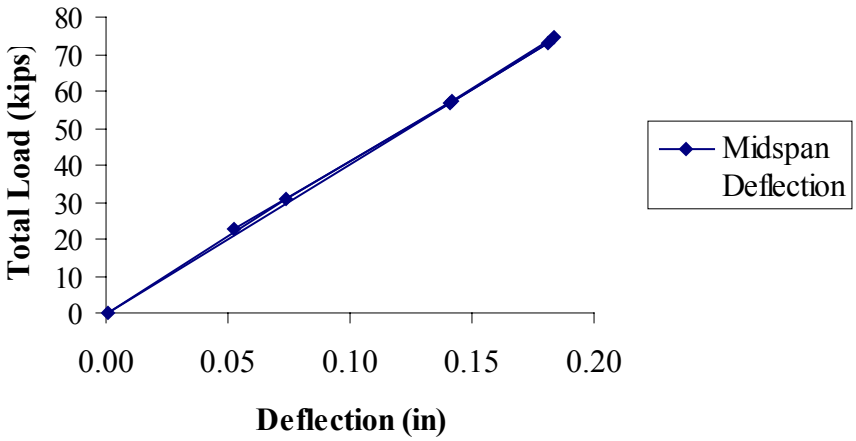

Figure 6.42 East beam: load vs. deflection

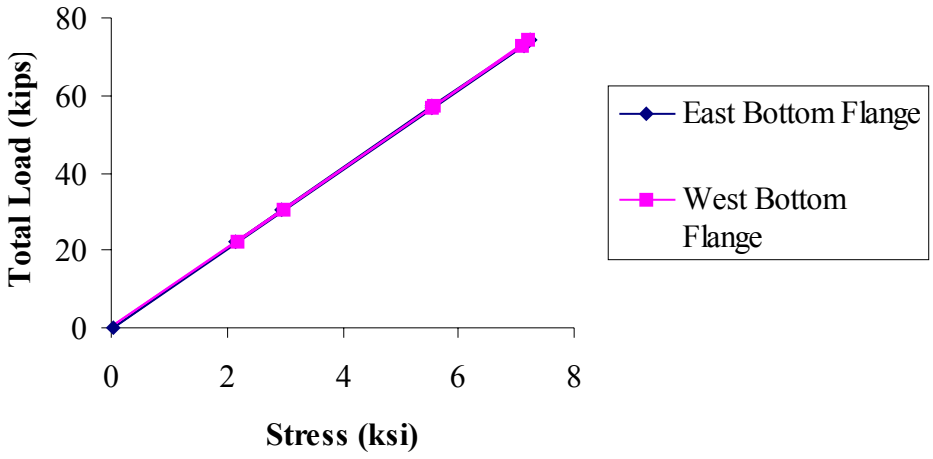

Figure 6.43 East beam: load vs. bottom flange stress

Figures 6.42 and 6.43 illustrate plots of load versus deflection and load versus bottom flange stress for the east beam. Both plots show a very linear response, more so than observed in the response of the stringers (Figures 6.25 and 6.26). Figure 6.44 shows load versus the ratio of deflection to load. This plot shows that the ratio of deflection to load remains reasonably constant with increasing load, as compared to stringers, which showed an increase in the deflection to load ratio with increasing load. Figure 6.45 shows the midspan deflections of both the east and west beams. This plot shows a linear response for both beams, with slightly higher deflections in the west beam for the same load. Recall that the east beam has a one-foot overhang of the slab. This overhang may have contributed to the stiffness of the cross section, and therefore reduced the deflections of the east beam. Figure 6.46 shows a similar higher response for stress in the west beam.

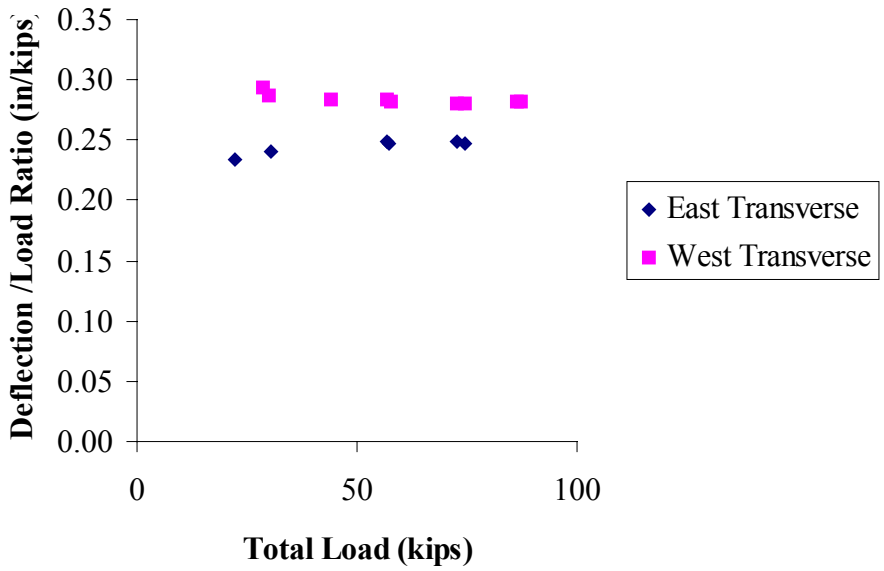

Figure 6.44 East and west beams: load vs. deflection to load ratio

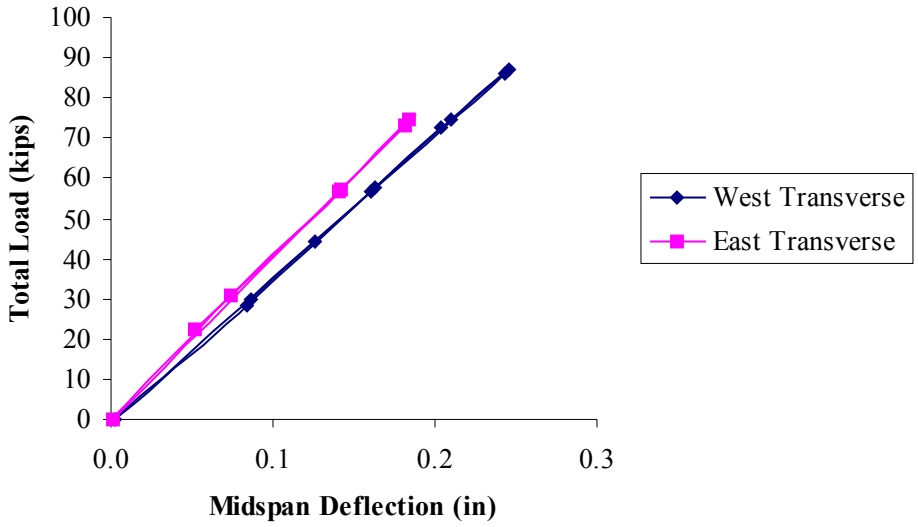

Figure 6.45 East and west beams: load vs. deflection

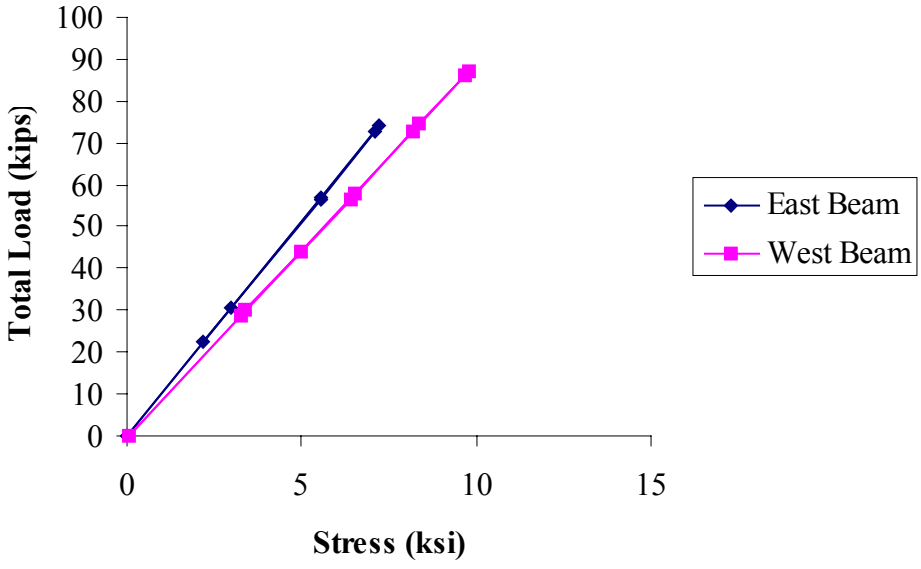

Figure 6.46 East and west beams: load vs. midspan stress

Figure 6.47 shows the load-stress plot for the top and bottom flanges of the west beam. The similar results between the two flanges indicate a nearly symmetrical stress distribution and therefore

little unintended composite behavior. This is reflected in Figure 6.48 as well, which shows the neutral axis location for increasing loads. Similar results are shown for the east beam in Figure 6.49. Consequently, compared to the stringers, the transverse beams showed little unintended composite action. Similar observations were made from the field test data at Llano and Goliad.

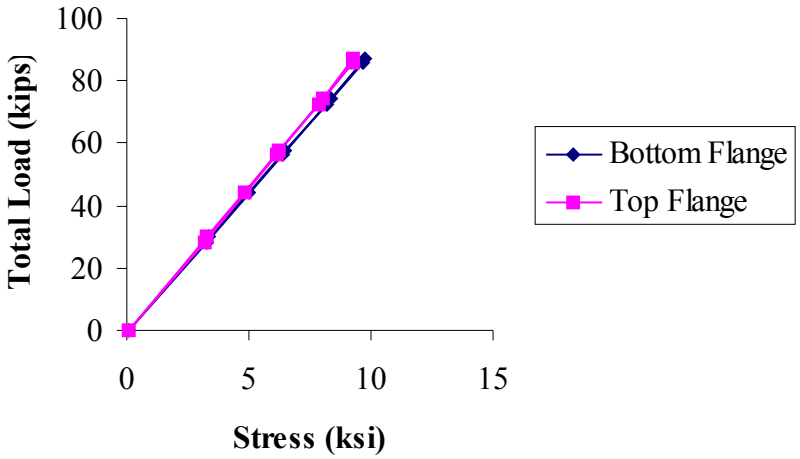

Figure 6.47 West beam: load vs. top and bottom flange stress

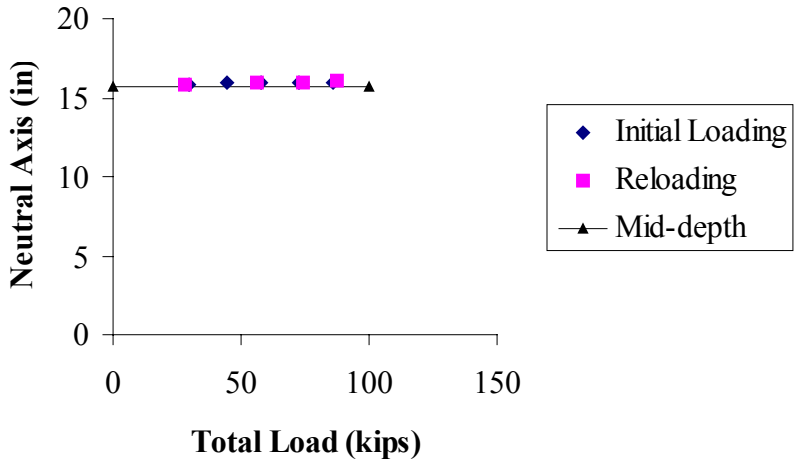

Figure 6.48 West beam: load vs. neutral axis

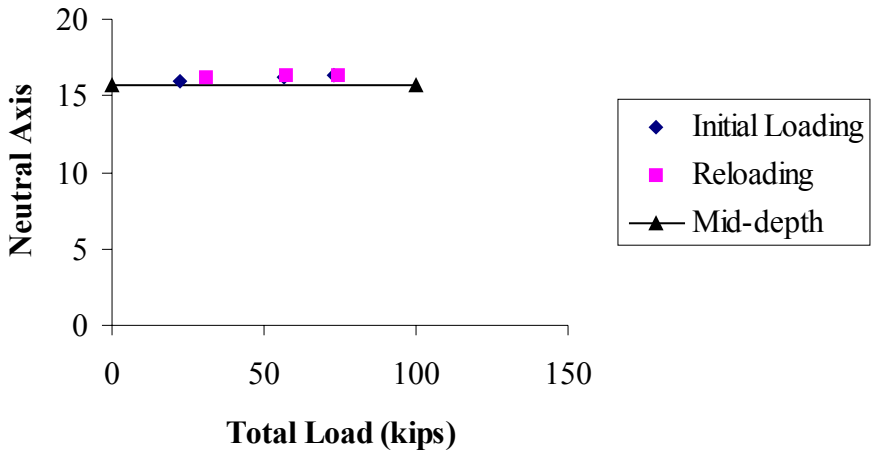

Figure 6.49 East beam: load vs. neutral axis location

6.5.4 Comparison of Experimental Results and Finite Element Analysis

As described in Section 6.4, a finite element model was used to analyze the test specimen under the laboratory imposed loads. Typical results of the finite element analysis are shown in Figure 6.50. This figure shows load versus midspan stress predicted by the finite element analysis for the stringers. These predictions follow the same general trends as exhibited by the laboratory test data. For a given load level, stringers S2 and S3 have similar stress levels, while stringer S1 exhibits approximately 50% higher stresses for the same loads. Figure 6.51 shows load versus deflection plots for the east and west beams predicted by the finite element analysis. Unlike the laboratory test data, the finite element analysis shows very little difference in response between the east and west beams. Experimental results (Figure 6.45) show approximately a 16% higher deflection in the west transverse beam as compared to the east transverse beam. The finite element analysis shows less than a 1% difference between the two beams. Experimental data for stress (Figure 6.46) showed a similar 16% higher stress in the west beam compared to the east beam. Again, the finite element analysis showed less than a 1% difference.

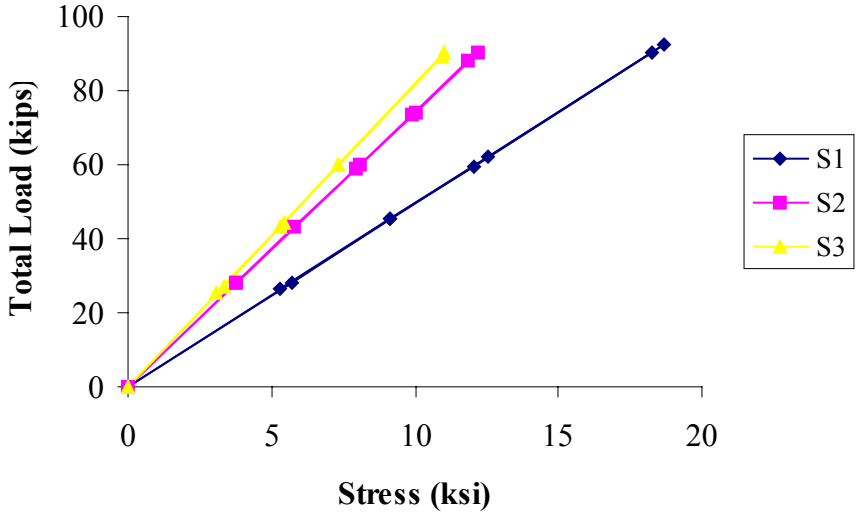

Figure 6.50 Finite element analysis prediction for load vs. midspan stress for stringers

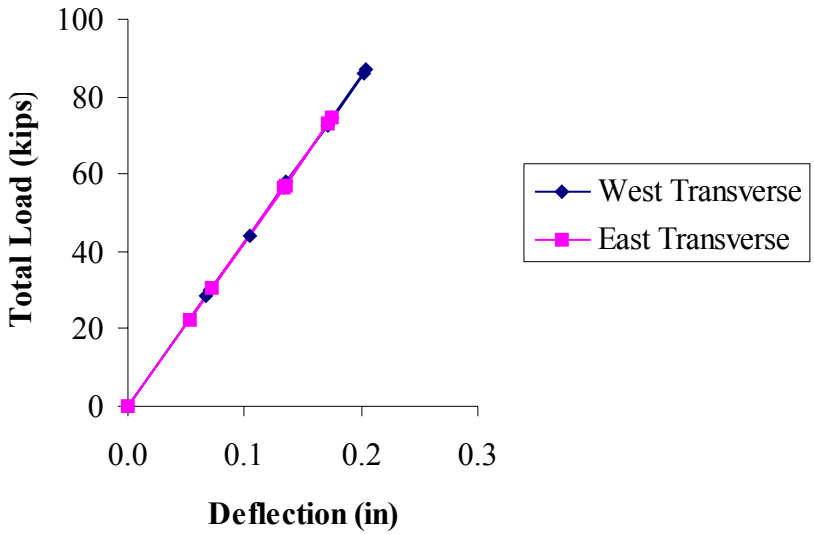

Figure 6.51 Finite element analysis prediction for load vs. deflection for transverse beams

Direct comparisons between predictions of the finite element analysis and the experimental data for the stringers are shown in Figures 6.52 through 6.57. Comparisons are provided both for deflection of the member and for maximum flange stress in the member. For stringers S1 and S2, the deflections predicted by the analysis are very close to and slightly larger than the measured values. Stresses predicted by the analysis are higher than the measured values. This is the same trend that was seen in both the Llano and Goliad field load tests, where stress predictions of the finite element analysis were somewhat higher than field measured values.

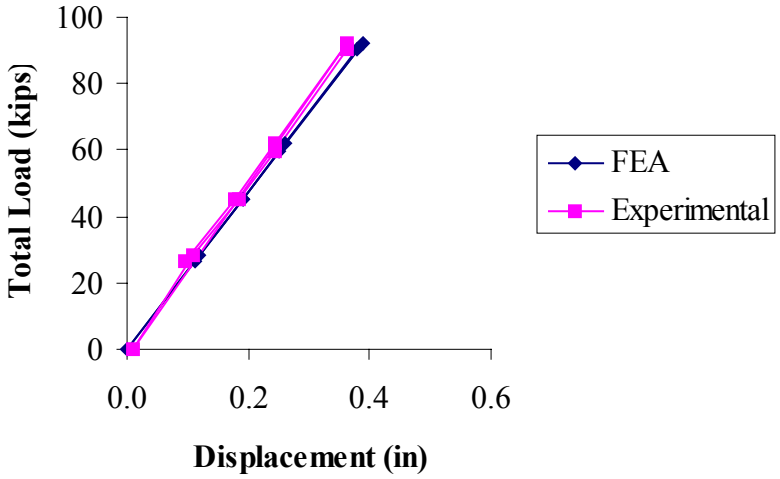

Figure 6.52 Comparison between FEA and experimental data for deflection of stringer S1

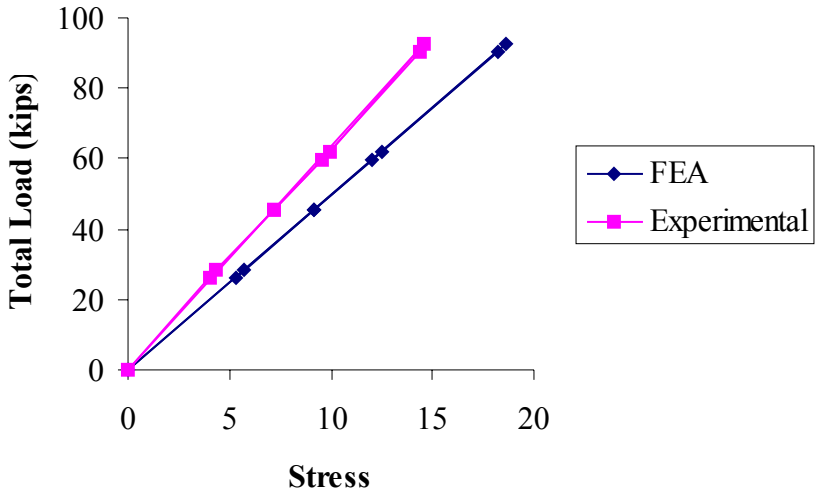

Figure 6.53 Comparison between FEA and experimental data for stress in stringer S1

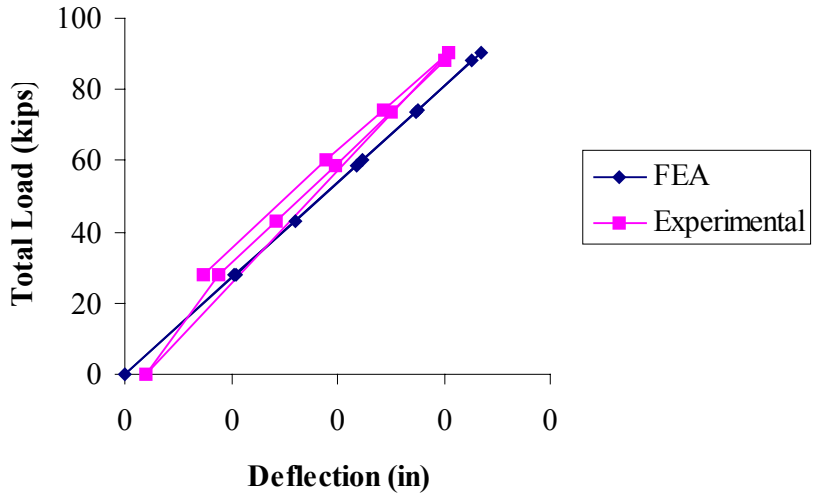

Figure 6.54 Comparison between FEA and experimental data for deflection of stringer S2

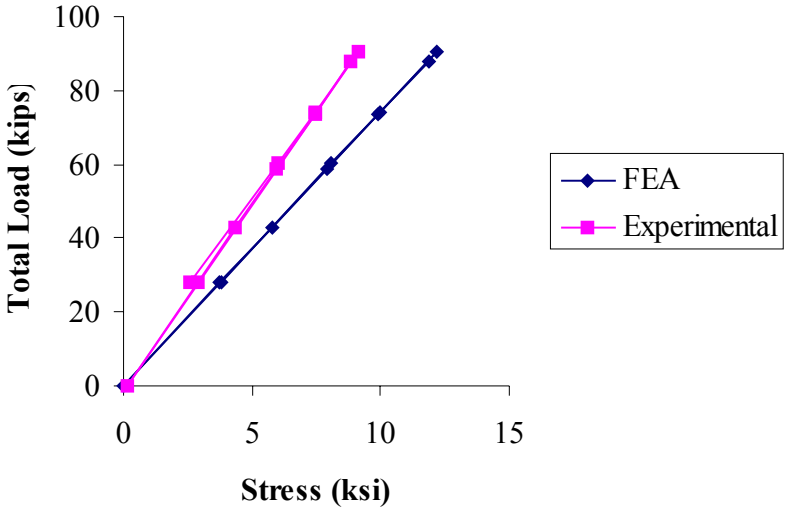

Figure 6.55 Comparison between FEA and experimental data for stress in stringer S2

Of interest to note is that the difference between the analysis and experimental data for deflections of S1 and S2 is smaller than the difference between analysis and experimental data for stresses. For stringer S1, finite element analysis over predicted displacement by 6%, and over predicted stress by 28%. For stringer S2, finite element analysis over predicted displacement by 15% and over predicted stress by 34%. Recall that the finite element model does not include composite action between the steel and concrete, whereas the experimental data for the stringers exhibited some influence of composite action. The absence of composite action in the finite element model likely accounts, at least in part, to the over prediction of both deflection and stress by the model.

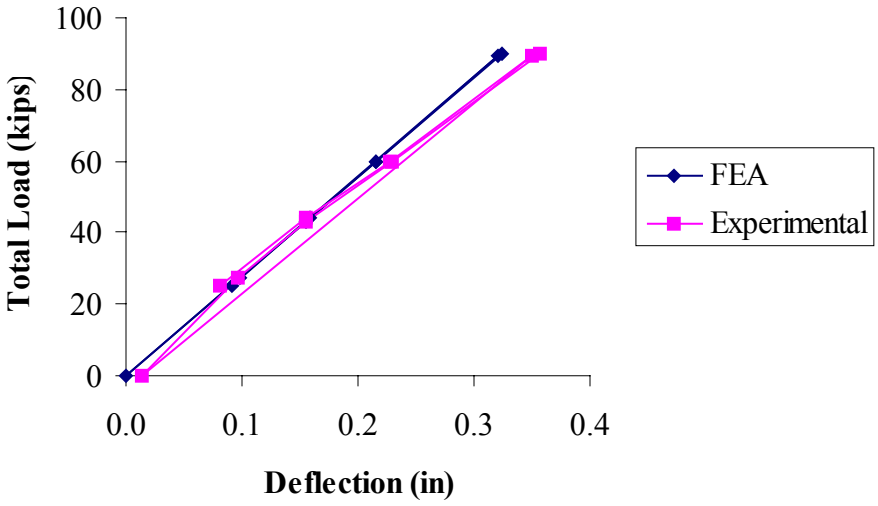

Figure 6.56 Comparison between FEA and experimental data for deflection of stringer S3

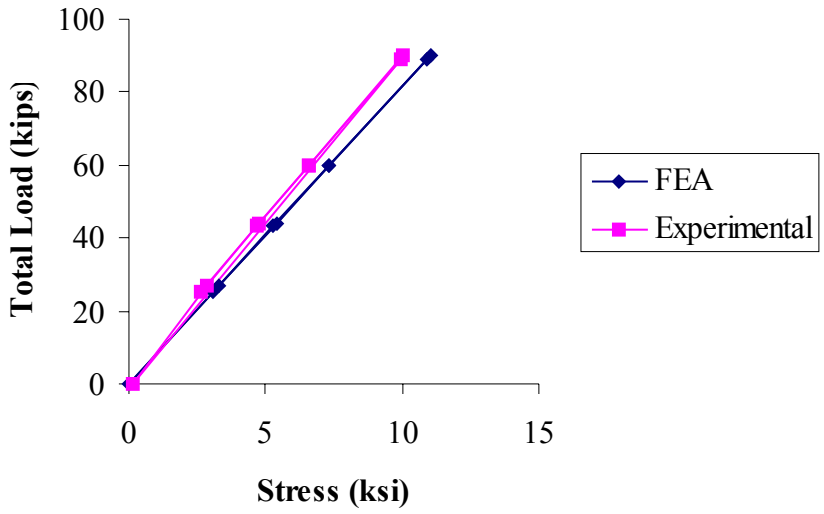

Figure 6.57 Comparison between FEA and experimental data for stress in stringer S3

The difference between the finite element analysis and experimental results was somewhat smaller for S3. Figure 6.56 shows that the analysis predicts deflections within approximately 2% of the measured values. Stresses in stringer S3 from the finite element analysis exceed the measured values by approximately 13%.

A distribution factor for stringer S3 was calculated from the laboratory test data, in a manner similar to that described in Section 4.6.2 for the Llano field test data. The distribution factor for S3 was computed as the maximum stress in S3 divided by the sum of the maximum stresses in all the stringers, for the load case producing maximum stress in S3. Table 6.3 compares the distribution factor from the experimental data with that based on the finite element analysis and based on AASHTO load rating procedures. The same comparison is shown for the distribution factor for stringer S3 in the Llano field test. The distribution factors based on measured stresses are quite similar between the laboratory bridge deck model and the actual Llano bridge deck. Further, both for the laboratory model and for the Llano bridge deck, the finite element analysis predicts the measured distribution factors significantly more accurately than standard AASHTO distribution factors.

Table 6.3 Distribution factor comparison for stringer S3

	DF (AASHTO)	DF (FEA)	DF (Experimental)
Laboratory	0.41	0.29	0.28
Llano field test	0.41	0.26	0.31

Figures 6.58 through 6.61 show the comparisons between finite element analysis and experimental data for the transverse beams. The finite element analysis predicted deflections that were close to but somewhat smaller than the measured values, and predicted stresses that were close to but somewhat larger than the measured values. Both for the longitudinal stringers and for the transverse beams, an important observation is that the finite element model predicts stresses that are close to but somewhat larger than the measured values. The same observation holds for the Llano and Goliad field tests. Since stresses are the key response quantity for load rating (as opposed to deflections), this suggest that load ratings based on finite element analysis will provide a conservative result.

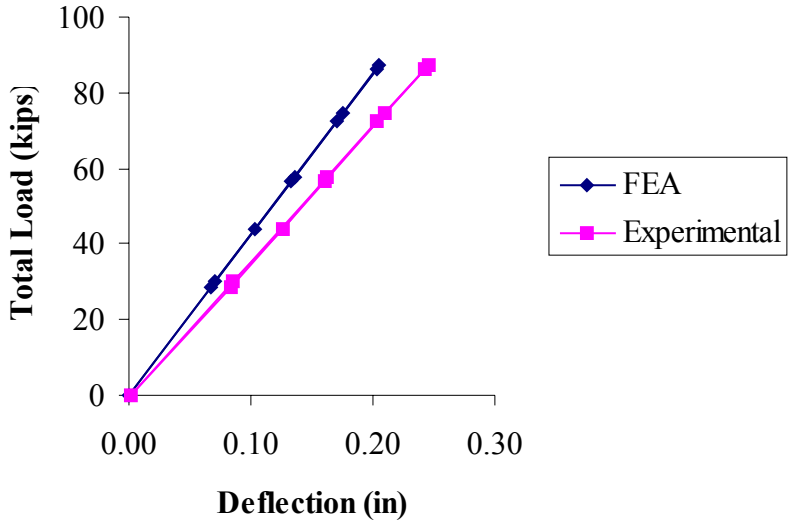

Figure 6.58 Comparisons between FEA and experimental data for deflection of west beam

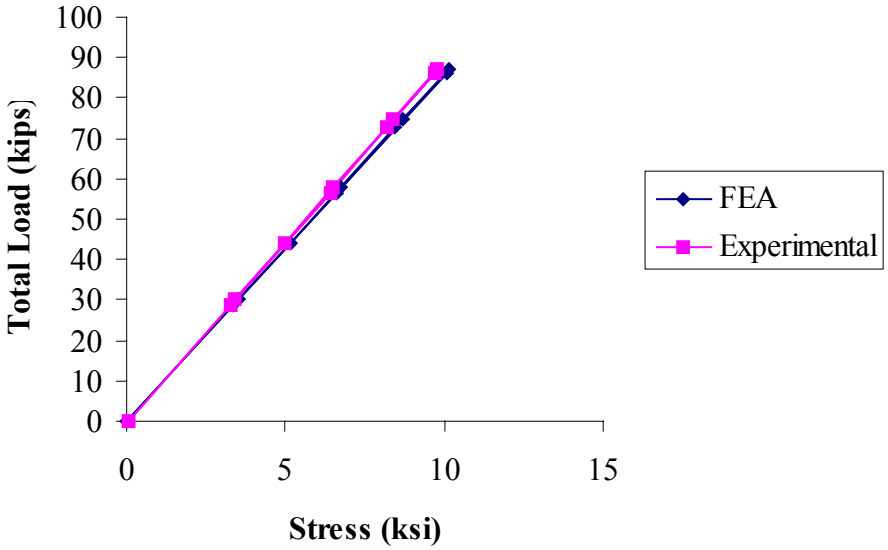

Figure 6.59 Comparison between FEA and experimental data for stress in west beam

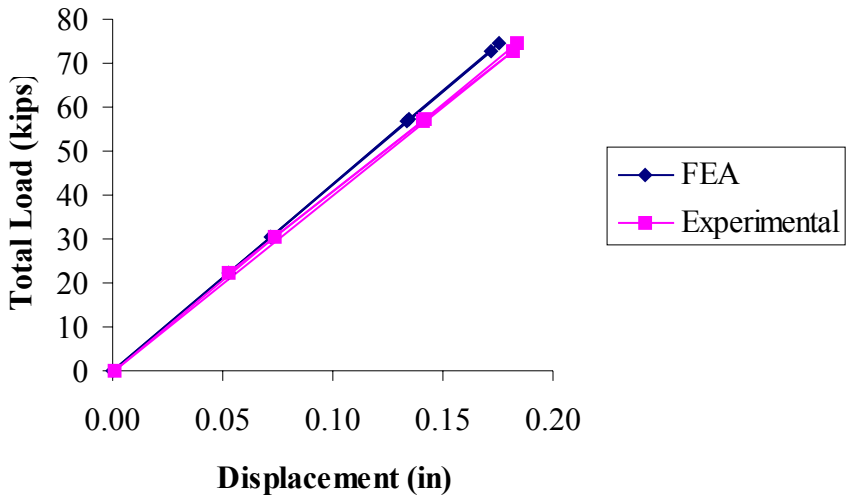

Figure 6.60 Comparison between FEA and experimental data for deflection of east beam

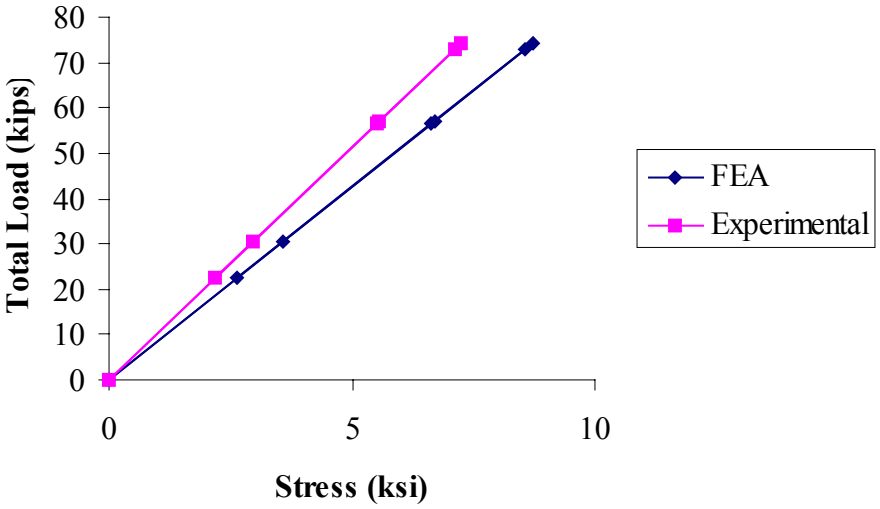

Figure 6.61 Comparison between FEA and experimental data for stress in east beam

6.5.5 Comparisons to Goliad Field Test Results

A clear trend seen in the Llano and Goliad field tests is that the measured stresses were lower than predicted either by AASHTO calculations or by finite element analysis. Further, the stresses predicted by the finite element analysis were significantly closer to the measured values than AASHTO calculations. These same trends were also clear in the laboratory testing. The laboratory deck model had simple well defined boundary conditions, as opposed to the actual bridge decks, where the deck support and boundary conditions were more complex. Comparisons between the lab and field results were examined to reaffirm that factors such as railings, curbs, end restraint, and other unidentified sources of

strength not present in the laboratory model did not play a significant role in the field response. If the field and laboratory responses were comparable, then it could be more reasonably concluded that the increased strength was due to slab contribution and load distribution effects, not the other factors noted above.

Since the members were not identical, an exact comparison between the laboratory and field test results is not possible. However, the spans in the Goliad bridge and laboratory model were equal, and the loading conditions in the laboratory were closer to the Goliad than the Llano field test. Hence the Goliad test is used in the comparison to the laboratory work. The Goliad field test results were compared to the laboratory results in only a general way, since the difference in parameters involved precluded any exact, definitive comparisons.

Comparisons are made between centerline (tandem centered transversely) loading cases. Since the laboratory model's transverse loading had the rear most axle of the tandem over the member (Figure 6.21), the same tandem position was used for comparing results in the field test. Given that the maximum response in the field test was due to the rear tandem straddling the transverse member, the response used in the comparisons was lower than the maximum response. In other words, for comparison, the response used was when the truck was 2 ft. further longitudinally than for the maximum response. These positions are shown in Figure 6.62.

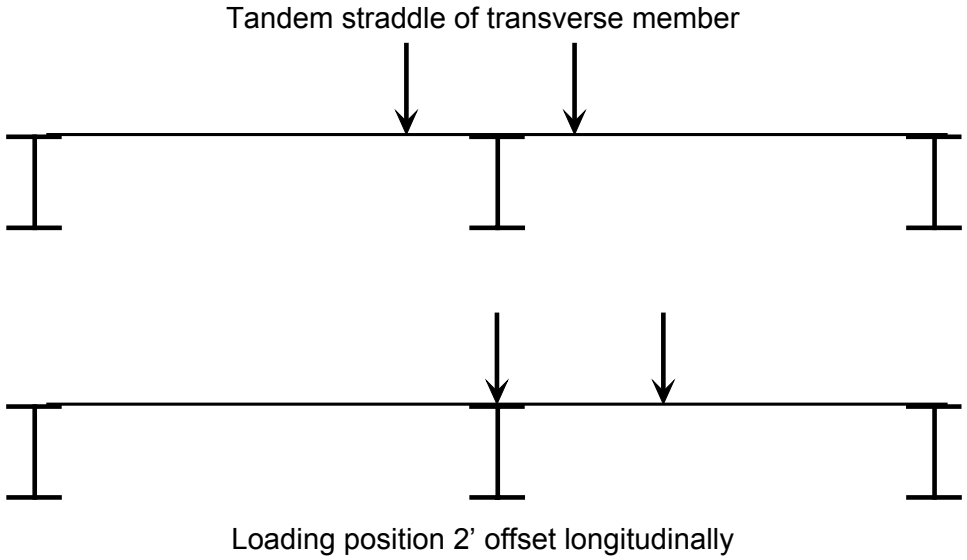

Figure 6.62 Loading position for maximum response (top) and loading position used for comparison with laboratory loading (bottom)

Since the members in the field differed slightly from the laboratory members, the stresses in the laboratory work were simply scaled up by a ratio of the individual member's section modulus $\left(\frac{S_{x\,lab}}{S_{x\,field}}\right)$ as shown in Table 6.4. Table 6.5 gives a general comparison between the laboratory and Goliad field results for specific tests.

Table 6.4 Comparison of member properties

Member section modulus (in^3)		
	Transverse	**Longitudinal**
Laboratory model	406	88.9
Goliad bridge	385	82.3
Ratio (lab/field)	1.05	1.08

Table 6.5 Stress comparisons between field and lab test results

Laboratory			**Field**		
Longitudinal Stringer			**Longitudinal Stringer**		
Load (k)	**Top Flange Stress (ksi)**	**Bottom Flange Stress (ksi)**	**Load (k)**	**Top Flange Stress (ksi)**	**Bottom Flange Stress (ksi)**
28.2	-2.0	3.7	28.6	-1.7	2.7
59.8	-5.4	7.9	57.3	-4.5	5.9
Transverse Beam			**Transverse Beam**		
Load (k)	**Top Flange Stress (ksi)**	**Bottom Flange Stress (ksi)**	**Load (k)**	**Top Flange Stress (ksi)**	**Bottom Flange Stress (ksi)**
28.0	-3.1	3.1	28.6	-2.8	2.8
57.9	-6.0	6.3	57.3	-6.1	6.3

The data in Table 6.5 show a reasonably close correlation for the transverse beam, and a lesser degree of correlation for the longitudinal stringer. Longitudinal stringers are more difficult to compare directly because of the differing degrees of composite action present between the laboratory model and the Goliad bridge deck. However, the results are generally within 10% to 35% for the longitudinal stringers, and within 10% for transverse beams. In each case, the laboratory results showed higher stresses.

Possible reasons for the differences between the laboratory tests and the Goliad field tests include:

1. The laboratory model slab was more heavily reinforced, using both top and bottom reinforcing bars instead of single bent bars.
2. Laboratory longitudinal member end connections were not tightened, and a small end restraint may have been present in the field.
3. Concrete strength in the field was unknown, the compressive strength estimated based on AASHTO guidelines.
4. Although the loading in the laboratory used an approximation of a tandem axle, the actual load vehicles contact area was larger, and had 8 contact points instead of four. This would spread the loading further in the field than in the model.

5. Exact truck location during the test is based on a constant vehicle speed, and judgment of participants in the field tests. Very precise transverse and longitudinal location was not possible. The controlled environment of the laboratory made load location more accurate.

6.6 RETROFIT OF LABORATORY MODEL

6.6.1 Retrofit Scheme

The results of the various tests and analyses conducted for the Llano and Goliad bridge decks as well as for the laboratory model consistently show that the load rating of the bridge decks can be increased through the use of improved structural analysis, specifically by finite element analysis, or by field load testing. In some cases, however, this improved load rating may still fall short of the desired load rating. For such cases, some degree of strengthening may be needed for selected bridge deck members. Consequently, as the final step in this investigation, a simple strengthening measure was examined using the laboratory bridge deck model. The trial method selected for strengthening was the addition of shear connectors between the steel beams and concrete floor slab. As described earlier, the existing decks in the Llano and Goliad bridges have no shear connectors, and similarly the laboratory model was constructed without shear connectors. As the field and laboratory test data show, a small degree of composite action is developed in these bridge decks, likely due to friction between the top of the steel beams and the bottom of the concrete slab. However, both the field test and experimental data suggests that this unintended composite action may be reduced due to slip at higher load levels, and therefore does not appear to provide a reliable or predictable source of additional strength. The addition of shear connectors was therefore investigated as a means to add a reliable and predictable degree of composite action to the bridge deck. The addition of shear connectors was also considered an attractive option for strengthening a historic steel truss bridge due to the rather minimal visual impact on the bridge.

The stiffness and strength of a composite system is far greater than a non-composite system. For full composite action in the laboratory model, the longitudinal stringers would have an increase in moment of inertia of 2.76 times the moment of inertia of the bare steel alone (2,210 in^4 versus 800 in^4). The transverse beams would have an increase of 2.27 times the moment of inertia of the bare steel alone (15,256 in^4 versus 6,710 in^4). Analysis of both the Llano and Goliad bridge deck members indicated that the transverse beams were the controlling members in the load rating. Consequently, strengthening measures were examined for the transverse beams in the laboratory model.

Many schemes were considered for post-installing shear connectors between the transverse steel beams and the concrete slab. A key issue in the choice of strengthening technique was constructabilty. A scheme was developed that permitted the installation of shear connectors from underneath the slab, so as to avoid any disruption to traffic on the bridge. The strengthening scheme that was ultimately chosen is shown in Figures 6.63 through 6.70.

Threaded studs with a diameter of 3/4-inch were welded to the inside top flange at the end of the transverse beams, between the connections of the two outermost longitudinal members, as shown in Figures 6.63 and 6.64. A 1/2 inch thick steel plate with holes drilled corresponding to the location of the welded threaded studs was then bolted to the flange, with approximately 6 inches of the plate protruding beyond the edge of the flange. To accommodate the weld metal at the base of the threaded stud and any slight misalignment in placing the studs, the holes in the plates were 1-1/4 inch in diameter. Since the plate was bolted to the bottom side of the top flange, and the slab rested on the topside of the top flange, the corresponding gap (equal to the thickness of the top flange, 0.855 inches) between the plate and slab was filled with grout, as shown in Figure 6.65.

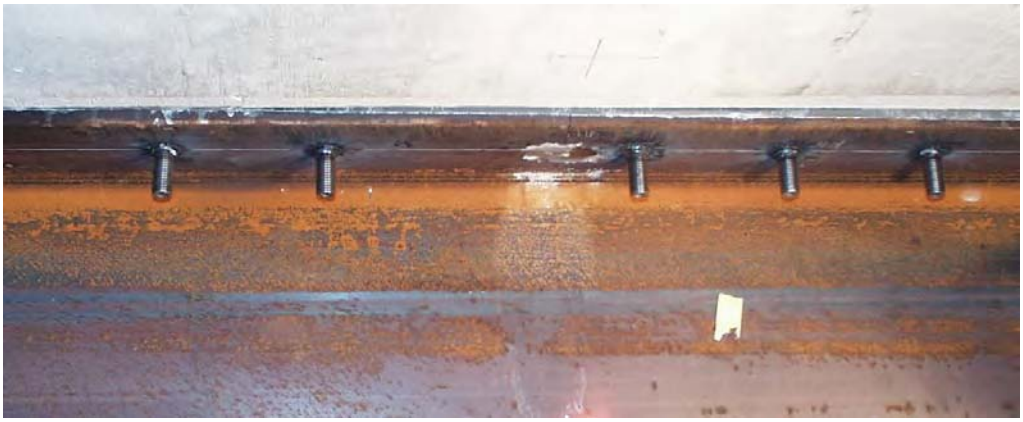

Figure 6.63 Threaded studs welded to the inside top flange of the transverse beam

Figure 6.64 Close up view of the threaded stud

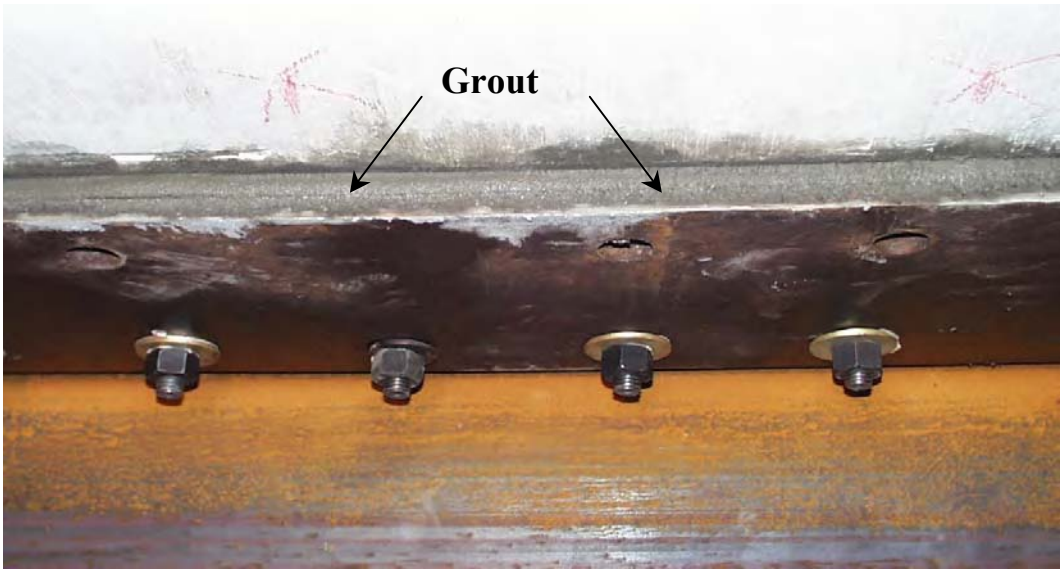

Figure 6.65 Plate attached to underside of beam top flange with threaded studs, and grouted

Holes that were 7/8 inch in diameter were drilled upward through the existing holes in the plate into the slab. Threaded rods were then placed in these holes, fastened with epoxy, and then tightened to the plate with nuts, as shown in Figures 6.66 through 6.68.

Figure 6.66 Holes drilled up through the plate into the slab

Figure 6.67 Threaded rod installed in slab with epoxy

Figure 6.68 Threaded rods bolted to plate

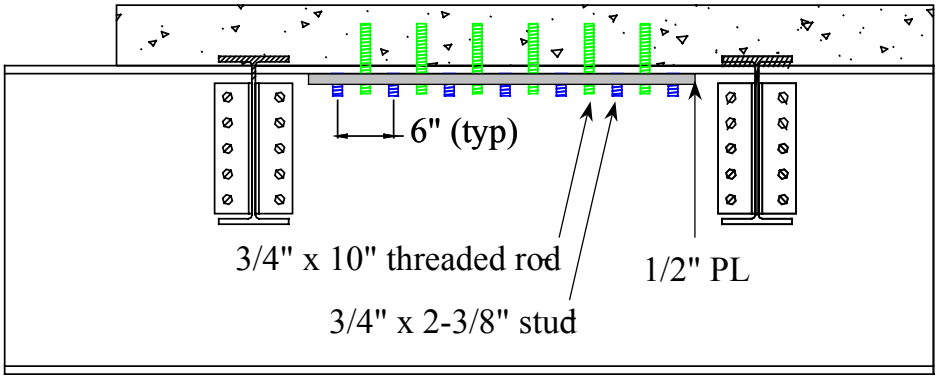

Figure 6.69 Section view of retrofit scheme

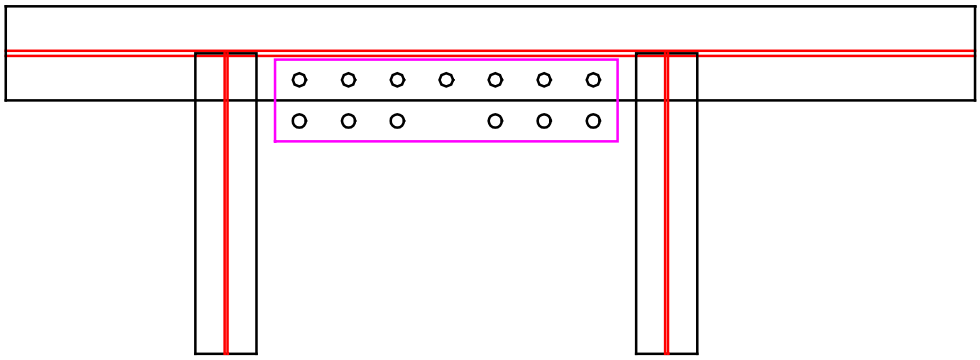

Figure 6.70 Plan view of retrofit scheme

6.6.2 Strengthening Details

The threaded studs welded to the top flange are essentially shear studs without heads that have threads cut into them. The specified minimum yield stress for the threaded studs was 55 ksi. The steel plate used was 1/2 inch thick and had a specified minimum yield stress of 50 ksi. Dimensions and hole placements are shown in Figure 6.71.

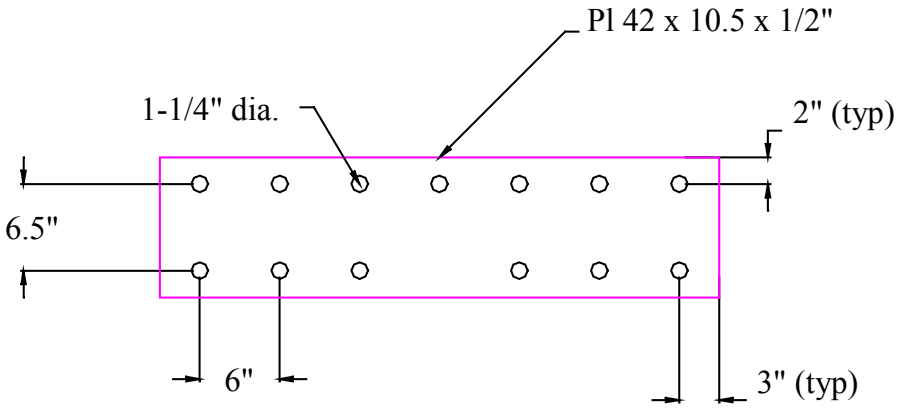

Figure 6.71 Retrofit plate specifications

The threaded rods inserted into the concrete, the epoxy, and the grout were all Hilti Corporation products. (Hilti, 2001) The rods (3/4"x10") are designated as "HAS Super Rods" and have material specifications (ASTM 193) similar to A325 bolts. Yield strength is specified to be 105 ksi and ultimate strength is 125 ksi. The size and number of shear connectors was designed to provide approximately 15% of the full composite capacity. This amount of composite action would provide enough capacity to load rate the transverse beams above HS20.

The grout used to fill the space between the plate and the slab is Hilti product "CG 200 PC" cementitious grout with a 28-day compressive strength between 8.5 and 11 ksi. This grout had the best combination of quick set up time (less than three hours), strength, and non shrink characteristics. "HSE 2421" high strength epoxy was used to anchor the treaded rods into the slab. The epoxy had a specified bond strength of 2 ksi, a specified compressive modulus of 290 ksi, and a specified tensile strength of 7.08 ksi. The epoxy was also used to fill the gap between the threaded studs and the holes drilled in the plate. As previously mentioned, oversized holes were necessary to fit the plates over the threaded studs. These particular epoxy and grout products were recommended by the manufacturer's technical staff.

Threaded rods were tightened to the maximum torque permitted by Hilti specifications, 180 foot-pounds. This was estimated to provide approximately 5 kips of tension in each threaded rod

6.6.3 Test Results

Loading was applied to the strengthened laboratory model in an identical manner as was earlier applied for the base model. Stresses and deflections were then compared before and after strengthening. Interestingly, test results did not show any increase in stiffness or reduced stress in the strengthened model as compared to the original unstrengthened model. The results were essentially identical for the retrofitted and unretrofitted deck. Figure 6.72 compares the retrofitted and unretrofitted data for stress, and Figure 6.73 compares the midspan deflections. Both plots show nearly identical response for the retrofitted and the unretrofitted model for both stress and deflection. Although the retrofit was intended to provide only partial composite action, before strengthening and after strengthening tests gave nearly identical results.

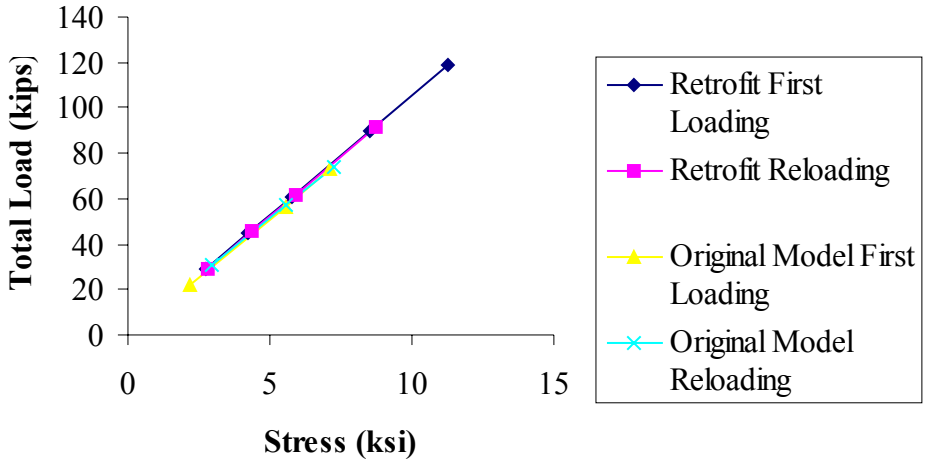

Figure 6.72 Load vs. stress for retrofitted and unretrofitted beam

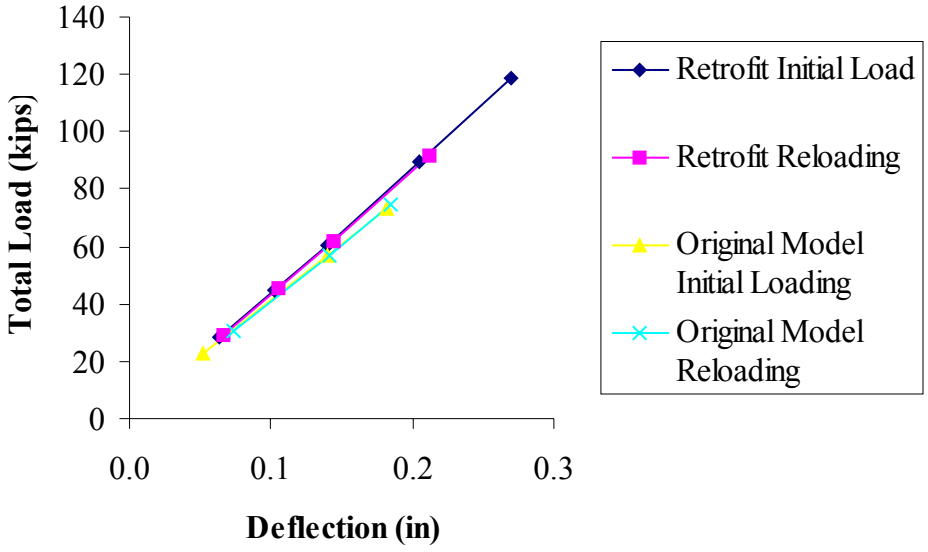

Figure 6.73 Load vs. deflection for retrofitted and unretrofitted beam

The intent of the retrofit was to prevent the relative end slip between the concrete and steel sections. Figure 6.74 shows the data for the end slip in the retrofitted and unretrofitted models. Although there is some scatter of data, again, the retrofit shows little difference in response as compared to the unretrofitted model.

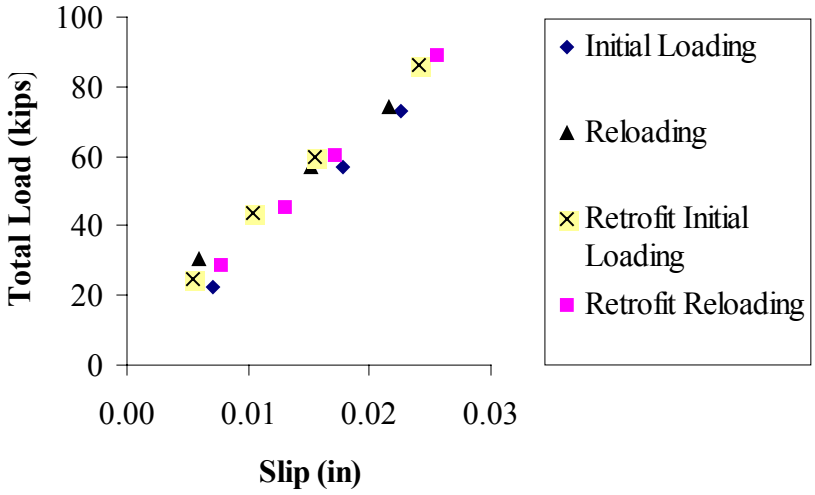

Figure 6.74 End slip of retrofitted and unretrofitted beam

Because of the absence of any change in response, it is believed that the threaded rods simply did not engage the steel and slab to transfer shear. Oversized holes were used in the plate around both the welded studs and the threaded rods in order to facilitate fit-up. The welded rods were 3/4 inch diameter,

and the plate holes were 1-1/4 inch in diameter. The gap around the welded rod is shown in Figure 6.75. These gaps were filled with epoxy, as shown in Figure 6.76. However, since the gaps were subsequently covered with washers and nuts (Figure 6.77), it was not possible to visually inspect to see if the gaps were fully filled with epoxy. The grout and epoxy were damaged during disassembly, and therefore it was not possible to verify after testing whether the gaps were filled.

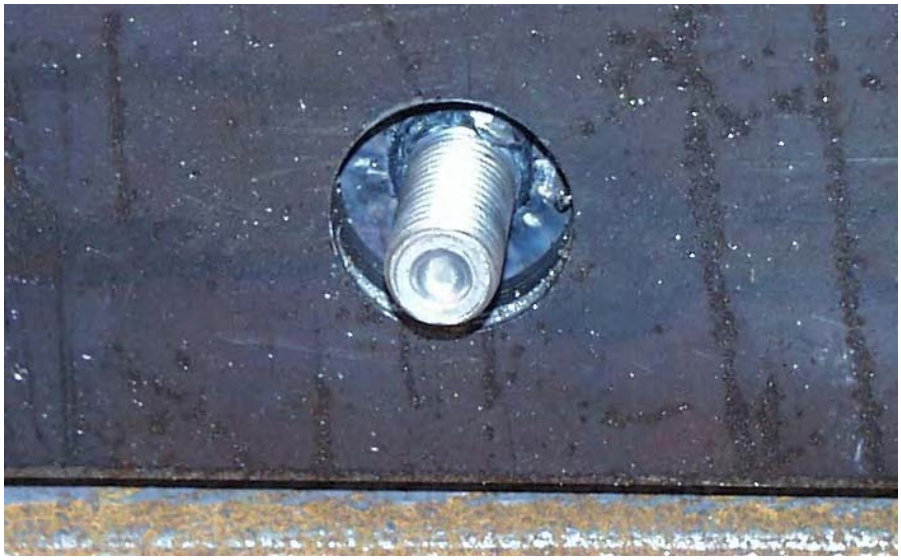

Figure 6.75 Gap around threaded stud

Figure 6.76 Gap filled with HSE 2421 epoxy

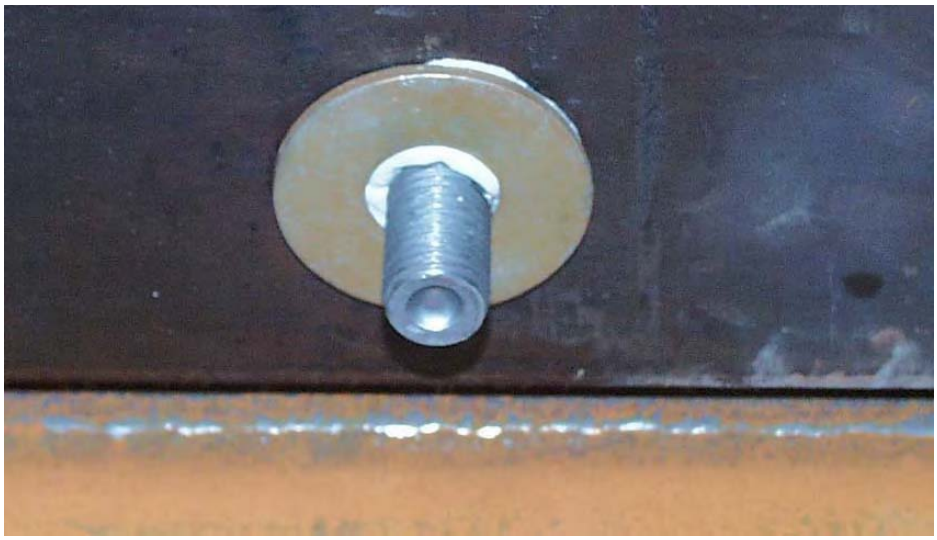

Figure 6.77 Washer covering epoxy filling

The epoxy was inserted overhead, and in some cases difficult to keep in place. The epoxy had a modulus that was 1/100 of steel. Hence, even if the gaps were filled completely, the compressive stiffness of the epoxy was much lower than that of steel. This lower stiffness would allow a greater relative movement between the rod and the plate as compared to the condition if the rods were bearing against the steel plate directly. Additionally, any shrinkage of the epoxy would likely contribute to reduced effectiveness in shear transfer.

Since the hole drilled up into the concrete slab was larger than the diameter of the inserted rod, there was also a gap between the threaded rod and the slab. This gap was much smaller however, as the drilled hole in the slab was only 1/8 inch larger than the threaded rod.

An additional problem may have been the space between the plate and slab that was filled by the cementitious grout. As with the epoxy, the grout was installed overhead, which proved to be somewhat difficult. The grout was not viscous enough to be simply plastered on the underside of the slab. Instead, the plate was loosely attached to the flange, and the grout was pushed into the space between the slab and the plate. It was not possible to inspect whether or not the entire space was completely filled. Also, if any shrinkage occurred, it would leave a gap between either the grout and the plate, or the grout and the slab. It is believed that the combination of gaps prevented engagement of composite action.

Although test results showed no decrease in measured deflections or stresses in the strengthened laboratory model under essentially elastic level loading, the effectiveness of the strengthening measures for increasing the ultimate strength of the bridge deck system could not be determined. Since the use of a full-scale laboratory model precluded loading the model to failure, the behavior of the retrofit scheme at very high load levels could not be examined. At higher load levels, the shear connectors would likely become engaged and contribute to the ultimate strength of the system. Again, however, this could not be confirmed from this test series. However, it is clear from the tests that the retrofit scheme was not effective in reducing stresses in the steel beams at the load levels used in these tests. Recall that the test loads were well above HS20, but still within the elastic range for this bridge deck system.

This attempt to retrofit the laboratory model of the bridge deck system was done at the end of this research project to provide a first look at the feasibility of strengthening existing non-composite decks by adding shear connectors. This was done at the end of this project simply due to the availability of the laboratory model. However, developing new strengthening techniques was not the primary objective of this research project, and so further attempts to strengthen the bridge deck model were not pursued as part

of this project. Nonetheless, strengthening the decks of historic truss bridges by the addition of shear connectors may still represent a useful technique for improving the load rating of the deck system. However, considerable additional work is needed to identify techniques for installing shear connectors that are effective and economical.

6.7 SUMMARY

A laboratory investigation was performed on a full-scale segment of a slab on steel girder bridge deck. The geometry and member sizes of the laboratory specimen closely matched the Llano and Goliad case study bridge decks. The deck was loaded in various positions and with varying loads. The model was then retrofitted in the attempt to create a partially composite system. Important results and observations are as follows.

- The stresses measured in the transverse beams and longitudinal stringers of the laboratory bridge deck model were significantly less than the stresses predicted using calculation methods typically used for AASHTO load rating. Simple finite element modeling of the laboratory bridge deck model predicted stresses much closer to the measured values. However, the stresses predicted by the finite element model were still somewhat higher than the measured values. Consequently, a simple finite element analysis of the bridge deck can provide a significantly improved prediction of stresses as compared to conventional AASHTO based calculations, while still providing overall conservative results.
- As in the field tests, some composite action was found in the longitudinal stringers of the laboratory model, but not the transverse beams. The degree of this unintended composite action was higher than what was found in the field, but still relatively small.
- After adjusting the laboratory results for differences in member sizes, the results from the Goliad field tests and the laboratory tests generally agreed well.
- The strengthening scheme used on the laboratory model was not effective in increasing stiffness or reducing stresses at the load levels used in the laboratory testing. It is believed that the installation procedure did not sufficiently affix the slab to the girders because of unintended gaps between the plates, rods, and the slab and the low compressive modulus of the epoxy. The ultimate strength of the strengthened bridge deck could not be determined in the laboratory tests due to limitations in the loading system. Strengthening existing non-composite bridge decks by the addition of shear connectors may still represent a useful retrofit strategy, but additional work is needed to develop effective and economical methods to install shear connectors.

Chapter 7:
Summary and Conclusions

7.1 Review of Project Scope and Objectives

There are a large number of older on-system metal truss bridges still in vehicular service in Texas. A number of these are of significant historical interest due to their age and other unique features, and are either listed or eligible for the National Register of Historic Places. Considerable interest exists in maintaining historic metal truss bridges in continued vehicular service. However, achieving this goal is often problematic due to structural and functional deficiencies found in these bridges. The structural load rating can often be low due to the initial low design loads used for the bridge combined with damage and deterioration that has occurred over the service life of the bridge.

The primary objective of the study reported herein was to address structural issues involved with historic on-system truss bridges in Texas. More specifically, the objective was to examine methods that can be used to develop an accurate and realistic load rating for an older truss bridge. Based on commonly used evaluation procedures, many of these older truss bridges may show deficient load ratings based on current standards such as HS20. This study examined if such low load ratings accurately reflect the true load carrying capacity of these bridges, and whether more realistic load ratings can be achieved through the use of more accurate structural analysis methods and field load testing. This study also briefly examined a potential technique for strengthening floor systems on older truss bridges.

In order to examine issues involved in the structural evaluation of older on-system metal truss bridges, two case study bridges were investigated in detail. The first case study bridge was located in Llano, Texas, and the second in Goliad, Texas. These bridges, typical of the circa 1930 on-system truss bridges, featured non-composite slab on steel girder bridge decks and Parker trusses. Each bridge was studied through the use of conventional AASHTO load rating techniques, the use of more advanced structural analysis models, and extensive field load testing. In addition to the two detailed case studies, a full scale laboratory experimental investigation was conducted on a single bay of a typical slab on steel girder truss bridge floor system in order to examine the structural response of the floor system in greater detail.

7.2 Summary of Major Project Tasks and Findings

7.2.1 Llano Case Study Bridge

The first case study bridge studied in detail was located in Llano, Texas. Known as the Roy Inks Bridge, the main structure spans approximately 800 ft. over the Llano River, and was constructed in 1936. The bridge consists of four main spans, each approximately 200 ft. in length. Each span is a Parker through-truss, with a non-composite slab on steel beam and stringer floor system.

Material properties such as yield strength of the steel and concrete compressive strength were not specified on the available drawings for the Llano Bridge. Given unknown material properties, AASHTO provides guidelines for values to use based on the date of construction. For the Llano Bridge, this resulted in estimates of yield strength of steel equal to 30 ksi, and concrete compressive strength of 2.5 ksi. These values were used in the initial load rating.

Initial evaluation of the bridge indicated that the truss members showed inventory load ratings well in excess of HS20 using standard AASHTO load rating techniques. Consequently, the truss members themselves did not pose a problem with respect to inadequate load rating. However, the steel

beams and stringers in the bridge floor system showed inventory ratings well below HS20, using standard AASHTO based load-rating techniques.

The original mill certificates for the steel used in the Llano Bridge were available in TxDOT files. These mill certificates indicated that the yield stress of the beams and stringers was approximately 36 ksi, a substantial increase over the initially assumed value of 30 ksi. To confirm the information on the mill certificates, samples were removed from the flanges of two of the transverse beams. Tensile tests performed on these samples showed yield stresses of approximately 36 ksi. Using this higher yield strength, longitudinal stringers rated approximately 25 percent over an HS20 loading. Transverse beams, while still rating under HS20, had their load deficiency reduced to approximately 10 percent. Obtaining more accurate estimates of steel material properties by recovering mill certificates and by removing and testing samples of steel from the bridge proved to be a useful and economical measure to develop an improved load rating.

Based on initial evaluation of the Llano Bridge, it was clear that the floor system was controlling the load rating, and was the primary structural issue of concern for the bridge. Subsequent studies of the Llano Bridge therefore focused on the floor system.

An elastic finite element model was developed for the bridge floor system to determine if a higher load rating could be justified by using analysis methods that are more advanced and more exact than used in conventional load rating. The model was constructed using the commercially available finite element analysis software package SAP2000. The bridge floor model used standard beam elements to represent the beams and stringers, and shell elements to represent the concrete slab. The model was constructed to represent a floor system with no composite action between the steel members and the concrete slab. AASHTO HS20 truck loads were applied in positions on the model to produce maximum flexural response for both stringers and beams. The maximum moments due to live load effects where computed and used to load rate the members.

The finite element analysis showed significantly lower moments in the stringers and beams than conventional AASHTO calculations. This reduction in moment was attributed to two factors. One factor was that the finite element analysis predicts that the reinforced concrete slab resists substantial moment, thereby reducing the moment that must be carried by the steel beams and stringers. Thus, even without composite action, the finite element analysis shows that the slab provides a significant contribution to the load carrying capacity of the bridge deck. Conventional AASHTO load rating procedures do not regard a non-composite slab as a load carrying part of the deck system. A second factor was that the finite element analysis predicted a different and more advantageous distribution of moments among the steel members than obtained from the AASHTO calculations.

The critical members controlling the load rating of the Llano Bridge were the transverse floor beams. With the reduction in live load moment predicted by finite element analysis combined with a yield stress based on measured values, it was possible to demonstrate an inventory load rating for the transverse beams, and therefore for the entire bridge, in excess of HS 20. Consequently, the use of simple finite element analysis for the bridge floor system proved to be a valuable tool for developing an improved load rating.

Field load tests were subsequently conducted on the Llano Bridge to obtain the most accurate assessment of live load effects on the floor system, and to assess the accuracy of the finite element model. In these tests, selected portions of the floor system were instrumented with strain gages. Trucks of known weight and geometry were then driven slowly over the bridge, and the response of the instrumented members was measured.

The field test data showed live load stresses in the floor beams and stringers that were significantly lower than predicted by the standard AASHTO load rating. In many cases, the field test data showed stresses that were less than half of those predicted by standard AASHTO calculations. This

confirmed that the bridge floor system was significantly stronger than indicated by the standard load rating, and that an increased load rating for the bridge floor members is justified.

The field test data also showed live load stresses smaller than predicted by the finite element model of the bridge floor system. However, the difference between the field test data and the finite element model predictions were much smaller than the difference with the standard load rating calculations. The field test data showed stresses that were 5 percent smaller than predicted by the finite element analysis for the stringers, and 25 percent smaller for the transverse beams. Thus, the finite element model, although predicting much smaller stresses than standard load rating calculations, still provided conservative predictions compared to field test data.

The field data showed that some of the floor members exhibited a small degree of unintended composite action with the concrete slab. Where composite action was measured, it most frequently occurred in the longitudinal stringers rather than in the transverse beams. The composite action, however, was not consistent in all loading positions nor was it necessarily constant along the length of the member. Based on the field test data, it appears that composite action cannot be relied upon as a significant or consistent source of additional strength in the bridge floor system.

7.2.2 Goliad Case Study Bridge

Subsequent to the Llano field tests, an opportunity arose to investigate a similar truss bridge located on US 183, crossing the San Antonio River in Goliad, Texas. The Goliad Bridge was very similar to the Llano Bridge, except that it was slightly smaller, and consisted of only one span, as compared to the four spans at Llano. The floor system of the Goliad Bridge was also very similar to that of the Llano Bridge, consisting of a non-composite slab over steel beams and stringers. As with the Llano Bridge, an initial evaluation of the Goliad Bridge indicated that floor beams and stringers controlled the load rating of the bridge.

The floor system of the Goliad Bridge was evaluated three ways: by conventional AASHTO load rating calculations, by elastic finite element analysis, and by field load testing. The Goliad Bridge was scheduled for replacement and demolition, and the bridge was load tested just prior to demolition. Consequently, the testing was performed to a much higher load, since a limited amount of yielding could be tolerated. The highest loading used in the Goliad test was approximately a 57 kip axle load, almost 80 percent higher than an HS20 axle.

The overall trend in results for Goliad was quite similar to the Llano Bridge. Stresses in the floor members predicted by the AASHTO calculations were significantly higher than the stresses predicted by finite element analysis. The stresses predicted by finite element analysis, in turn, were somewhat higher than those measured in the field test.

The Goliad field load test confirmed that the finite element model of the bridge deck provided a significantly more accurate prediction of member response than that obtained from conventional AASHTO calculations. The stresses measured in the floor beams and stringers were significantly lower than predicted by the AASHTO calculations, indicating that the conventional AASHTO calculations significantly underestimate bridge deck capacity. The stresses predicted by the finite element analysis were much closer, although still somewhat higher, compared to those measured in the field test. Thus, as was the conclusion from the Llano test, the Goliad test indicated that the finite element analysis provides a very useful tool for load rating. The finite element analysis provides a more realistic, but still somewhat conservative prediction of the response of the bridge floor members to truck loading.

As with the Llano Bridge, the deck of the Goliad truss bridge did not have shear connectors for the development of composite action. The field test data for the Goliad Bridge showed the development of some composite action, primarily in the longitudinal stringers. A similar observation was made in the Llano field tests. Other researchers have observed such unintended composite action in other field tests

on bridges without mechanical shear connectors. The question arises as to whether this additional strength can be utilized in the evaluation and load rating of the bridge deck.

Data collected in the Goliad field test showed that at higher load levels slip occurred between the steel and concrete, and that most of the unintended composite action was in fact lost. Some researchers have suggested taking advantage of unintended composite action in load rating bridges. However, based on the data collected in the Goliad field test, it appears that such unintended composite action may not be sufficiently reliable for use in capacity determinations.

7.2.3 Laboratory Investigation

The final task of this research study was an experimental investigation of a full-scale portion of a non-composite slab on steel girder bridge deck. The laboratory model was similar in member sizes and geometry to the bridge decks on the Llano and Goliad truss bridges. The primary goal of the experimental study was to provide further data on the distribution of forces and stresses within the beams and stringers of the floor system and to corroborate the field test data and finite element analysis. The laboratory model of the floor system provided the opportunity to conduct more extensive testing than possible in the field and permitted the use of simpler and better defined boundary conditions for comparison with finite element models. The laboratory bridge deck model was also subsequently used for preliminary evaluation of a potential strengthening scheme for the bridge deck.

Loads were applied to the laboratory model at a variety of locations and with varying magnitudes. For each load case, the stresses measured in the beams and stringers were compared to the stresses predicted using conventional AASHTO load rating calculations and using an elastic finite element model.

The same trends seen in the case study bridges were also seen in the laboratory experimental investigation. The stresses measured in the transverse beams and longitudinal stringers of the laboratory bridge deck model were significantly less than the stresses predicted using calculation methods typically used for AASHTO load rating. Simple finite element modeling of the laboratory bridge deck specimen predicted stresses much closer to the measured values. However, the stresses predicted by the finite element model were still somewhat higher than the measured values. The laboratory model confirmed that a simple finite element analysis of the bridge deck can provide a significantly improved prediction of stresses as compared to conventional AASHTO based calculations, while still providing overall conservative results.

As in the field tests, some composite action was found in the longitudinal stringers of the laboratory model, but not the transverse beams. The degree of this unintended composite action was higher than what was found in the field, but still relatively small.

The results of the various tests and analyses conducted for the Llano and Goliad Bridge floor systems as well as for the laboratory model consistently showed that the load rating of the floor beams and stringers can be increased through the use of improved structural analysis, specifically by finite element analysis. In some cases, however, this improved load rating may still fall short of the desired load rating. For such cases, some degree of strengthening may be needed for selected bridge floor members. Consequently, as the final step in this investigation, a simple strengthening measure was examined using the laboratory bridge deck model. The trial method selected for strengthening was the addition of shear connectors between the transverse steel beams and concrete floor slab. The existing floor systems in the Llano and Goliad bridges had no shear connectors, and similarly the laboratory model was constructed without shear connectors. The field and laboratory test data show a small degree of composite action was developed in these bridge decks, likely due to friction between the top of the steel beams and the bottom of the concrete slab. However, both the field test and experimental data show that this unintended composite action may be reduced due to slip at higher load levels, and therefore does not provide a reliable source of additional strength. The addition of shear connectors was therefore

investigated as a means to add a reliable and predictable degree of composite action to the bridge floor system.

In the strengthening scheme, threaded steel studs were stud welded to the bottom side of the top flange of the transverse beams. The threaded studs were connected to steel plates, which extended beyond the edge of the beam flange. Threaded rods where then installed through predrilled holes in the plate up into the underside of the slab, and secured with epoxy, and then tightened down to clamp the top flange to the slab.

Test results did not show any measurable increase in stiffness or reduced stress in the model after the retrofit was completed, under the load levels used in the tests. Although the retrofit was intended to provide only partial composite action, before retrofit and after retrofit tests gave nearly identical measured stresses and deflections. Because of the absence of any change in response, it is believed that the threaded rods simply did not engage the steel and slab in any shear transfer. Gaps around the threaded rods and welded shear studs may not have been adequately filled with the epoxy.

The test loads used on the laboratory model were well above HS20, but still within the elastic range of the model. The ultimate strength of the strengthened bridge deck could not be determined in the laboratory tests due to limitations in the laboratory loading system. Strengthening existing non-composite bridge decks by the addition of shear connectors may still represent a useful retrofit strategy, but additional work is needed to develop effective and economical methods to install shear connectors and testing to ultimate strength levels is needed.

7.3 CONCLUSIONS

The circa 1930 Parker truss bridges investigated in this research program had adequate strength in the truss members to permit an HS20 load rating. However, the steel beams and stringers in the bridge floor systems generally showed load ratings well below HS20 using standard AASHTO based load rating techniques. Consequently, the floor systems in these truss bridges are the critical element controlling the load rating.

The results of this study have shown that the use of standard AASHTO load rating techniques substantially underestimates the strength of the floor beams and stringers. A significantly more accurate prediction of the structural response of the floor members to truck live loads can be achieved by conducting an elastic finite element analysis of the bridge floor system. Comparison with extensive field load test results and with laboratory test results shows that finite element analysis provides a more realistic but still somewhat conservative prediction of floor member response. Analysis of the floor system using a finite element model can be used to support a significantly improved load rating for older truss bridges.

References

American Association of State Highway and Transportation Officials (AASHTO). (1994). *Manual for Condition Evaluation of Bridges,* Washington, D.C.

American Association of State Highway and Transportation Officials (AASHTO). (1996). Standard Specifications for Highway Bridges, 16th ed., Washington, D.C.

American Association of State Highway and Transportation Officials (AASHTO). (1998). *LRFD Bridge Design Specifications*, Customary Units, 2nd ed., Washington, D.C.

American Concrete Institute (ACI) Committee 318. (1999). *Building code Requirements for Structural Concrete (ACI 319-99) and Commentary (ACI 318R-99)*, American Concrete Institute, Farmington Hills, Michigan

American Institute of Steel Construction (AISC). (2001). *Manual of Steel Construction, Load and Resistance Factor Design*, 3rd Edition. Chicago, IL.

American *Institute of Steel Construction (AISC). (1990)*. Iron and Steel Beams 1873 to 1952, Chicago, IL, 1990.

American Society of Civil Engineers (ASCE). (1974). "Composite Steel-Concrete Construction", Report of the Subcommittee on the State-of-the-Art Survey of the Task Committee on Composite Construction of the Committee on Metals of the Structural Division, *Journal of the Structural Division*, ST5, American Society of Civil Engineers.

Bakht, B.(1988). "Ultimate Load Test of a Slab-on-Girder Bridge," The Research and Development Branch, Ministry of Transportation of Ontario.

Bakht, B, and Noses, Fred. (1988). "Lateral Distribution Factors for Highway Bridges," *Journal of Structural Engineering*, Vol. 113, No. 8, American Society of Civil Engineers.

Baldwin, J. W. (1965). "Field Tests of a Three-Span Continuous Highway Bridge," *Highway Research Record*, No. 76, pgs. 140-167.

Barbero. Ever. (1996). "Stiffening of Steel Stringer Bridges With Carbon Fiber Reinforced Plastics for Improved Bridge Rating," 4th Annual Wilson Forum, San Francisco, CA.

BDI (1999). "Bridge Response Investigation: U. S. Army Heavy Equipment Transportation System (HETS)," Bridge Diagnostics, Inc., Boulder, CO.

Boothby, Thomas, and Craig, Richard. (1997). "Experimental Load Rating Study of a Historic Truss Bridge", *Journal of Bridge Engineering*, American Society of Civil Engineers.

Chajes, Michael, Mertz, Dennis, and Commander, Brett. (1997). "Experimental Load Rating Of A Posted Bridge." *Journal of Bridge Engineering*, American Society of Civil Engineers.

Chien, P. and Ritchie, J.K. (1984*). Design and Construction of Composite Floor Systems.* Canadian Institute of Steel Construction, Ontario, Canada.

Davies, Colin. (1969), "Tests on Half-Scale Steel-Concrete Composite Beams with Welded Stud Connectors", *Structural Engineer*, Vol. 47, No. 1.

Goodman, J. R., and Popov, E., (1968), "Layered Beams Systems with Interlayer Slip," *Journal of the Structural Division*, ST11, American Society of Civil Engineers.

Hays, C. O., Consolazio, G. R., Hoit, M.I., and Kakhandiki, A. (1994). "Bridge Rating of Girder-Slab Bridges using Automated Finite Element Technology." Structures and Materials Research Report No. 94-1, Engineering and Industrial Experiment Station, University of Florida, Gainesville, Florida.

Hilti corporation (2001), *Hilti North America Product Technical Guide*, Hilti Corporation, Tulsa, OK.

Jauregui, David, V. (1999). "Measurement Based Evaluations of Non-Composite Steel Girder Bridges," Dissertation, The University of Texas at Austin, August, 1999.

Klaiber, F. W., and Dedic, David, J. (1984). "High Strength Bolts as Shear Connectors in Rehabilitation Work," *Concrete International.*

Li, Wulin, and Albrecht, Pedro. (1995), "Strengthening of Composite Steel-Concrete Bridges," *Journal of Structural Engineering*, American Society of Civil Engineers.

Lichtenstein, A. G., (1993). "Manual For Bridge Rating Through Load Testing, Final Draft." National Cooperative Highway Research Program, (NCHRP), NCHRP 12-28(13)A.

Mabsout, Mounir, Tarhini, Kassim, Frederick, Gerald, and Tayar, Charbel. (1997). "Finite-Element Analysis of Steel Girder Highway Bridges." *Journal of Bridge Engineering*, American Society of Civil Engineers.

Maniar, D.R., Engelhardt, M.D. and Leary, D.E. (2003). "Evaluation and Rehabilitation of Historic Metal Truss Bridges: A Case Study of an Off-System Historic Metal Truss Bridge in Shackelford County, Texas," *Research Report 1741-3*, Center for Transportation Research, University of Texas at Austin.

Marshall, W.T., Nelson, H.M., Banerjee, H.K.(1971). "An experimental study of the use of high-strength friction-grip bolts as shear connectors in composite beams", *The Structural Engineer*, No. 4, Volume 49.

Mertz, Dennis, and Gillespie, John. (1966). "Rehabilitation of Steel Bridge Girders Through the Application of Advanced Composite Materials," Report of Investigation, Transportation Research Board, National Research Council, IDEA Program, Washington, DC.

Mosher Steel and Machinery Company (Mosher). (1923). "Structural Data Appertaining to the Use of Structural Steel, Cast Iron, Ornamental Steel and Iron, Reinforced Concrete and Steel Lumber for Engineers, Architects and Builders," Dallas, Texas.

Newmark, N. M., Siess, D. P., and Viest, I.M.. (1951), "Test and Analysis of Composite Beams with Incomplete Interaction," *Proceedings, Society for Experimental Stress Analysis*, Vol. 19, No. 1, 1951.

Oehlers, D. J., and Sved, G. (1995). "Composite Beams with Limited-Slip-Capacity Shear Connectors", *Journal of Structural Engineering*, American Society of Civil Engineers.

Pennings, Karl. (1999). "Lateral Load Distribution on Transverse Floor Beams in Steel Plate Girder Bridges," MS Thesis, The University of Texas at Austin.

Rabbat, B., G., and Russell, H, G. (1985). "Friction Coefficient of Steel on Concrete or Grout", *Journal of Structural Engineering*, Vol. 111, No. 3, American Society of Civil Engineers.

Salmon, Charles G., and Johnson, John E. (1996). *Steel Structures Design and Behavior.* 4th ed., Upper Saddle River, NJ, Addison, Wesley, Longman.

Saraf, Vijay, Nowak, Andrezej. (1998). "Proof Load Testing of Deteriorated Steel Girder Bridges." *Journal of Bridge Engineering*, American Society of Civil Engineers.

Seracino, R., Oehlers, D. J., and Yeo, M. F. (2001). "Partial-interaction flexural stresses in composite steel and concrete bridge beams." *Engineering Structures*, Vol. 23, p. 1186-1193.

Slutter, R. G., and Driscoll, G. C.. (1965), "Flexural Strength of Steel-Composite Beams", *Journal of the Structural Division*, ST2, American Society of Civil Engineers.

Thiel, M.E., Zulfiquar, K. and Engelhardt, M.D. (2002). "Evaluation and Rehabilitation of Historic Metal Truss Bridges: Survey of Literature and Current Practices," *Research Report 1741-1*, Center for Transportation Research, University of Texas at Austin.

Timoshenko, S., and Goodier, J. (1959). *Theory of Elasticity*, McGraw-Hill, NY.

Troitsky, M. S. (1987) "Orthotropic Bridges, Theory and Design," 2nd ed., Cleveland, OH. The James F. Lincoln Arc Welding Foundation.

Viest, I., V. (1960). "Review of Research on Composite Steel-Concrete Beams," *Journal of the Structural Division*, ST6, June, American Society of Civil Engineers.

Wang, Y. C. (1998). "Deflection of Steel-Concrete Composite Beams with Partial Shear Interaction," *Journal Of Structural Engineering*, American Society of Civil Engineers.

Zuk, Wiliam, Newlon, Howard, and McKeel, Wallace. (1980). "Methods of Modifying Historic Bridges for Contemporary Use," Virginia Highway and Transportation Research Council, Charlottesville, VA.

Appendix A:

Field Load Test Data: Llano Test No. 1

As described in Chapter 4, two field tests were conducted on the case study bridge located in Llano, Texas. Appendix A contains results from the first Llano field load test, conducted on February 9, 1999. In this test, selected portions of the deck system were instrumented with strain gages. Trucks of known weight and geometry were then driven slowly over the bridge, and the response of the instrumented members was measured. The measured strains were converted to stress and plotted versus the position of the load truck on the bridge. The load vehicles were driven south. Consequently, the graphic showing gage location on each plot faces in a southerly direction. The stringers are numbered 1 though 6, with stringer 1 the western-most stringer. Figure A1 shows the truck dimensions and average weight of the two trucks used in the test.

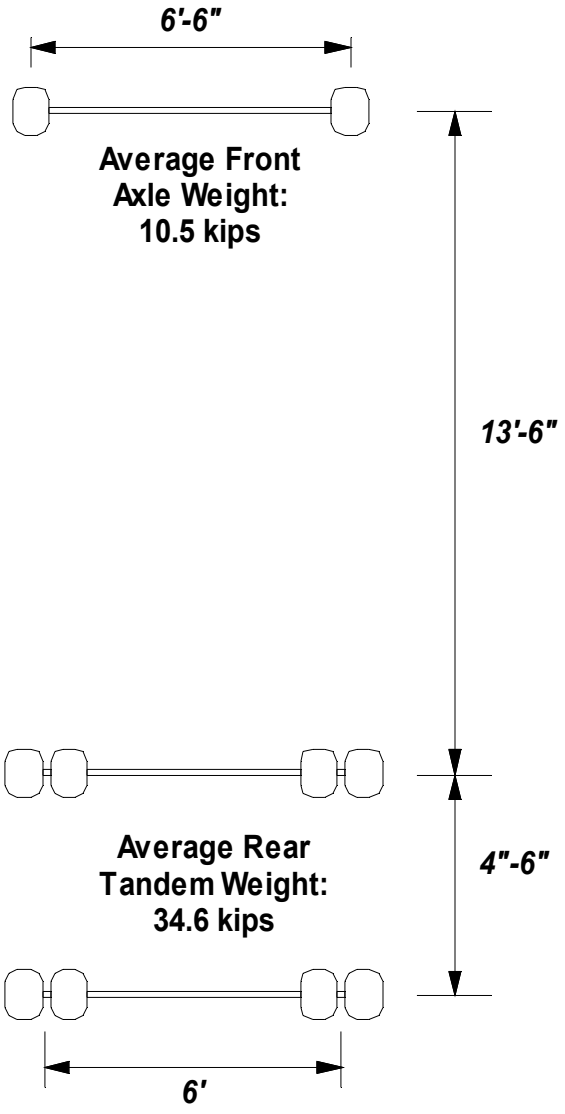

Figure A 1: Load truck dimensions and average weights for Llano field test No. 1

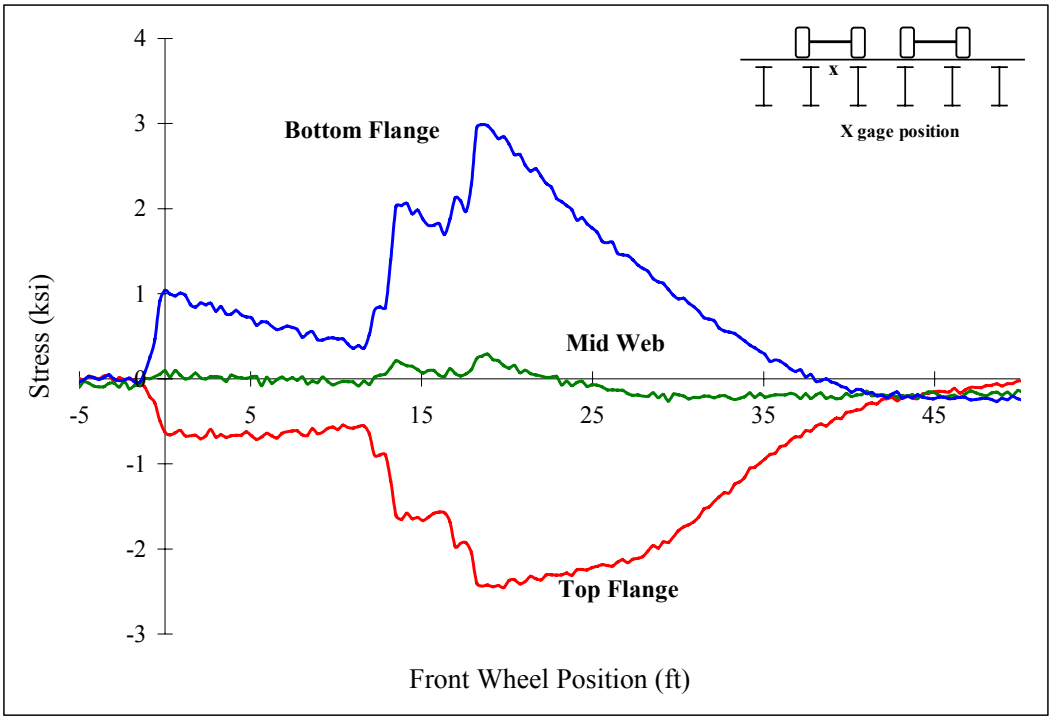

Figure A 2: Beam 1

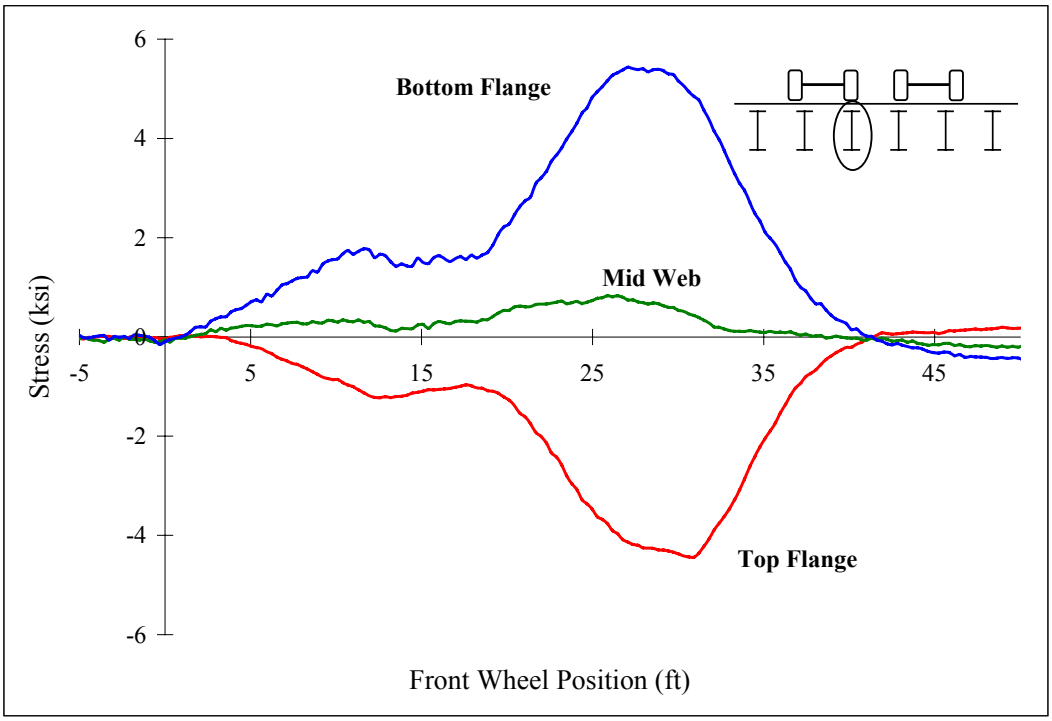

Figure A 3: Midspan stringer 4

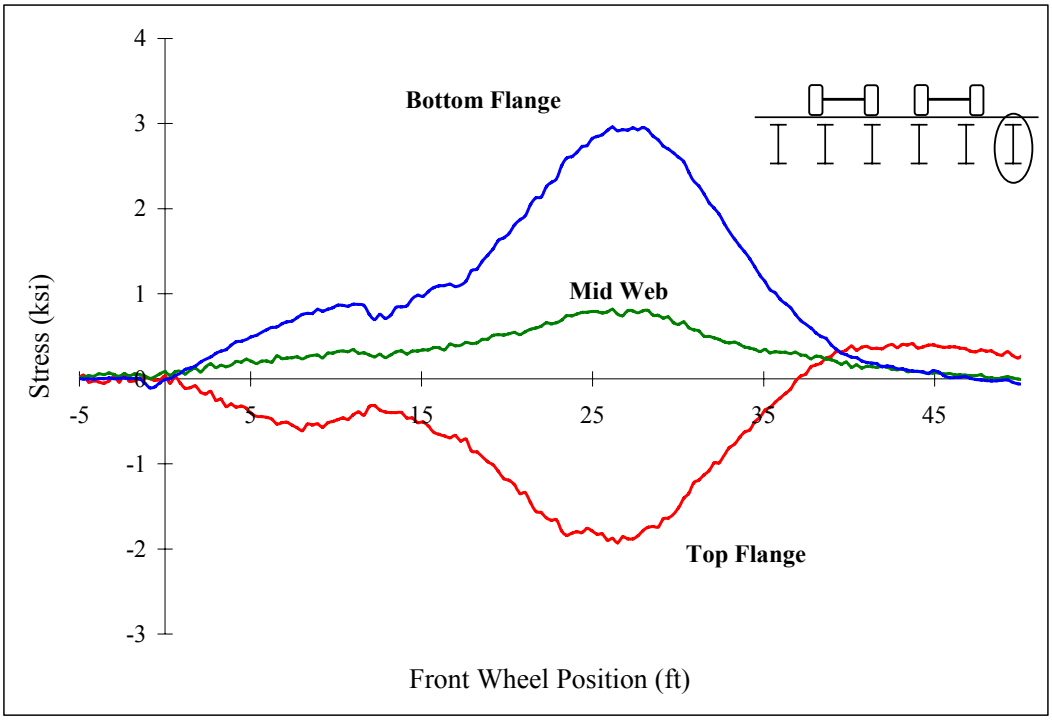

Figure A 4: Midspan stringer 1

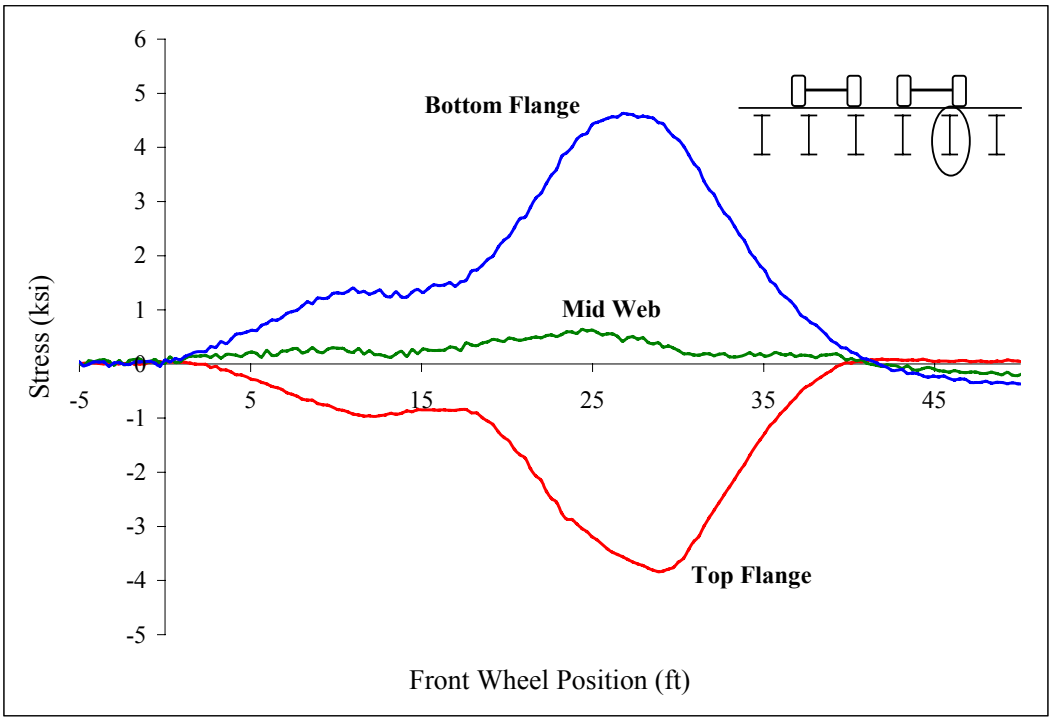

Figure A 5: Midspan stringer 2

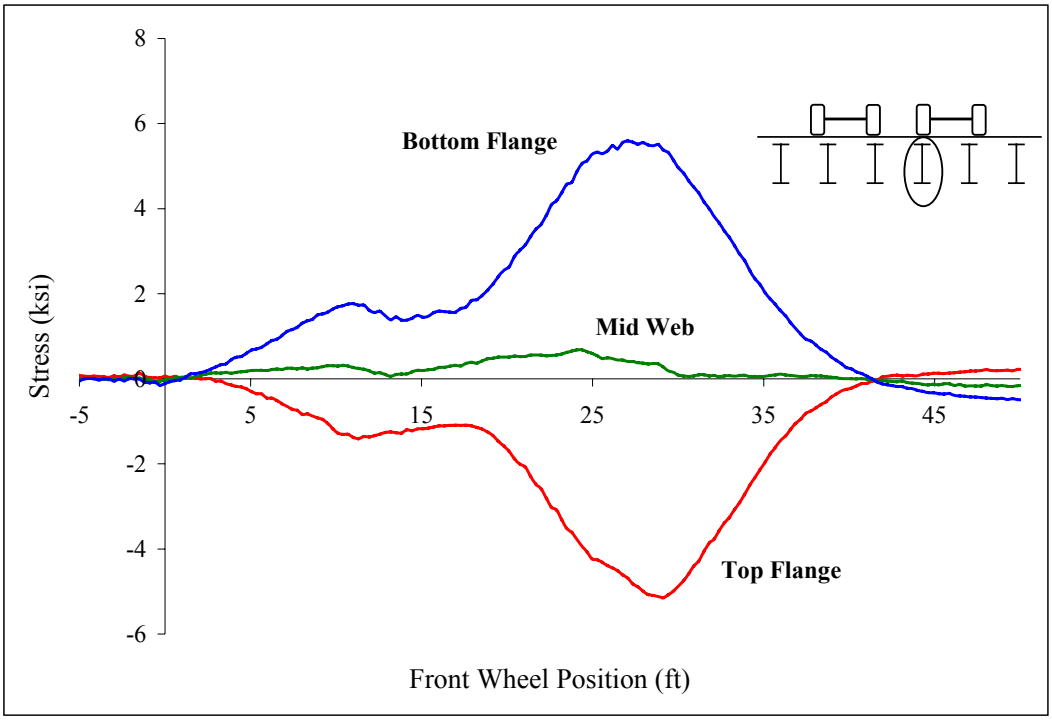

Figure A 6: Midspan stringer 3

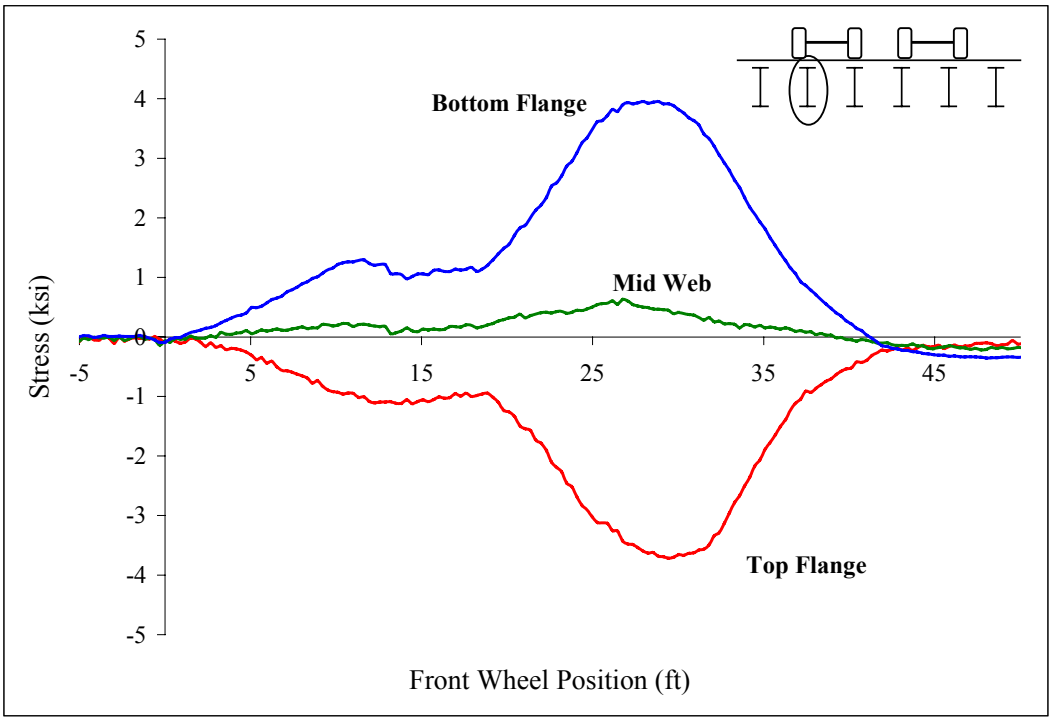

Figure A 7: Midspan stringer 5

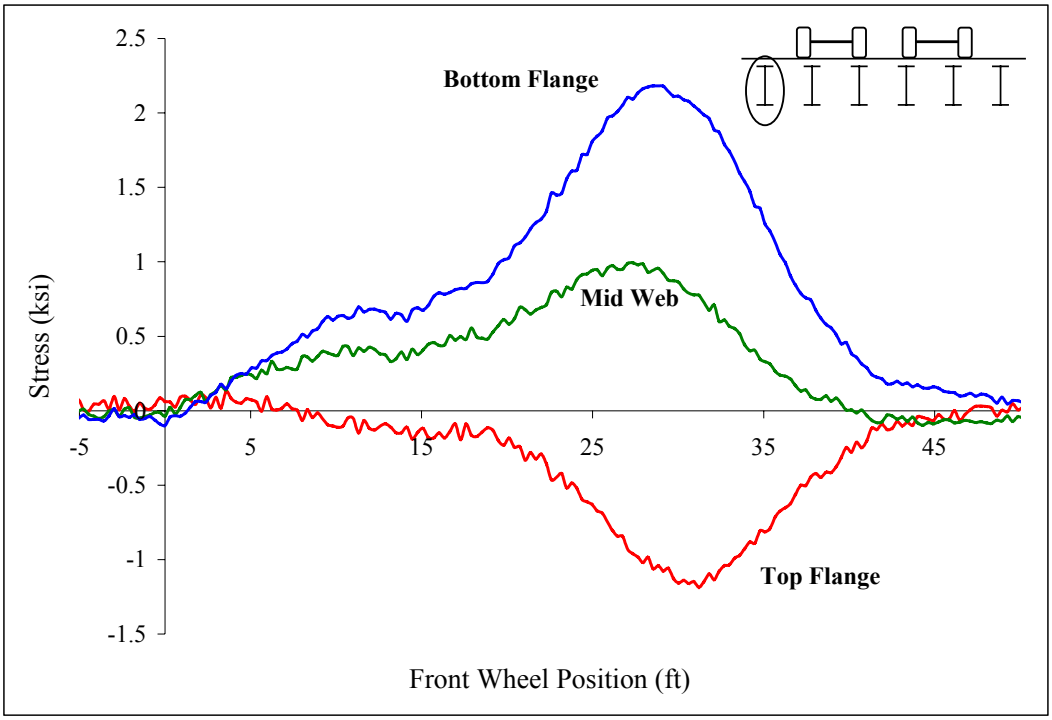

Figure A 8: Midspan stringer 6

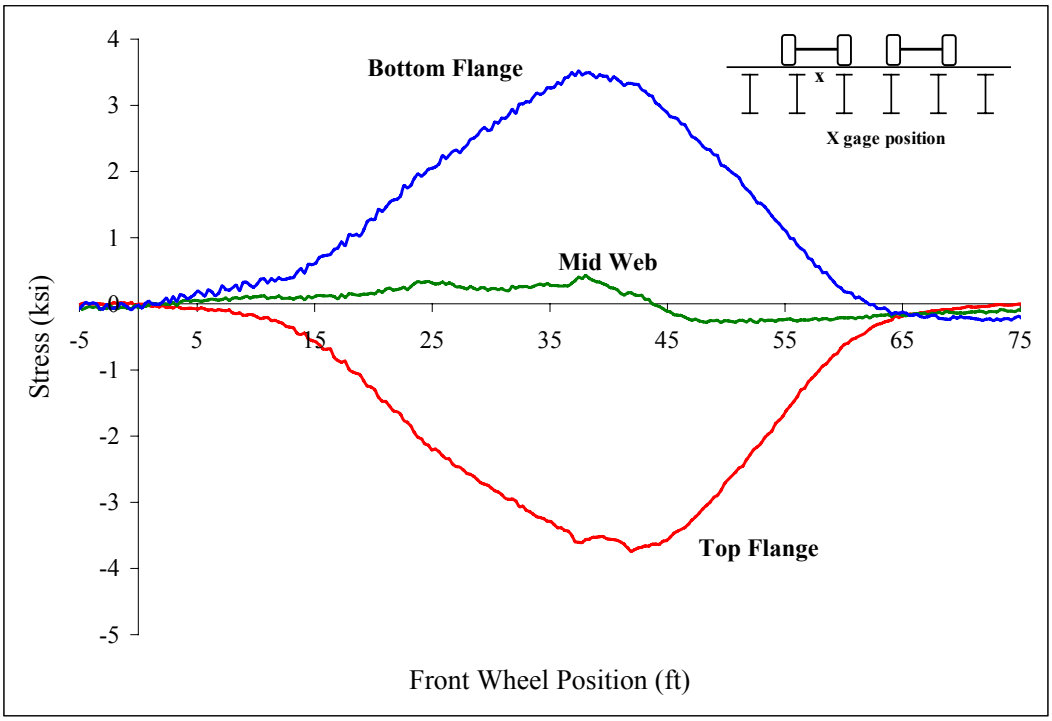

Figure A 9: Beam 2

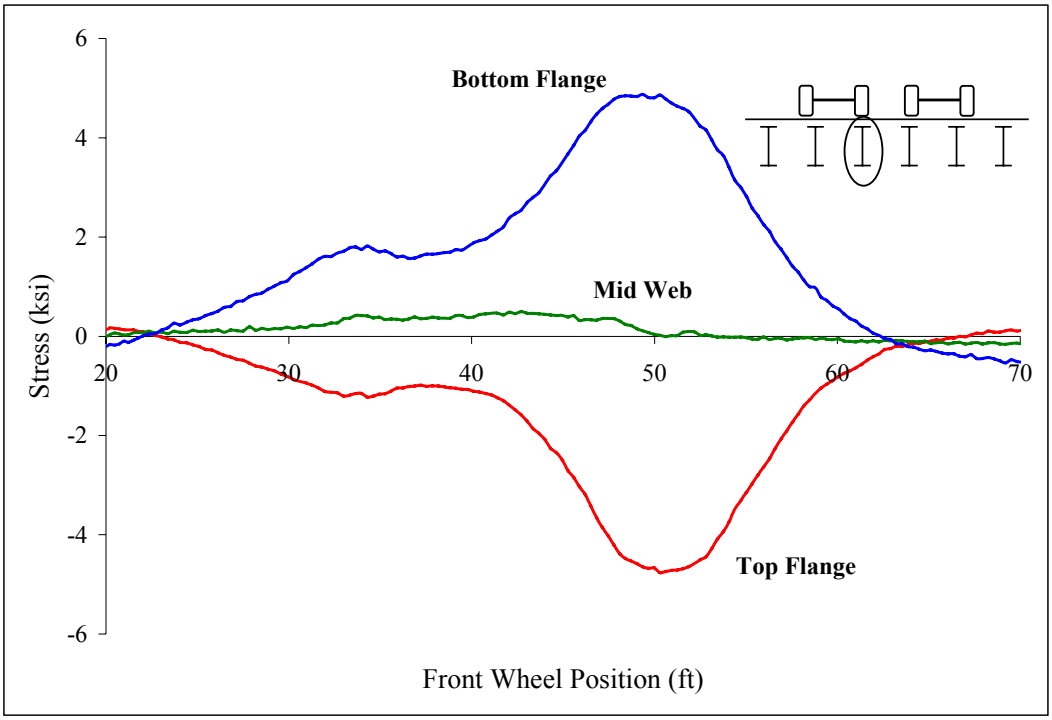

Figure A 10: Midspan stringer 7

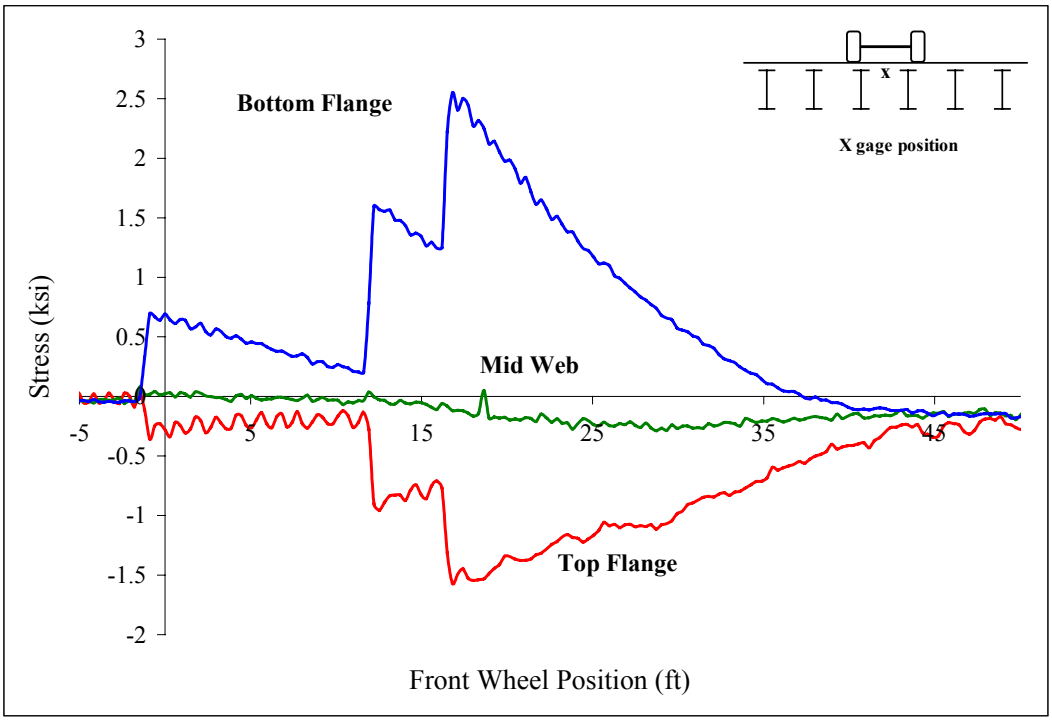

Figure A 11: Beam 1

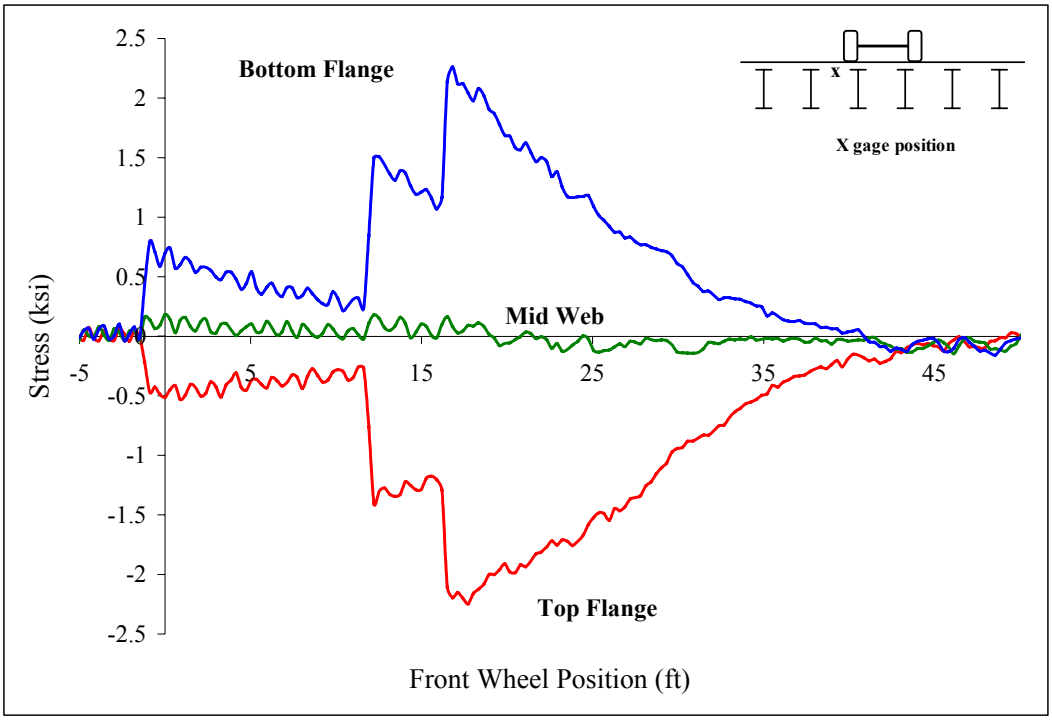

Figure A 12: Beam 1

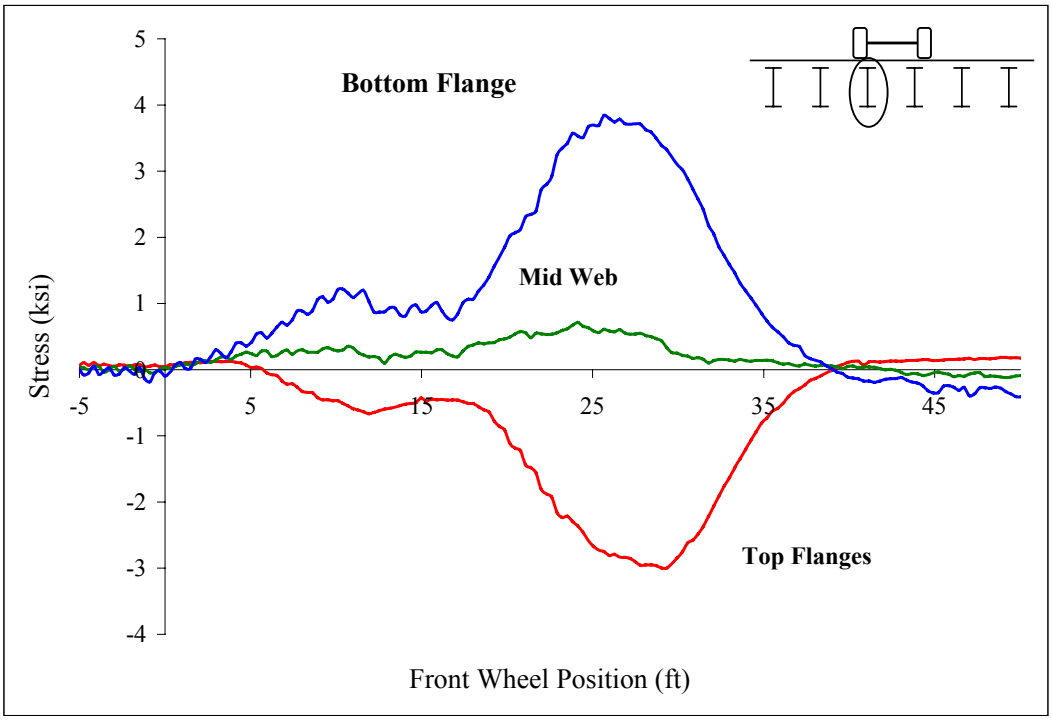

Figure A 13: Midspan stringer 4

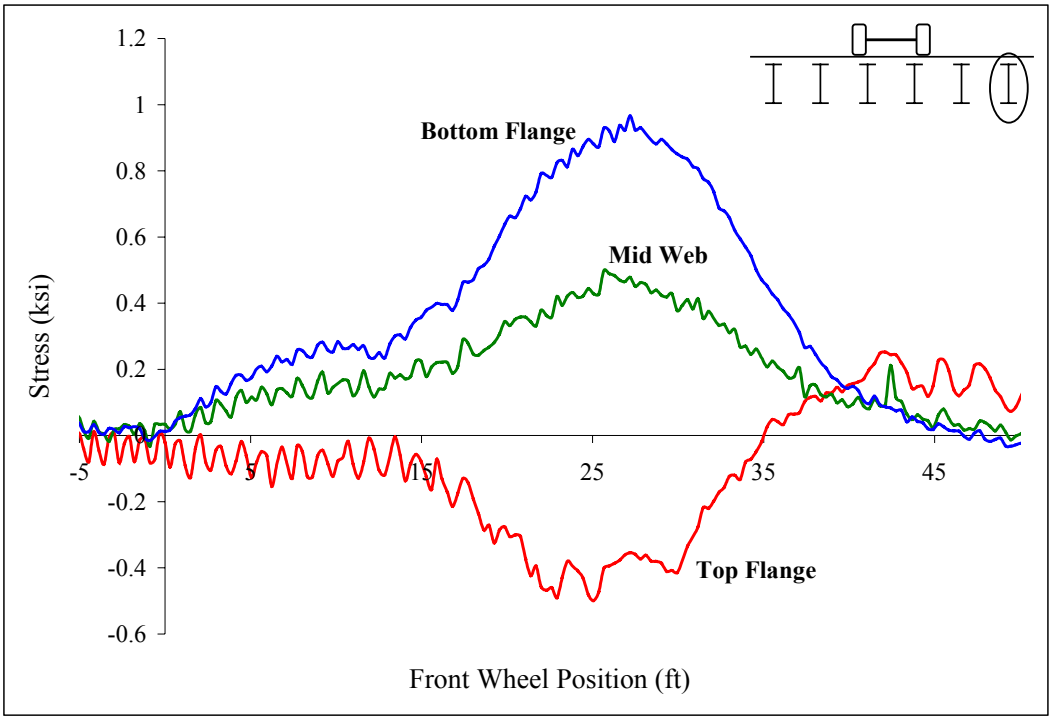

Figure A 14: Midspan stringer 1

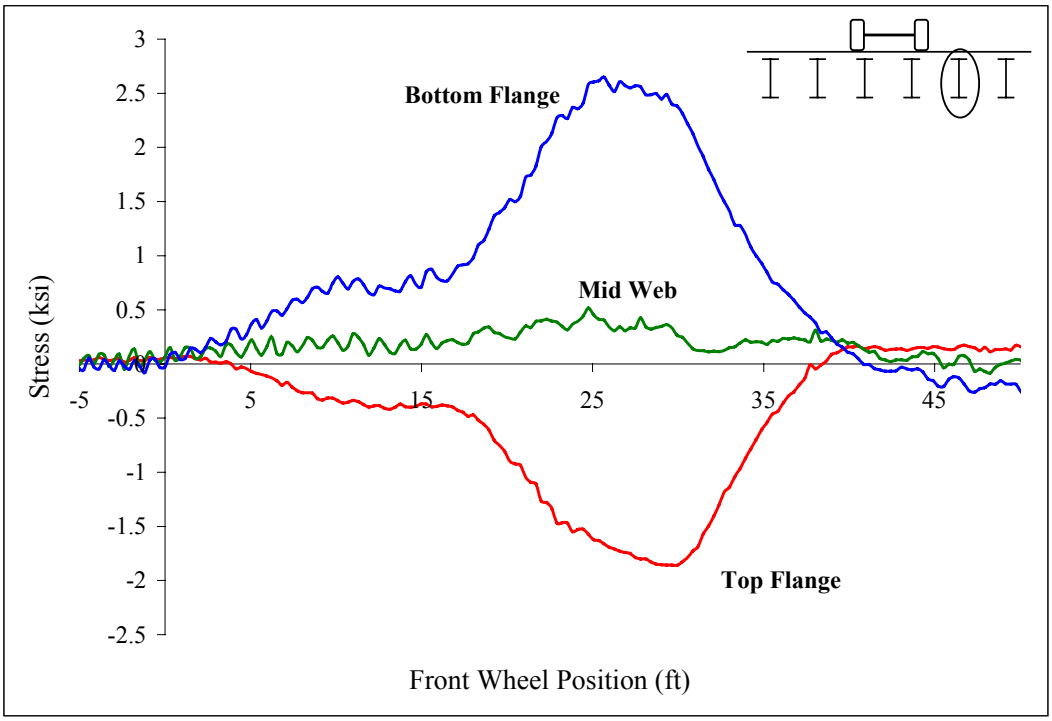

Figure A 15: Midspan stringer 2

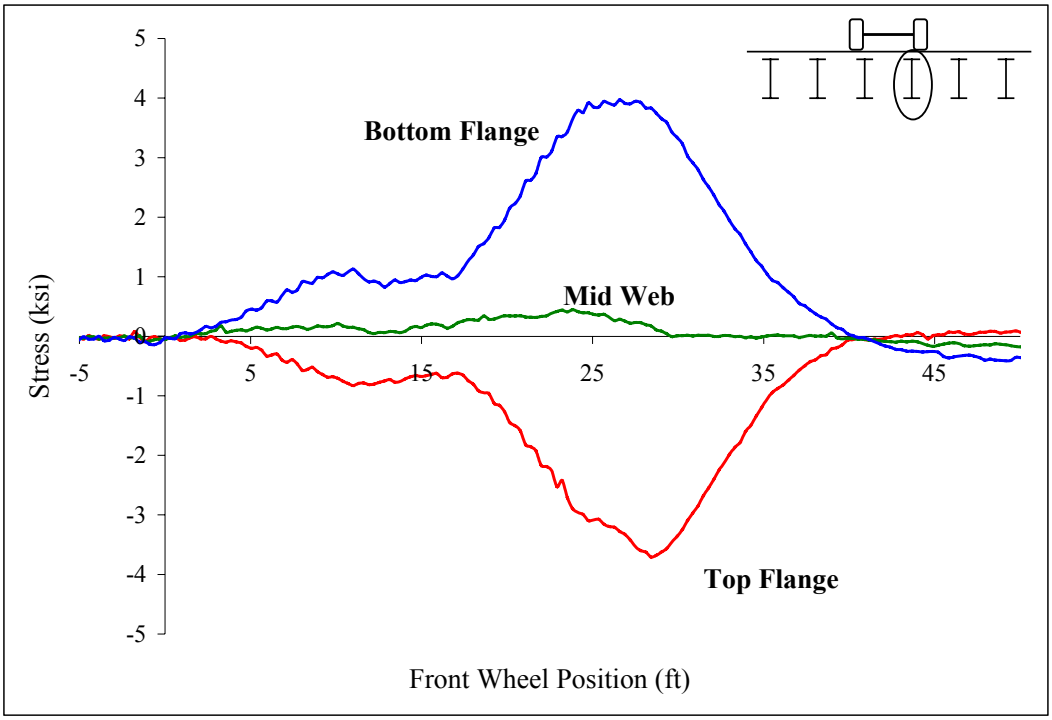

Figure A 16: Midspan stringer 3

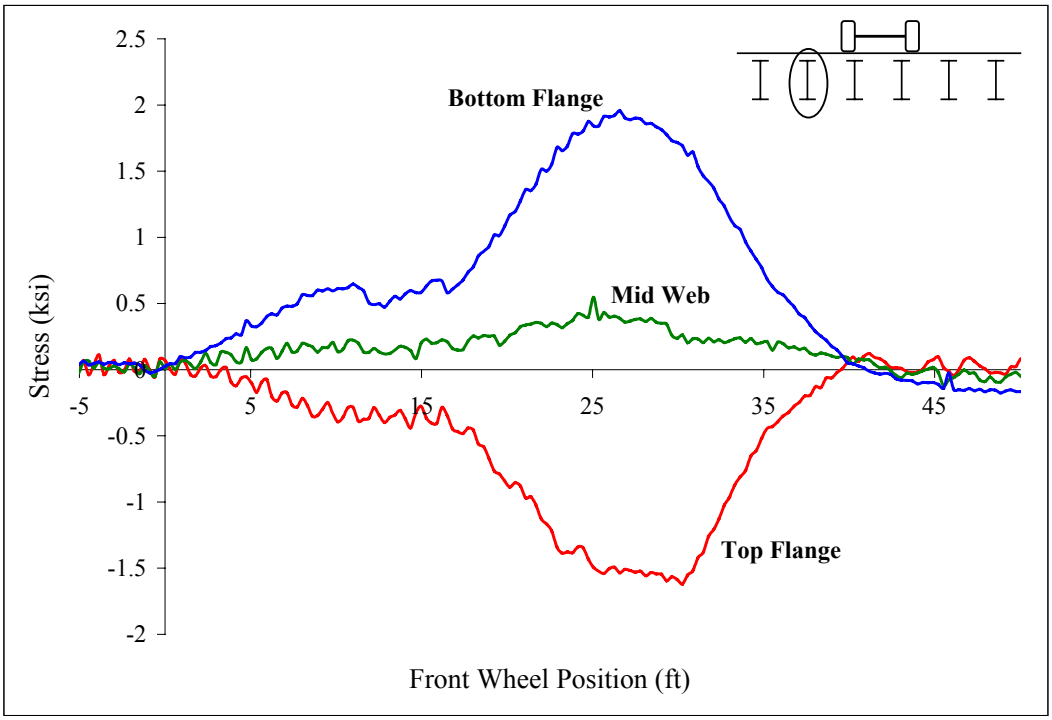

Figure A 17: Midspan stringer 5

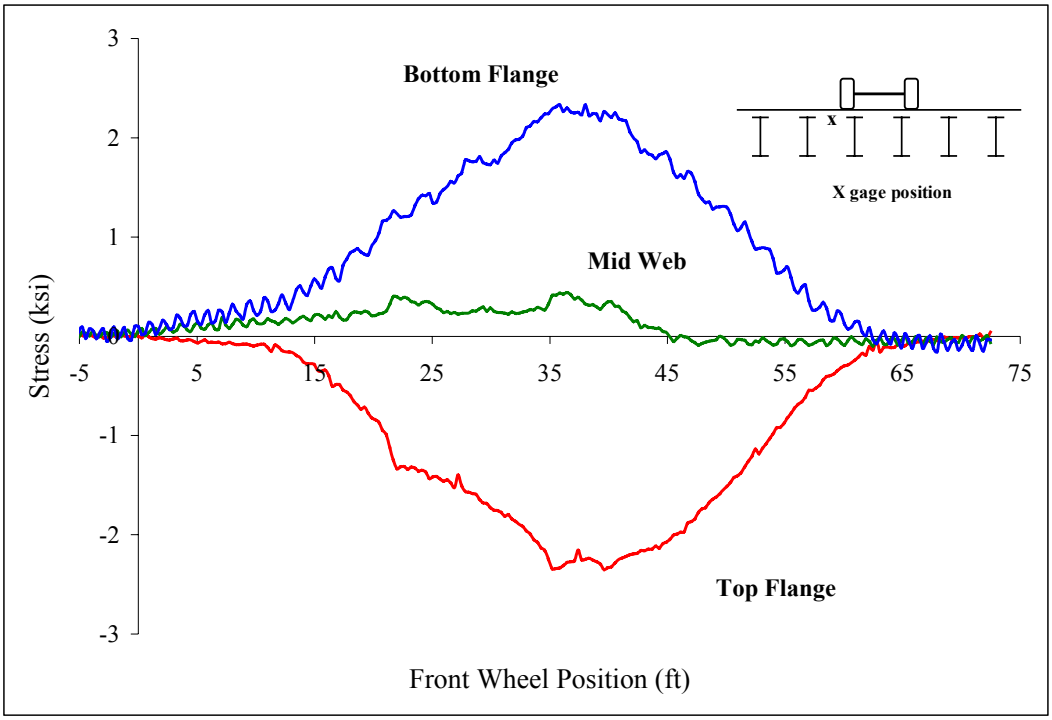

Figure A 18: Beam 2

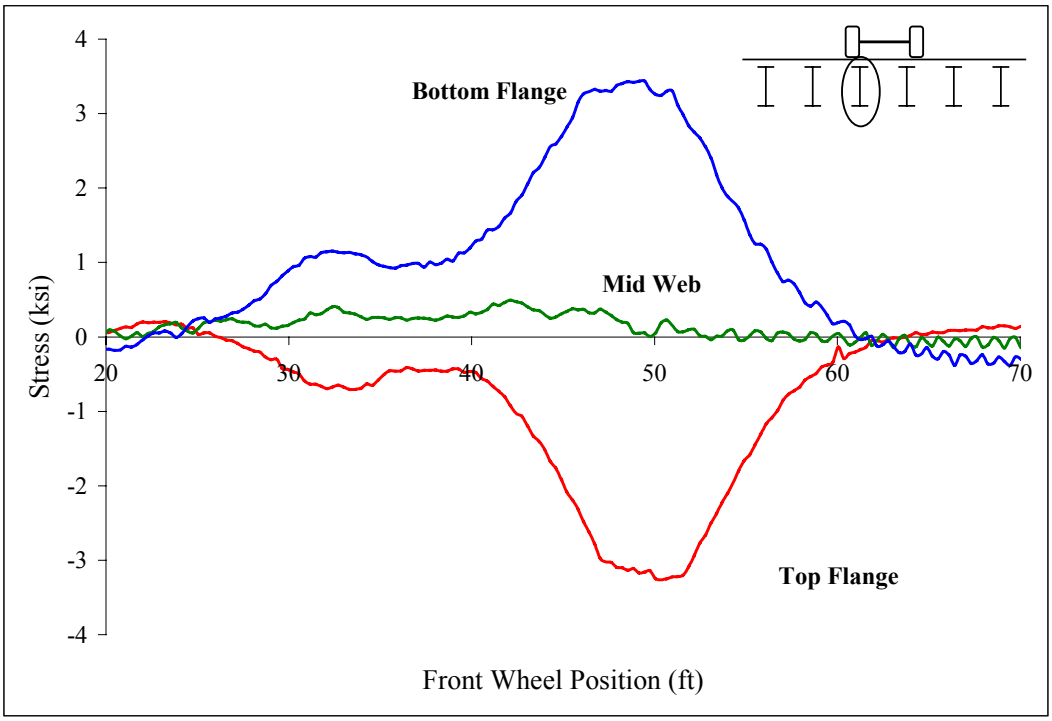

Figure A 19: Midspan stringer 7

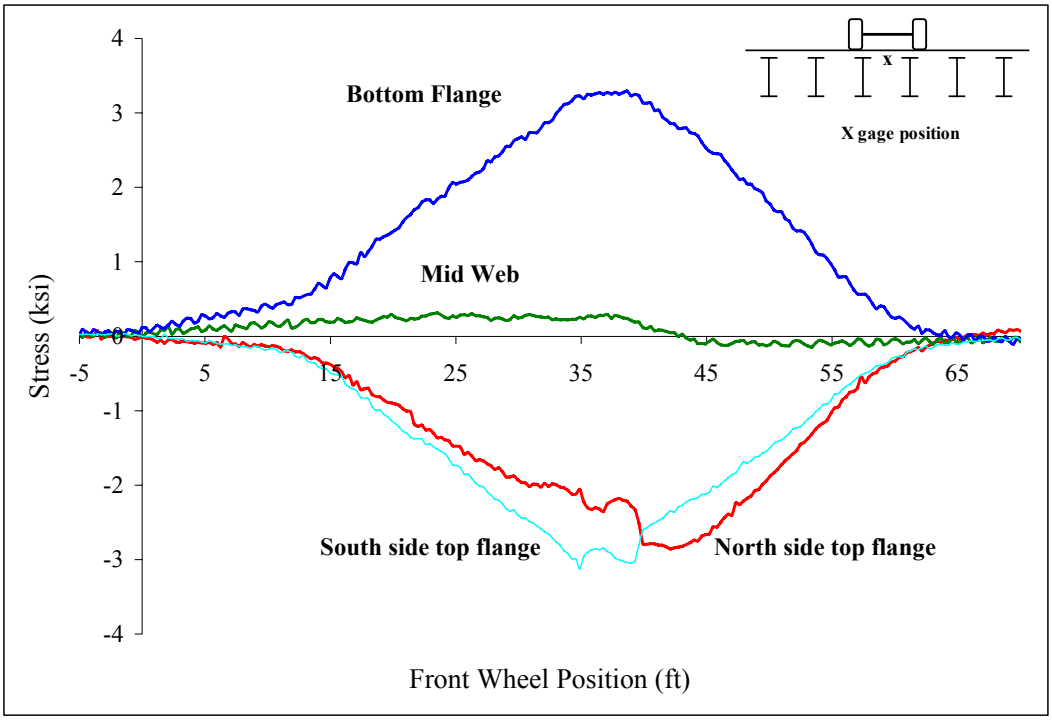

Figure A 20: Beam 2

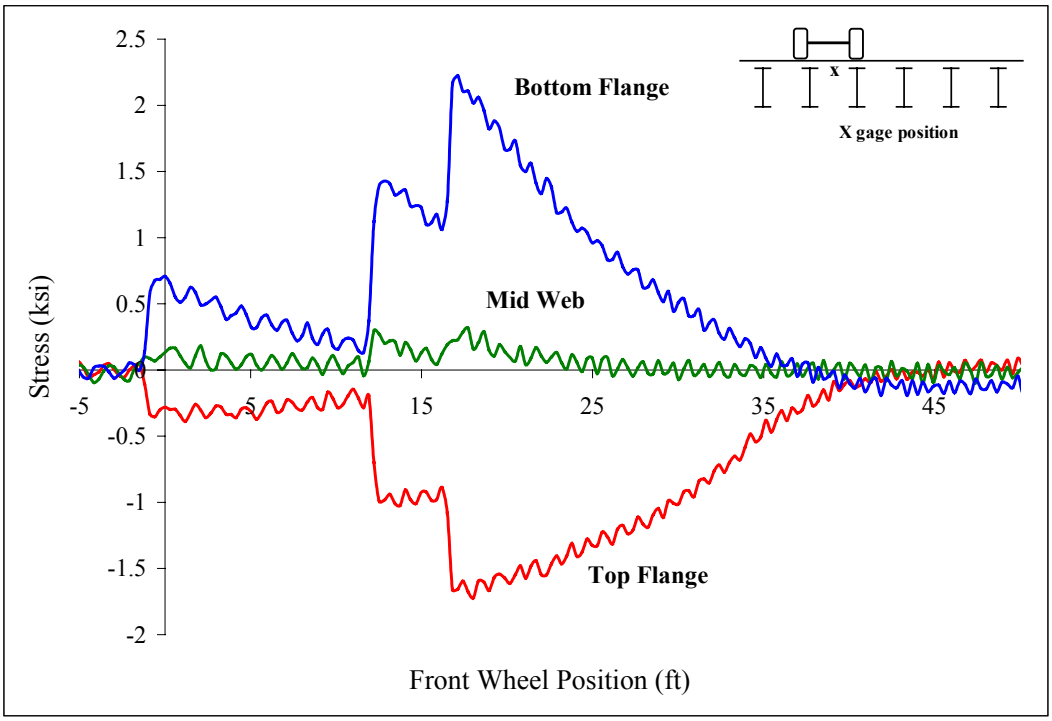

Figure A 21: Beam 1

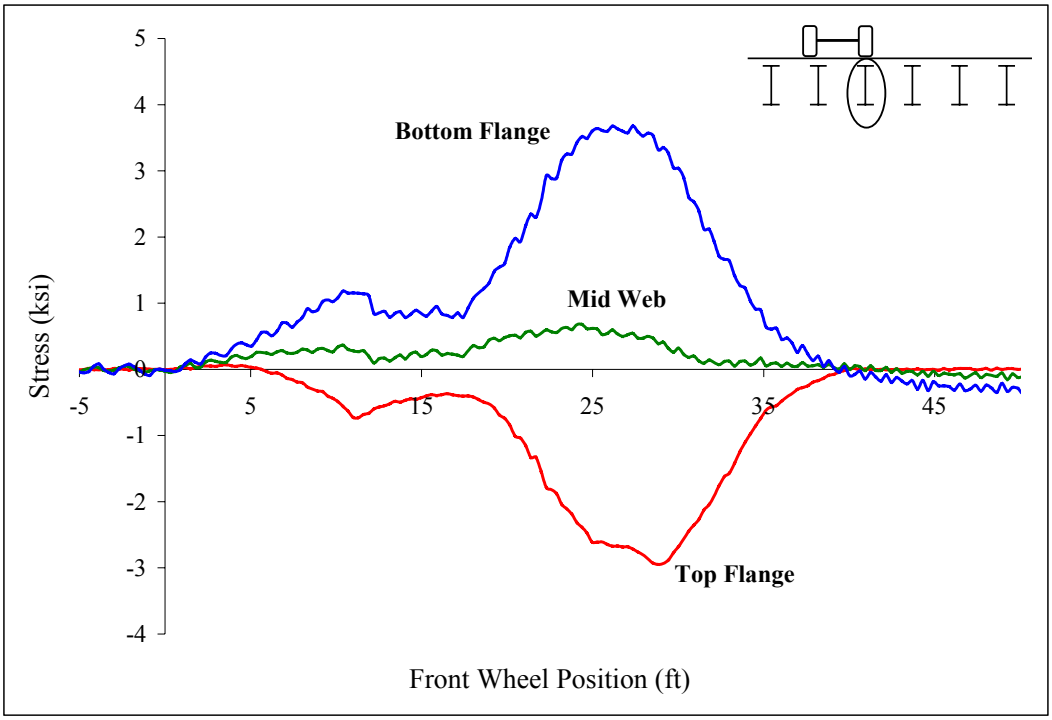

Figure A 22: Midspan stringer 4

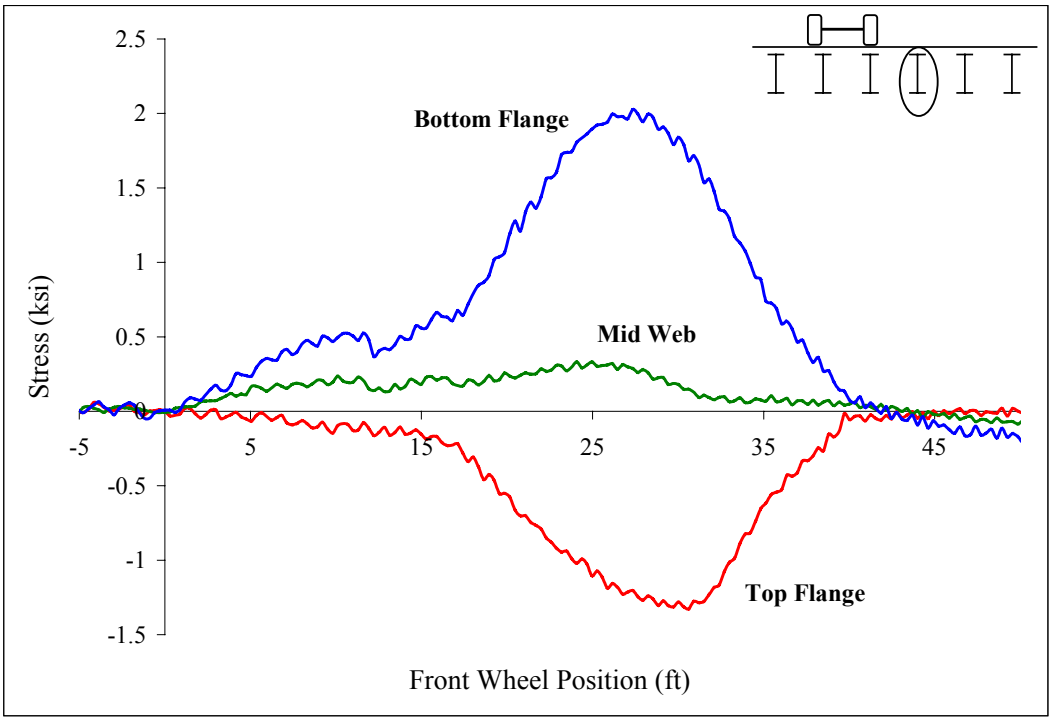

Figure A 23: Midspan stringer 3

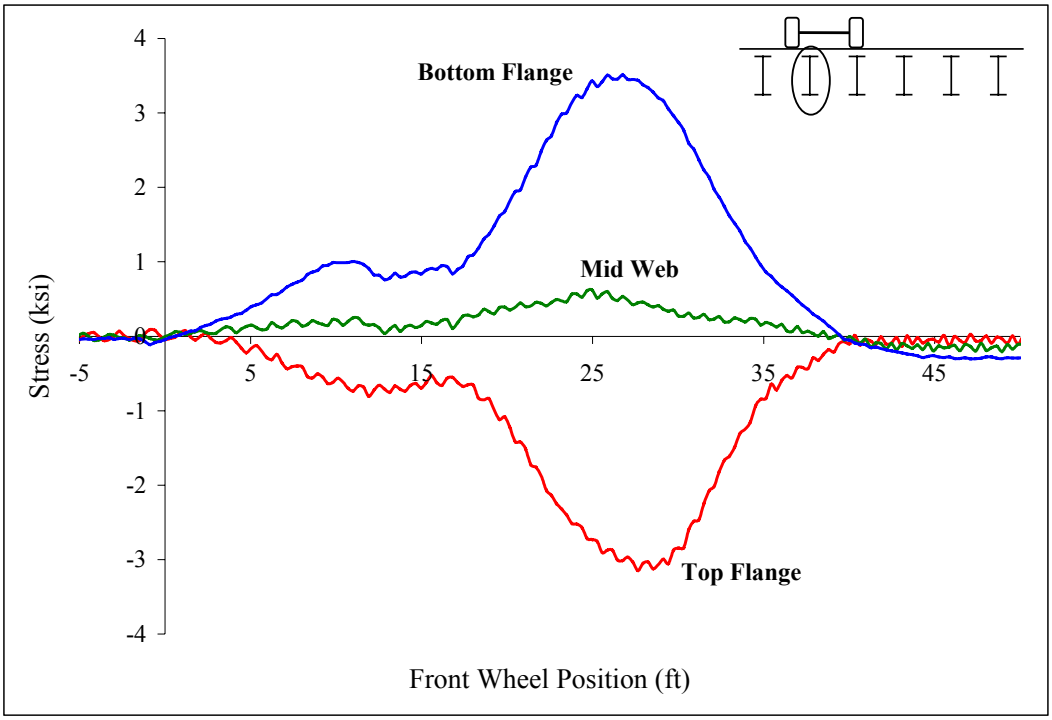

Figure A 24: Midspan stringer 5

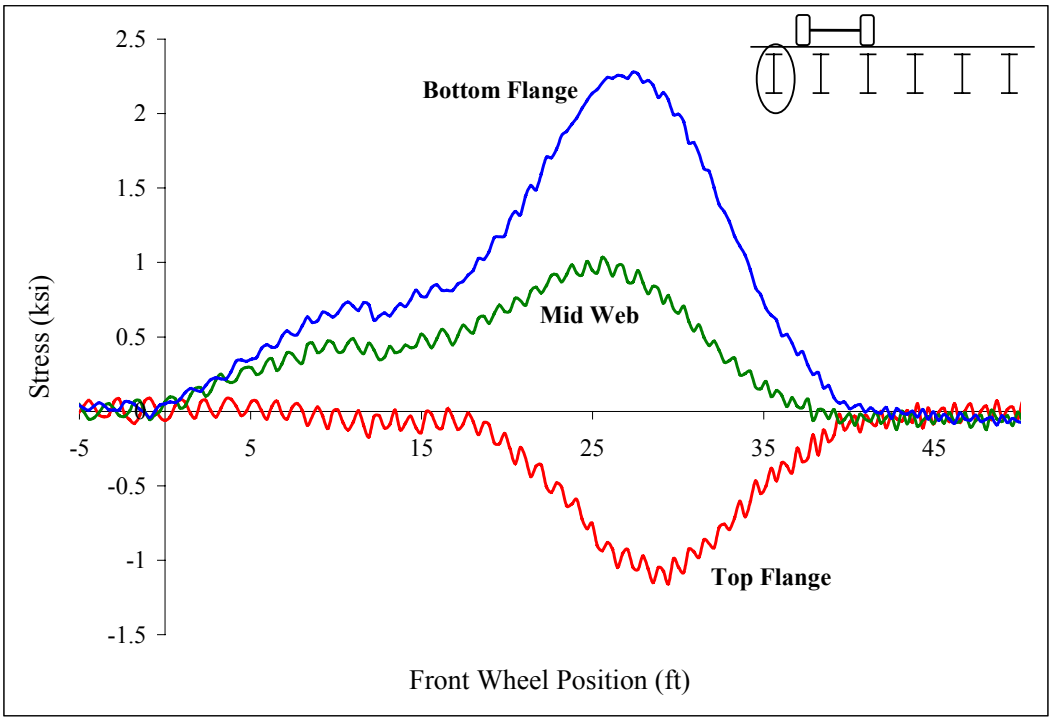

Figure A 25: Midspan stringer 6

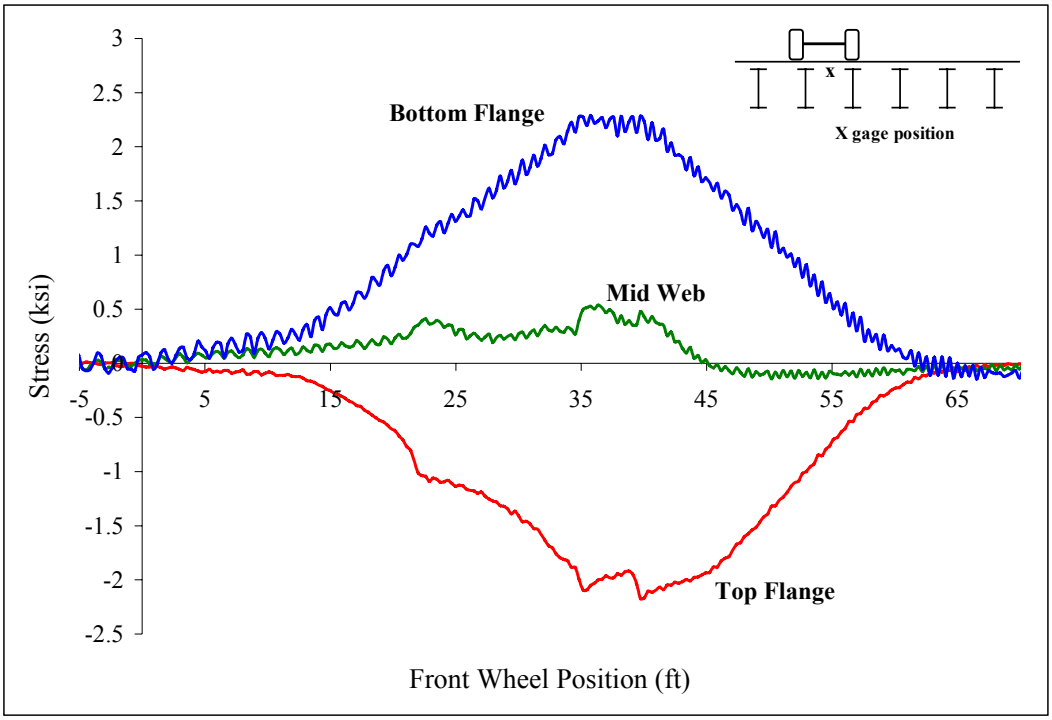

Figure A 26: Beam 2

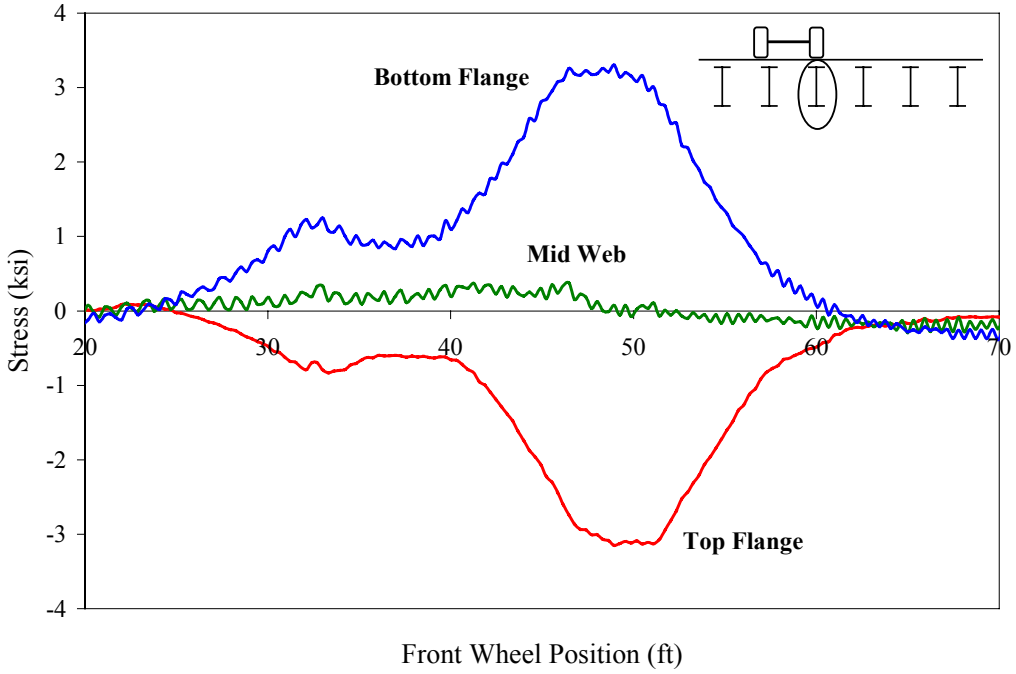

Figure A 27: Midspan stringer 7

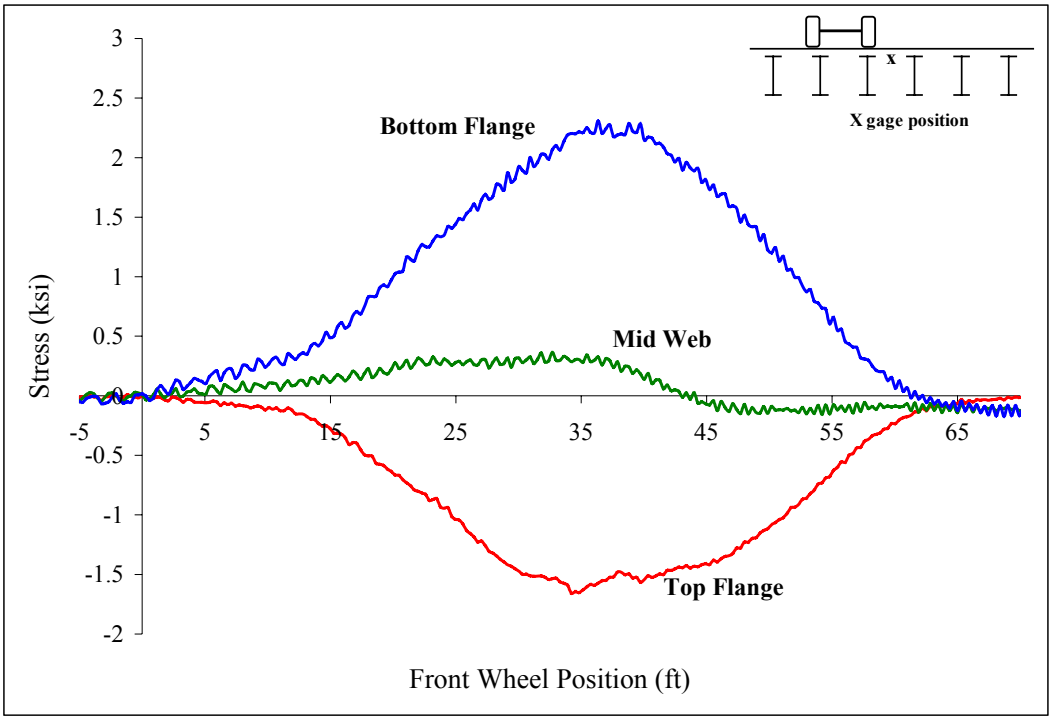

Figure A 28: Beam 2

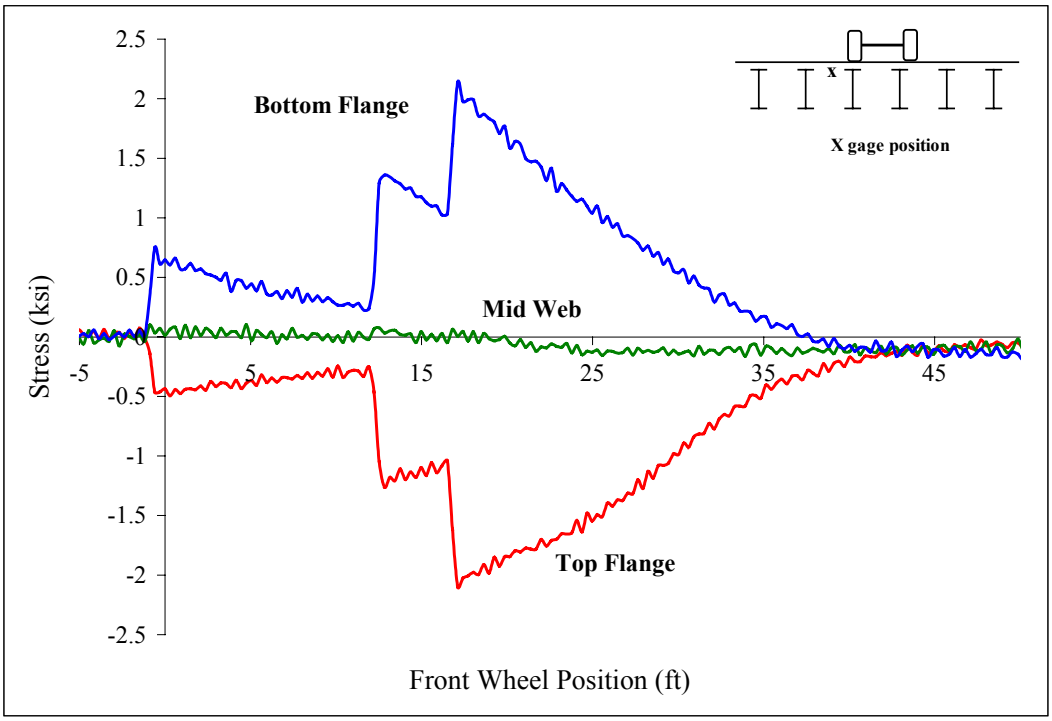

Figure A 29: Beam 1

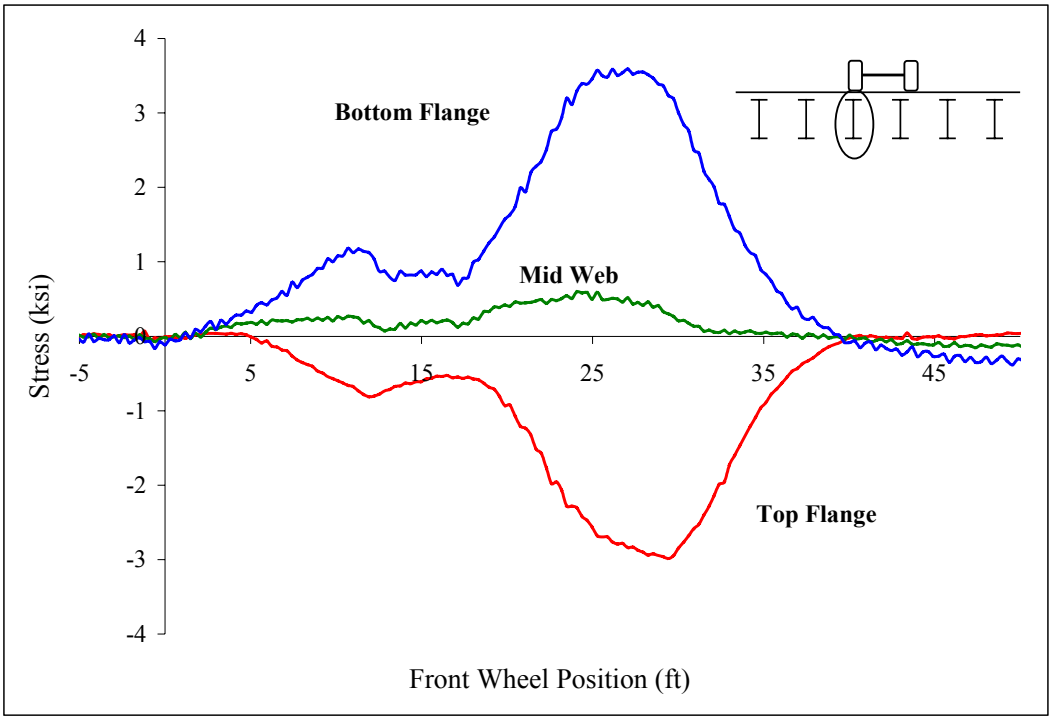

Figure A 30: Midspan stringer 4

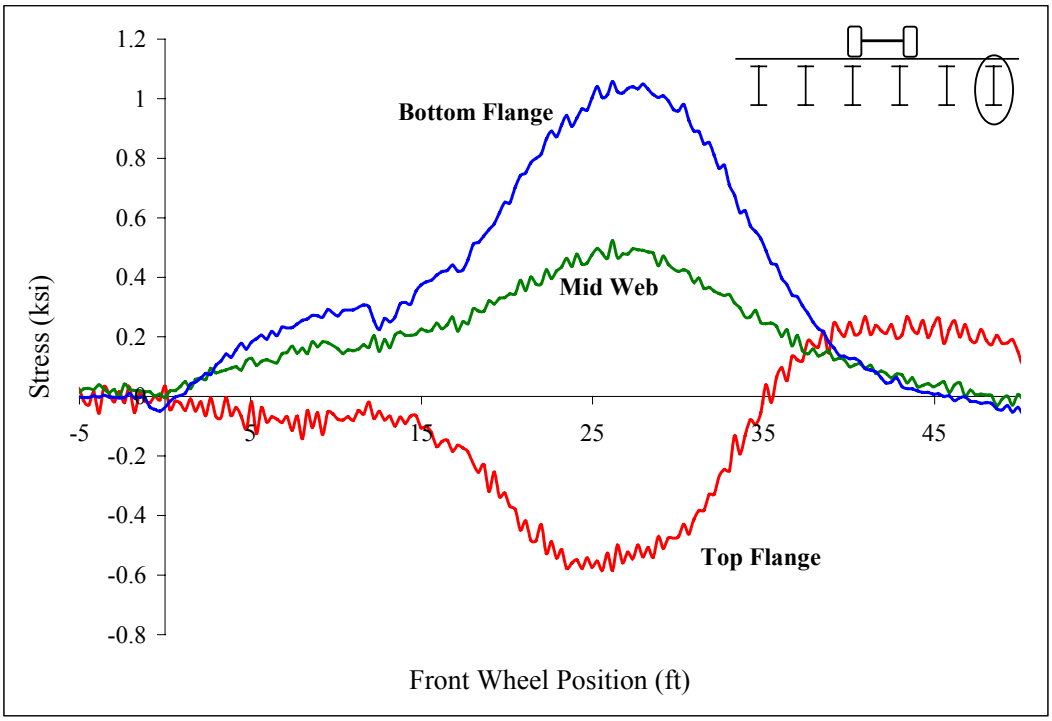

Figure A 31: Midspan stringer 1

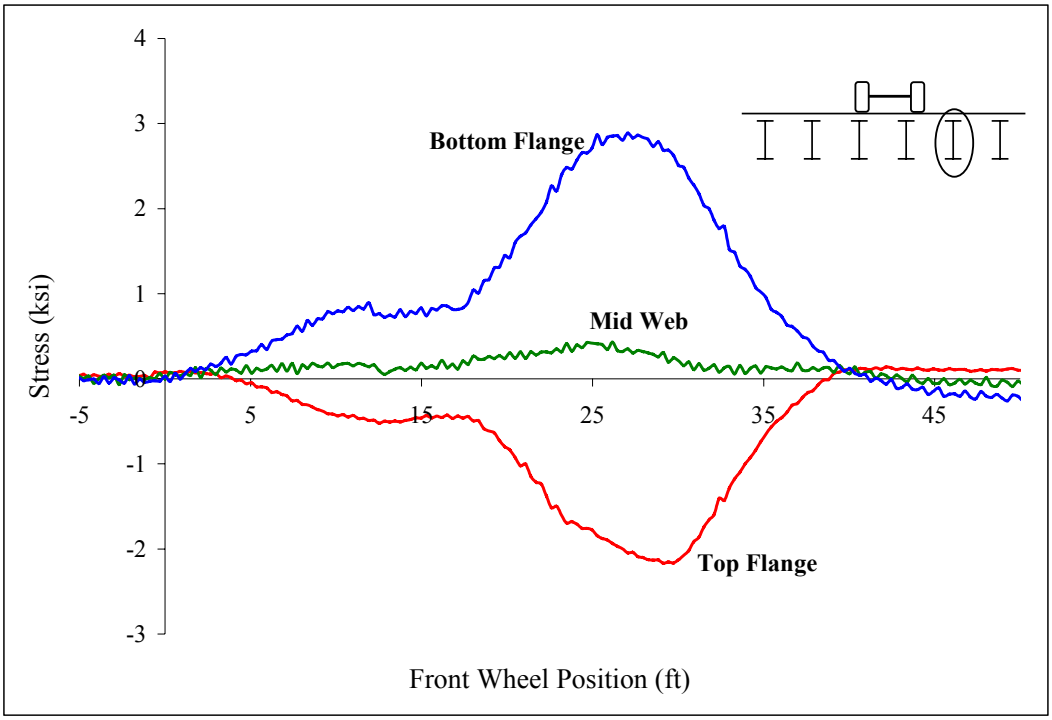

Figure A 32: Midspan stringer 2

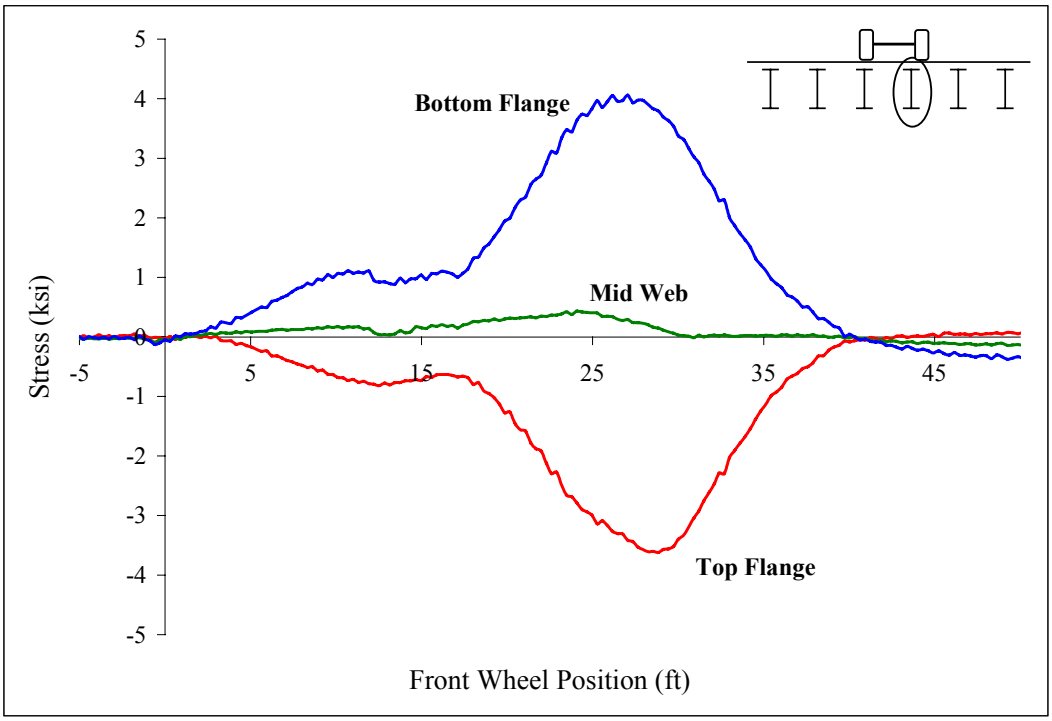

Figure A 33: Midspan stringer 3

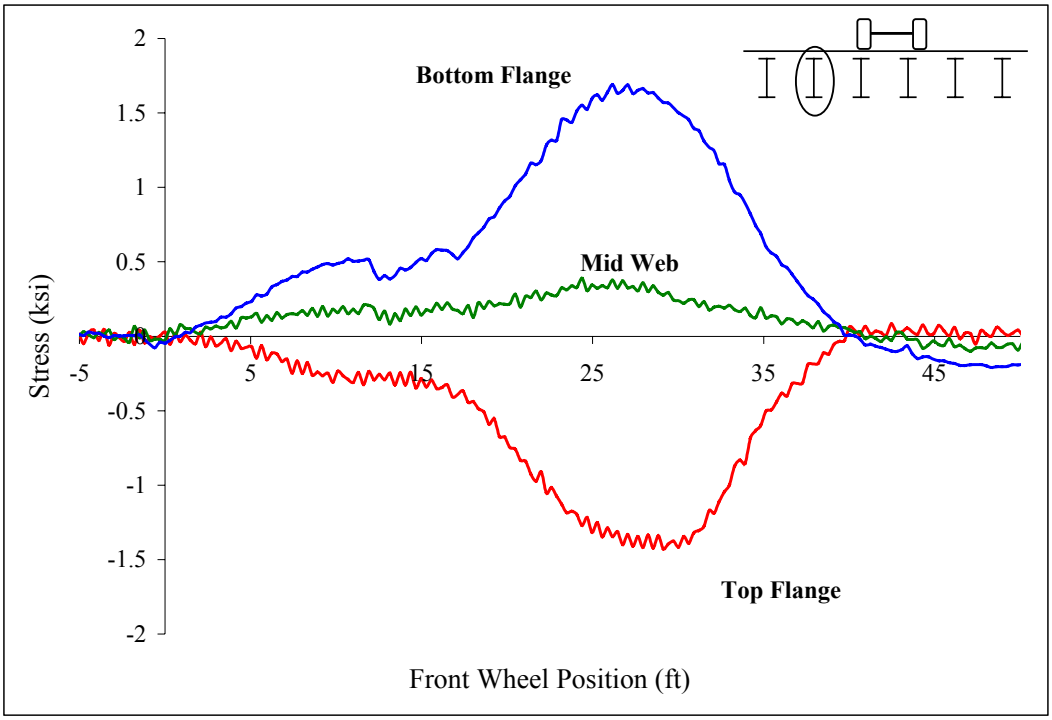

Figure A 34: Midspan stringer 5

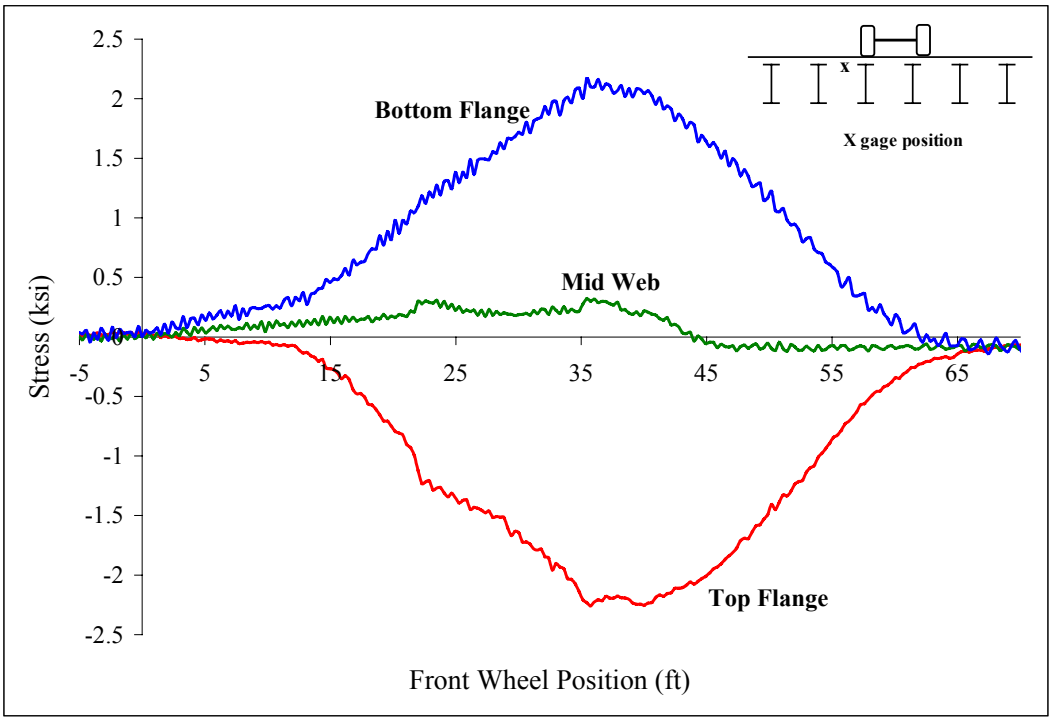

Figure A 35: Beam 2

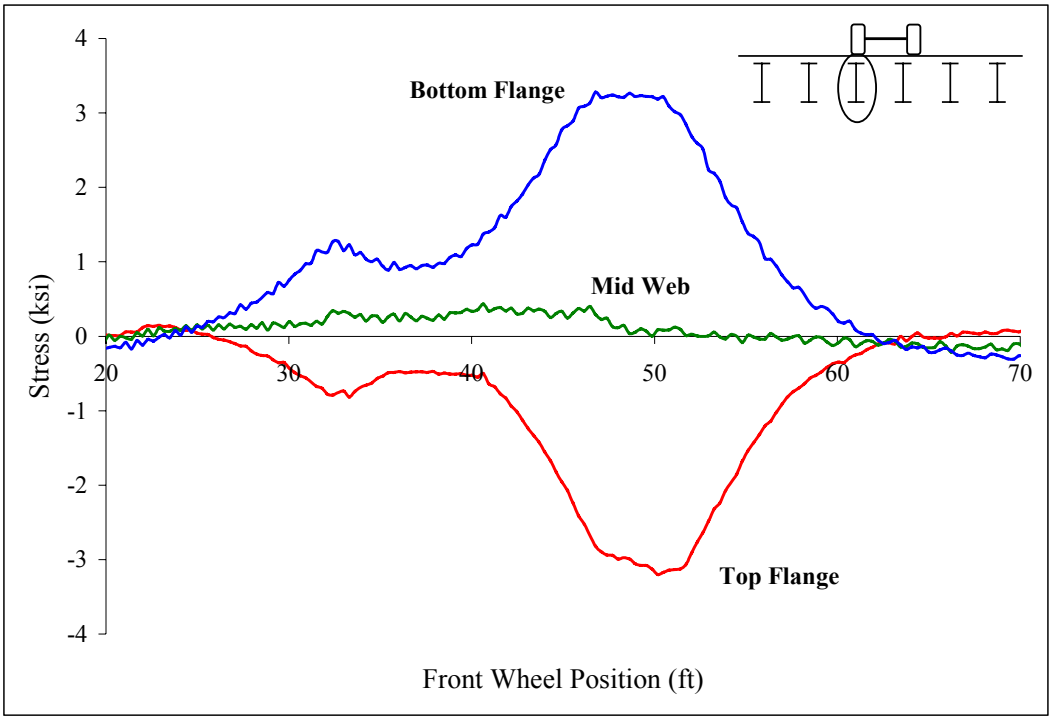

Figure A 36: Midspan stringer 4

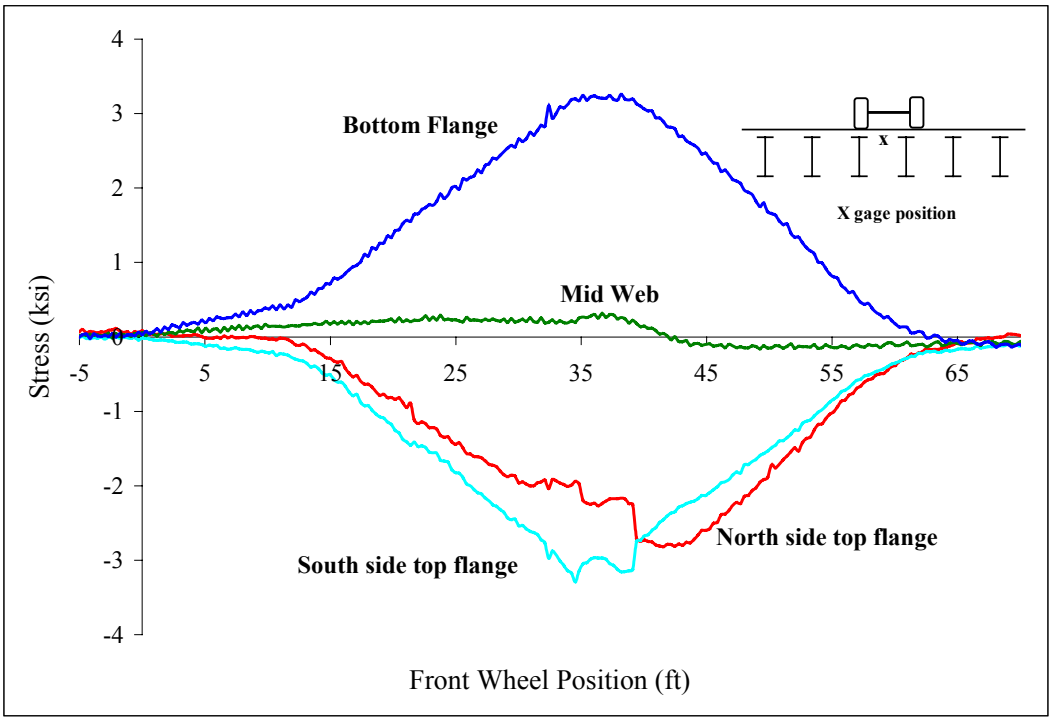

Figure A 37: Beam 2

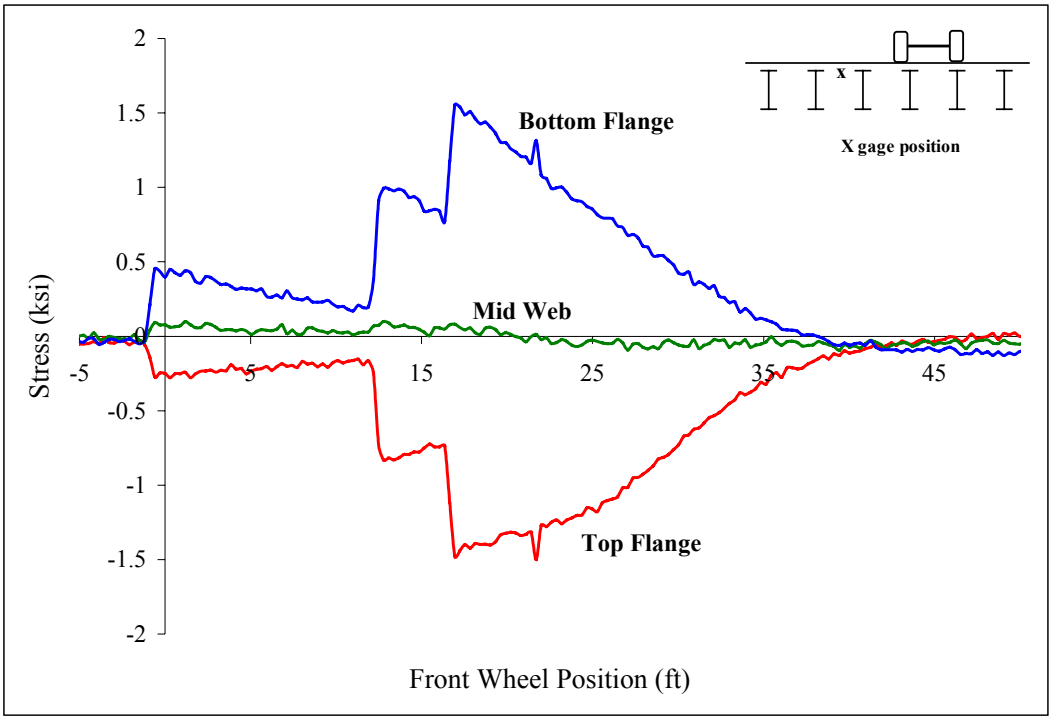

Figure A 38: Beam 1

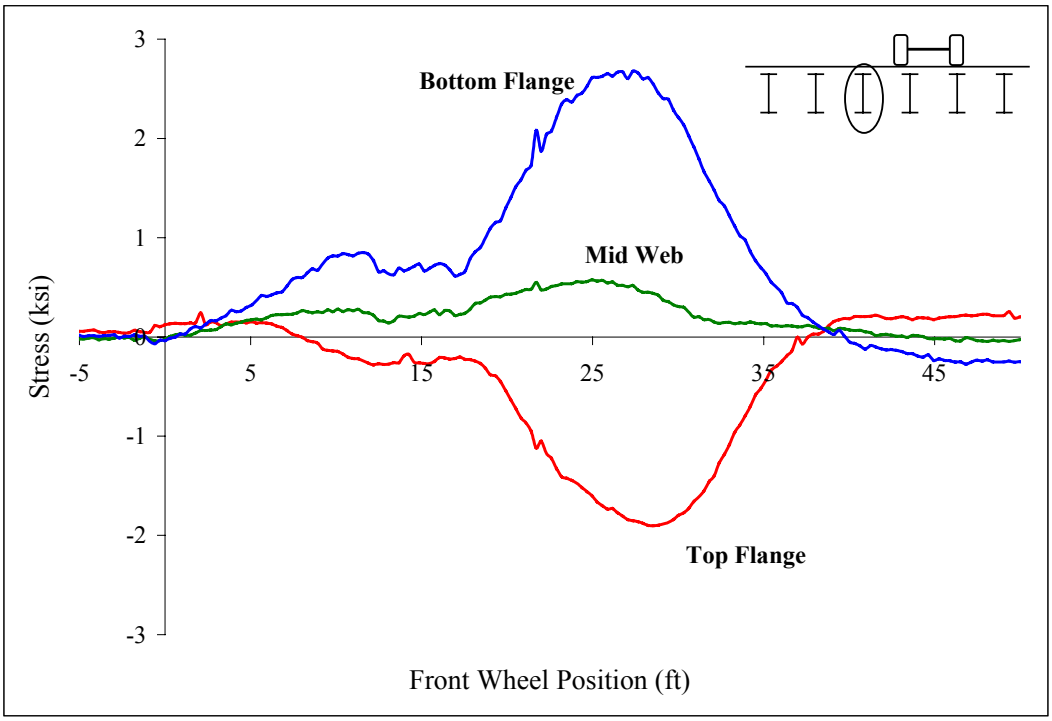

Figure A 39: Midspan stringer 4

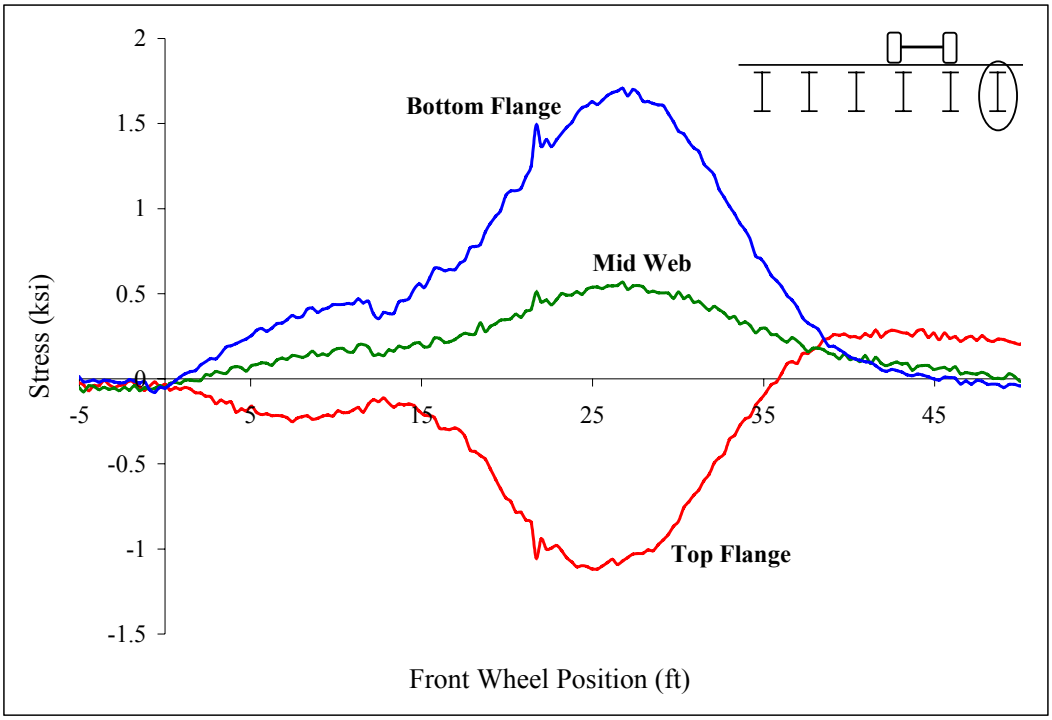

Figure A 40: Midspan stringer 1

Figure A 41: Midspan stringer 2

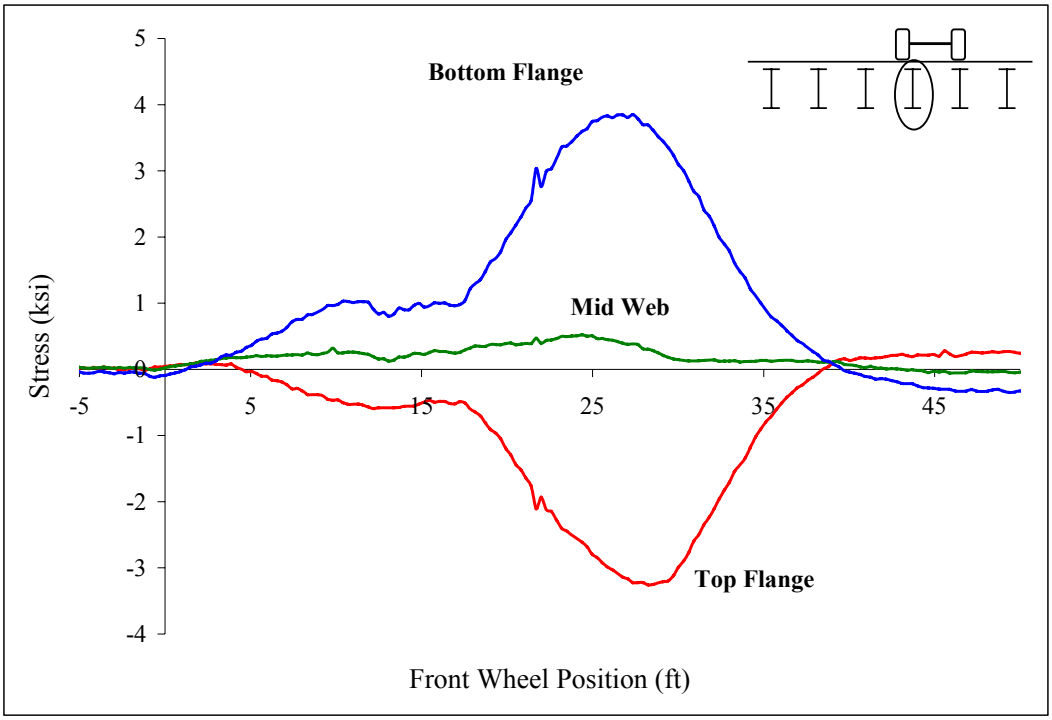

Figure A 42: Midspan stringer 3

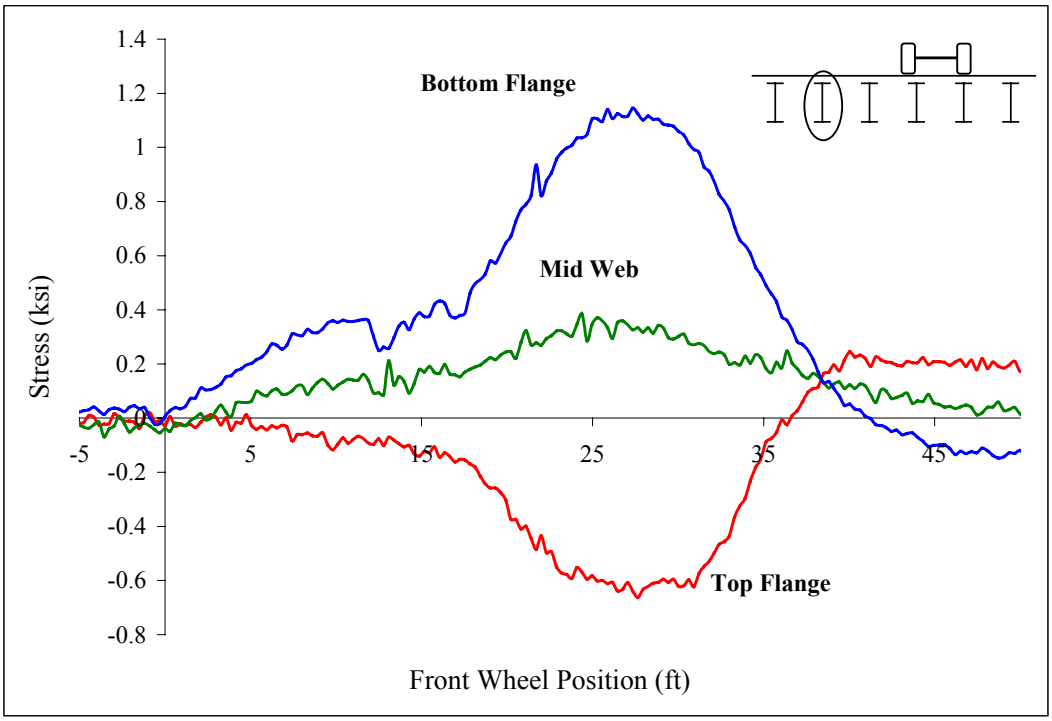

Figure A 43: Midspan stringer 5

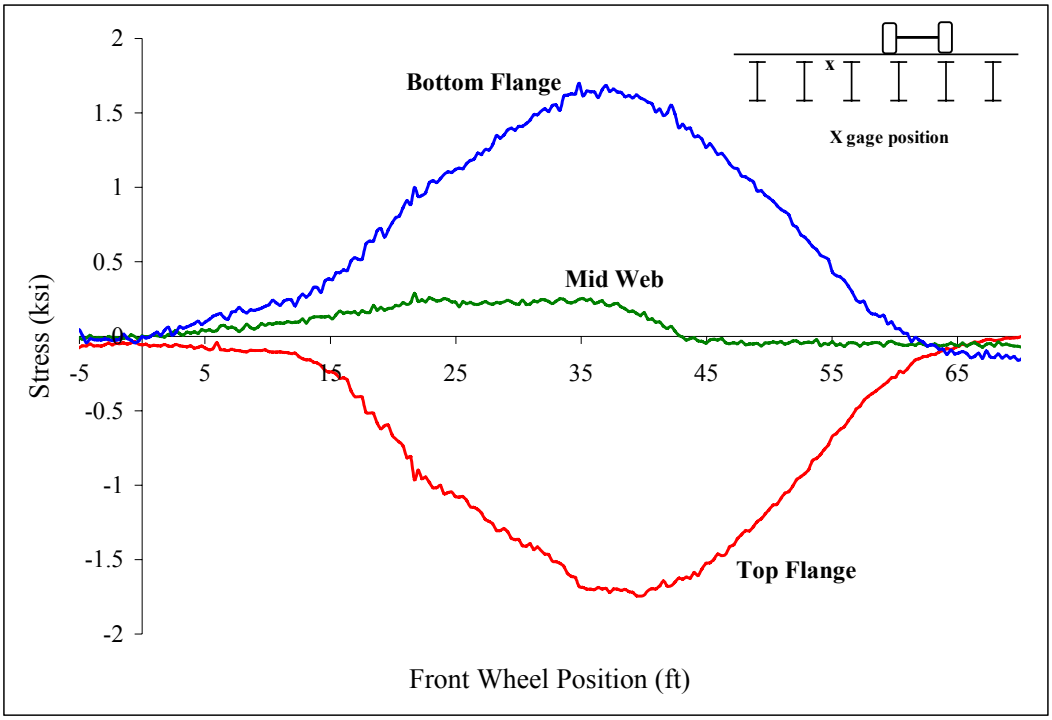

Figure A 44: Beam 2

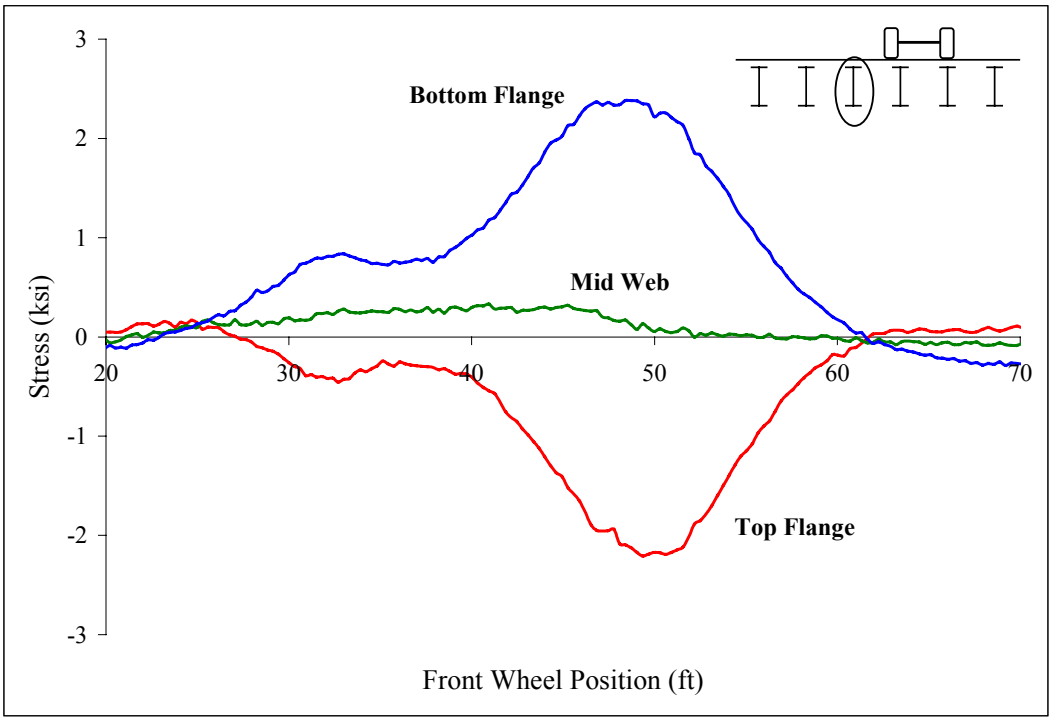

Figure A 45: Midspan stringer 7

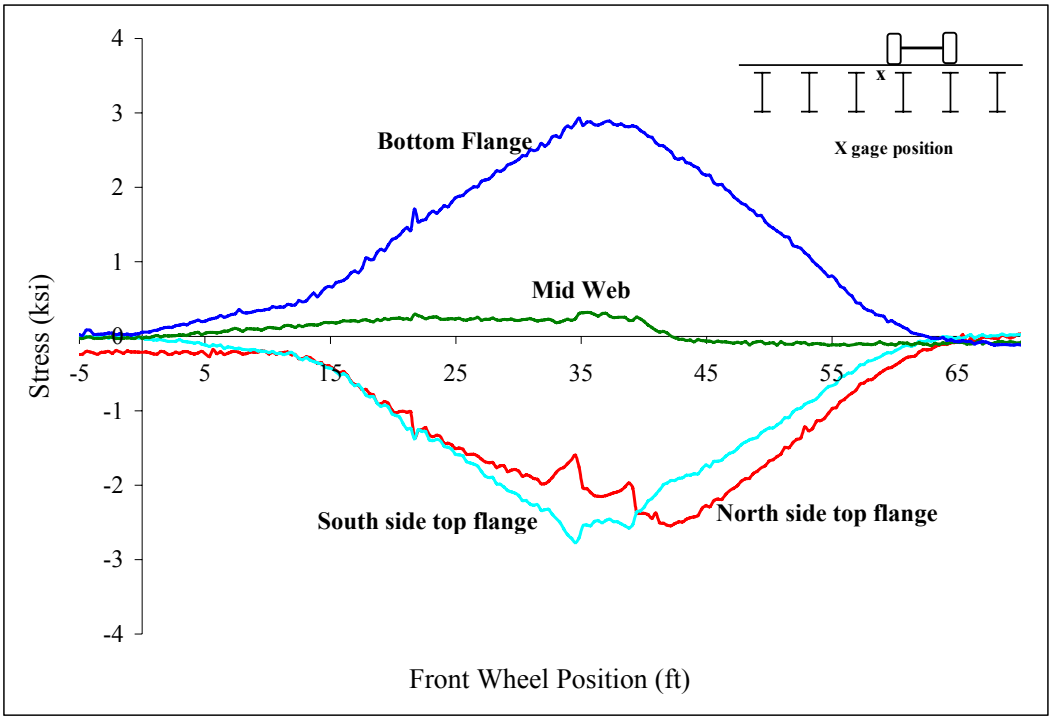

Figure A 46: Beam 2

Appendix B:

Field Load Test Data: Llano Test No. 2

Appendix B contains results from the second Llano field load test, conducted on April 15, 1999. In this test, selected portions of the deck system were instrumented with strain gages. Trucks of known weight and geometry were then driven slowly over the bridge, and the response of the instrumented members was measured. The measured strains were converted to stress and plotted versus the position of the load truck on the bridge. The load vehicles were driven south. Consequently, the graphic showing gage location on each plot faces in a southerly direction. The stringers are numbered 1 though 6, with stringer 1 the western-most stringer. Figure B1 shows the truck dimensions and average weight of the two trucks used in the test.

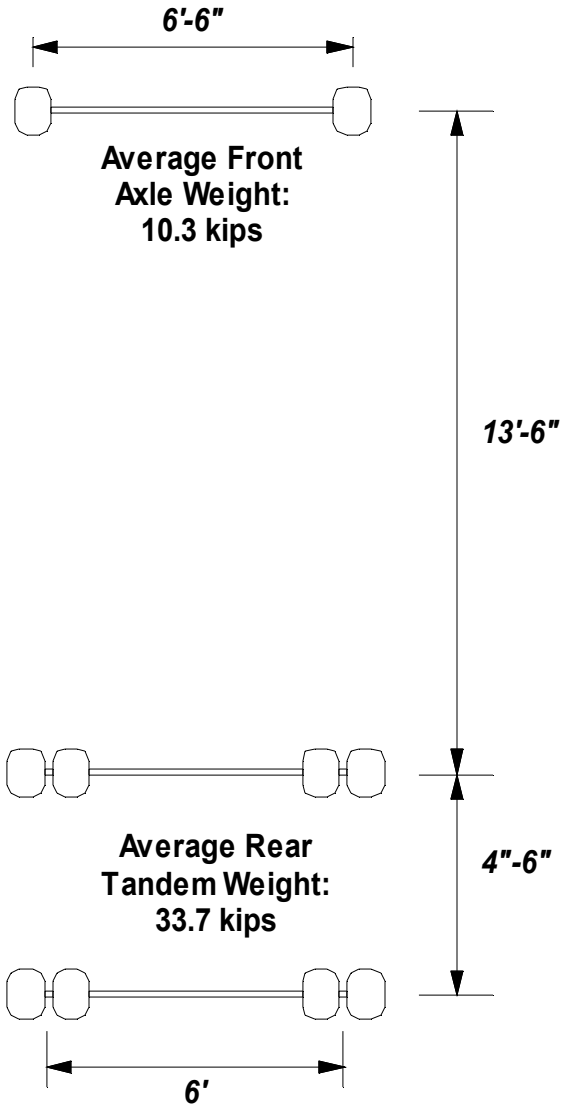

Figure B 1: Load truck dimensions and average weights for the second Llano test

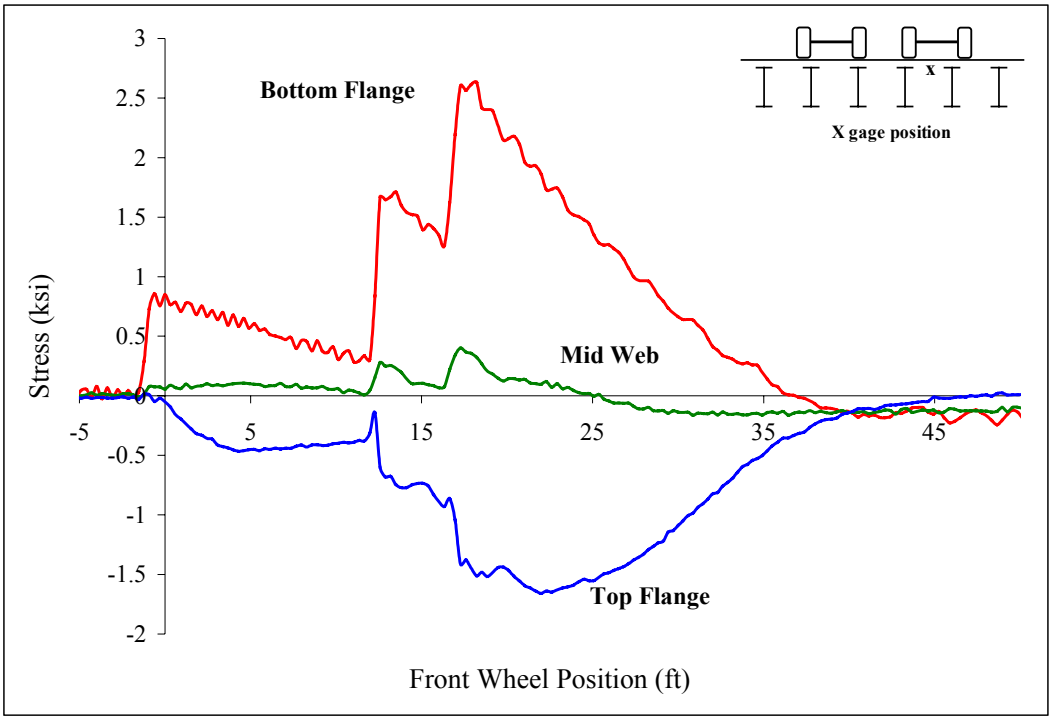

Figure B 2: Beam 1

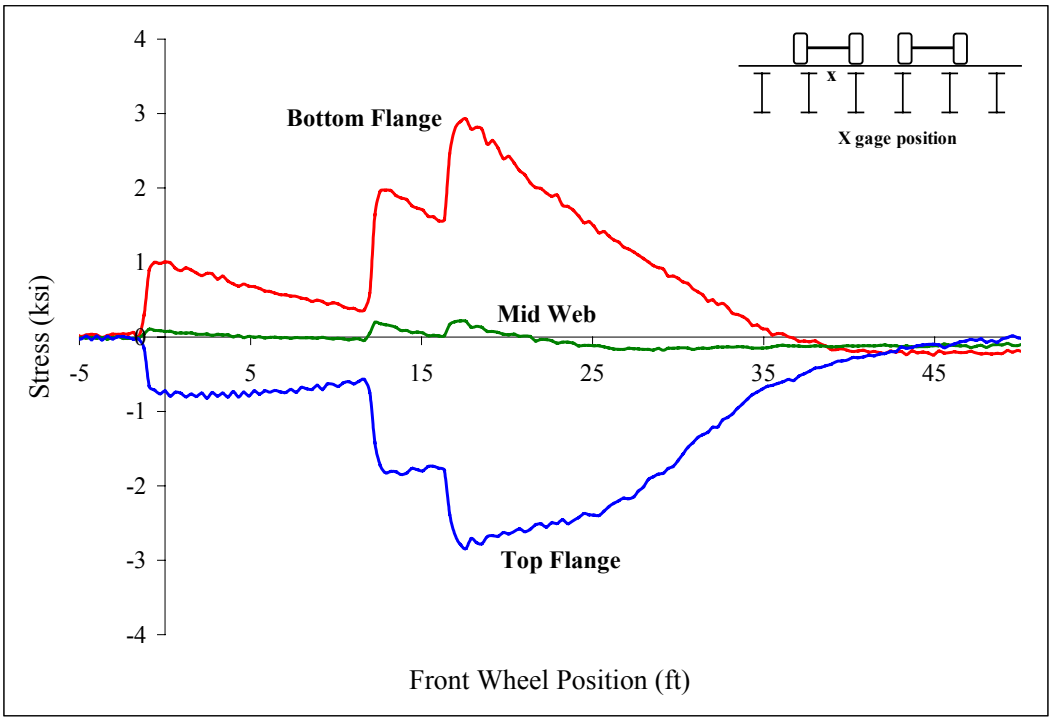

Figure B 3: Beam 1

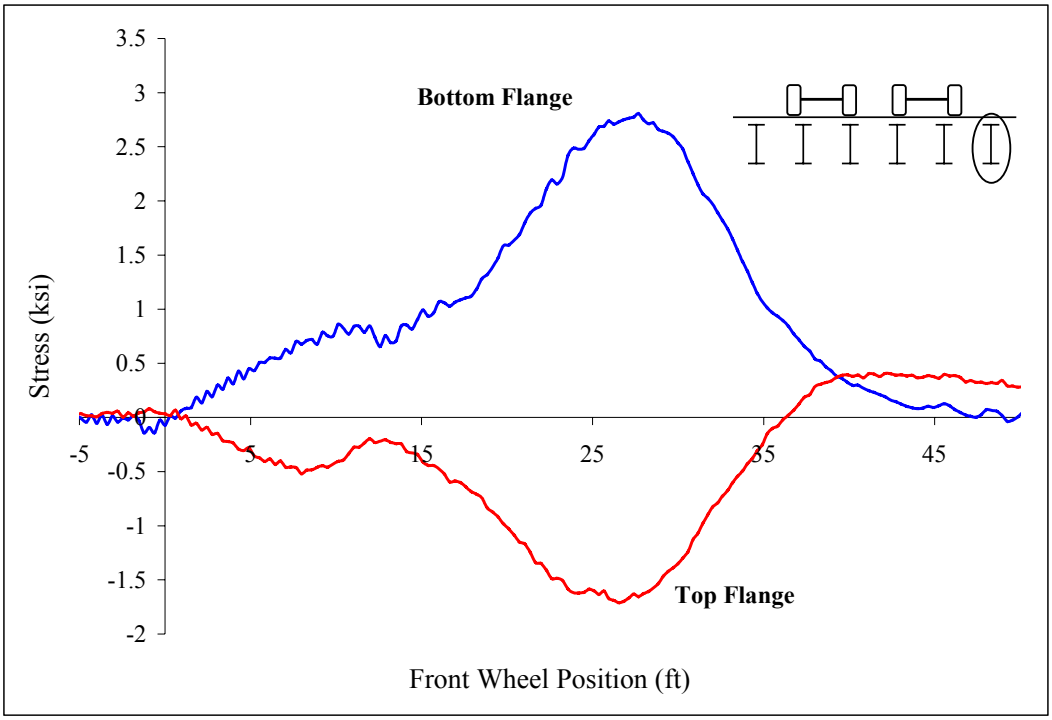

Figure B 4: Midspan stringer 1

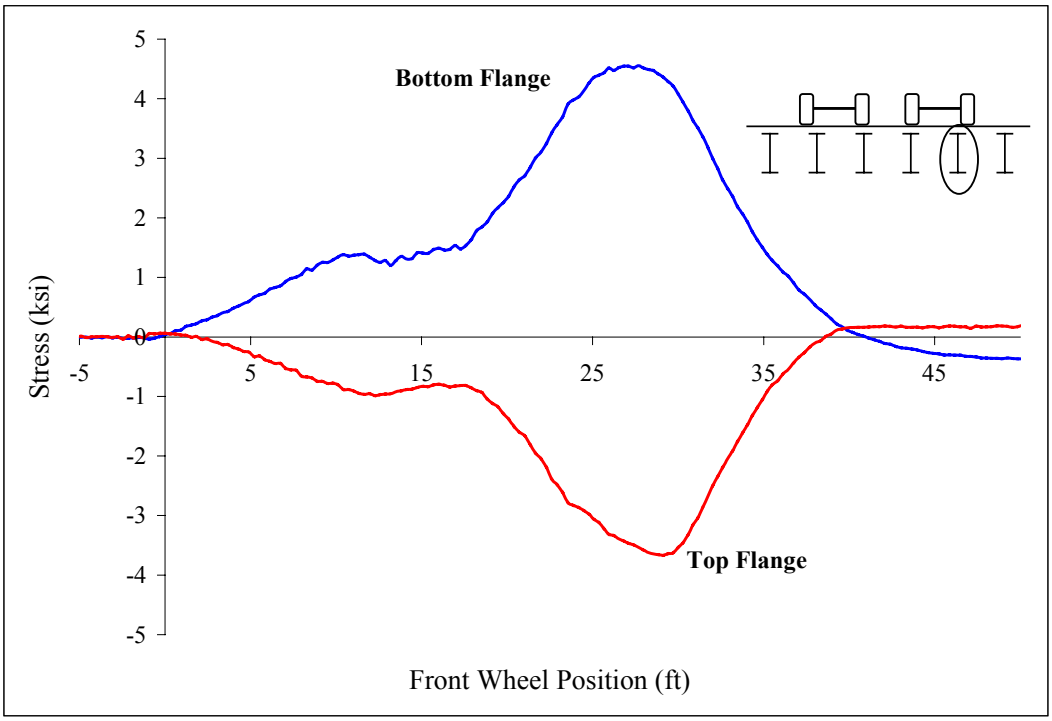

Figure B 5: Midspan stringer 2

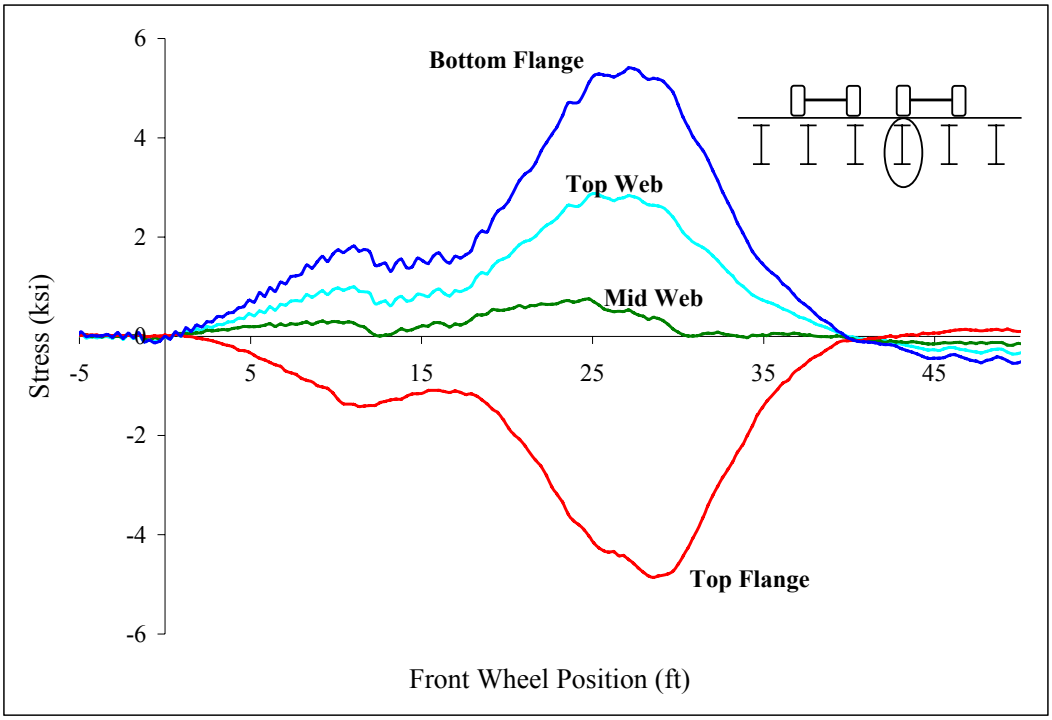

Figure B 6: Midspan stringer 3

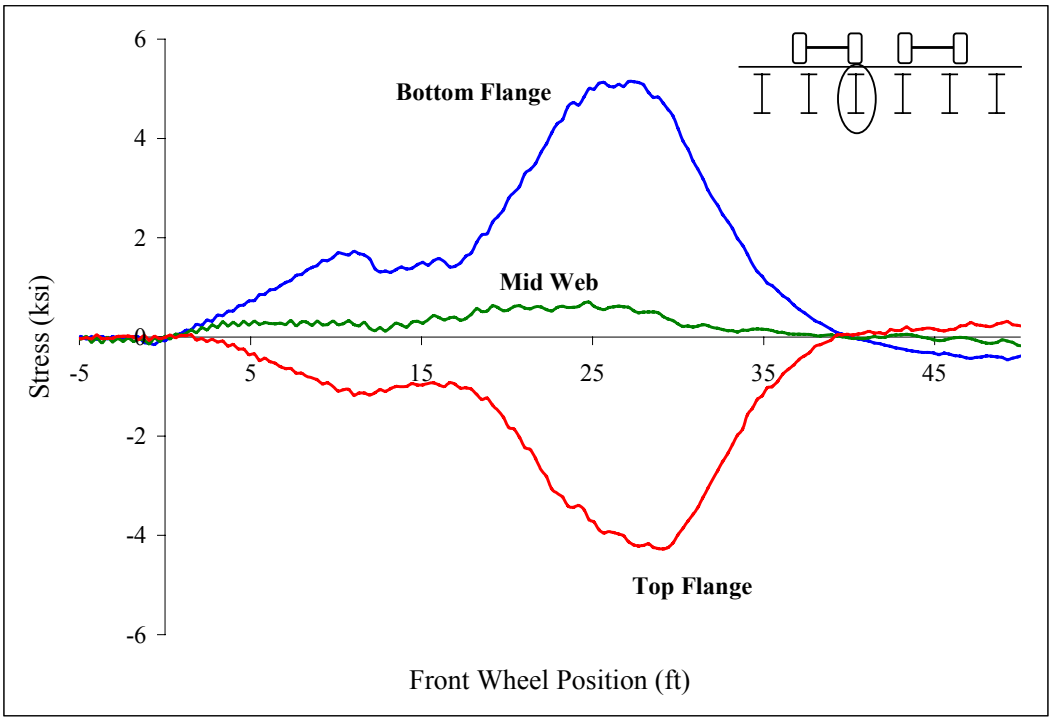

Figure B 7: Midspan stringer 4

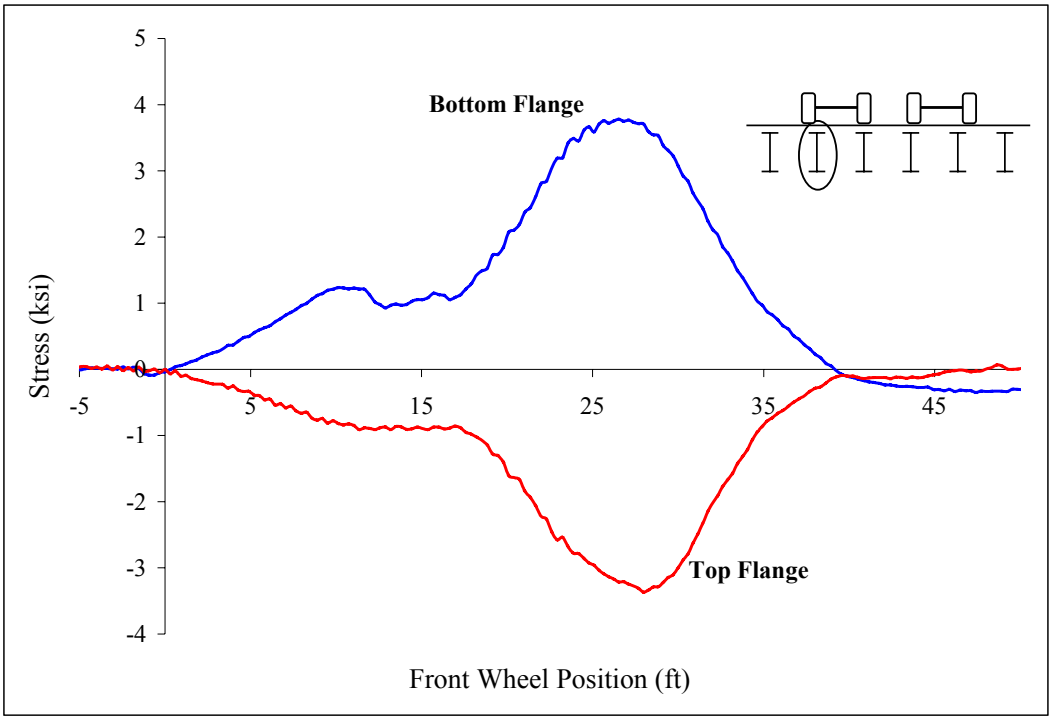

Figure B 8: Midspan stringer 5

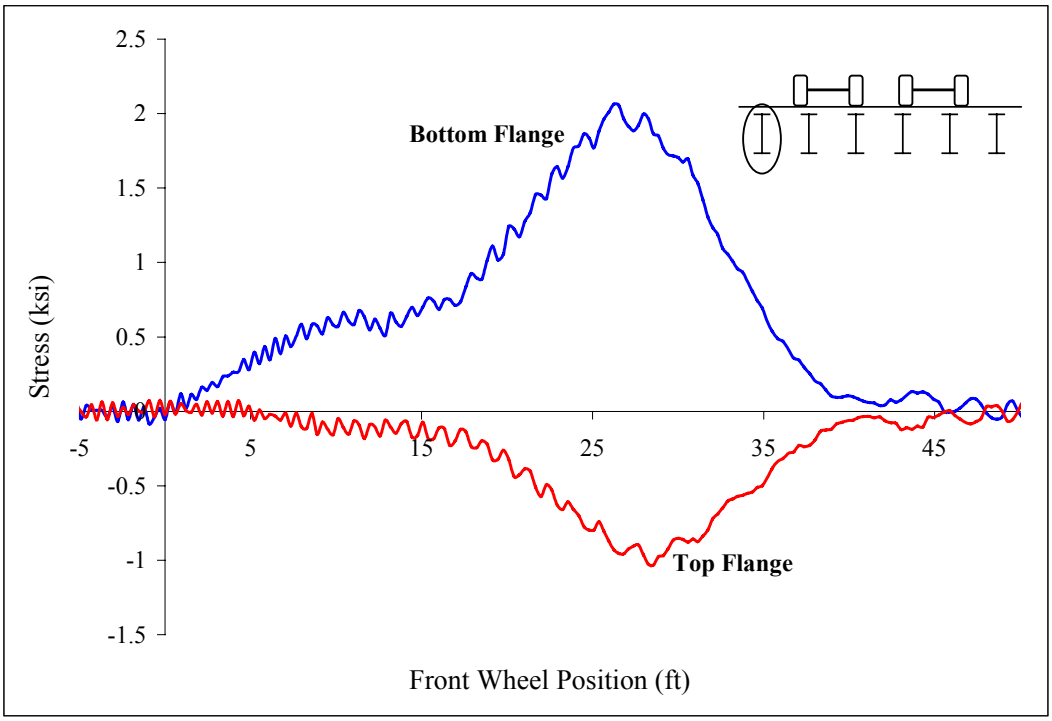

Figure B 9: Midspan stringer 6

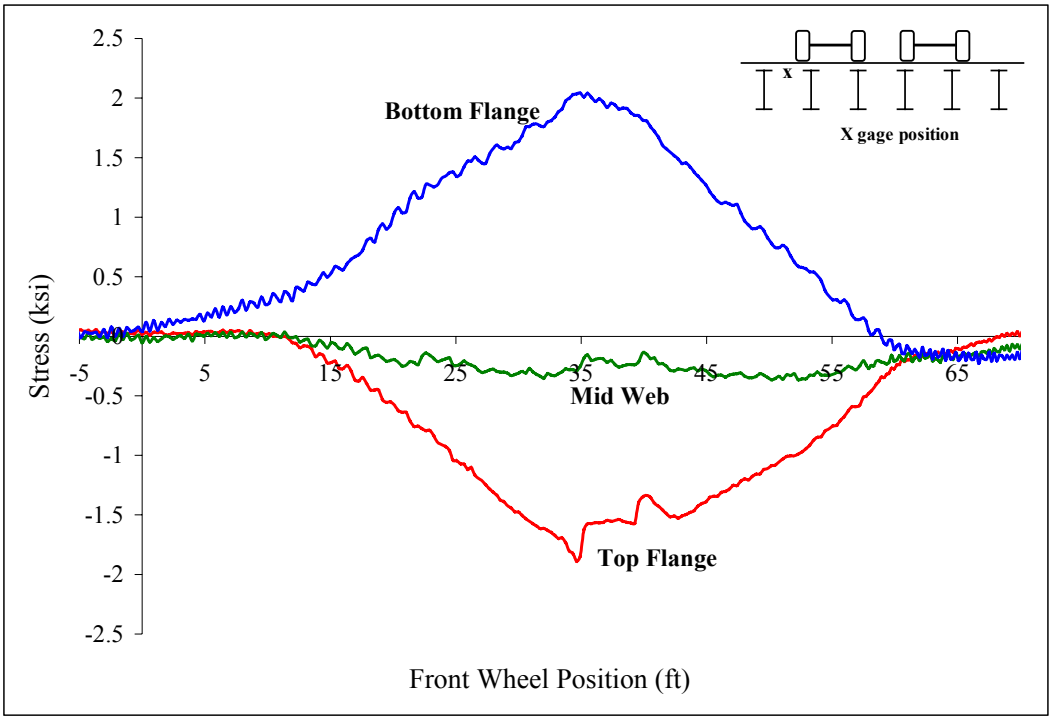

Figure B 10 Beam 2

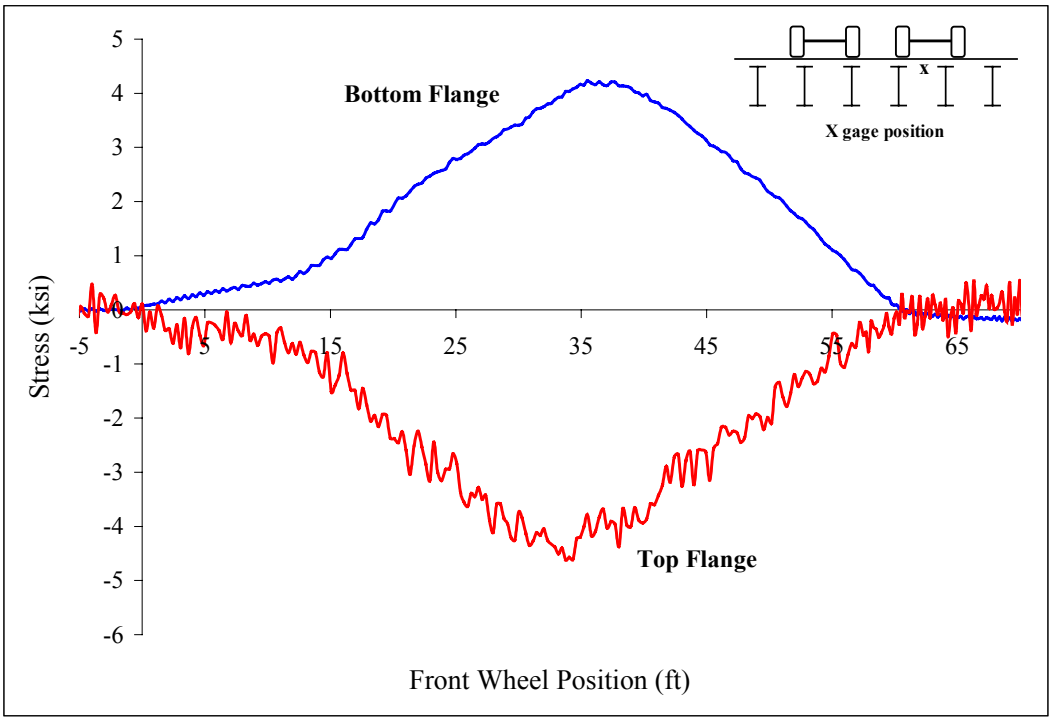

Figure B 11: Beam 2

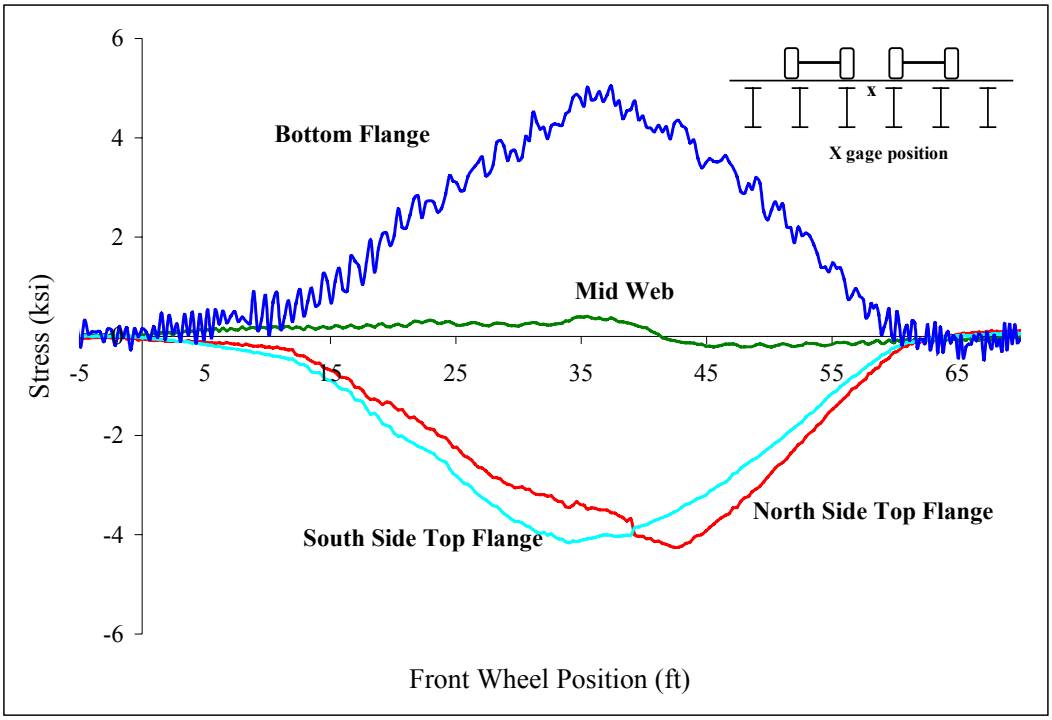

Figure B 12: Beam 2

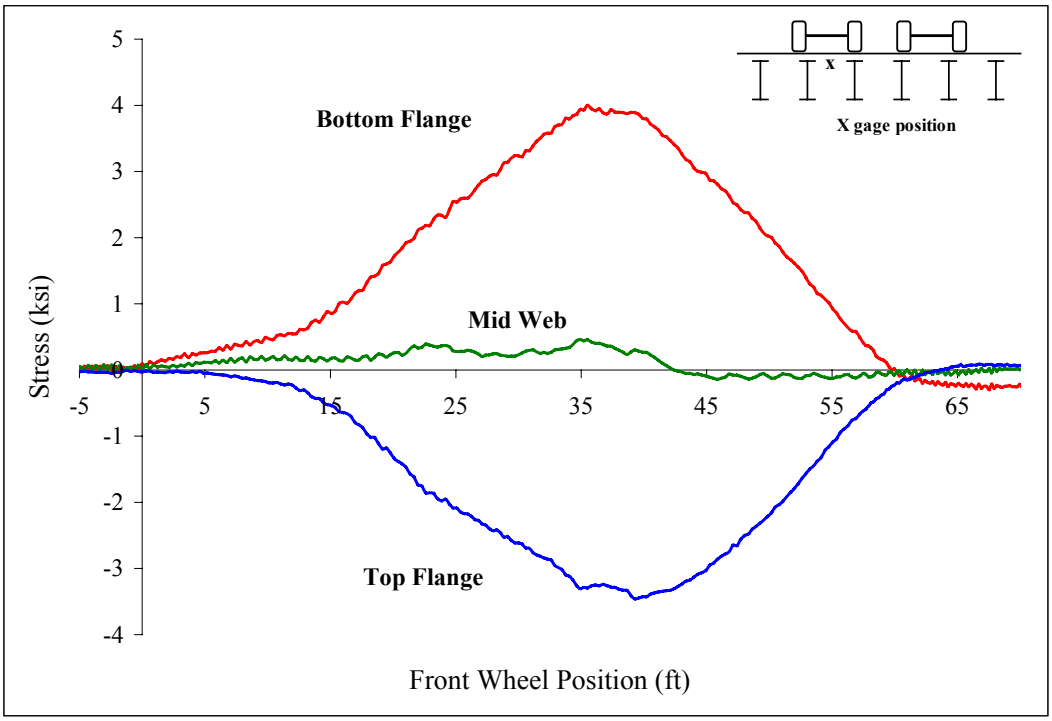

Figure B 13: Beam 2

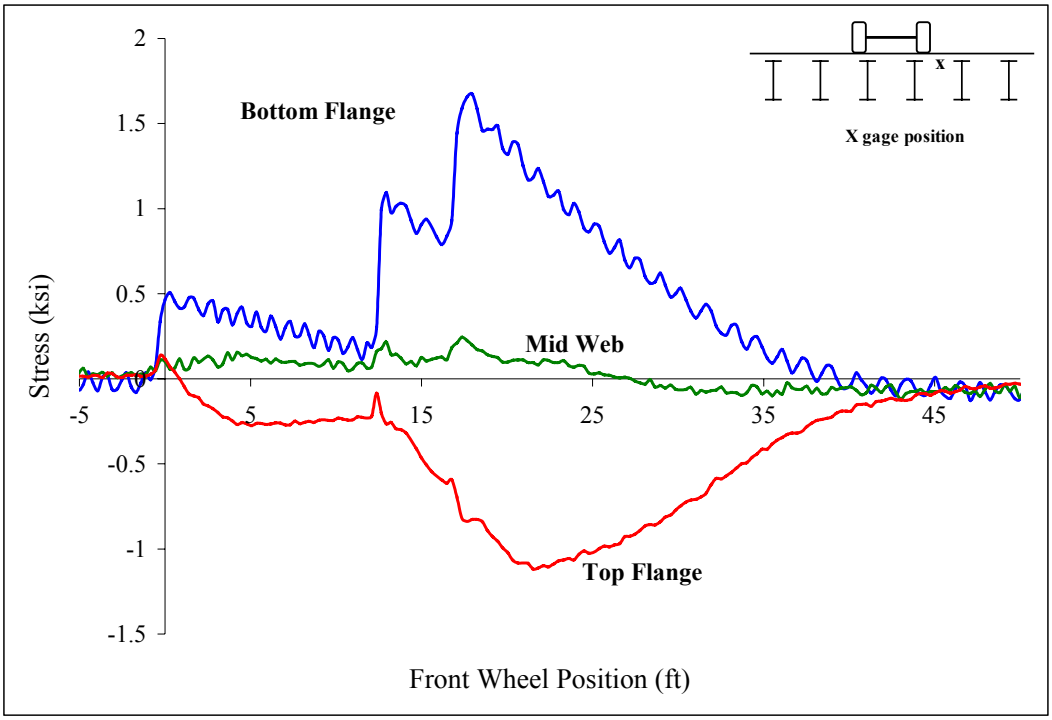

Figure B 14: Beam 1

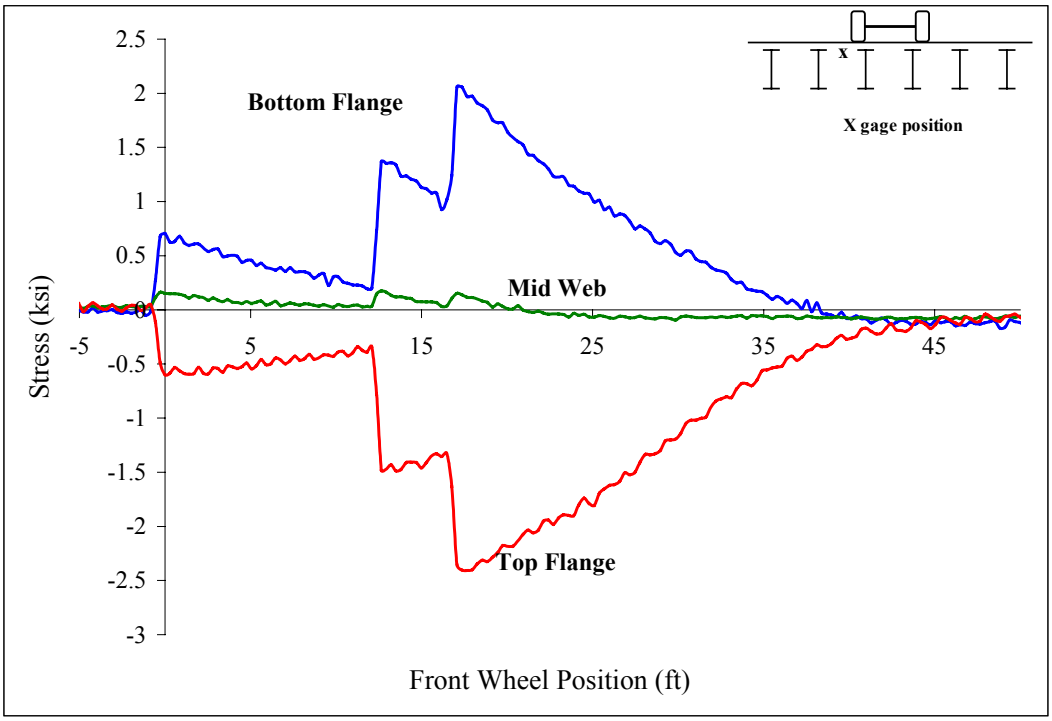

Figure B 15: Beam 1

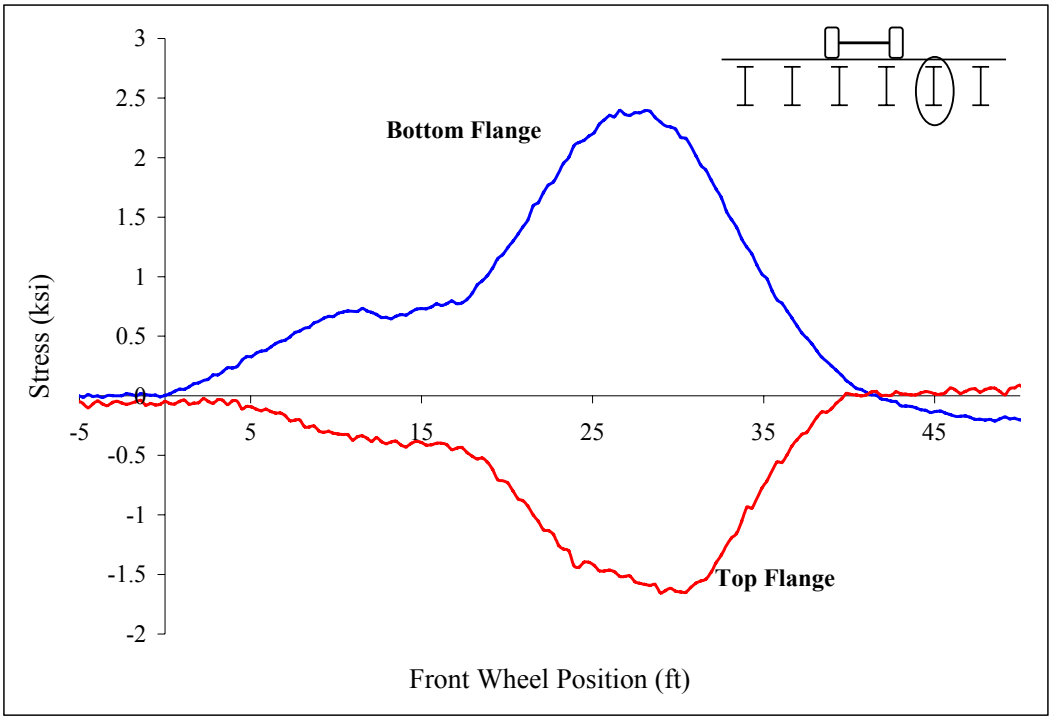

Figure B 16: Midspan stringer 2

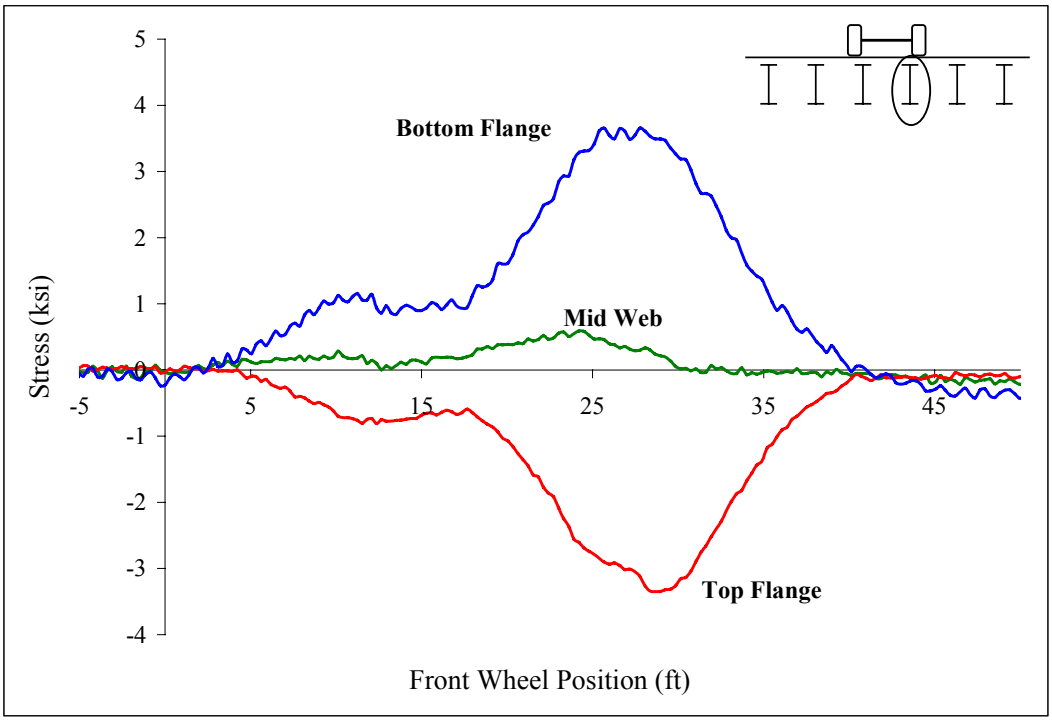

Figure B 17: Midspan stringer 3

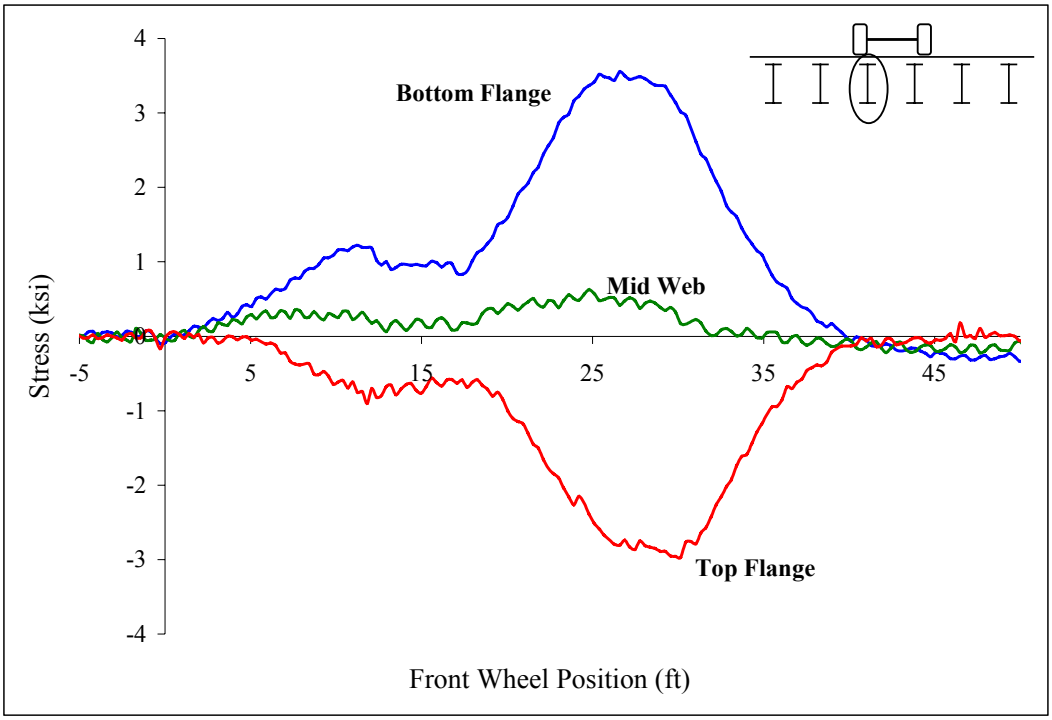

Figure B 18: Midspan stringer 4

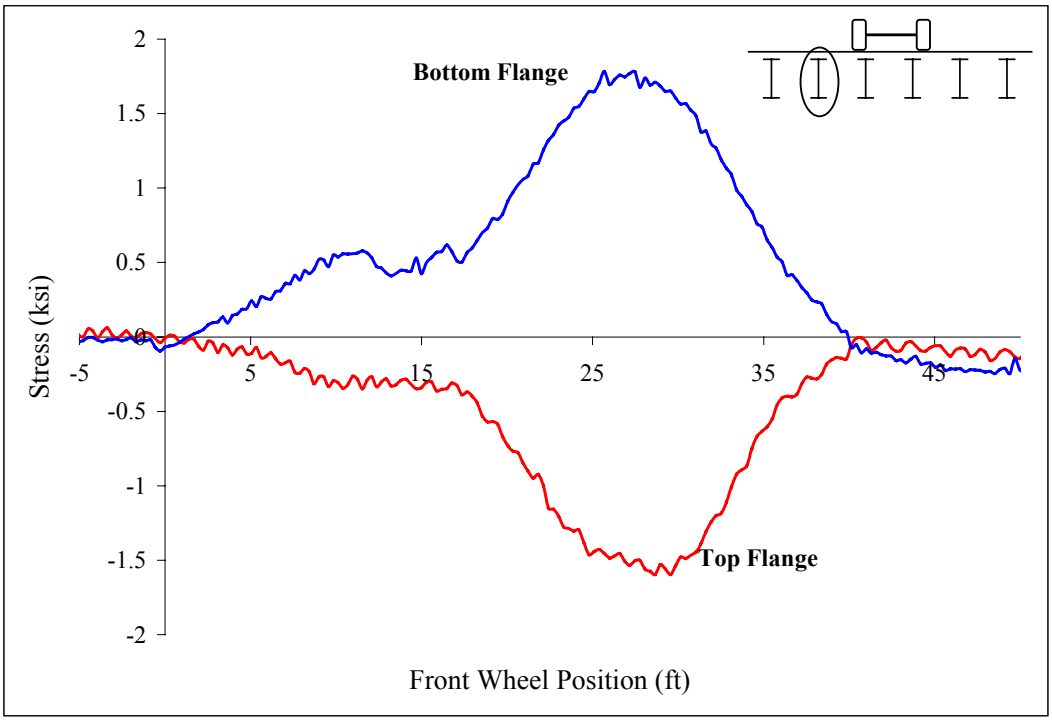

Figure B 19: Midspan stringer 5

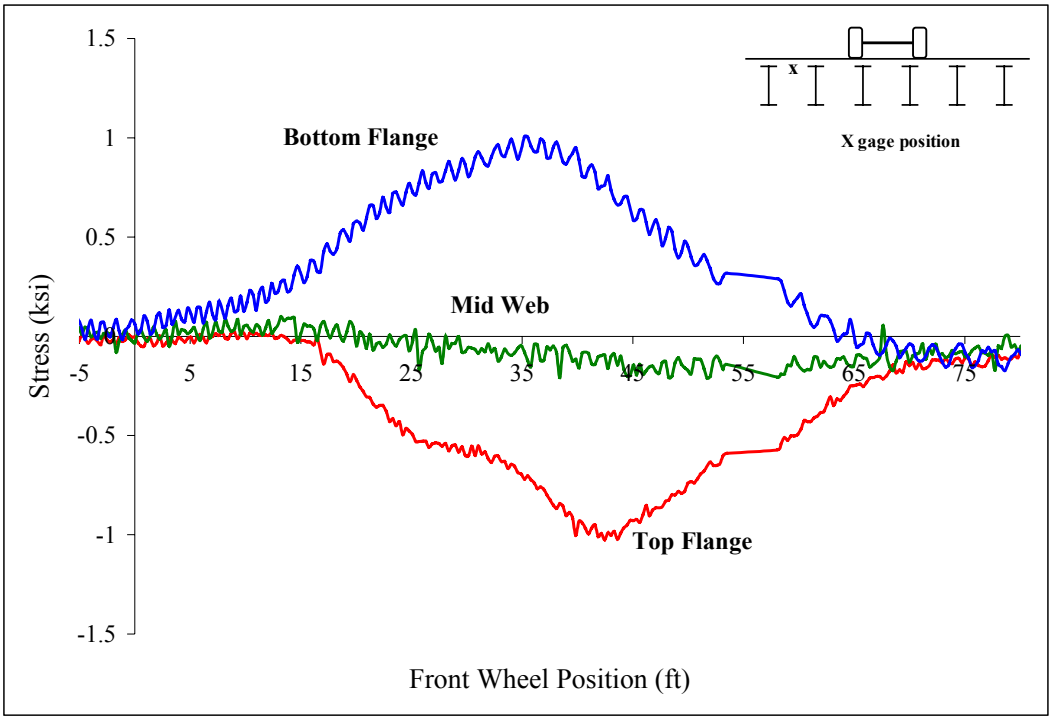

Figure B 20: Beam 2

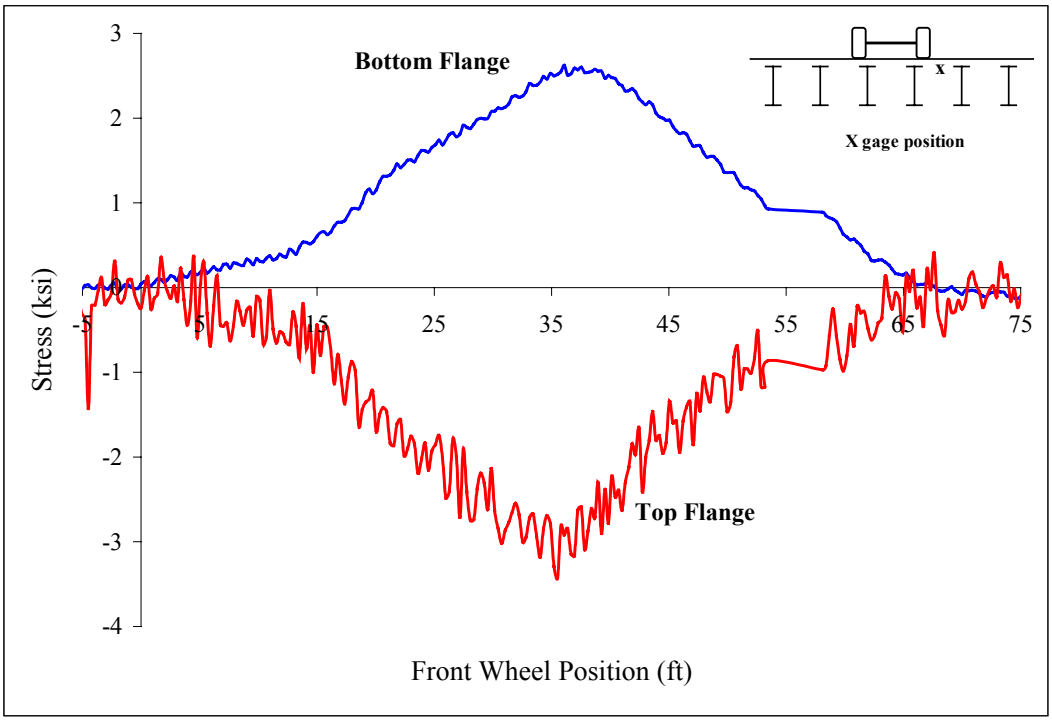

Figure B 21: Beam 2

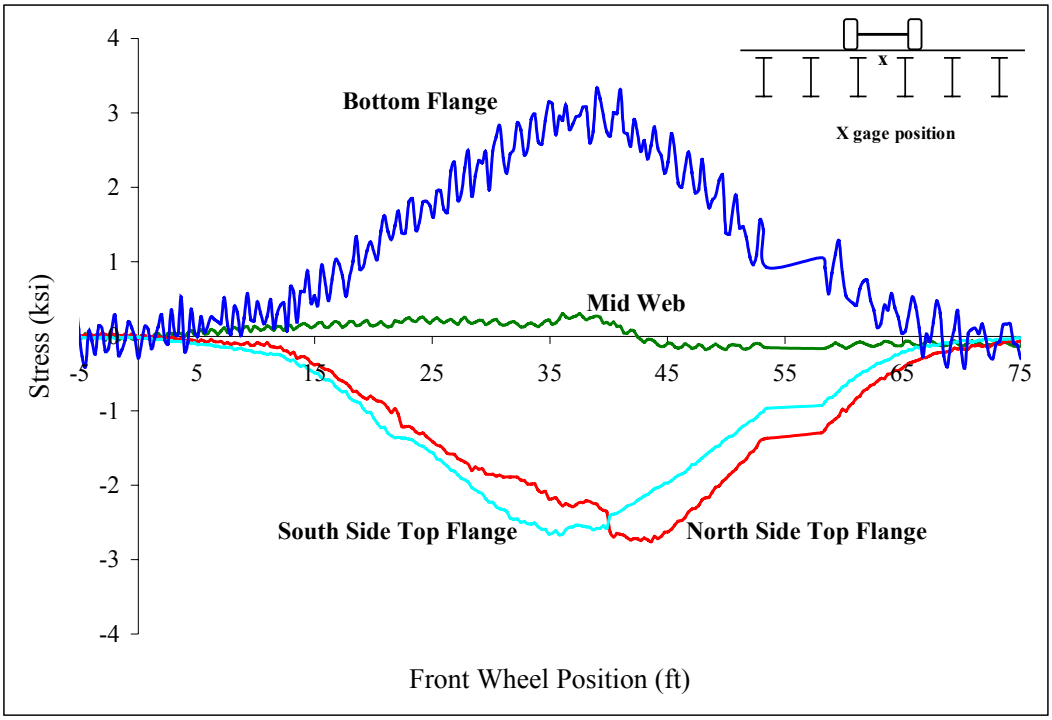

Figure B 22: Beam 2

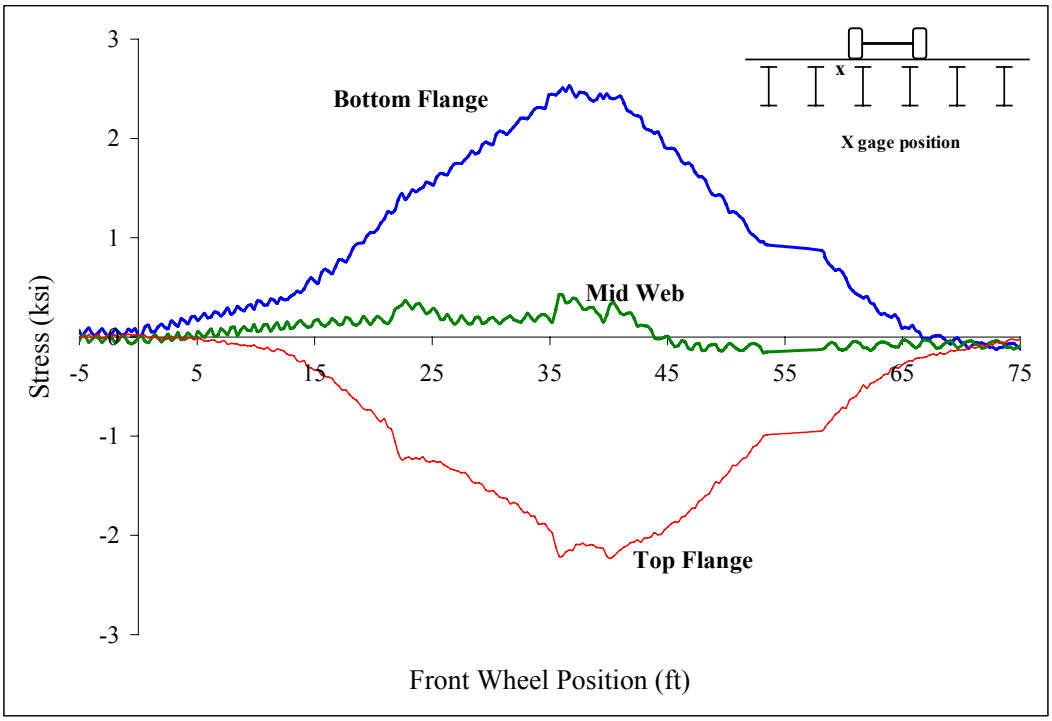

Figure B 23: Beam 2

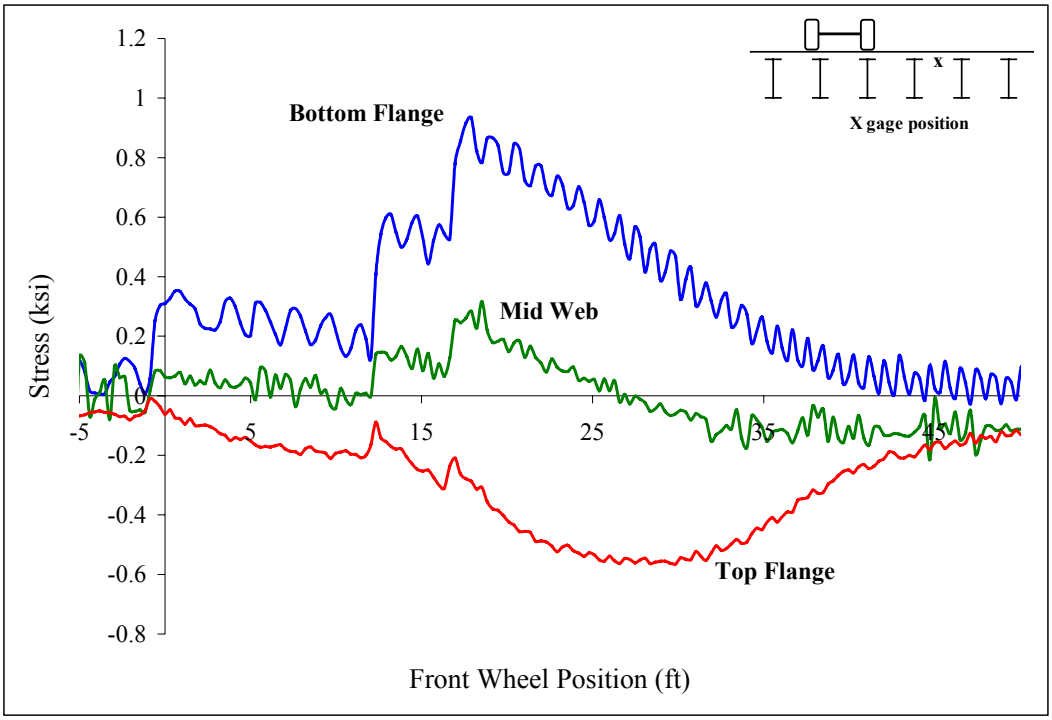

Figure B 24: Beam 1

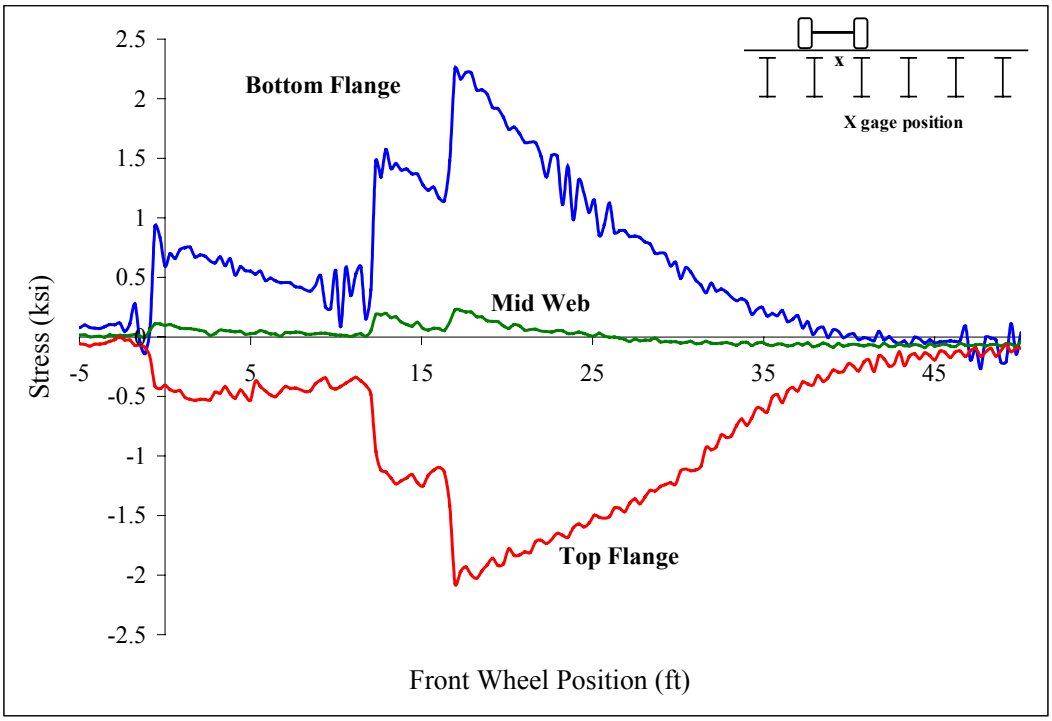

Figure B 25: Beam 1

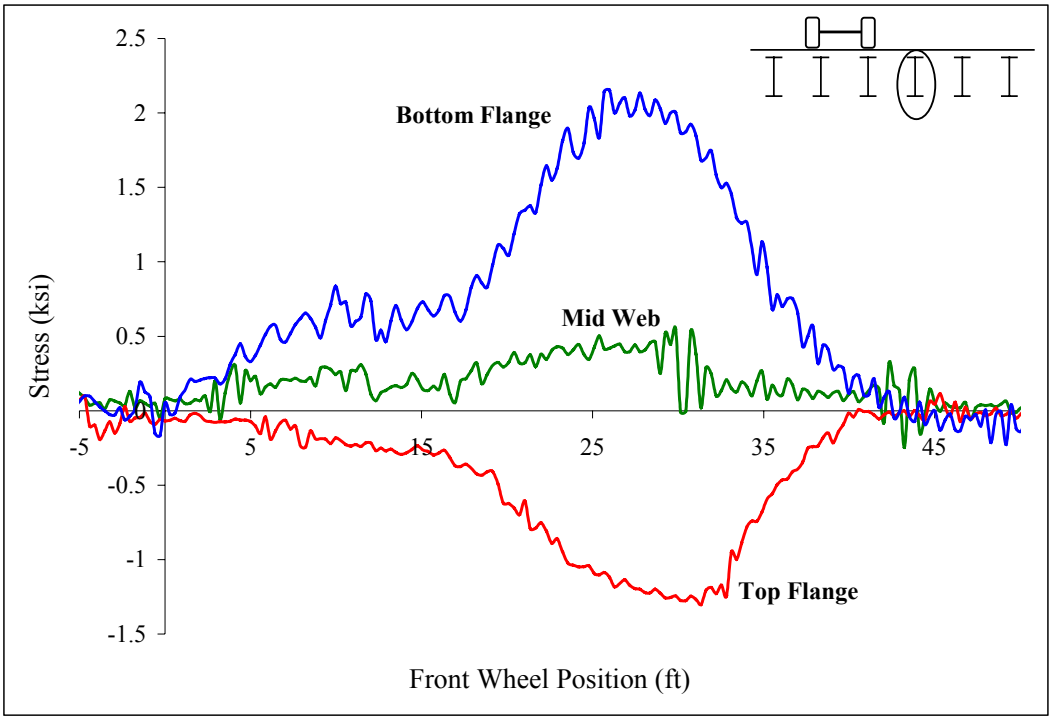

Figure B 26: Midspan stringer 3

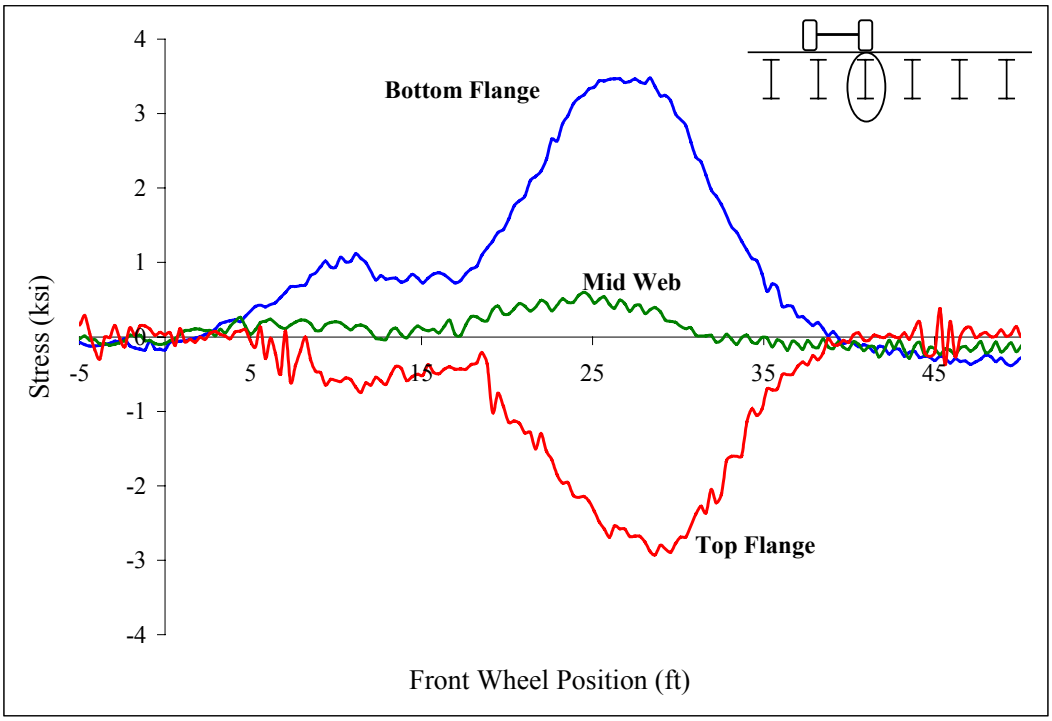

Figure B 27: Midspan stringer 4

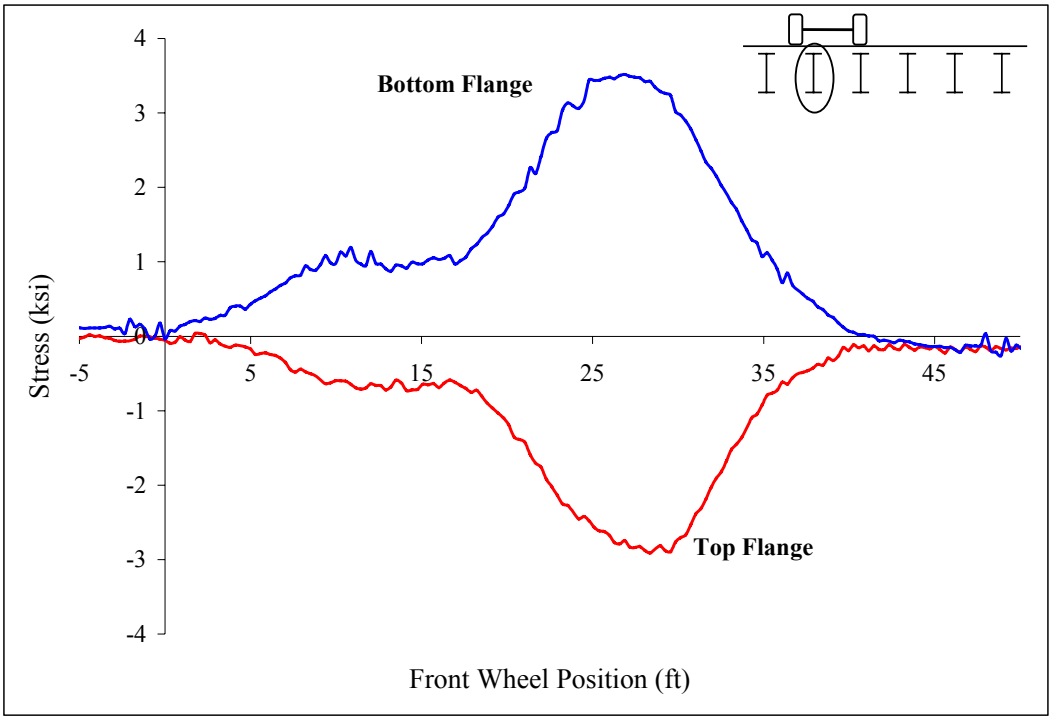

Figure B 28: Midspan stringer 5

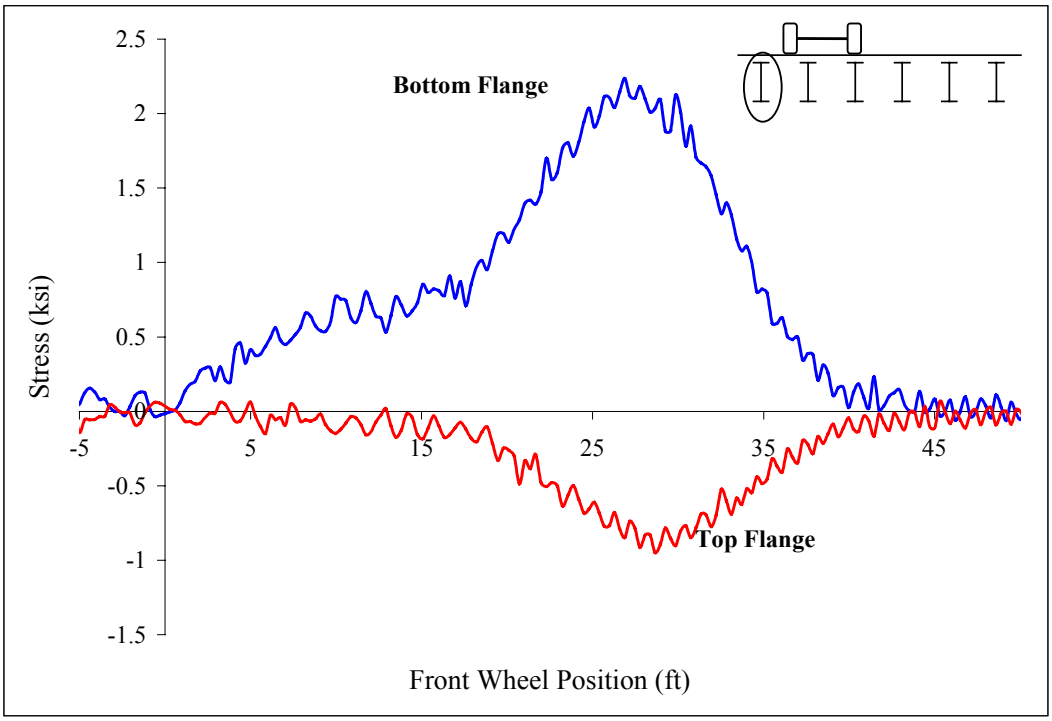

Figure B 29: Midspan stringer 6

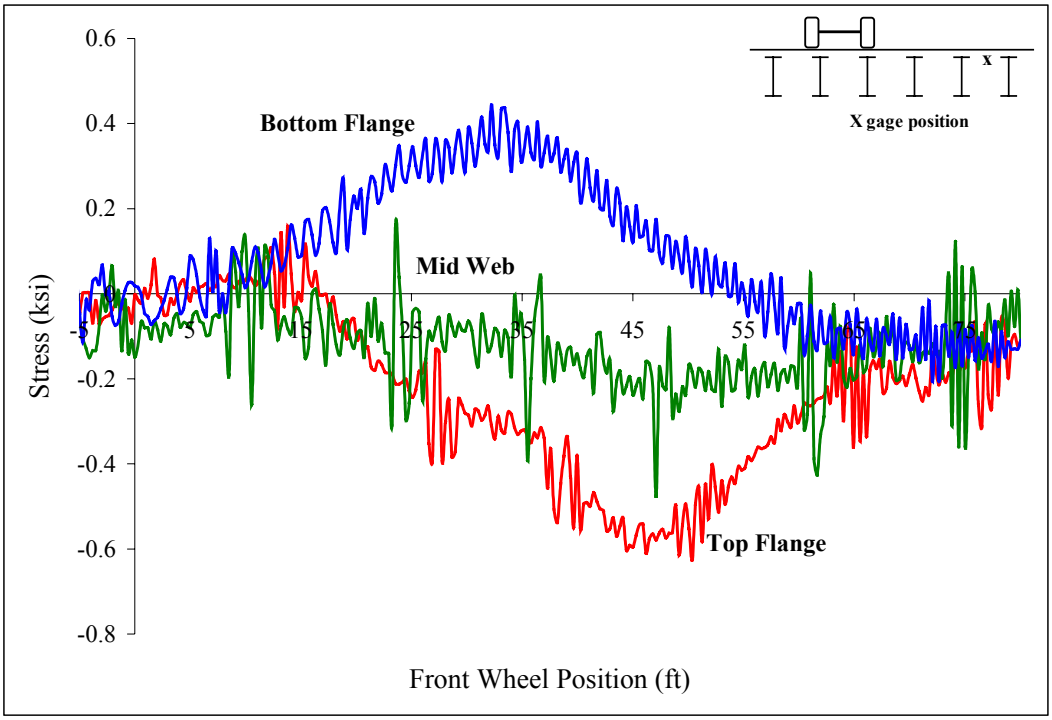

Figure B 30: Beam 2

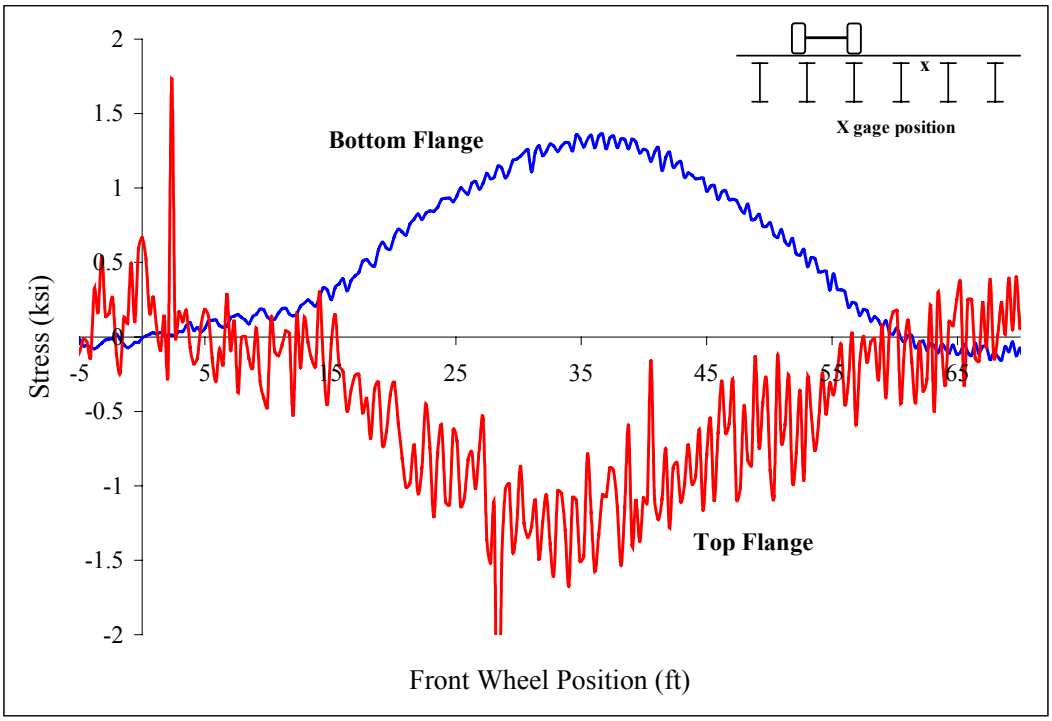

Figure B 31: Beam 2

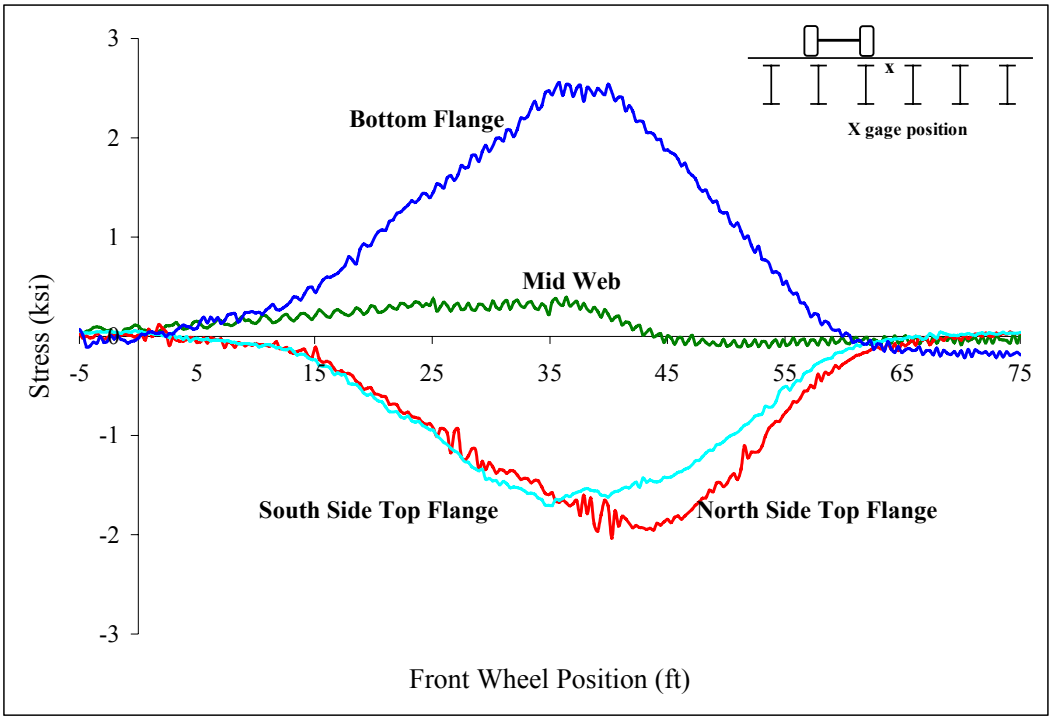

Figure B 32: Beam 2

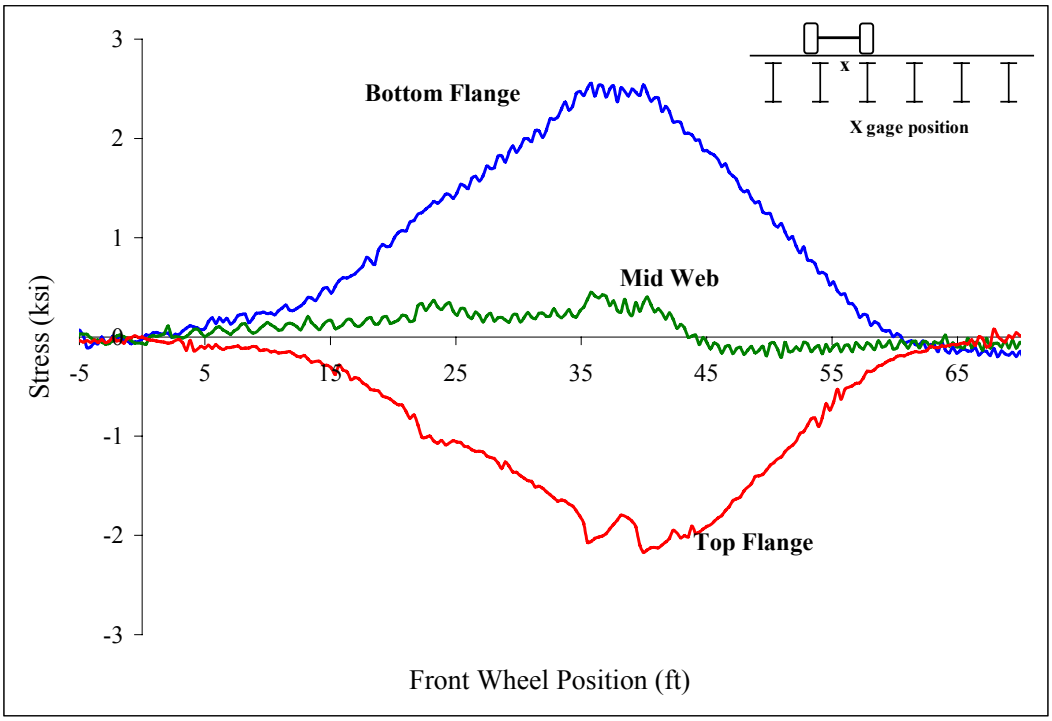

Figure B 33: Beam 2

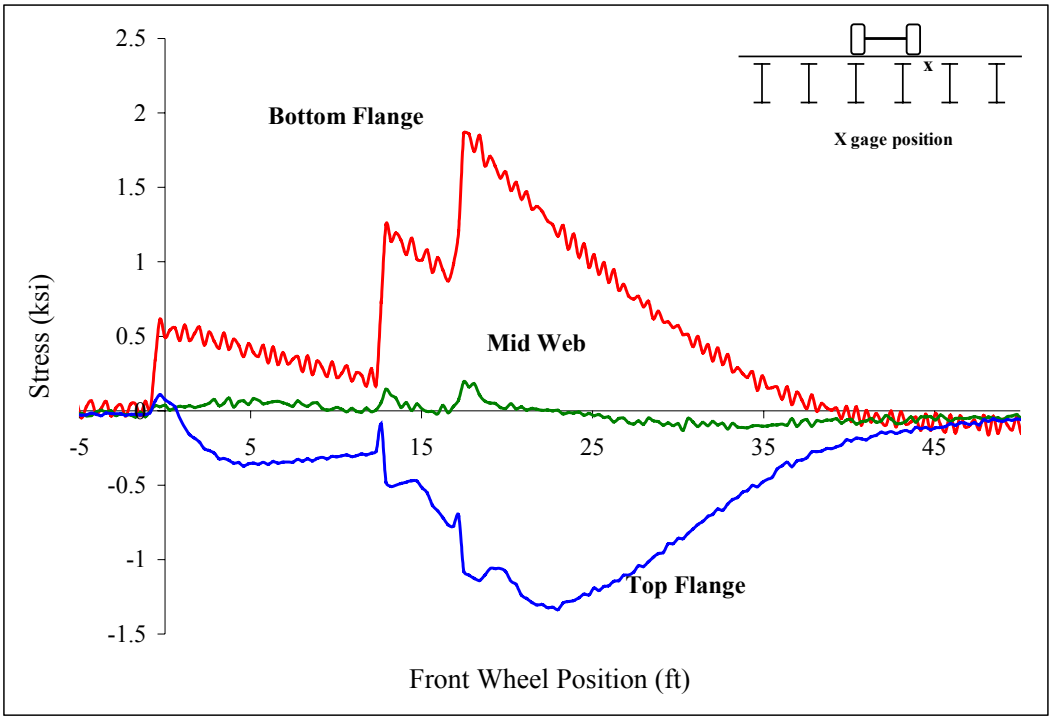

Figure B 34: Beam 1

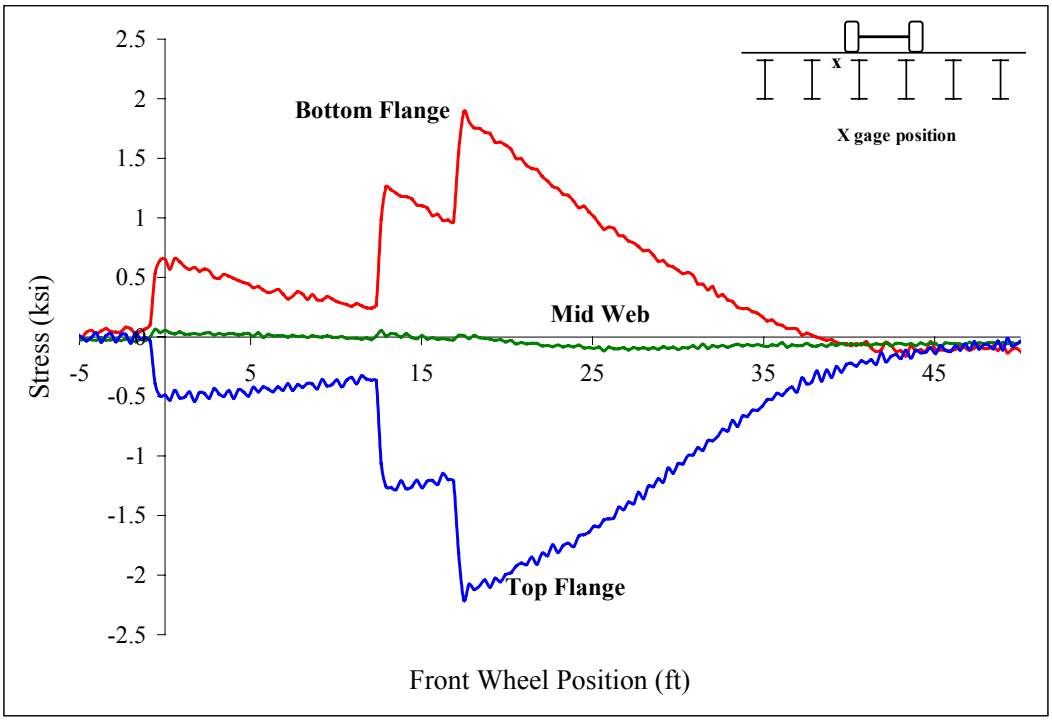

Figure B 35: Beam 1

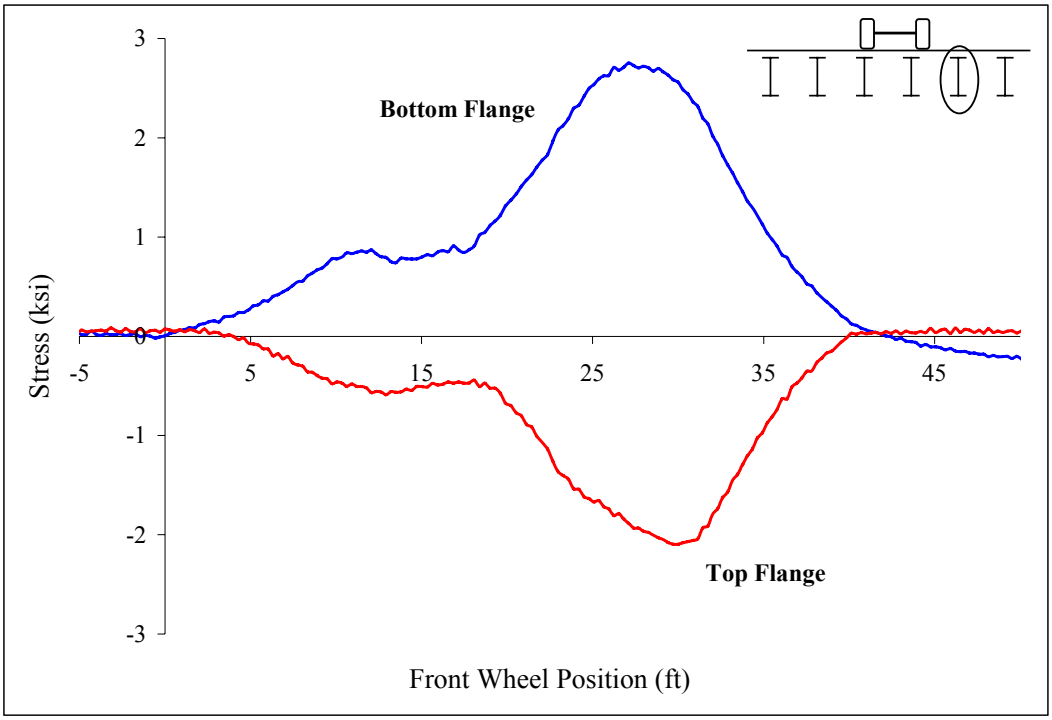

Figure B 36: Midspan stringer 2

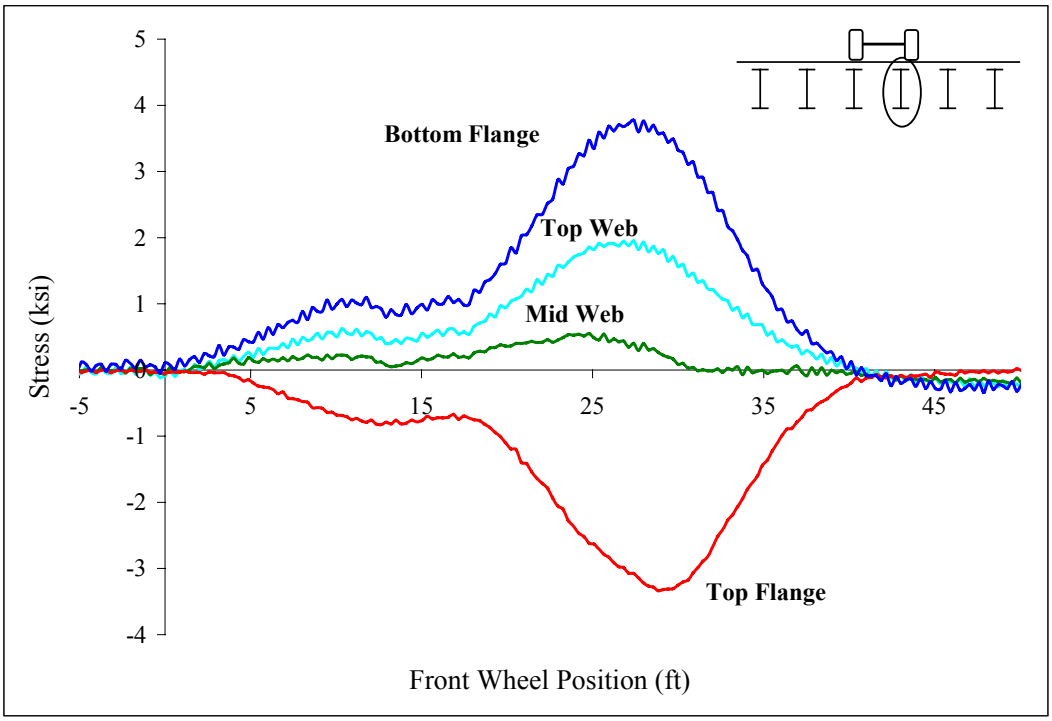

Figure B 37: Midspan stringer 3

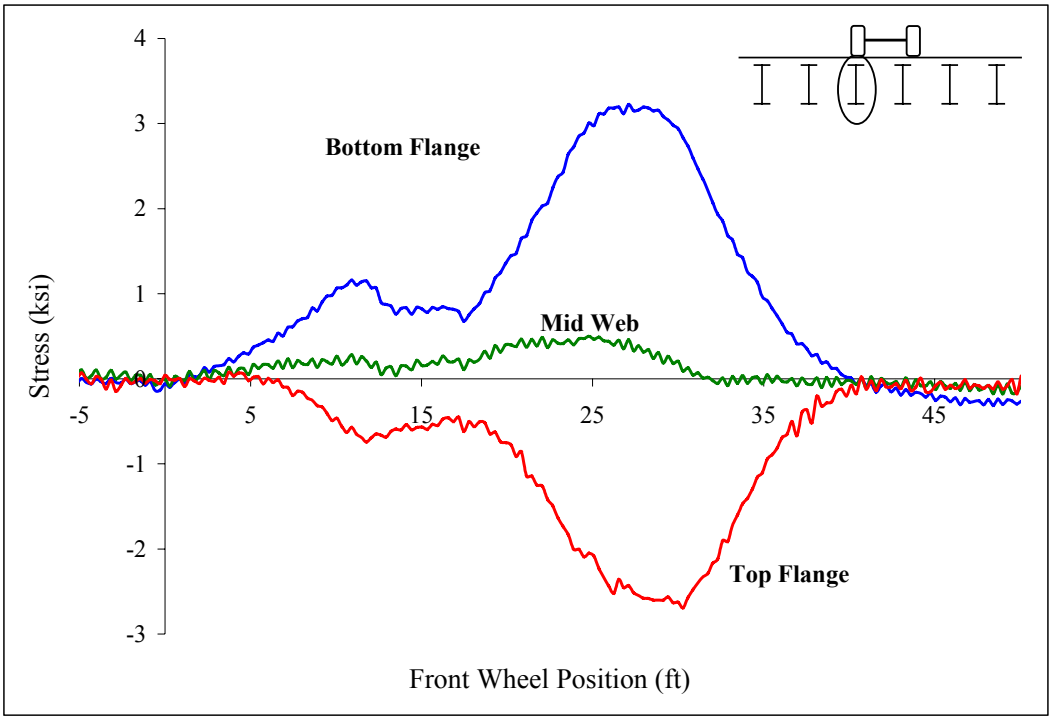

Figure B 38: Midspan stringer 4

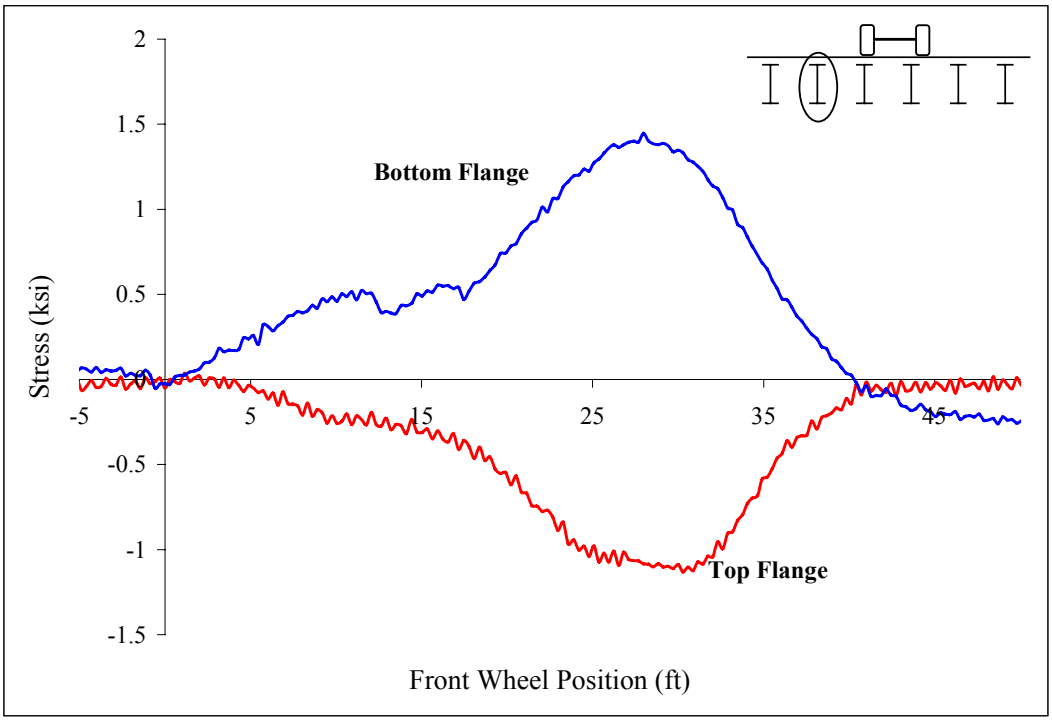

Figure B 39: Midspan stringer 5

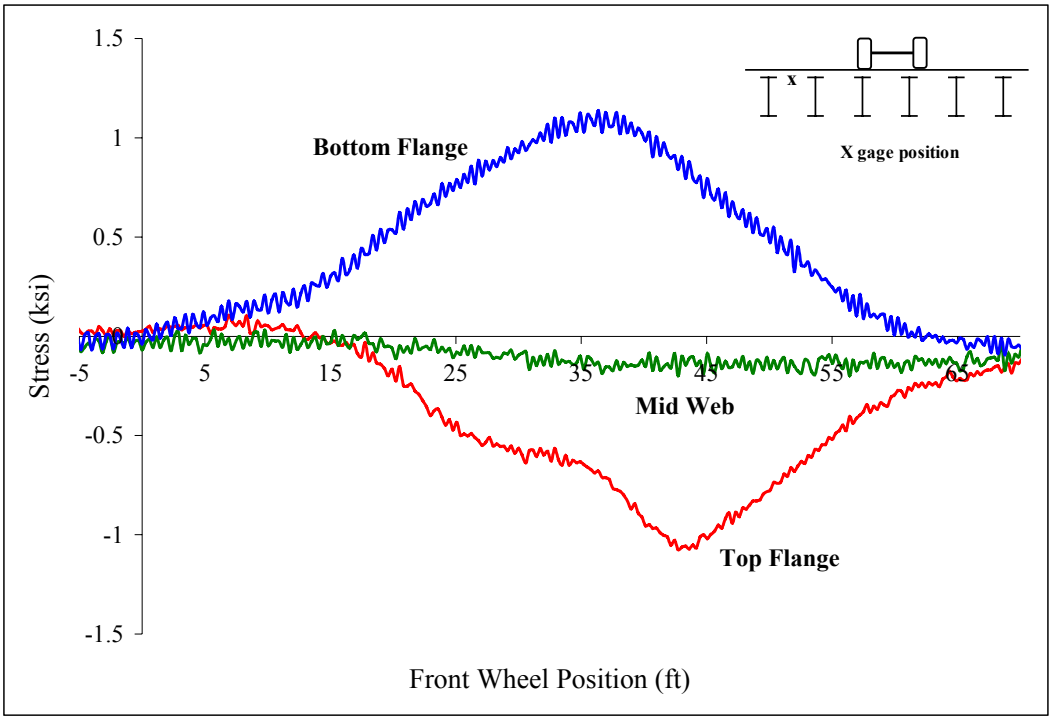

Figure B 40: Beam 2

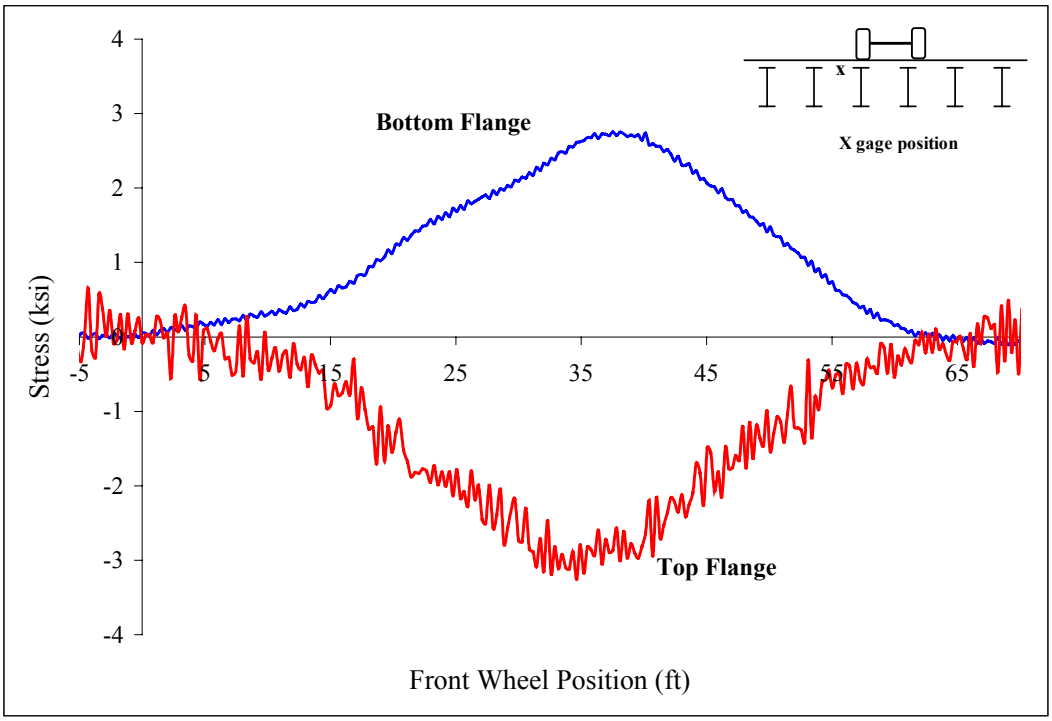

Figure B 41: Beam 2

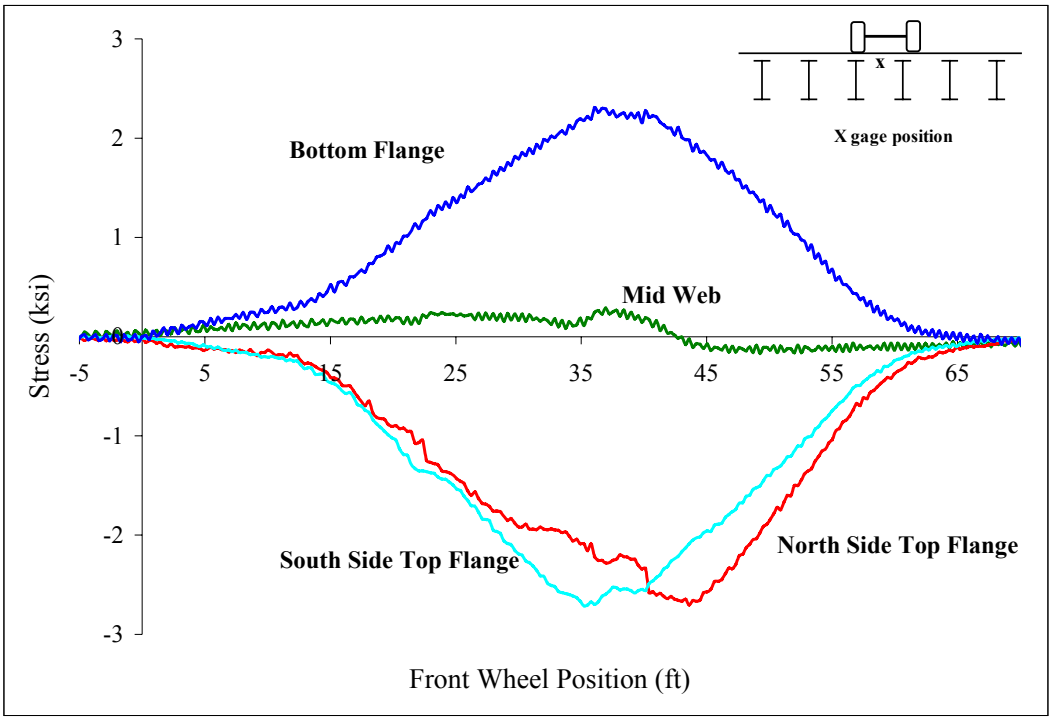

Figure B 42: Beam 2

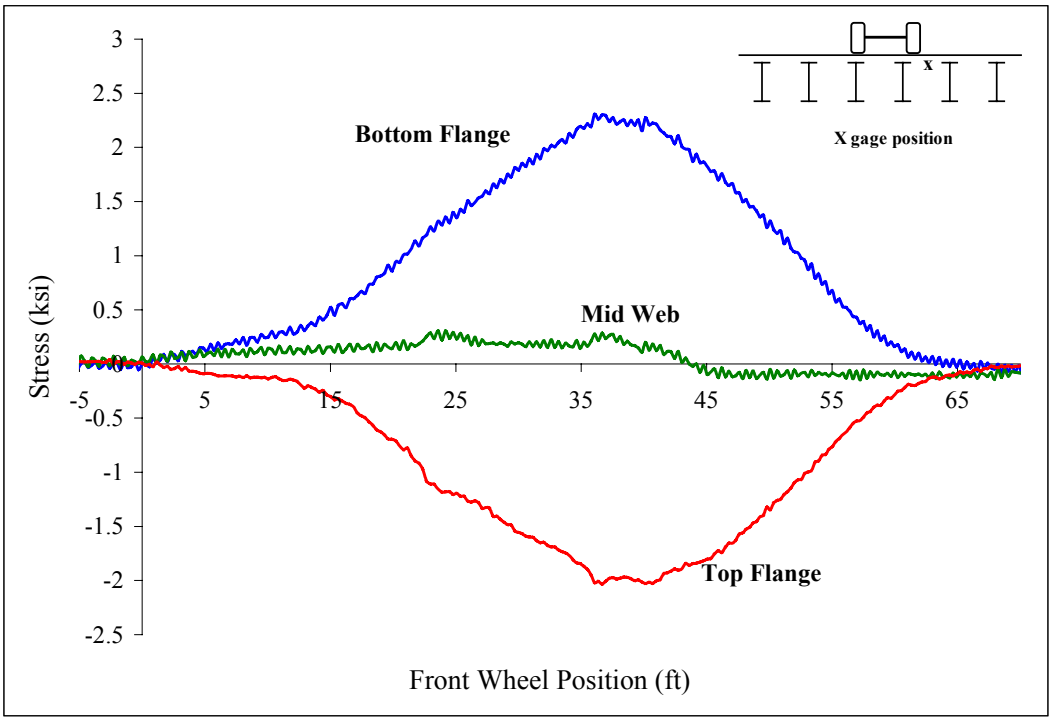

Figure B 43: Beam 2

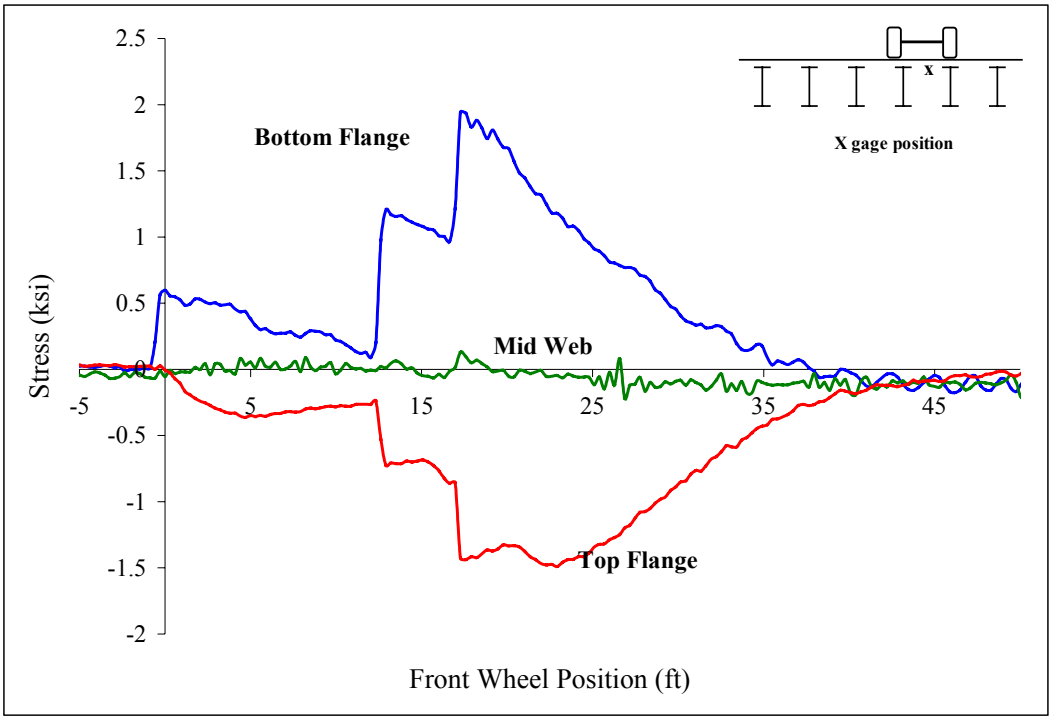

Figure B 44: Beam 1

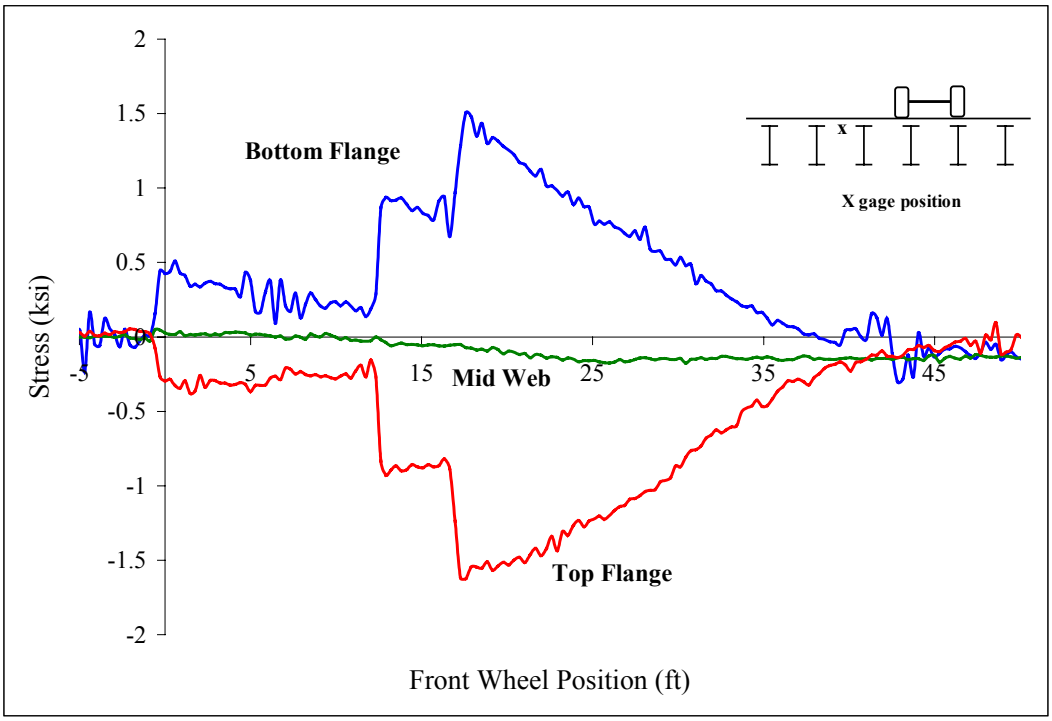

Figure B 45: Beam 1

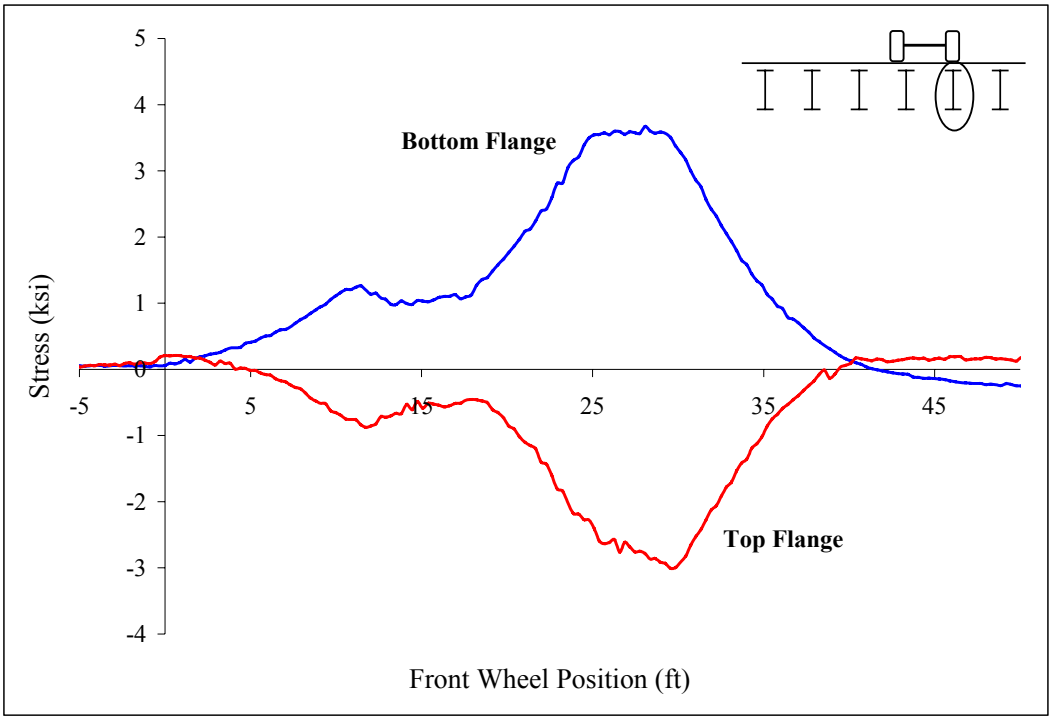

Figure B 46: Midspan stringer 2

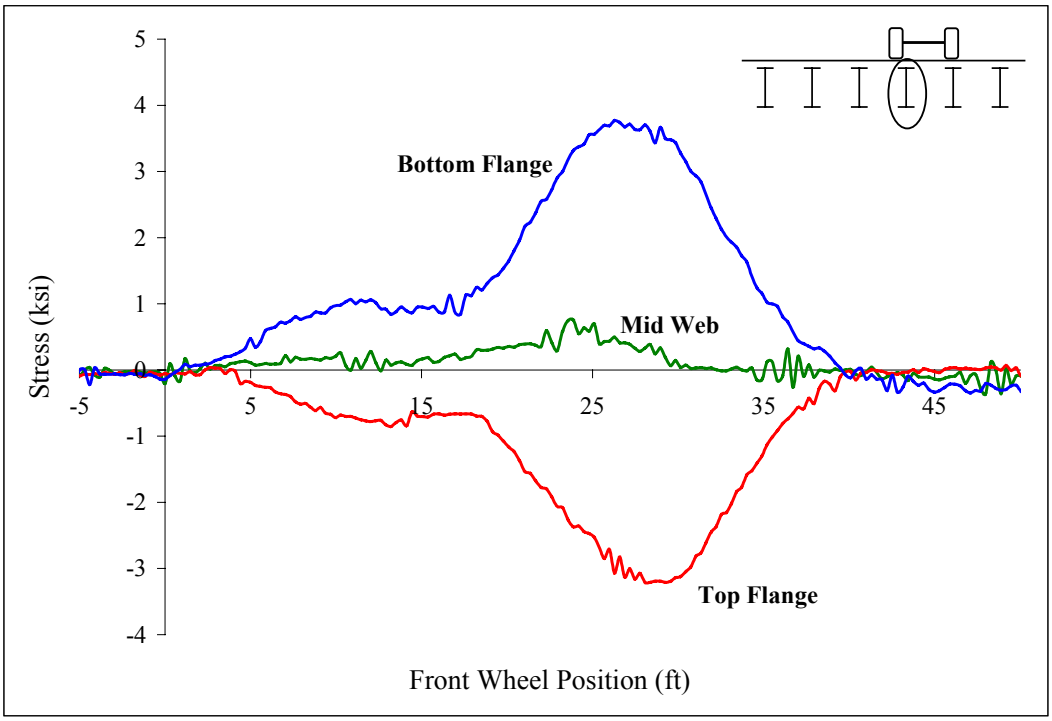

Figure B 47 Midspan stringer 3

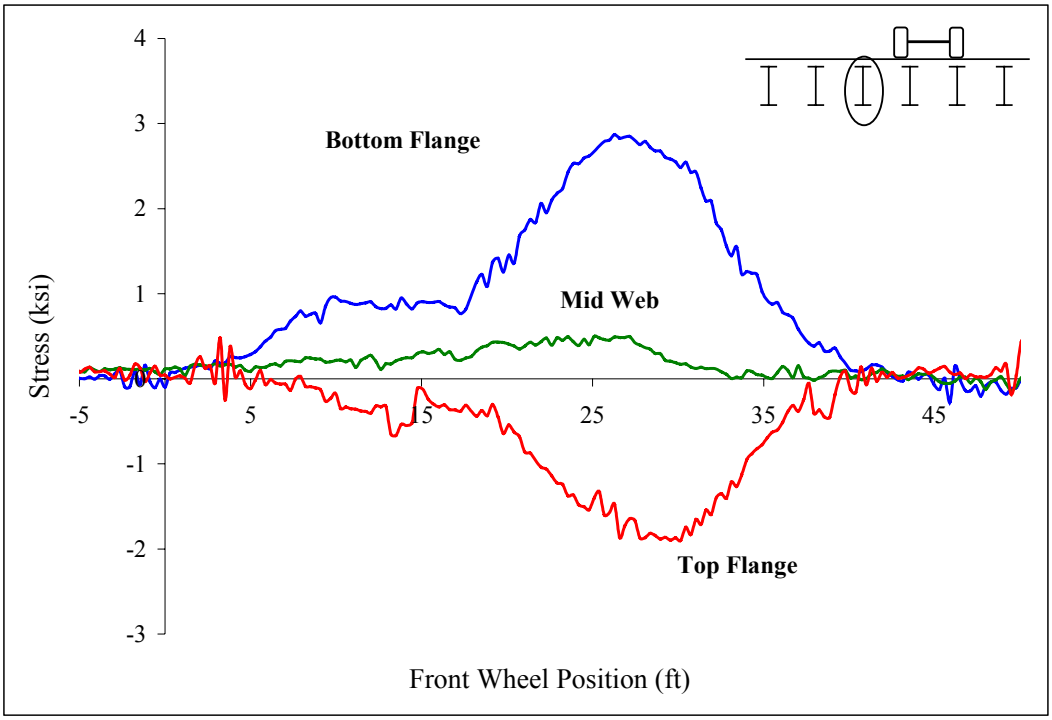

Figure B 48 Midspan stringer 4

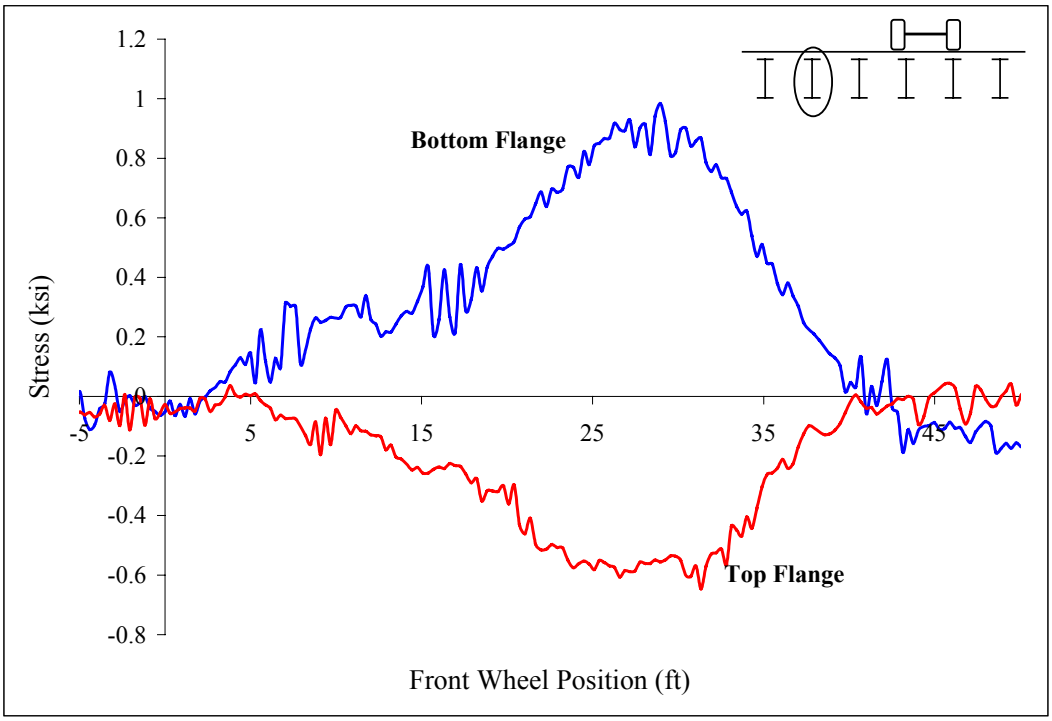

Figure B 49: Midspan stringer 5

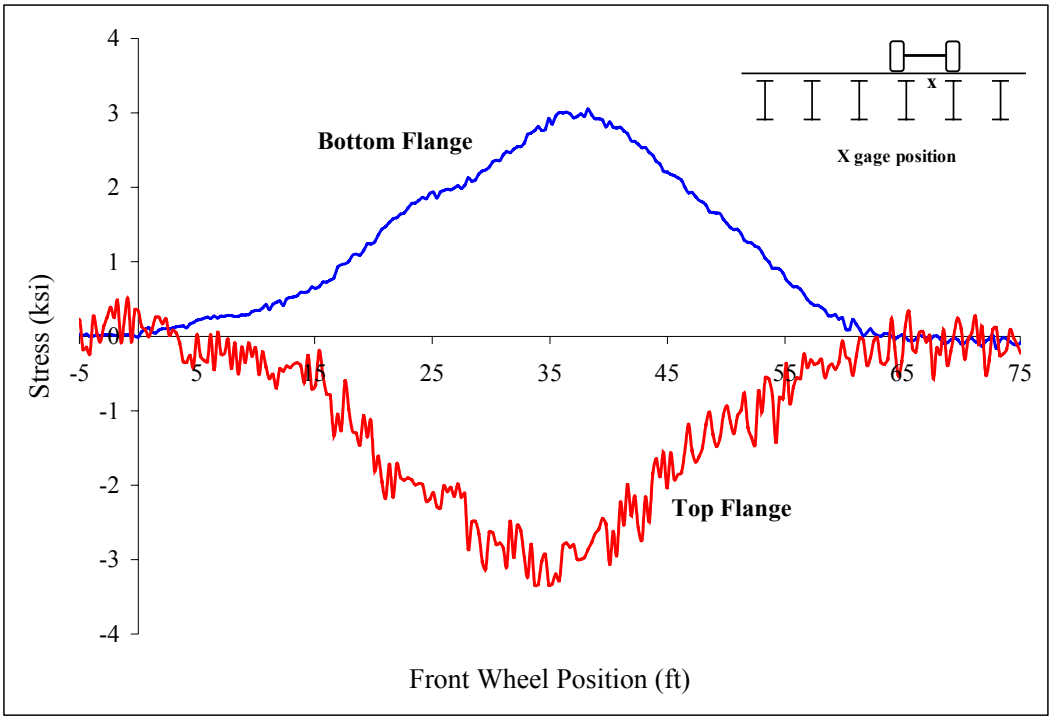

Figure B 50: Beam 2

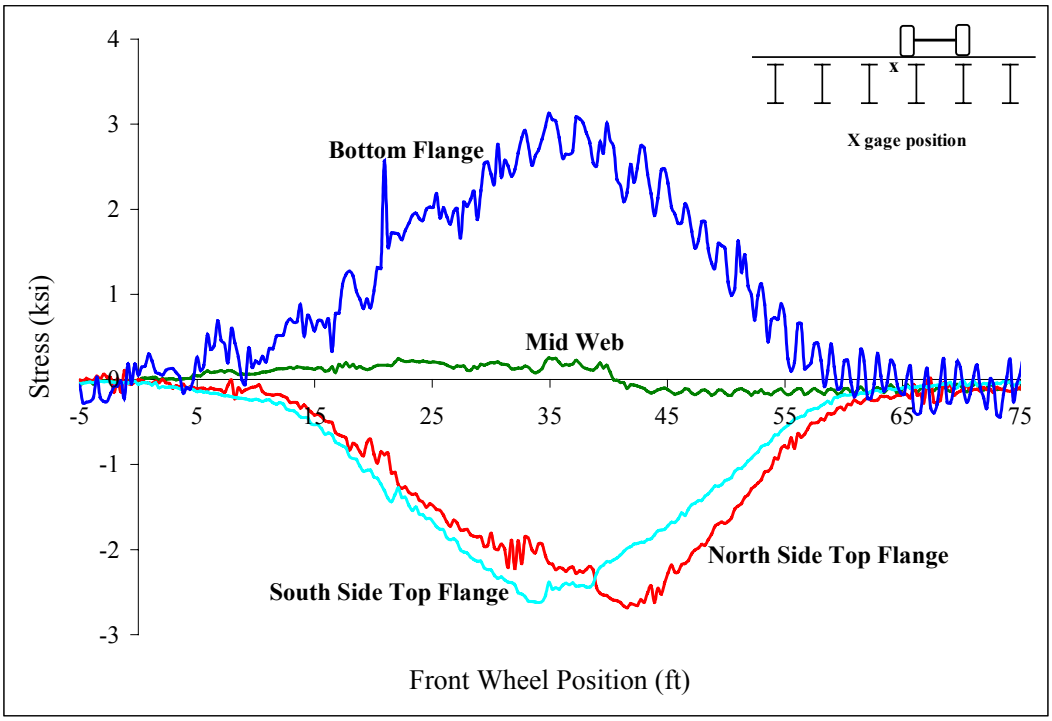

Figure B 51: Beam 2

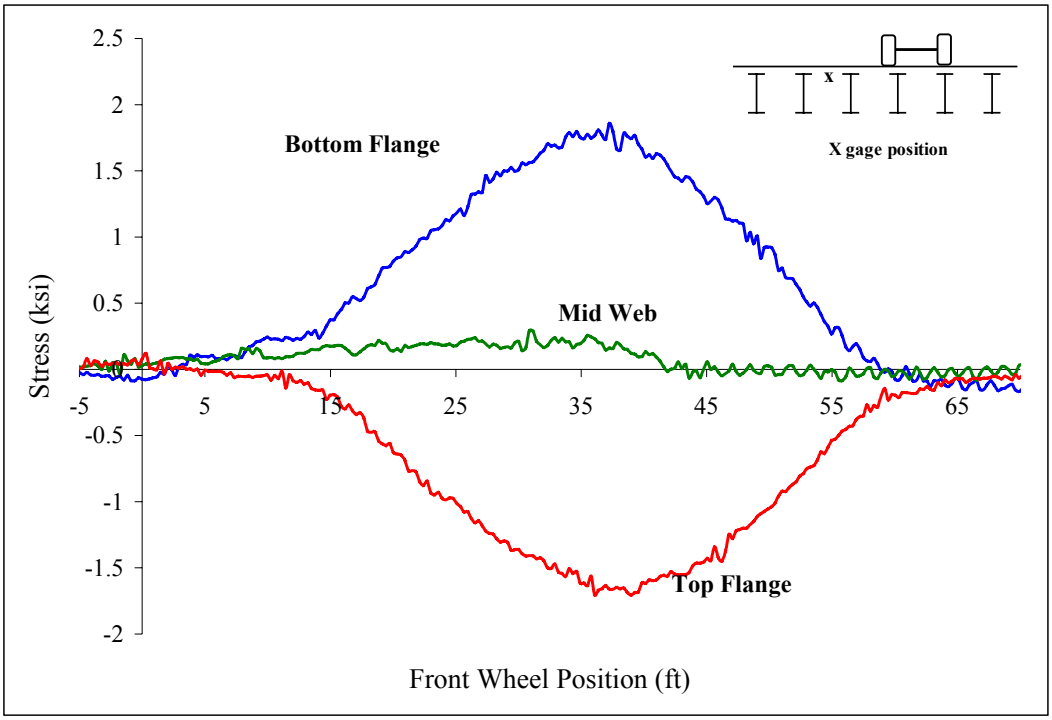

Figure B 52: Beam 2

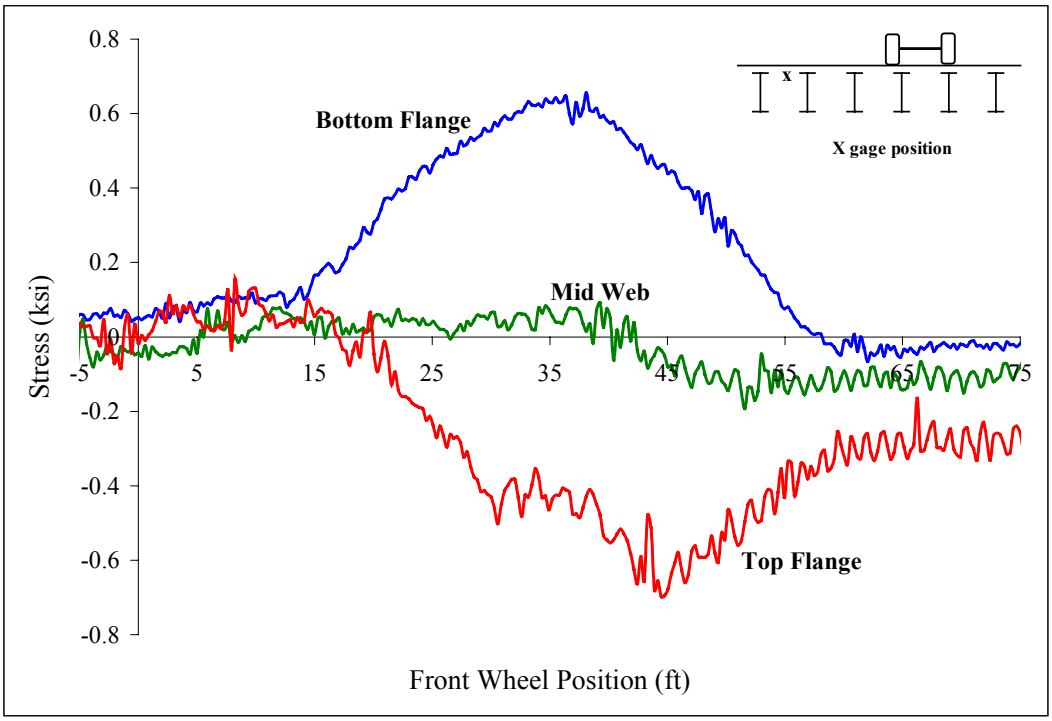

Figure B 53: Beam 2

Appendix C:
Field Load Test Data: Goliad Test

Appendix C contains results from the Goliad field load test. In this load test, selected portions of the deck system were instrumented with strain gages. A truck of known weight and geometry was then driven slowly over the bridge, and the response of the instrumented members was measured. The measured strains were converted to stress and plotted versus the position of the load truck on the bridge. For the Goliad tests the load vehicles were driven north. Consequently, the graphic showing gage location on each plot faces in a northerly direction. The stringers are numbered 1 though 6, with stringer 1 the western-most stringer. Figure C1 shows the truck dimensions. Each individual plot has a graphic depicting the axle weights used in that particular test run.

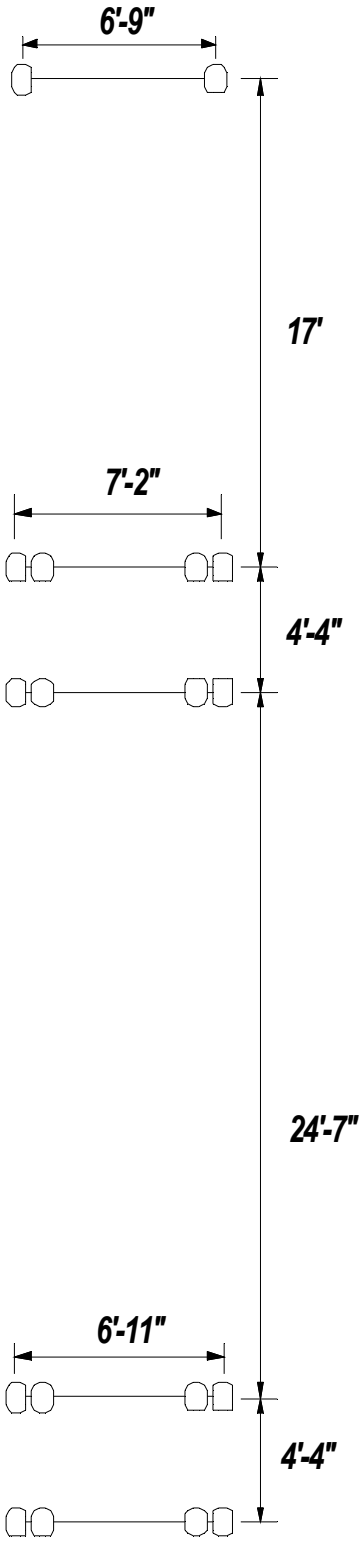

Figure C 1: Load truck dimensions for the Goliad field load test

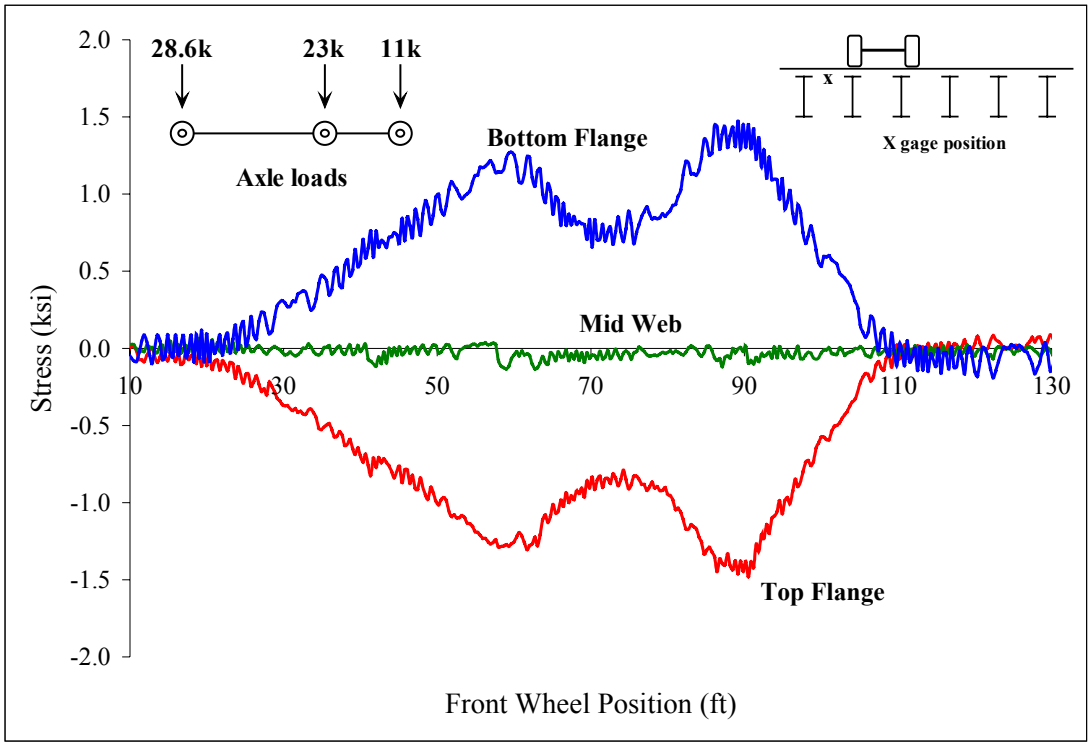

Figure C 2: Beam 4

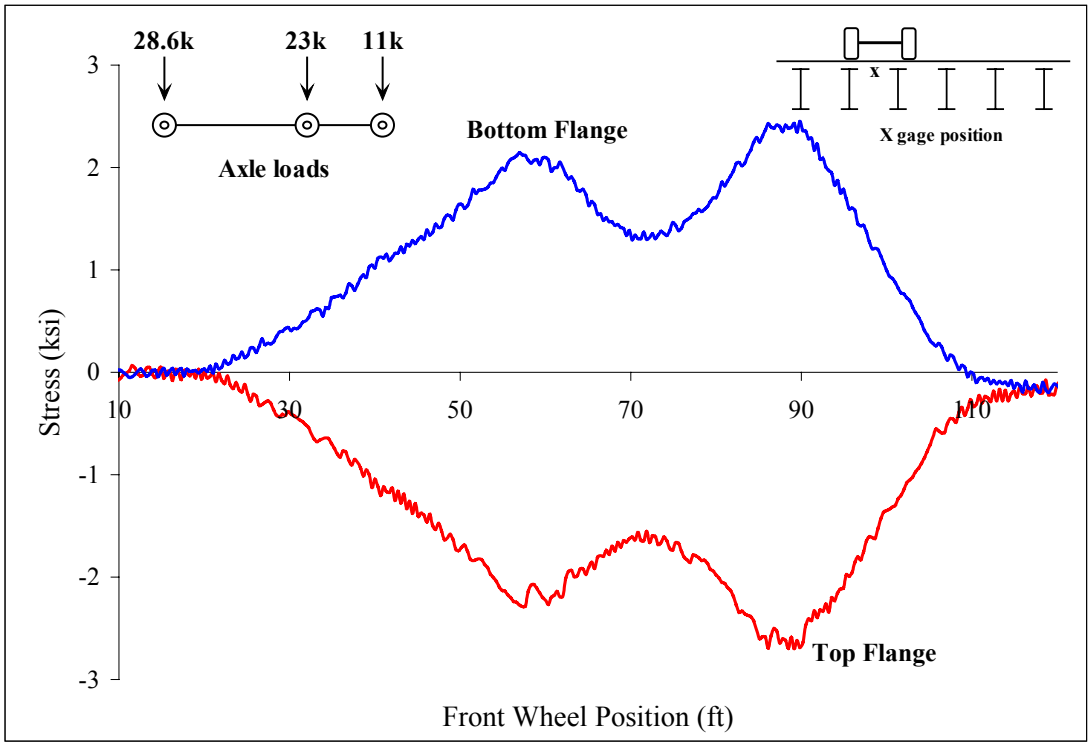

Figure C 3: Beam 4

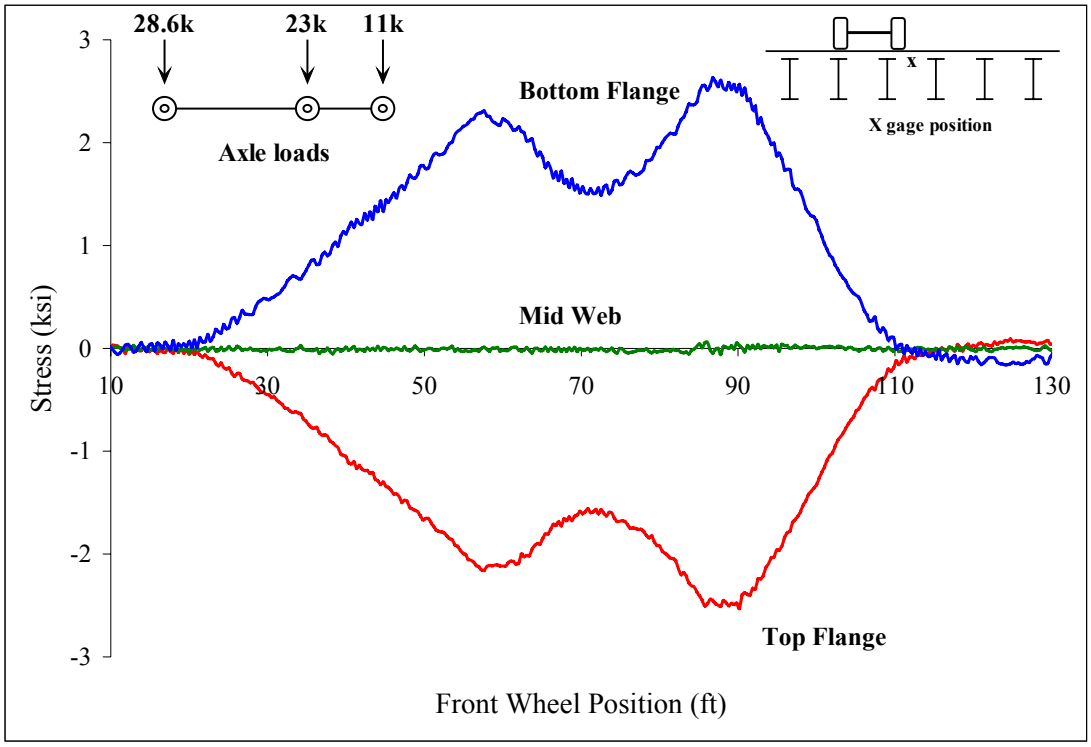

Figure C 4: Beam 4

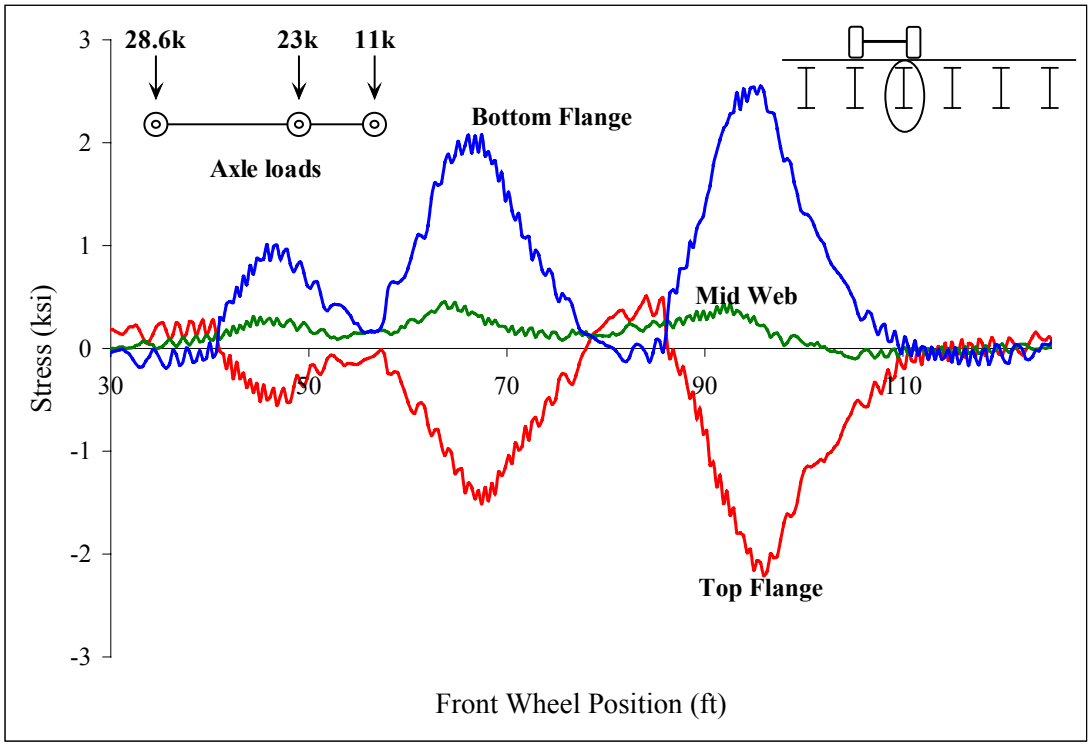

Figure C 5: South quarter point of stringer 3

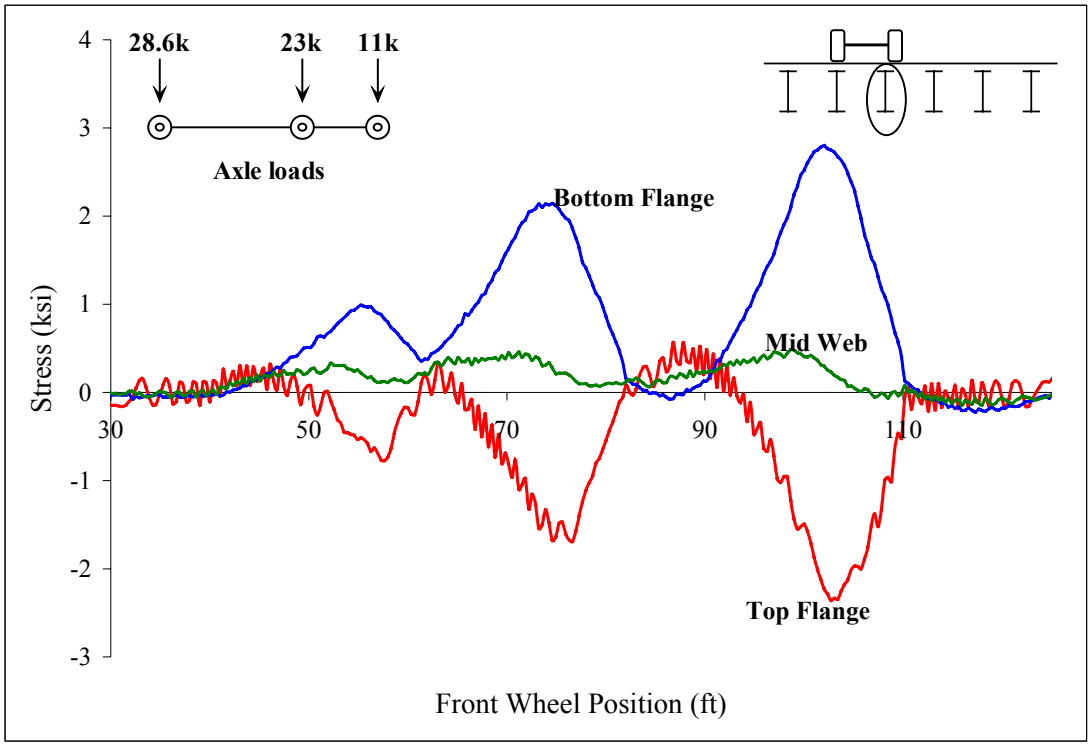

Figure C 6: North quarter point of stringer 3

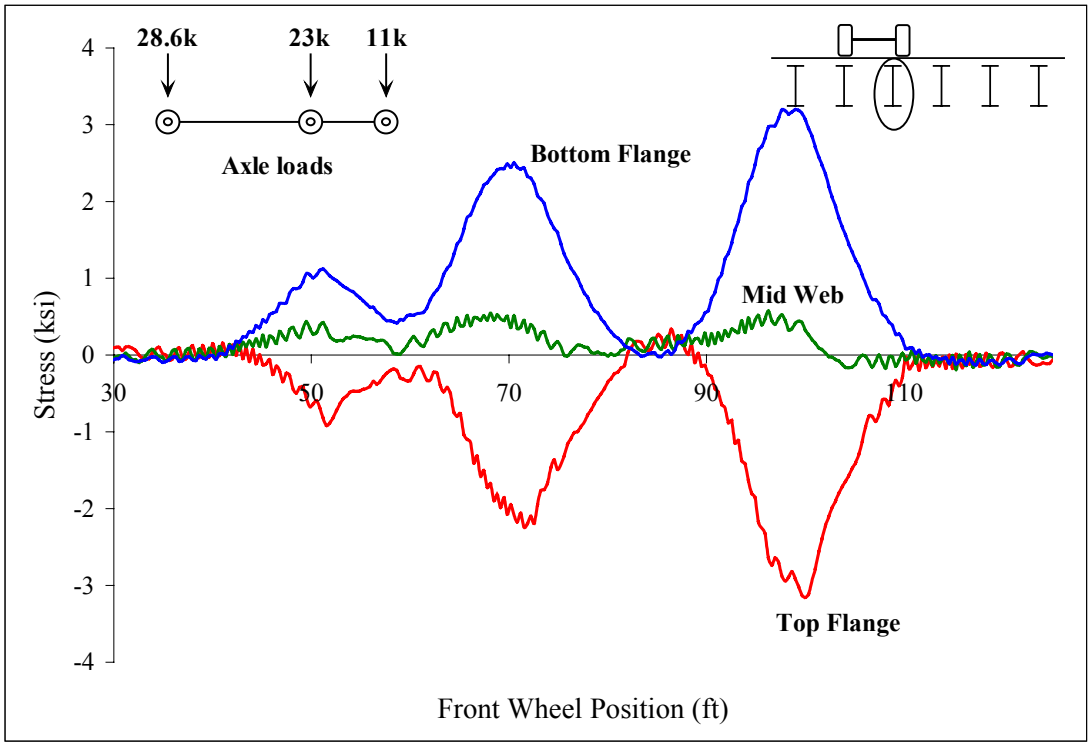

Figure C 7: Midspan stringer 3

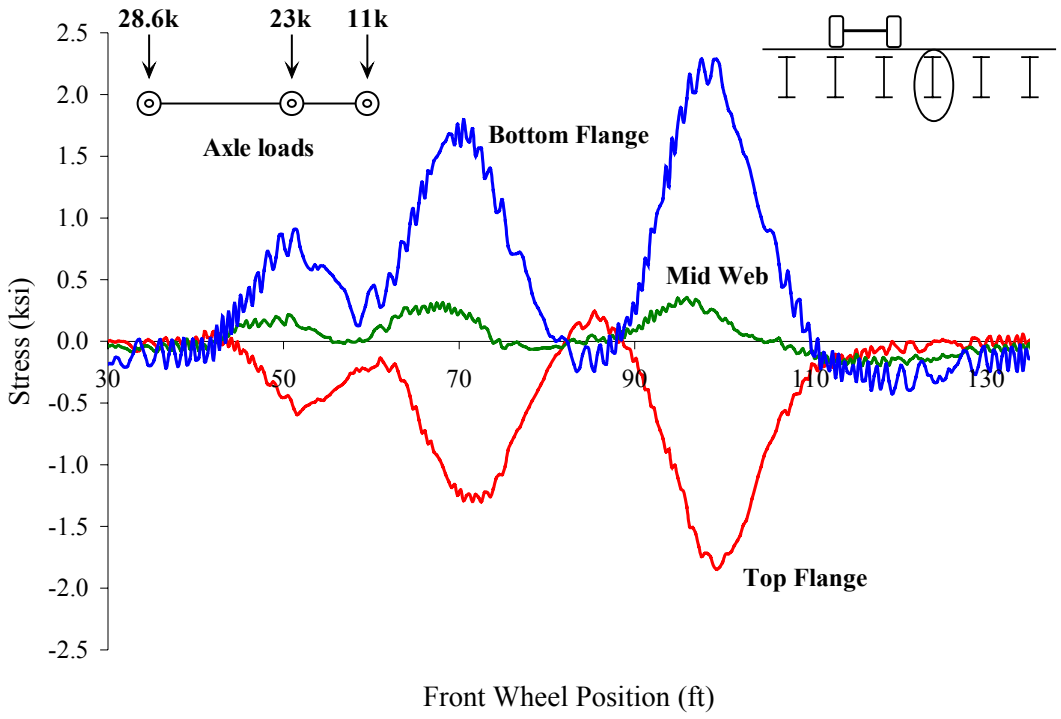

Figure C 8: Midspan stringer 4

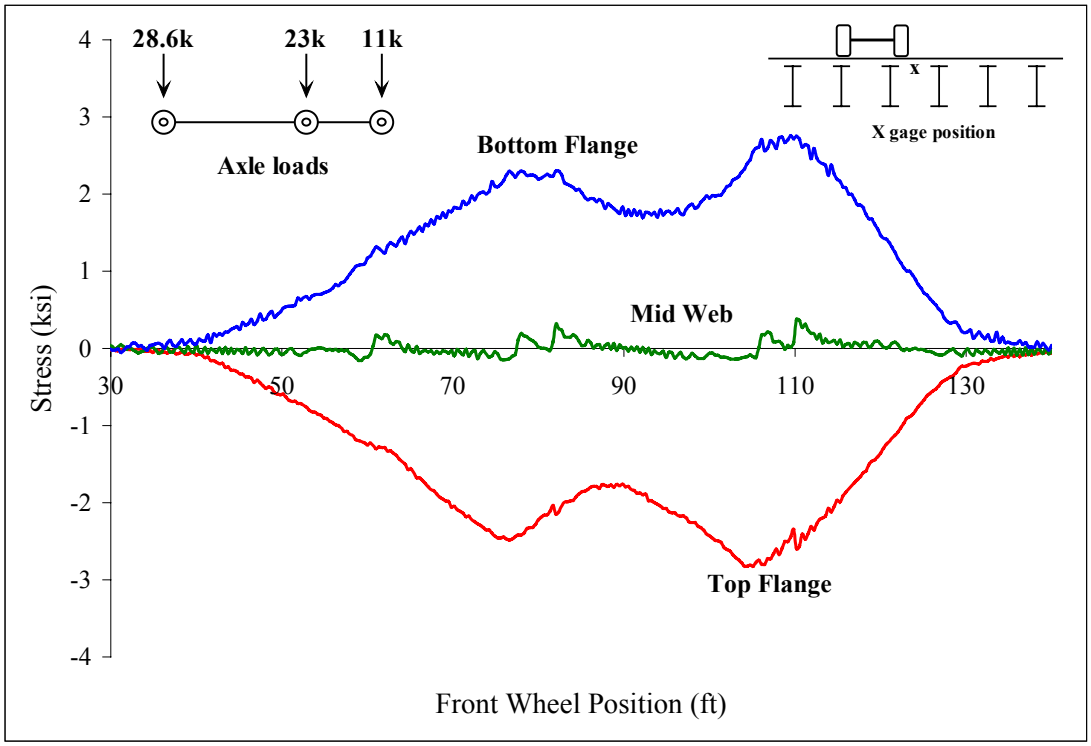

Figure C 9: Beam 5

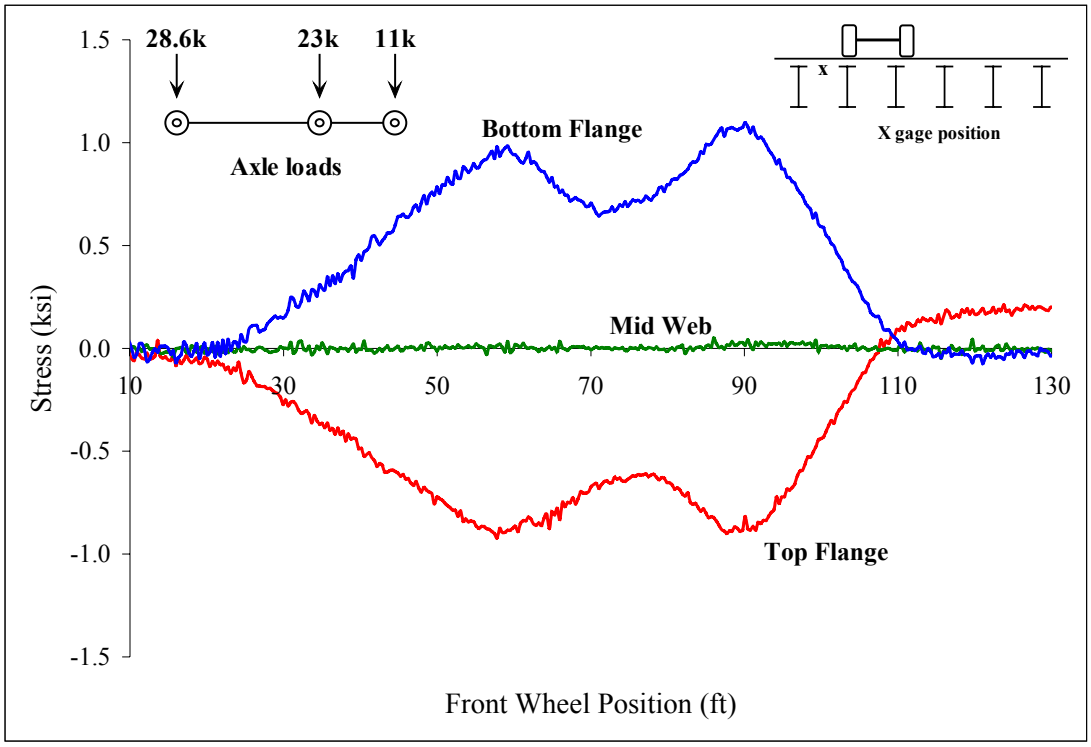

Figure C 10: Beam 4

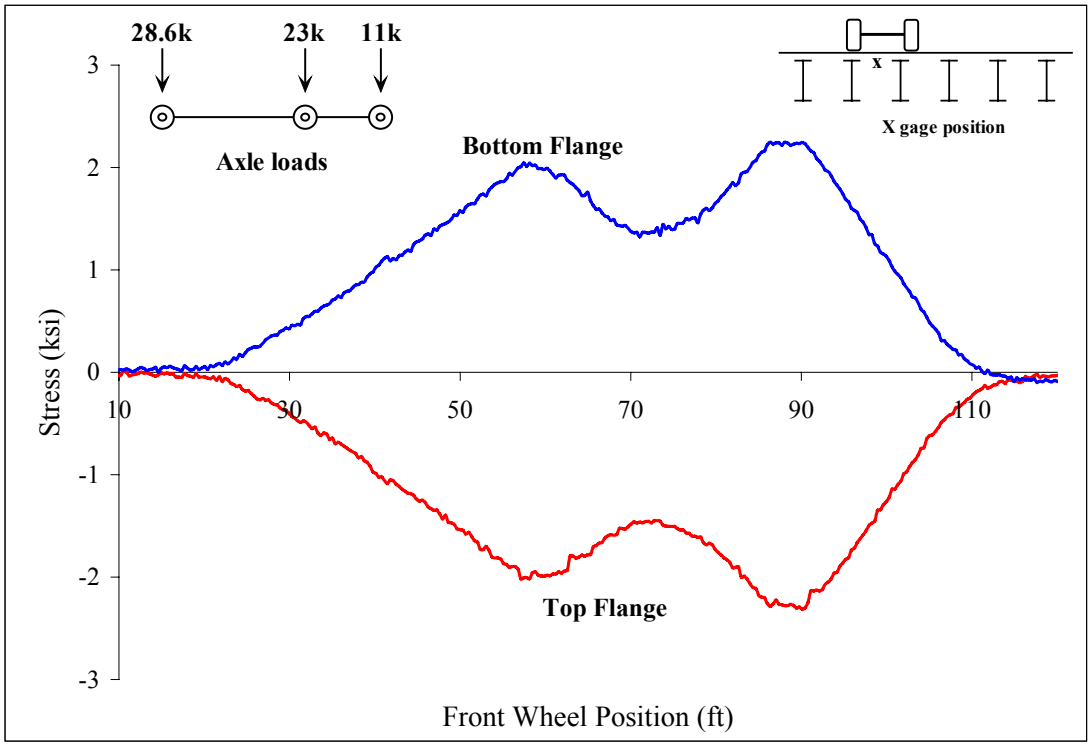

Figure C 11: Beam 4

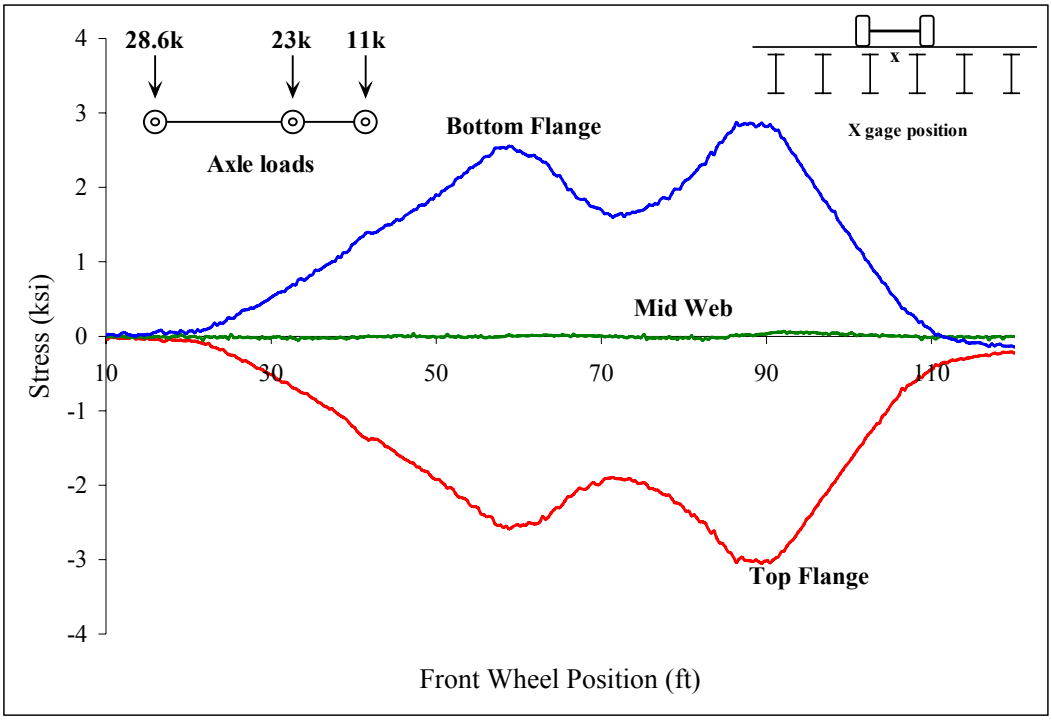

Figure C 12: Beam 4

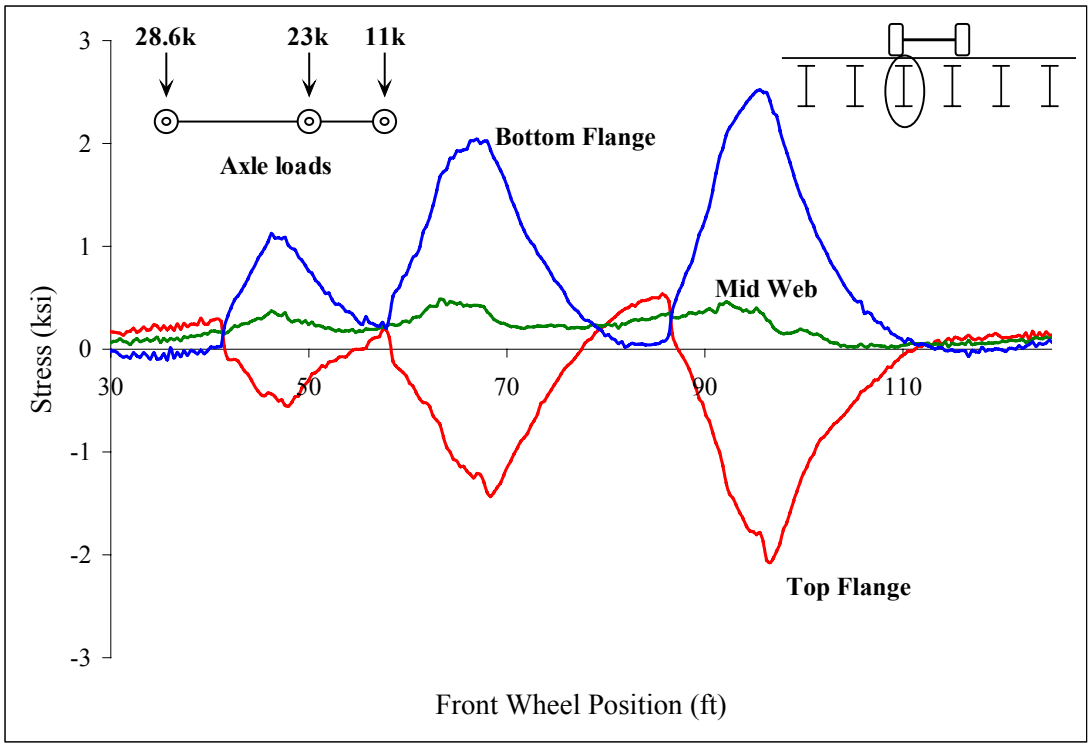

Figure C 13: South quarter point of stringer 3

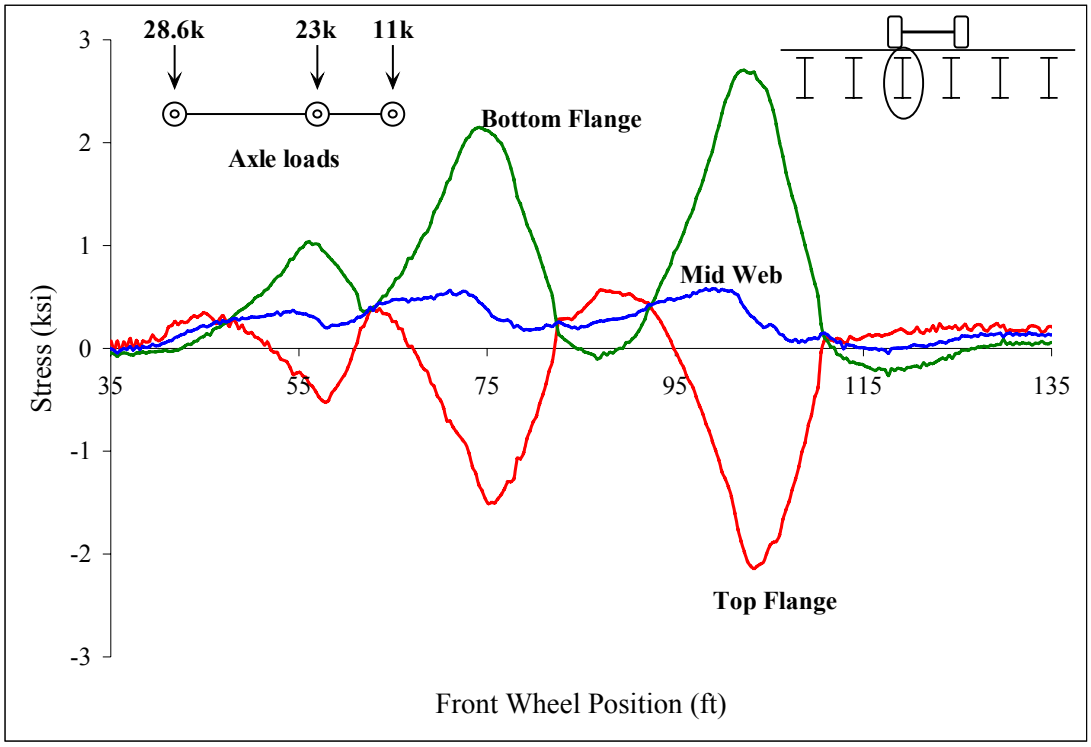

Figure C 14: North quarter point of stringer 3

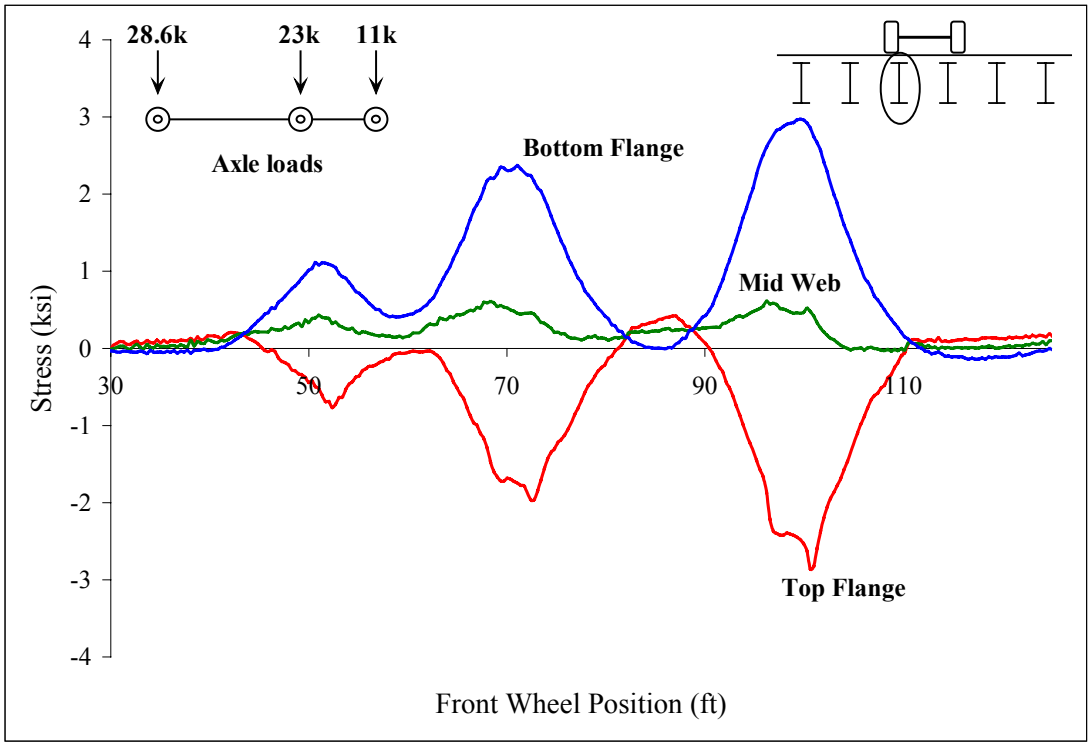

Figure C 15: Midspan stringer 3

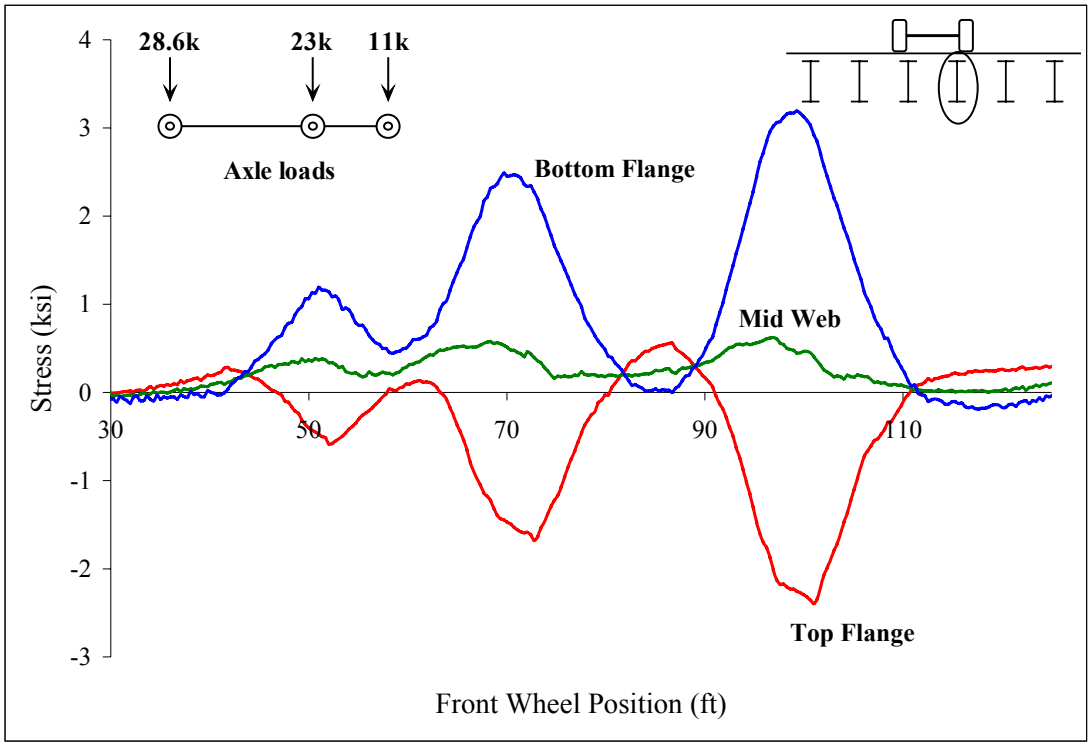

Figure C 16: Midspan stringer 4

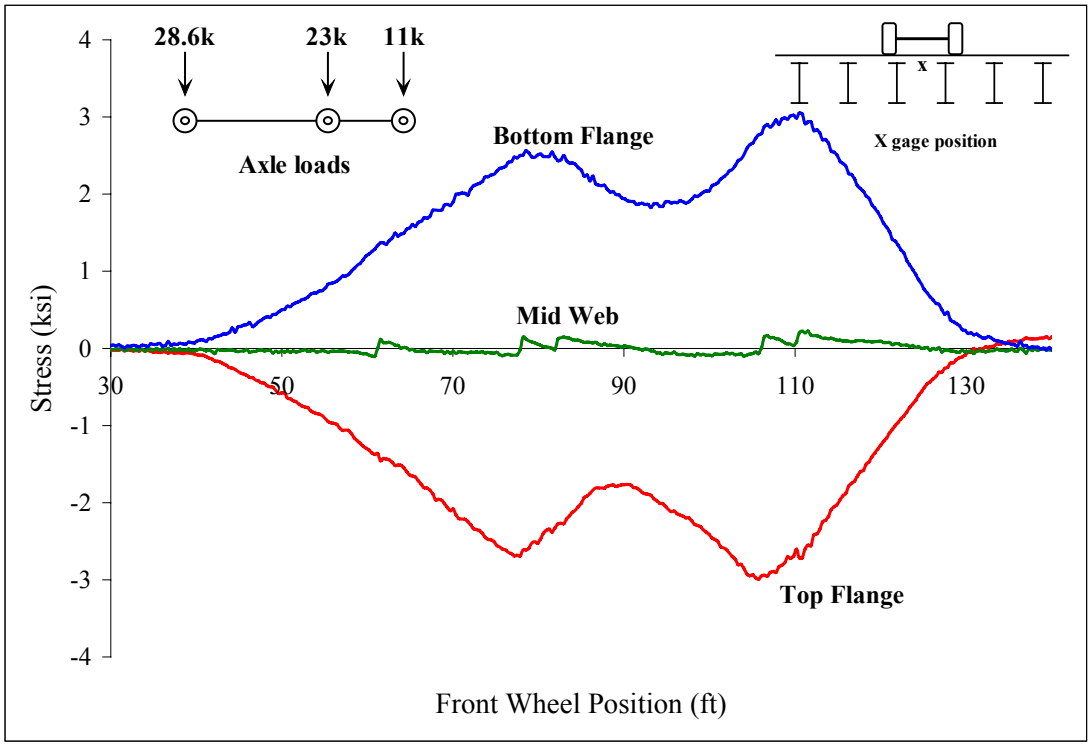

Figure C 17: Beam 5

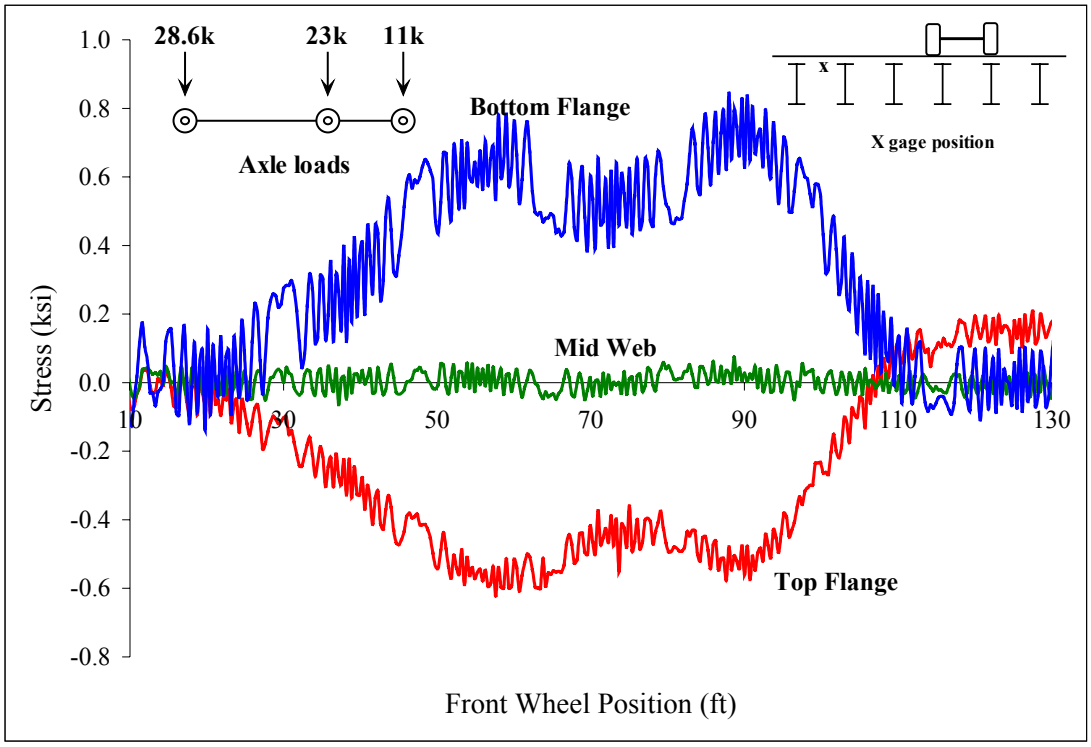

Figure C 18: Beam 4

Figure C 19: Beam 4

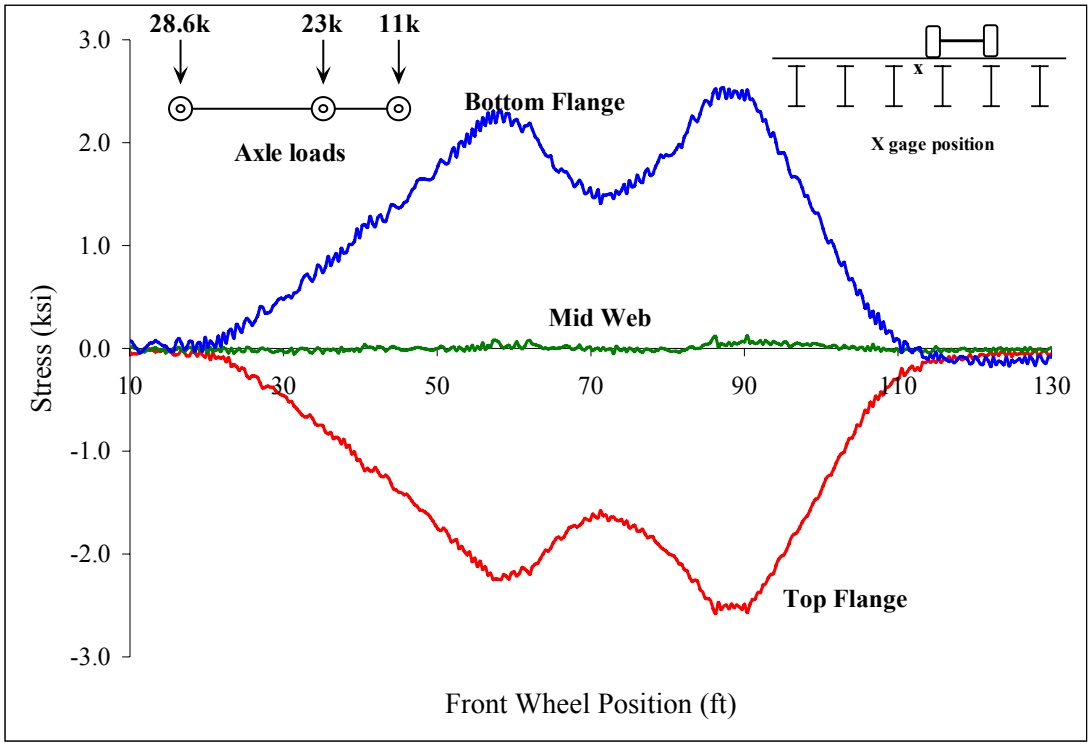

Figure C 20: Beam 4

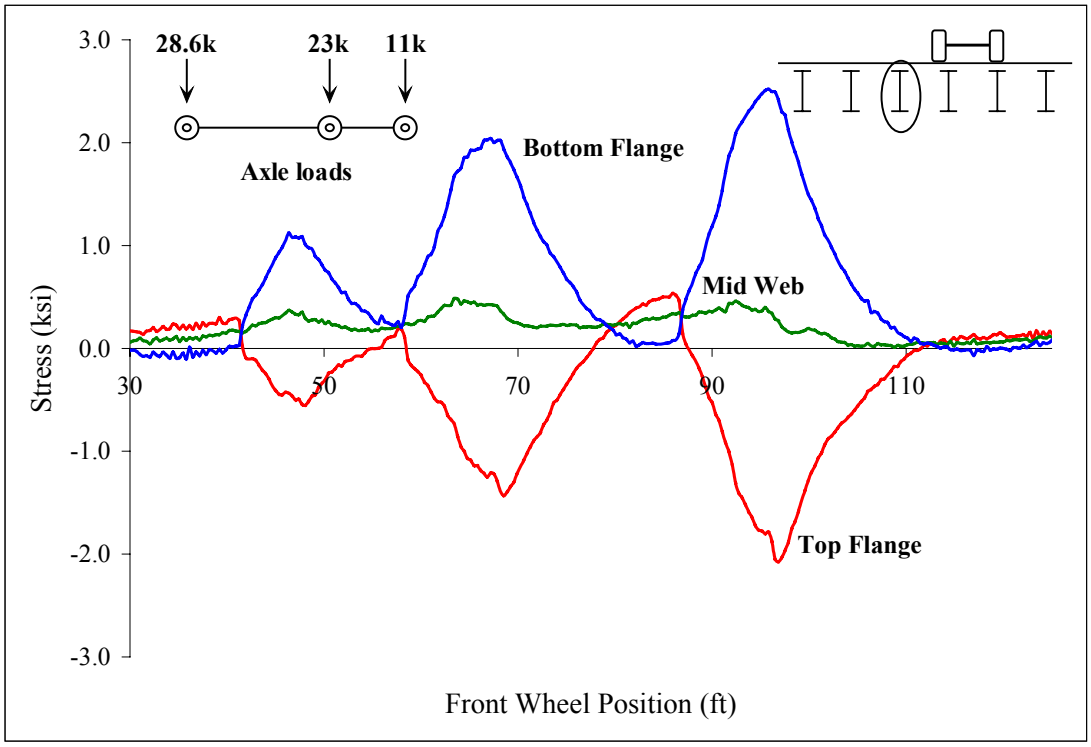

Figure C 21: South quarter point of stringer 3

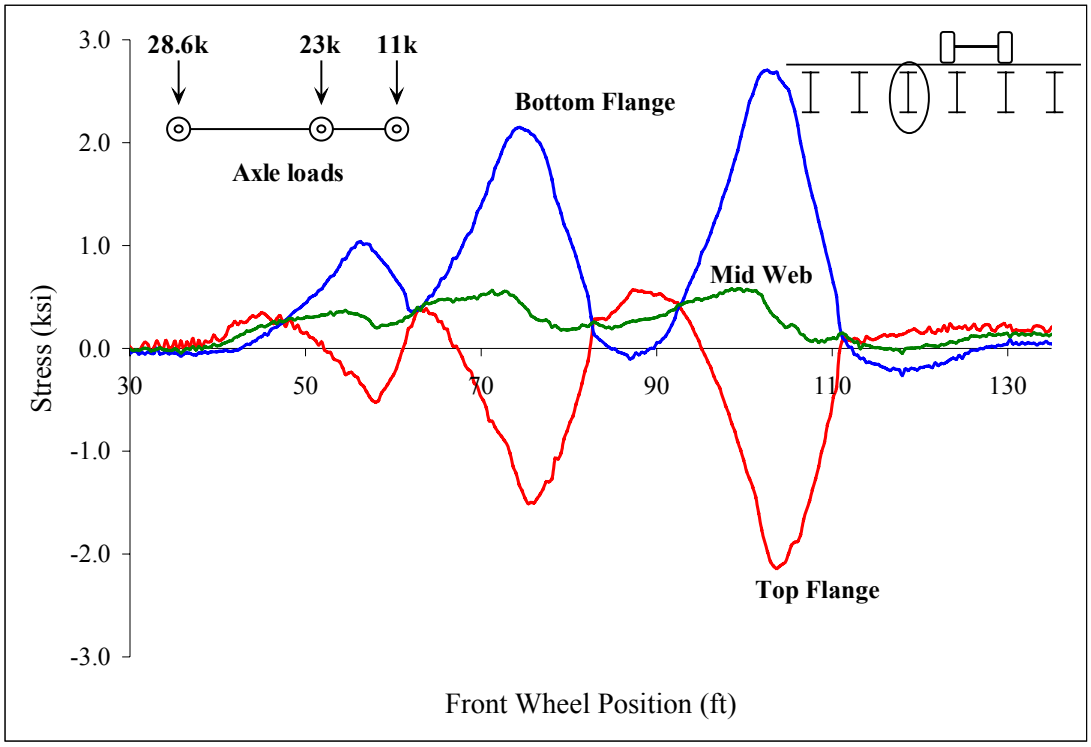

Figure C 22: North quarter point of stringer 3

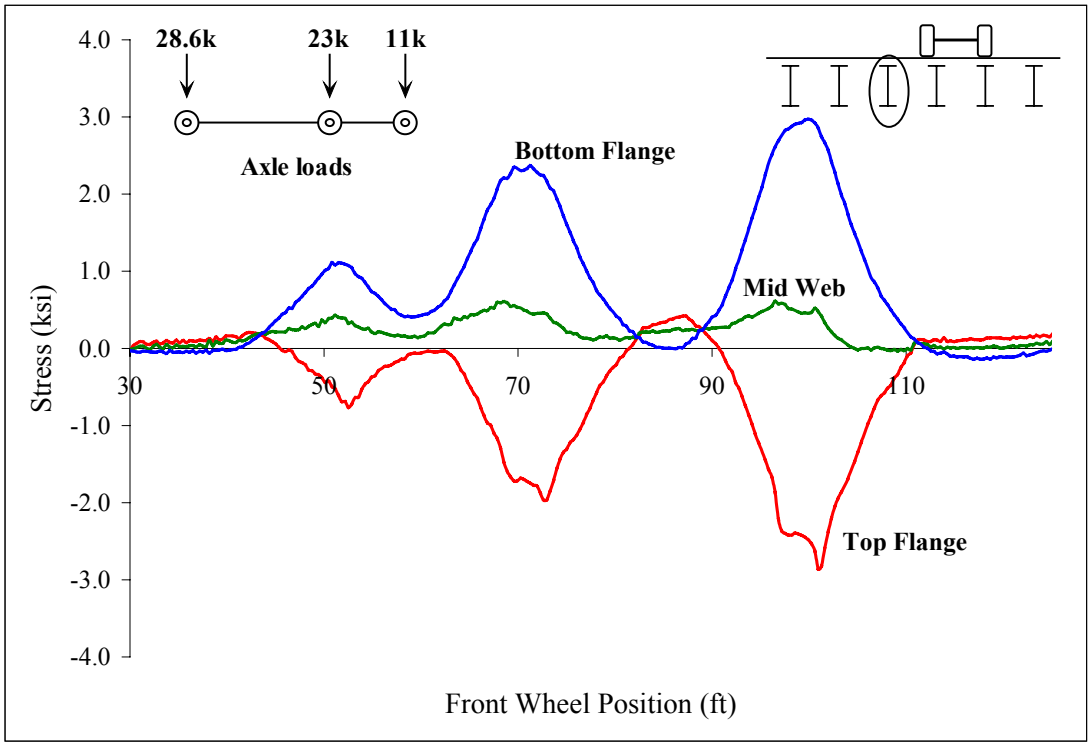

Figure C 23: Midspan stringer 3

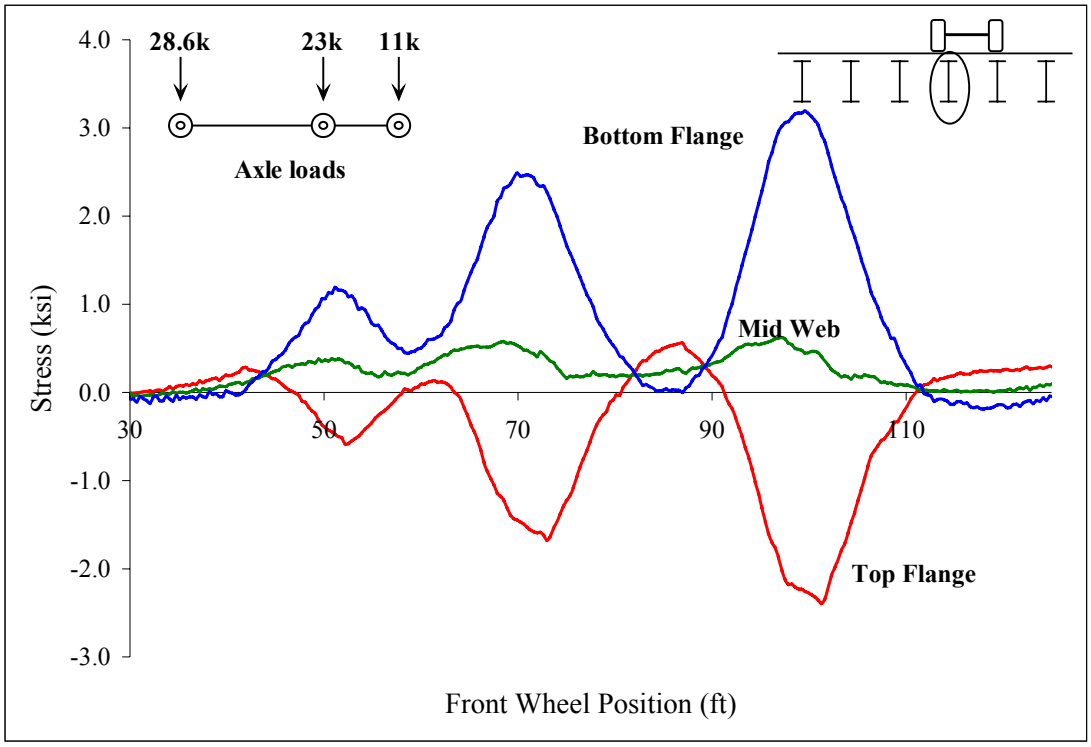

Figure C 24: Midspan stringer 4

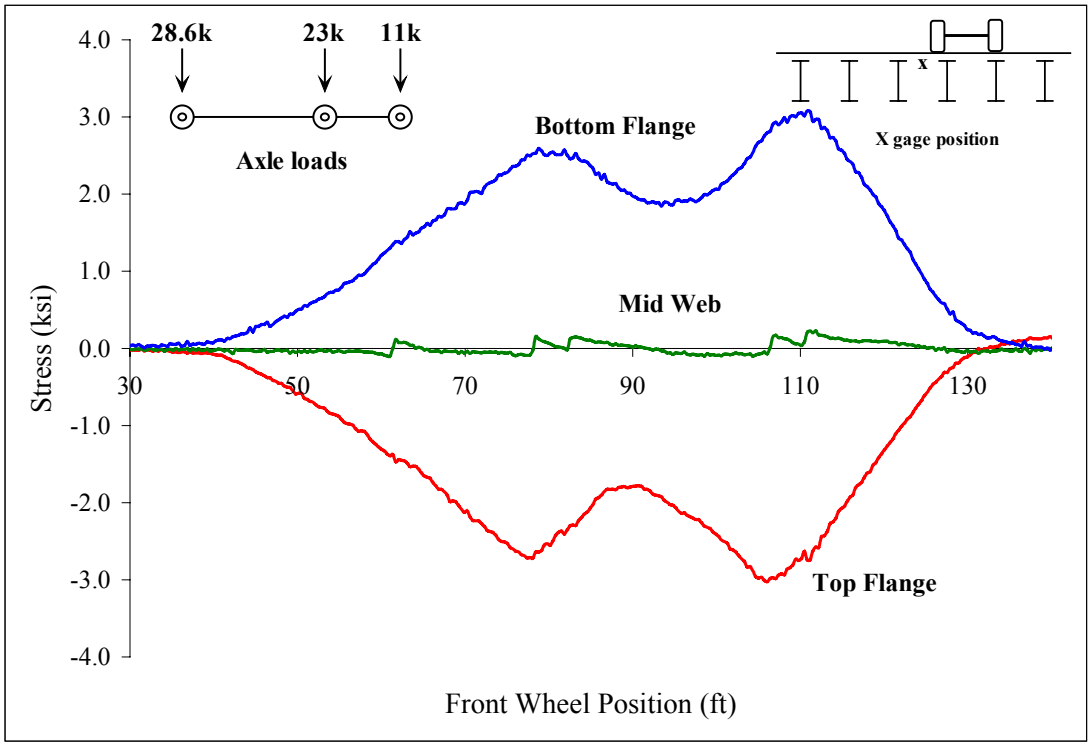

Figure C 25: Beam 5

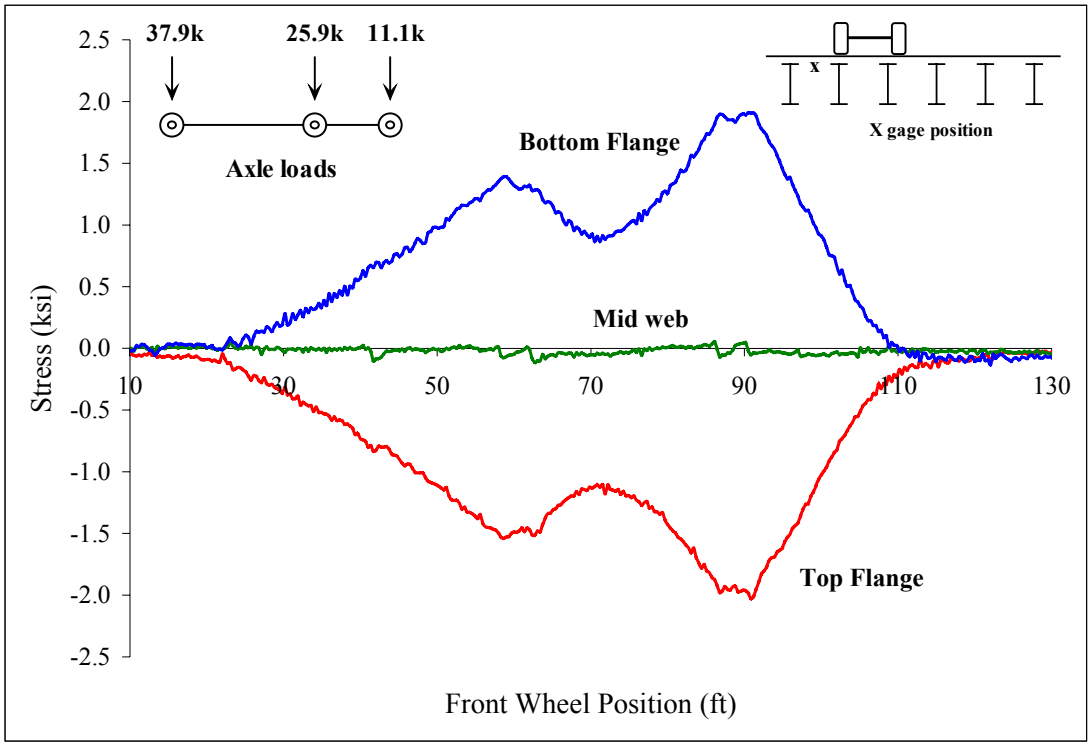

Figure C 26: Beam 4

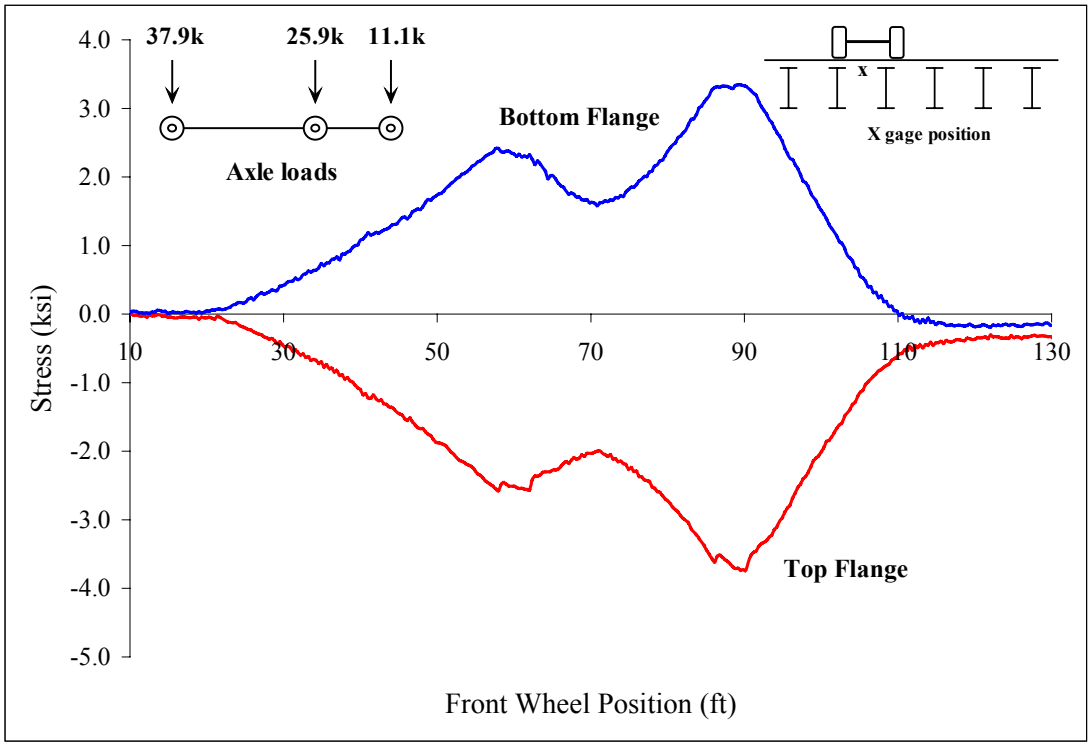

Figure C 27: Beam 4

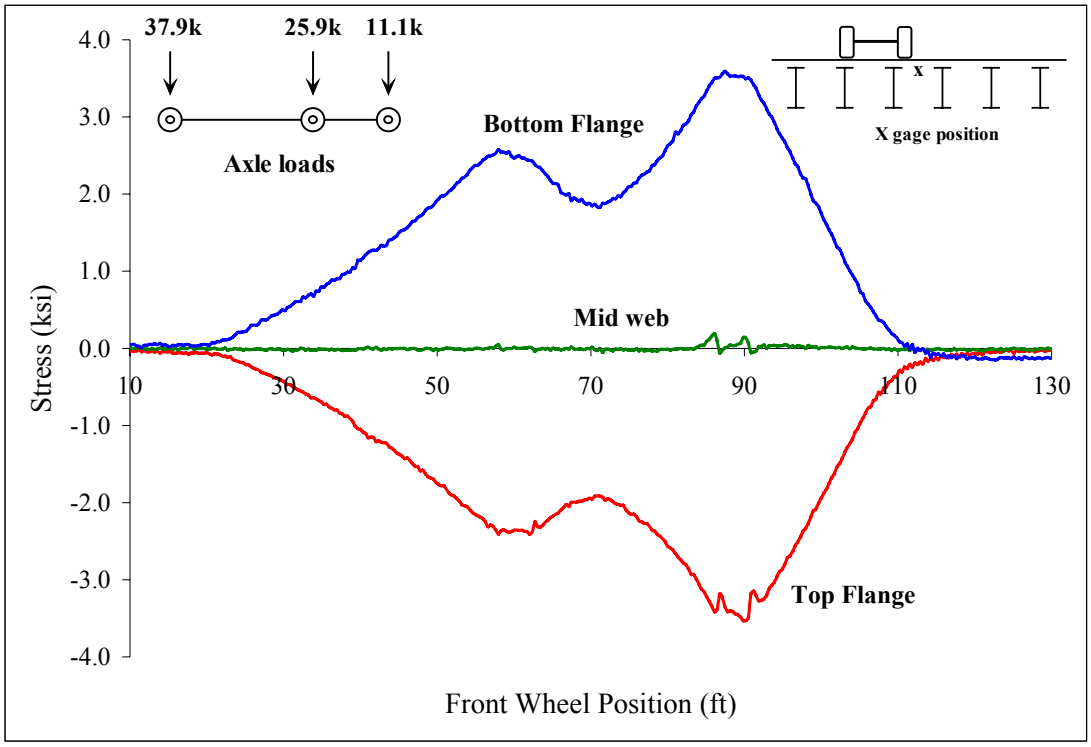

Figure C 28: Beam 4

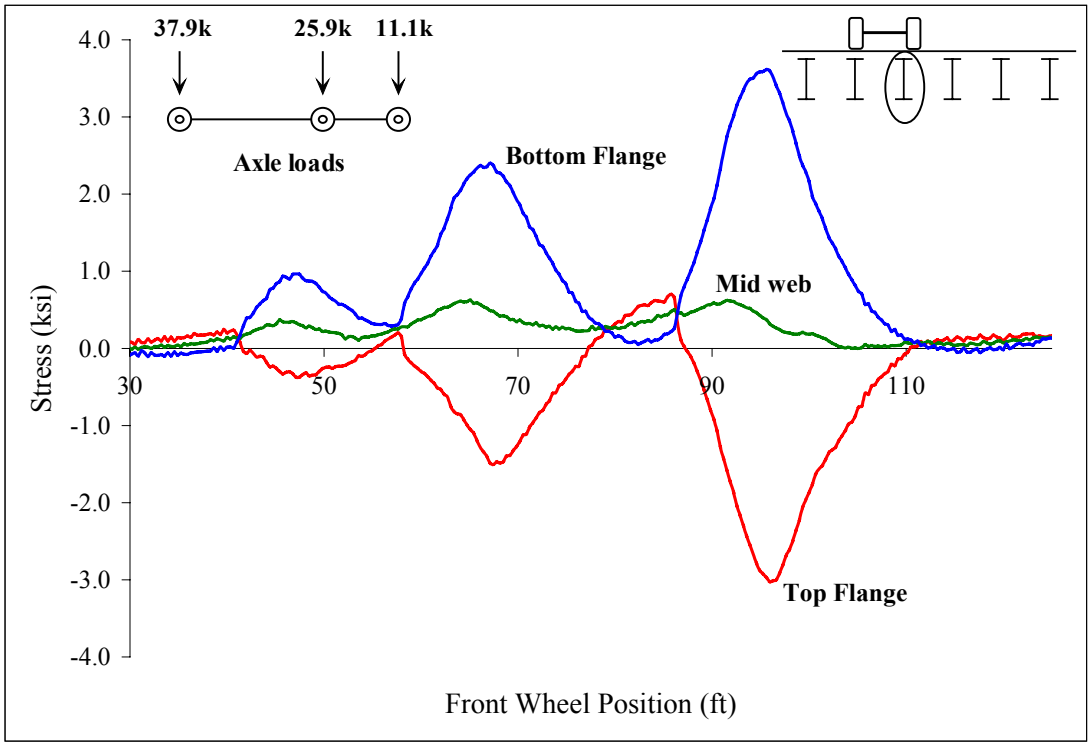

Figure C 29: South quarter point of stringer 3

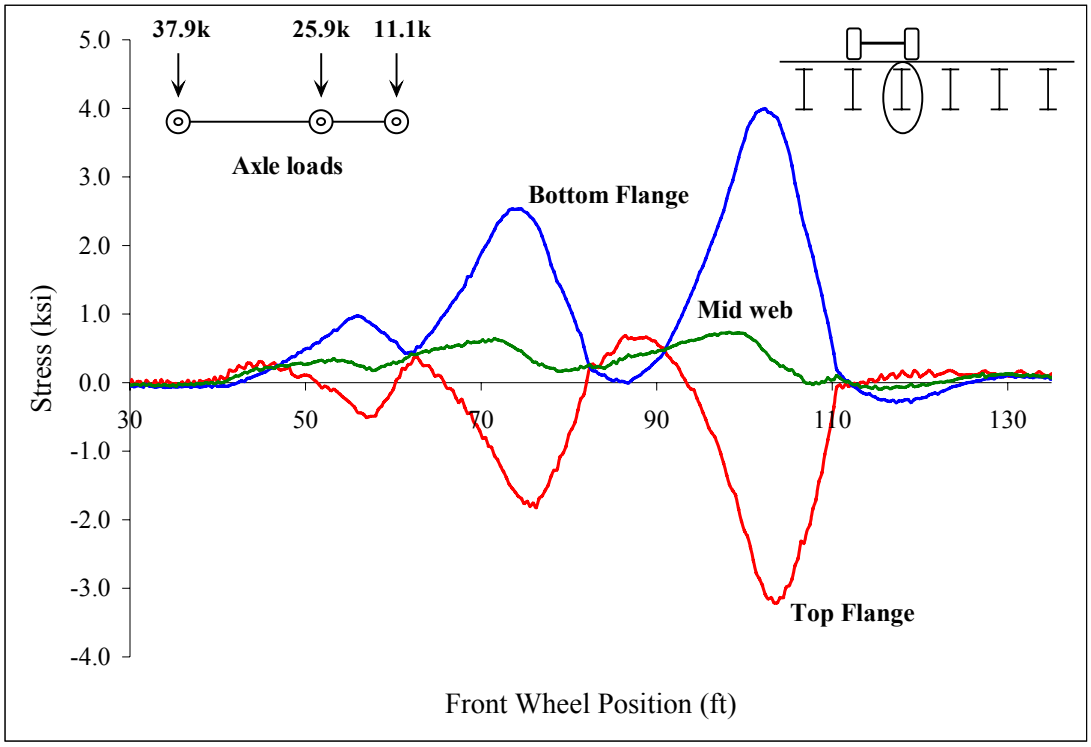

Figure C 30: North quarter point of stringer 3

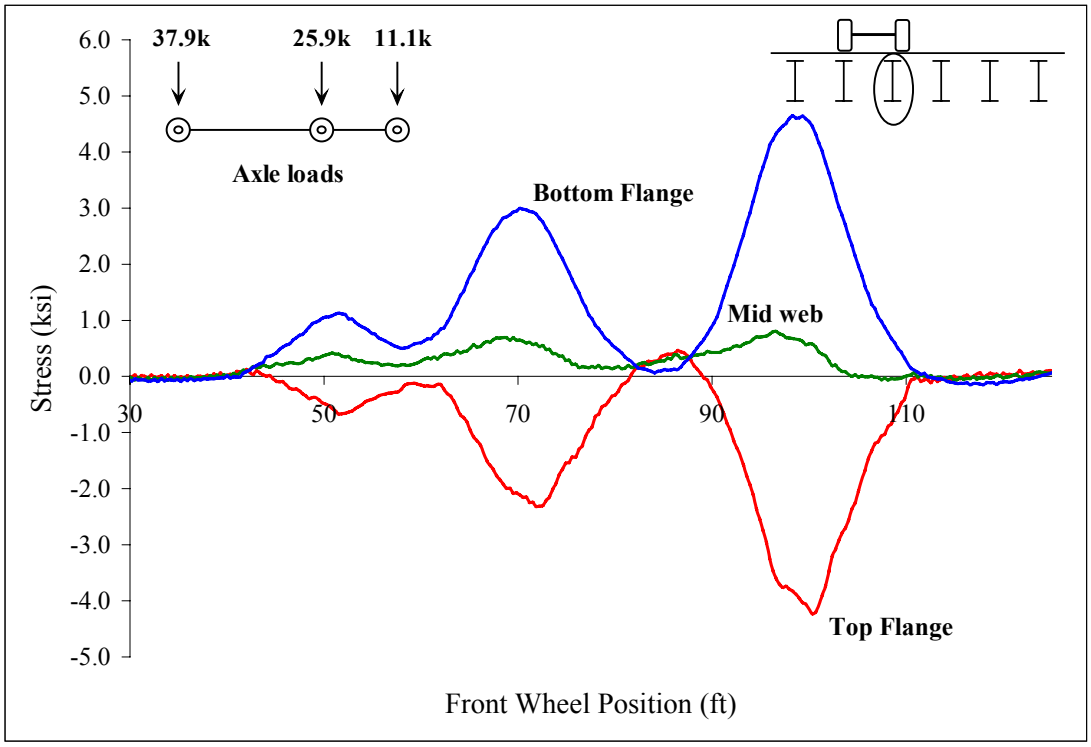

Figure C 31: Midspan stringer 3

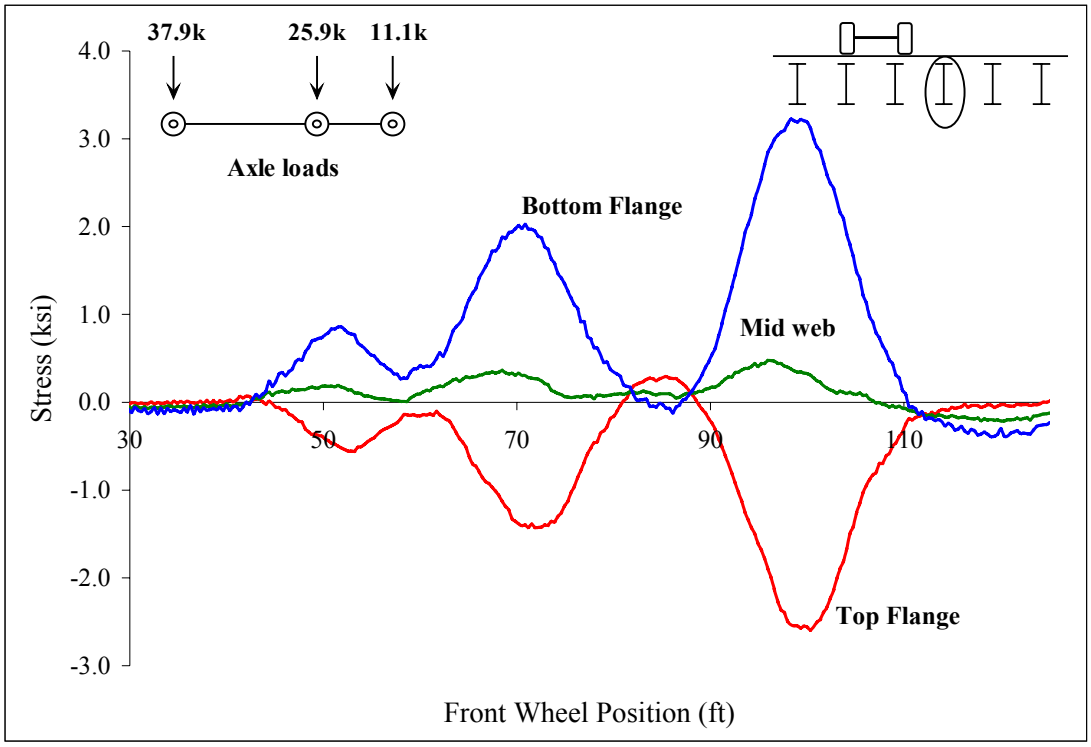

Figure C 32: Midspan stringer 4

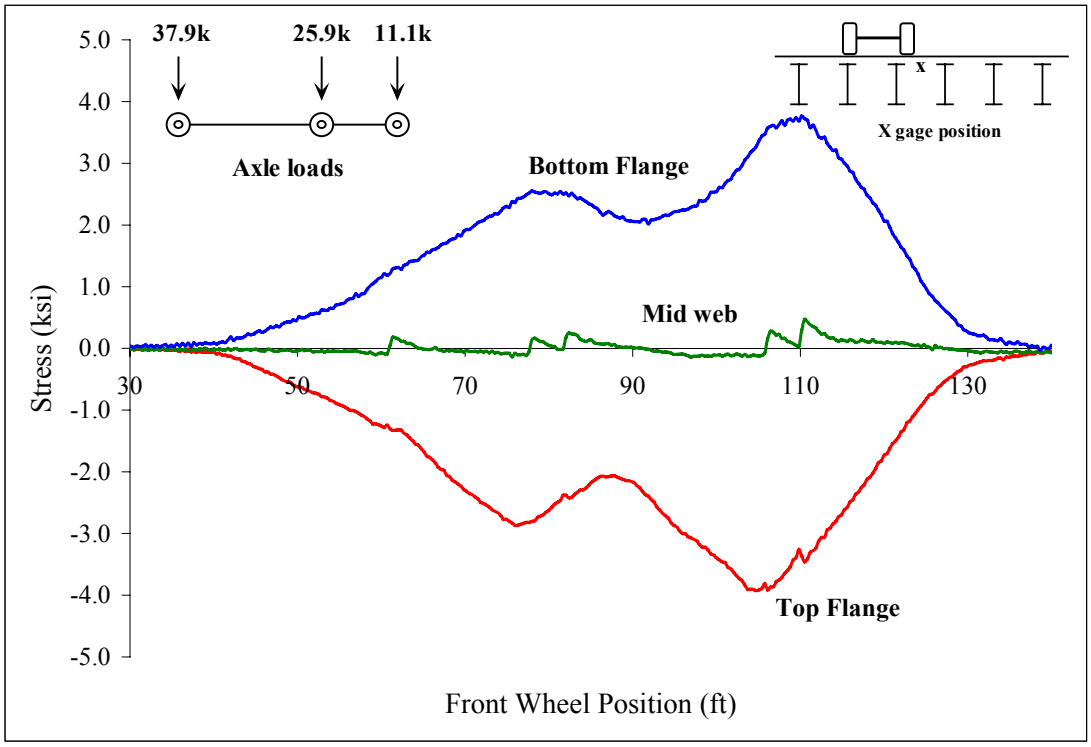

Figure C 33: Beam 5

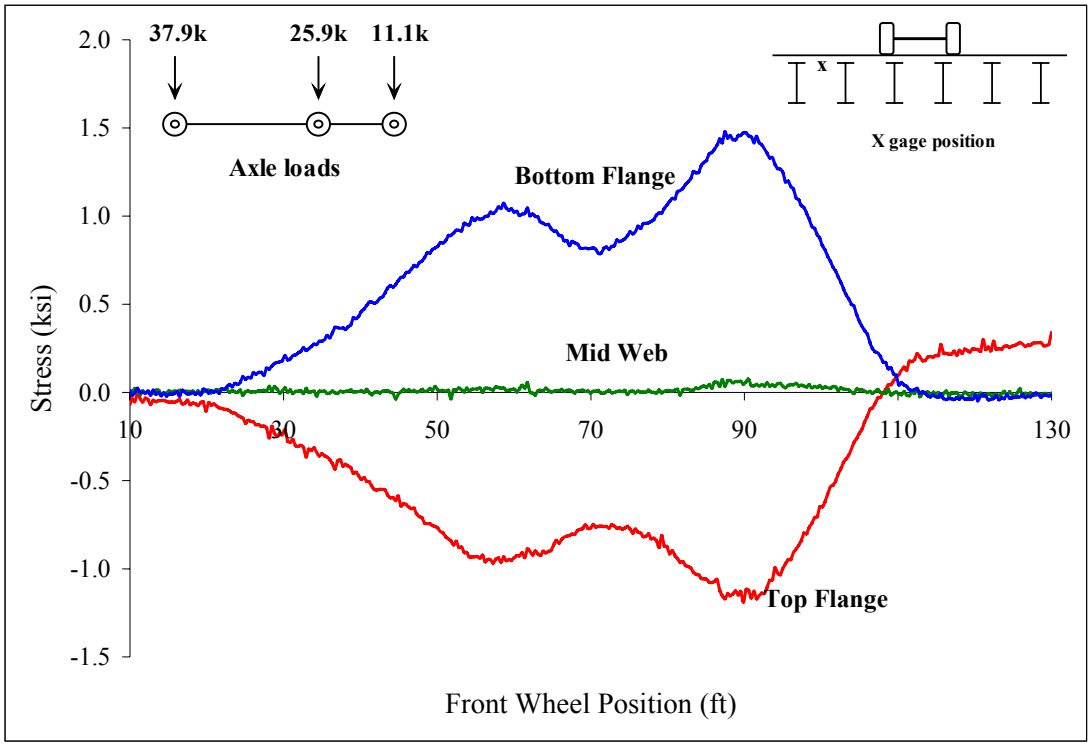

Figure C 34: Beam 4

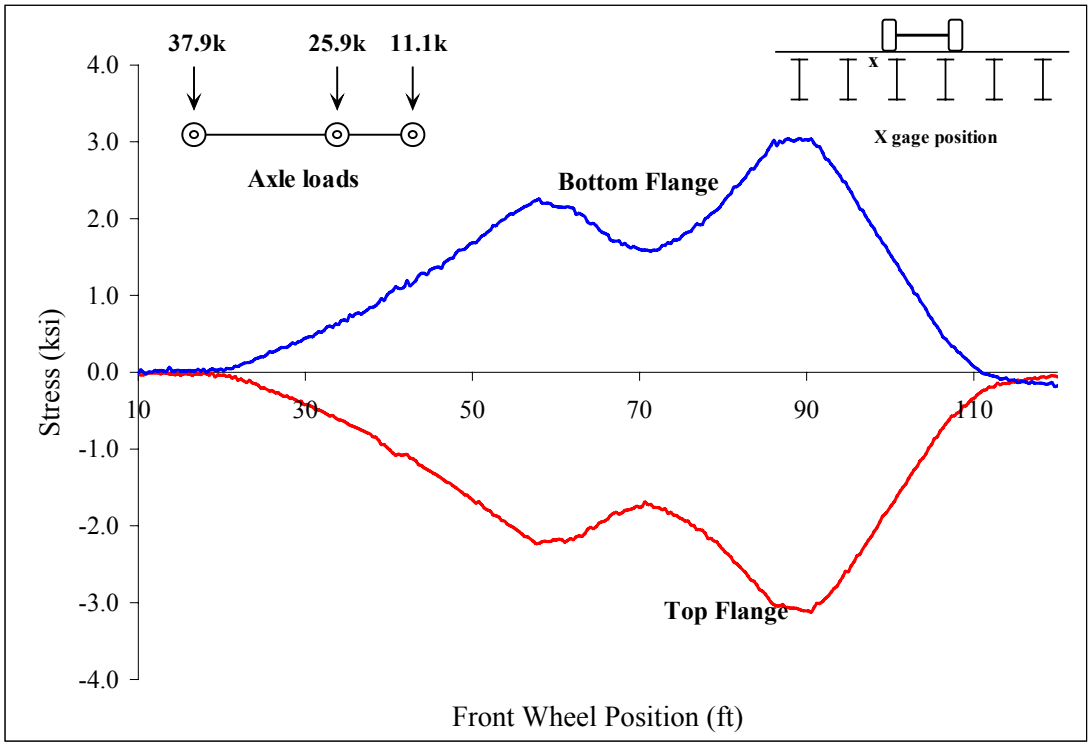

Figure C 35: Beam 4

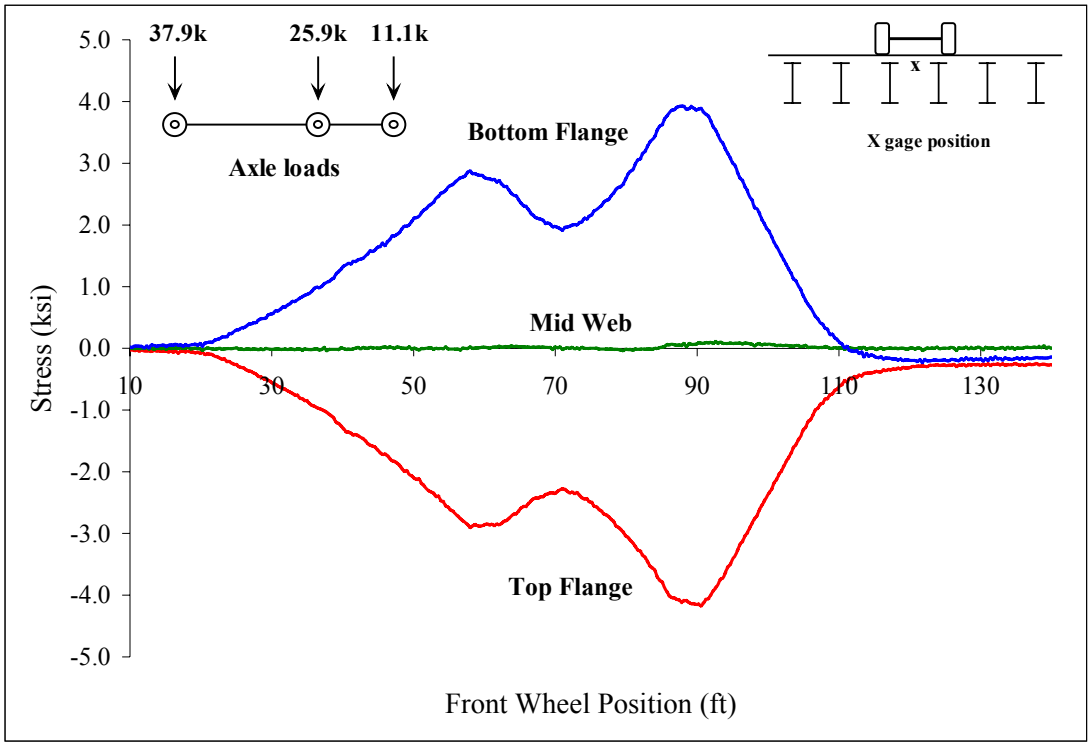

Figure C 36: Beam 4

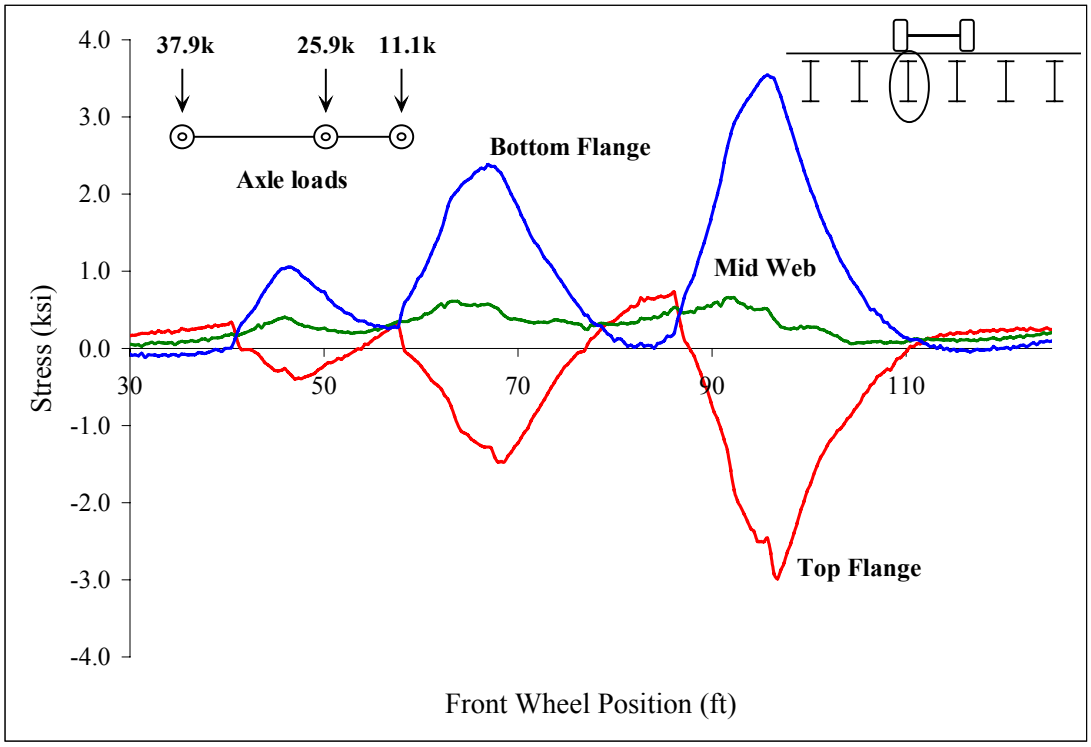

Figure C 37: South quarter point of stringer 3

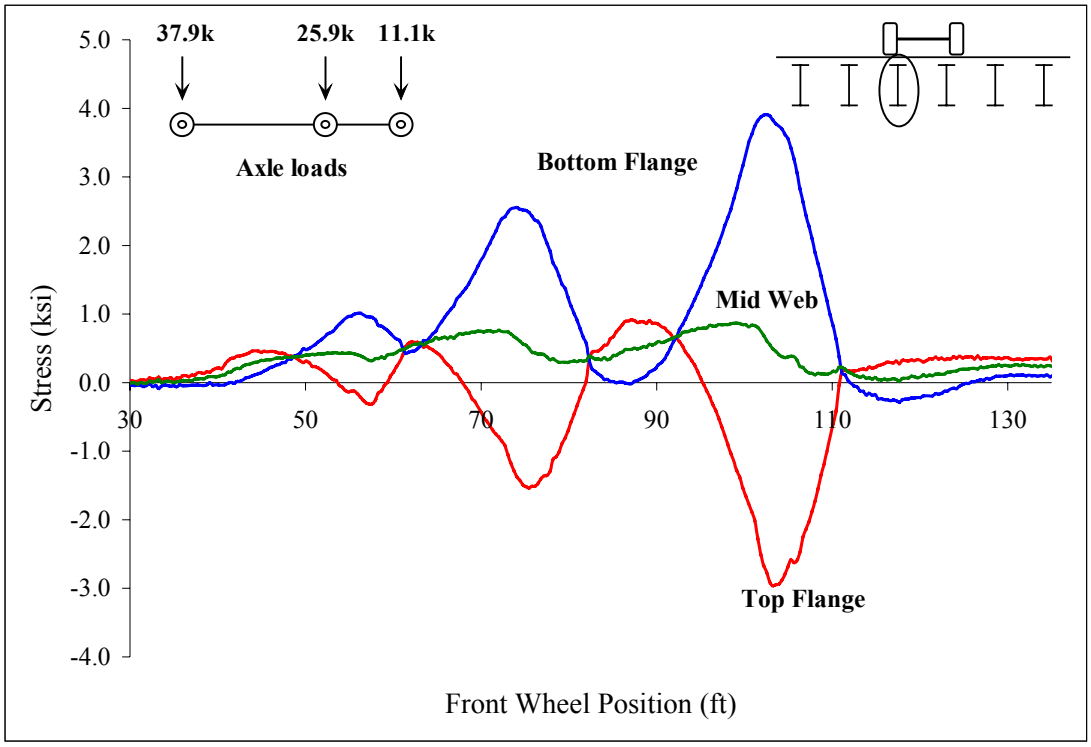

Figure C 38: North quarter point of stringer 3

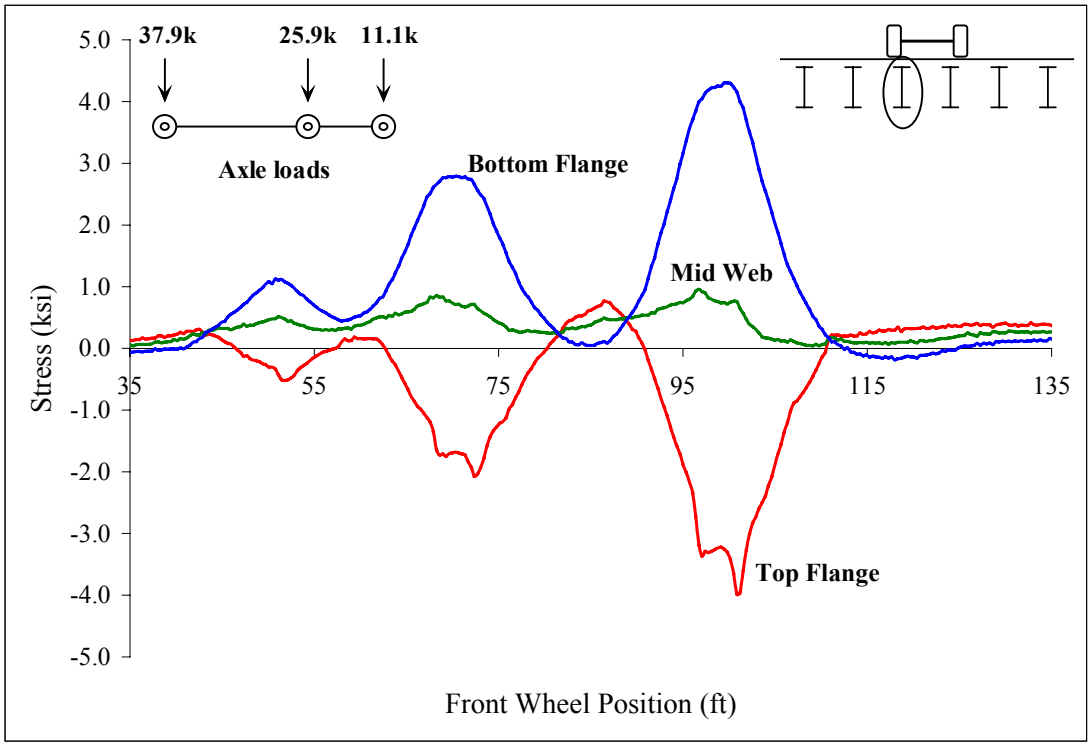

Figure C 39 Midspan stringer 3

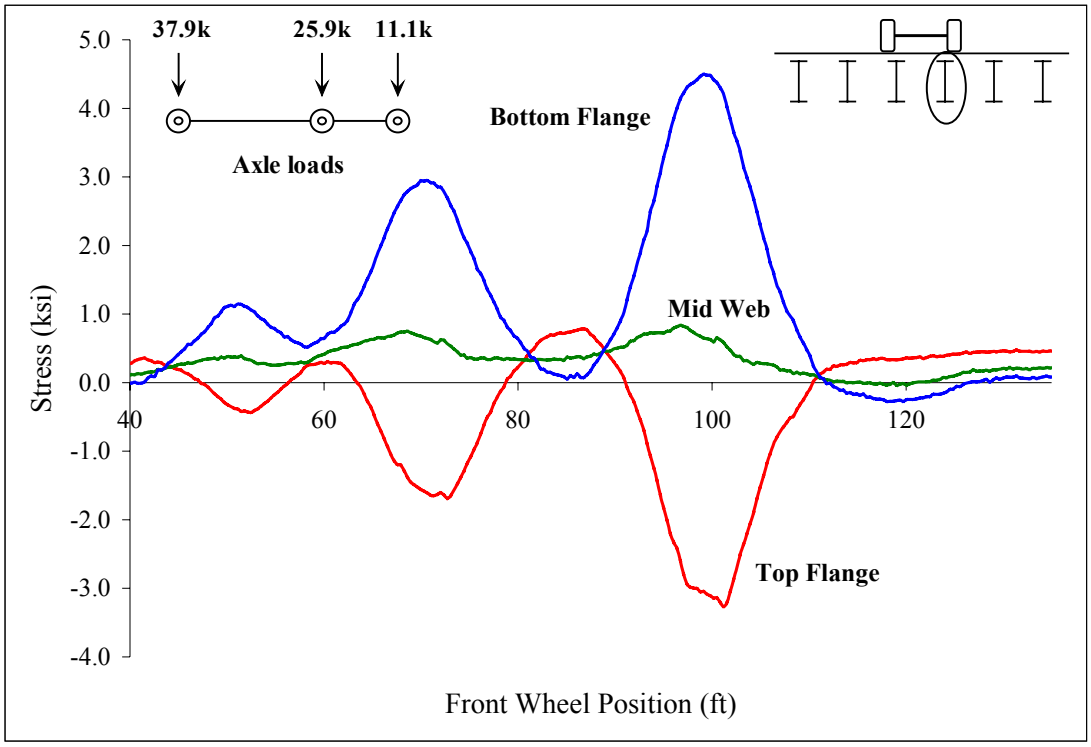

Figure C 40: Midspan stringer 4

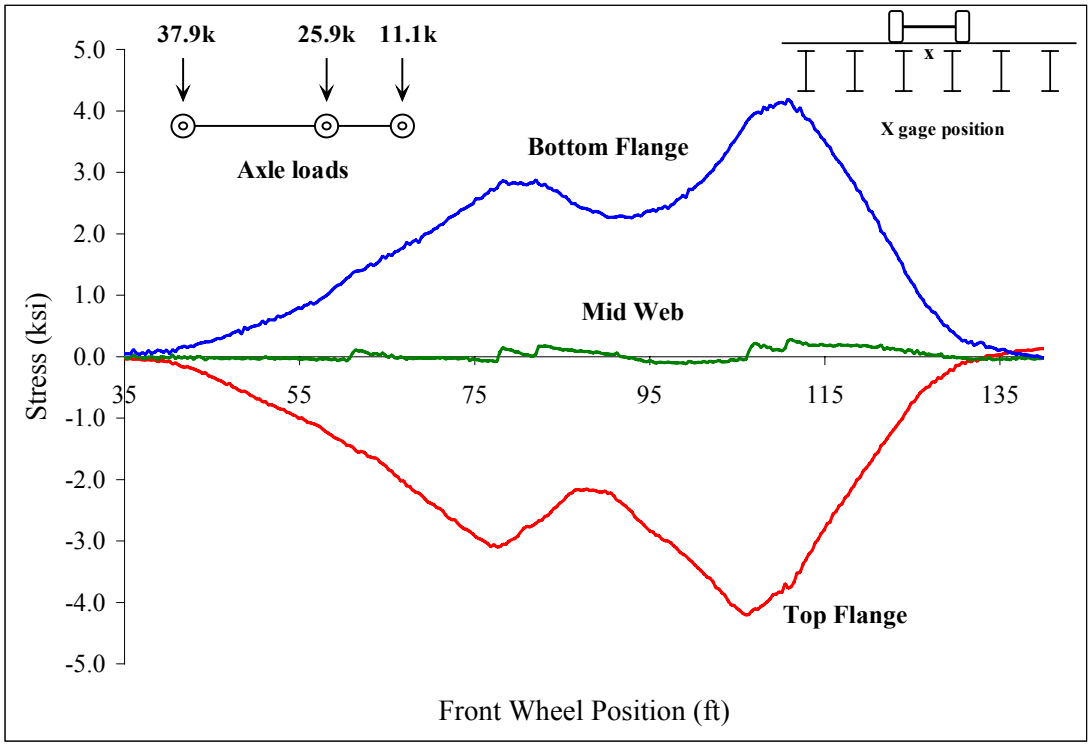

Figure C 41: Beam 5

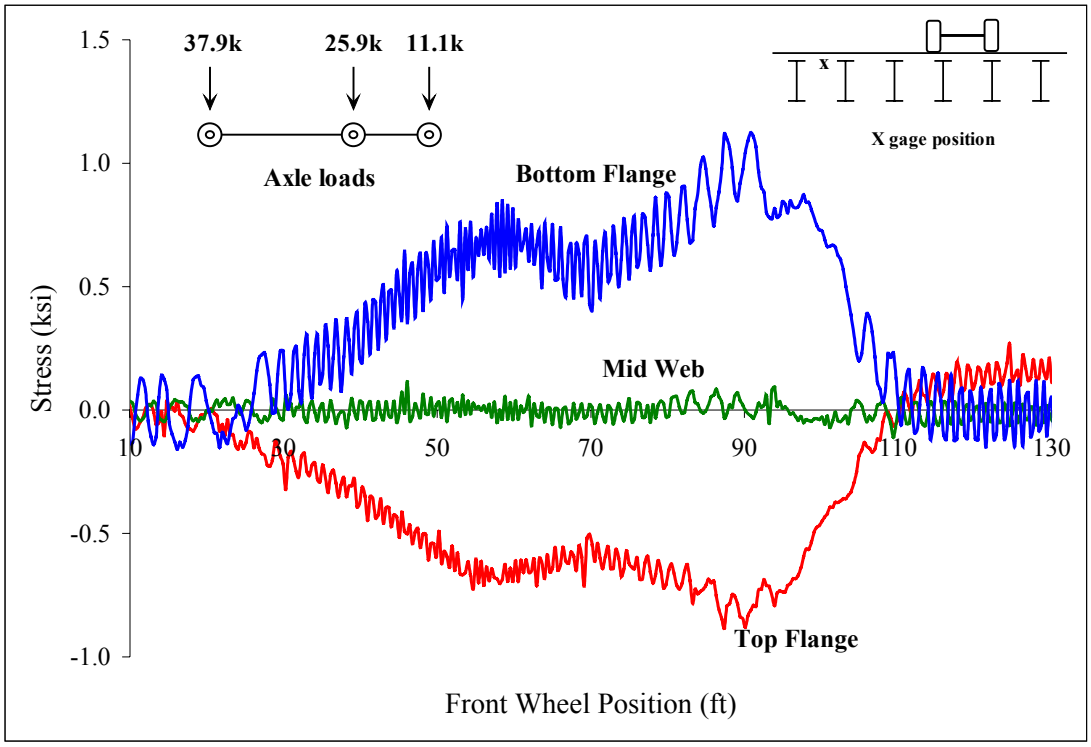

Figure C 42: Beam 4

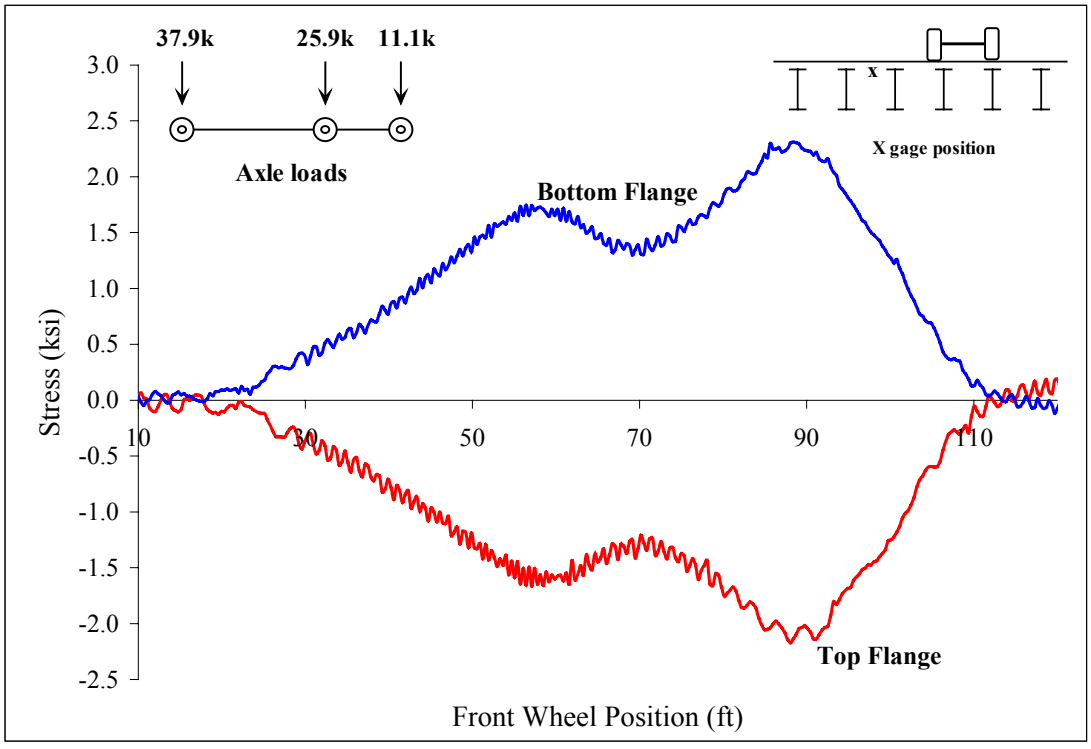

Figure C 43: Beam 4

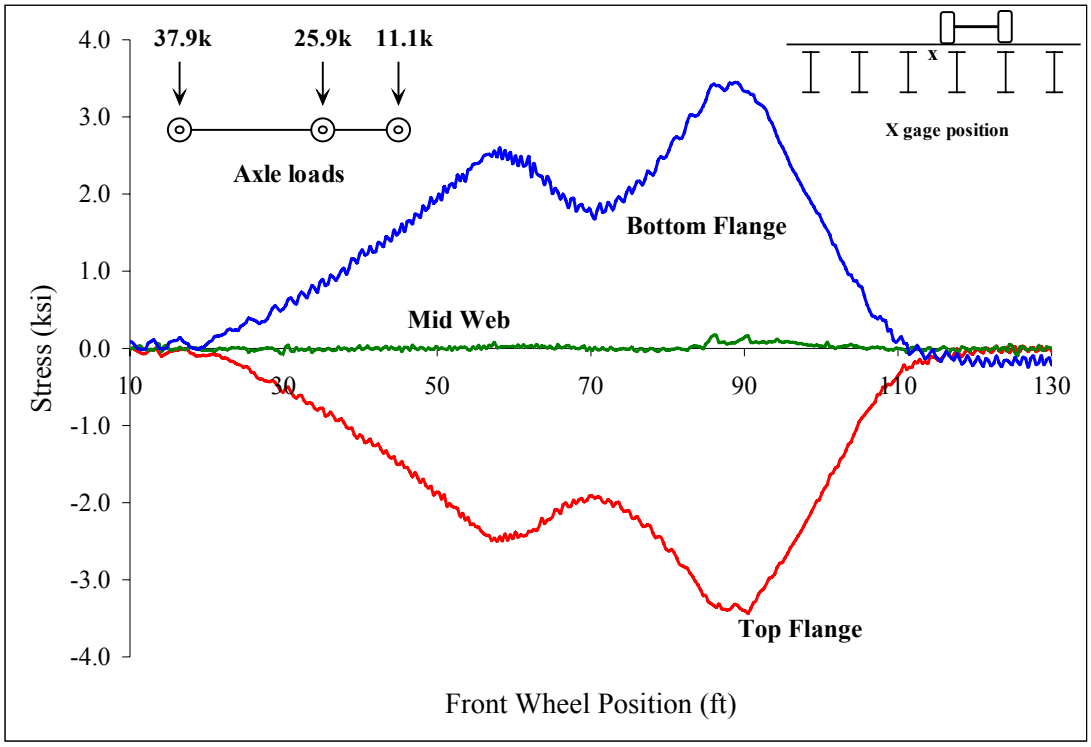

Figure C 44: Beam 4

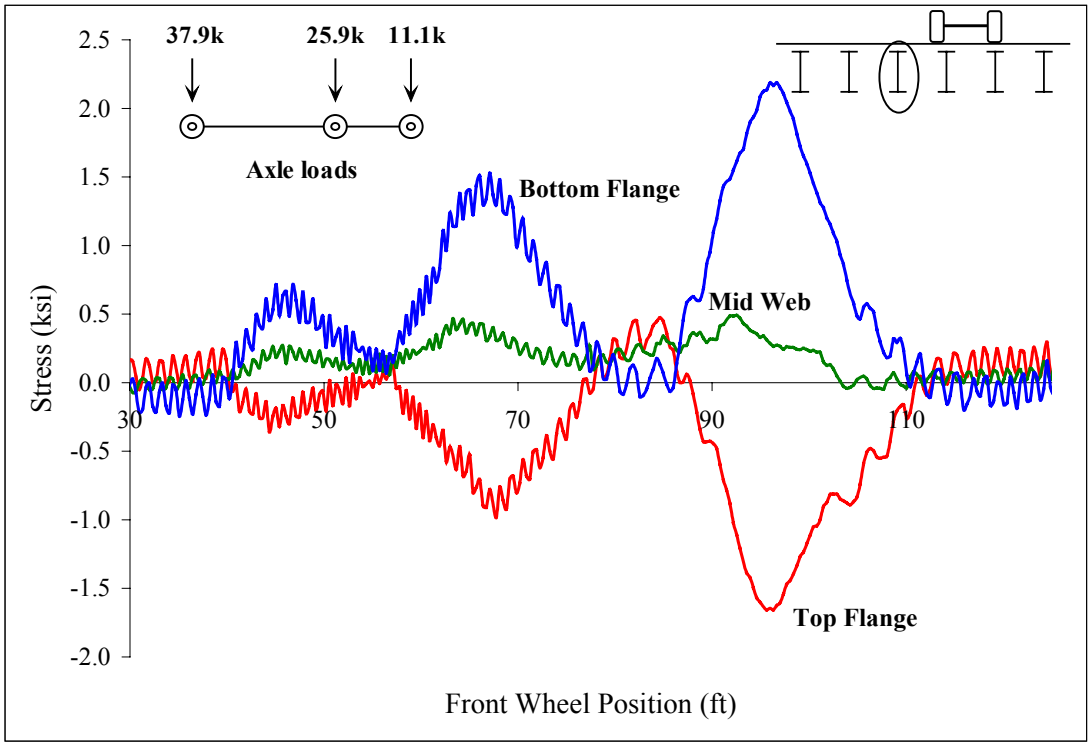

Figure C 45: South quarter point of stringer 3

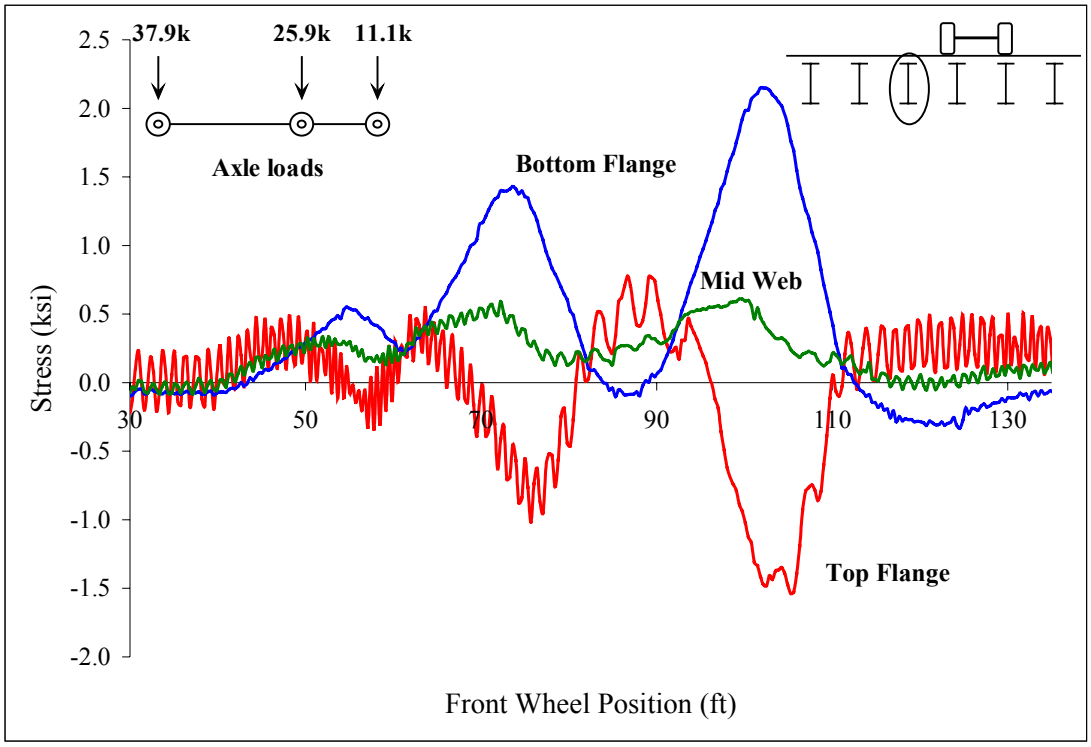

Figure C 46: North quarter point of stringer 3

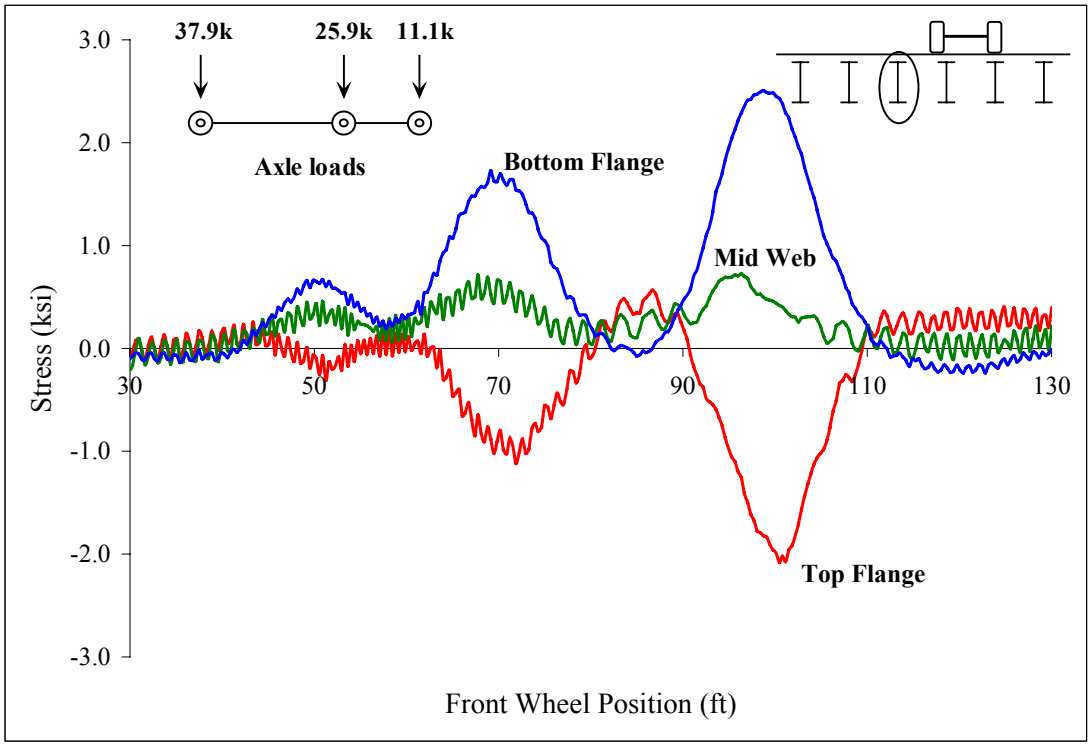

Figure C 47: Midspan stringer 3

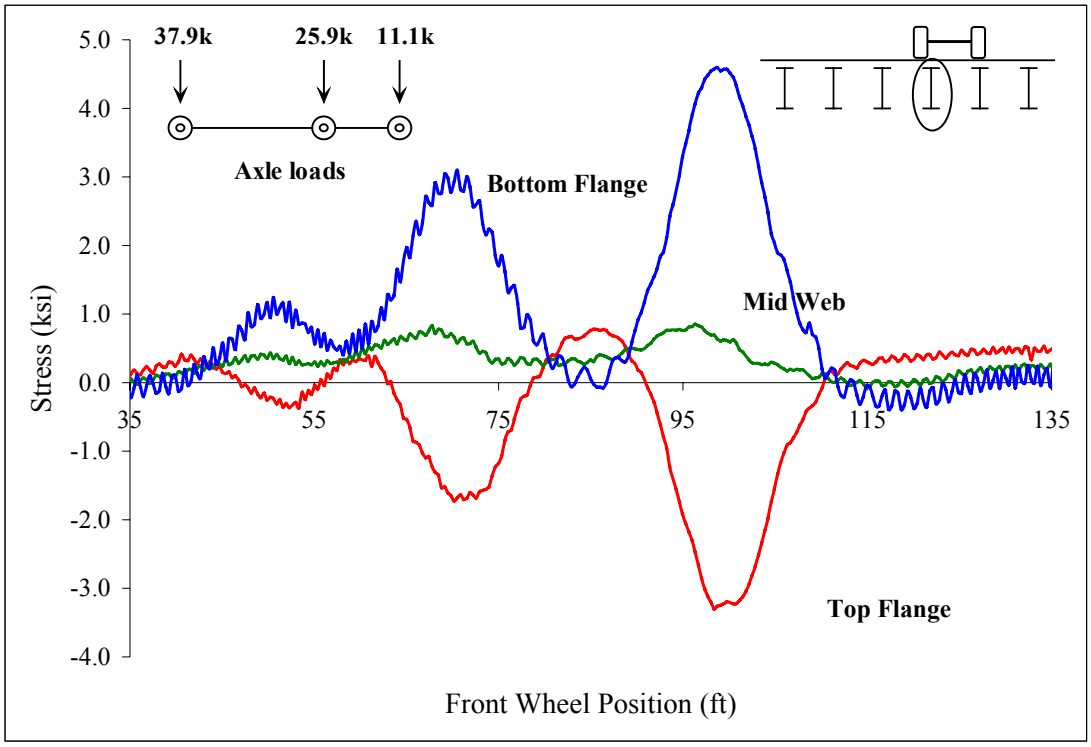

Figure C 48: Midspan stringer 4

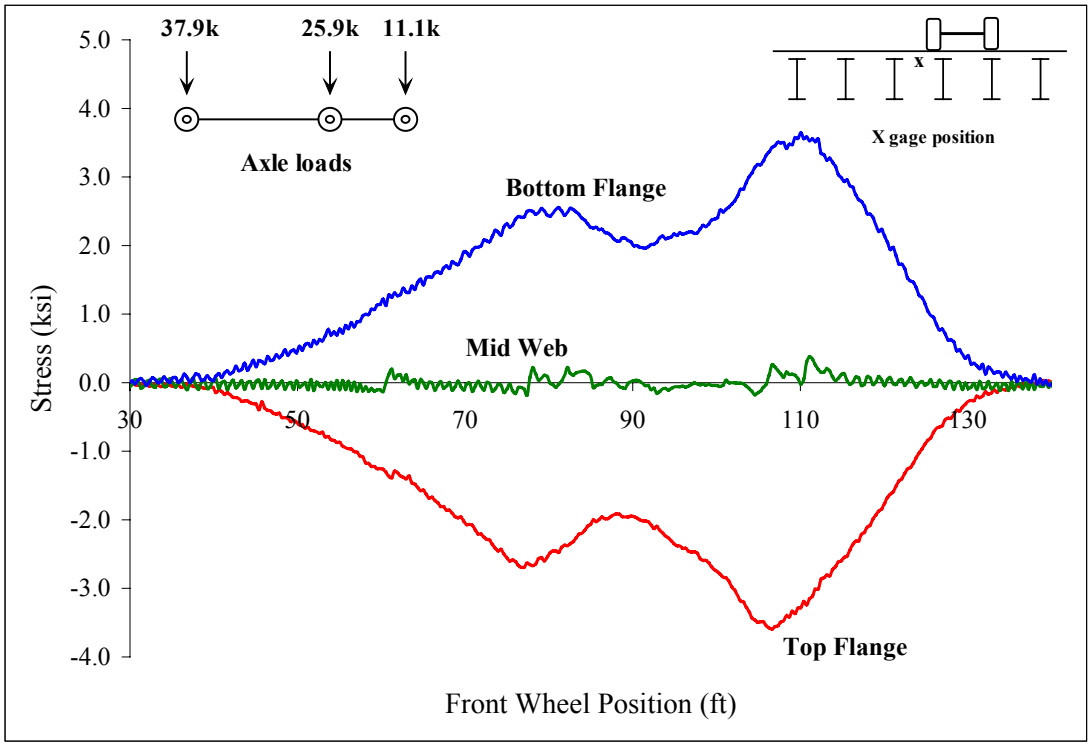

Figure C 49: Beam 5

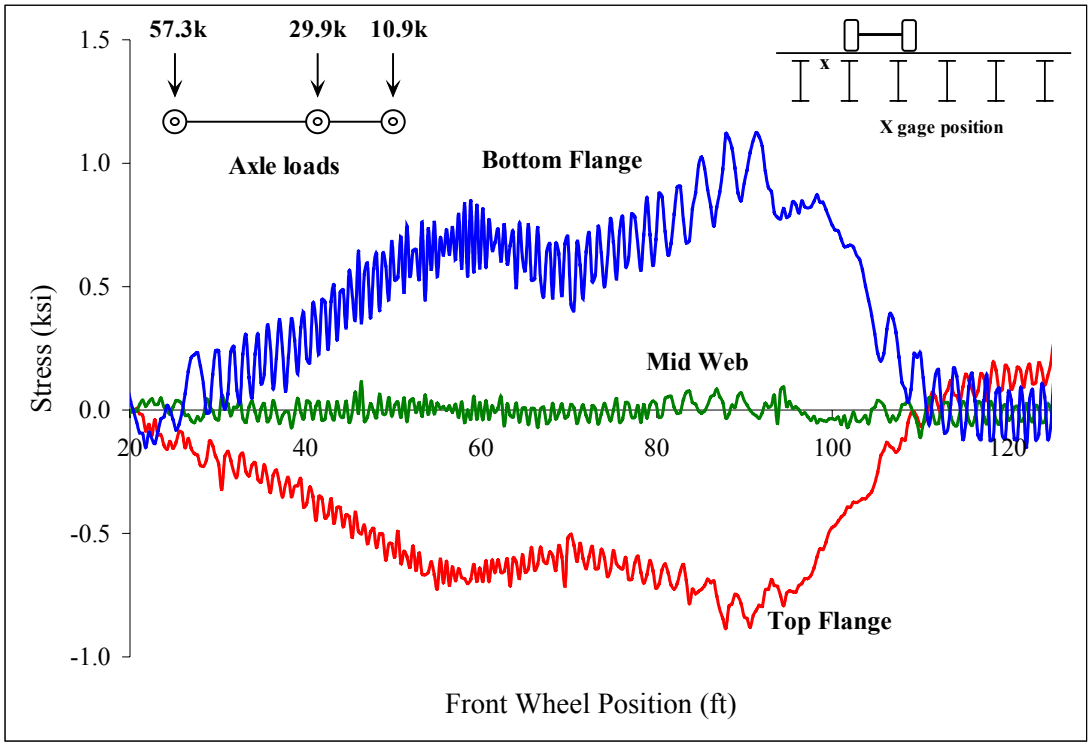

Figure C 50: Beam 4

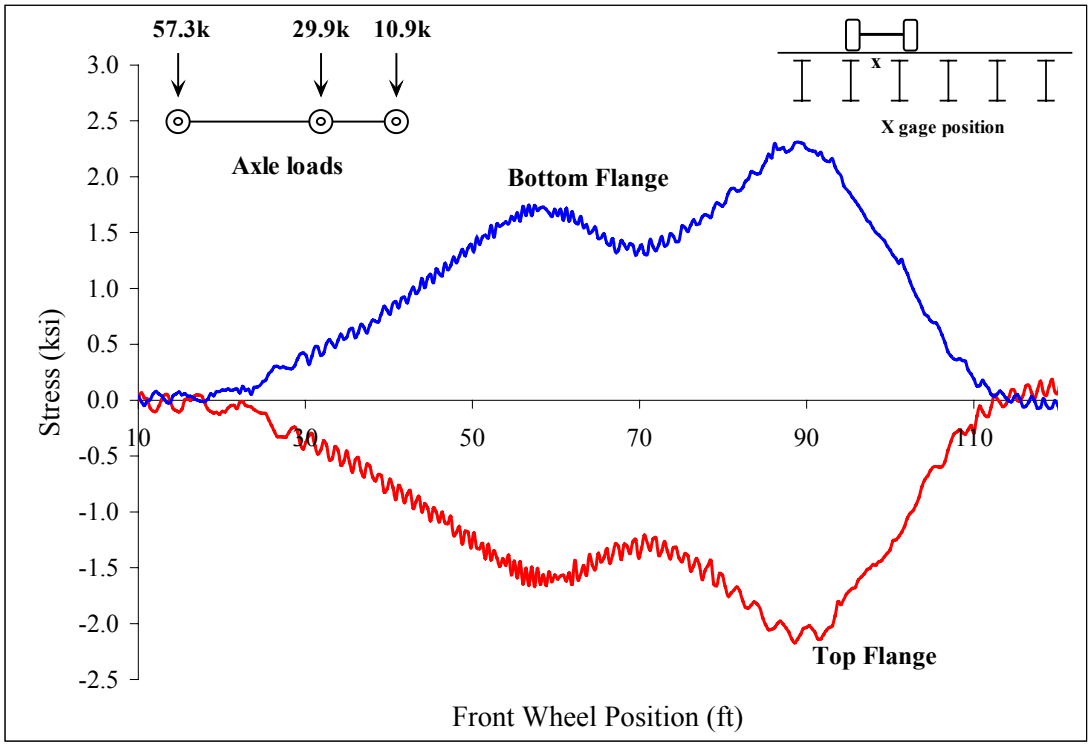

Figure C 51: Beam 4

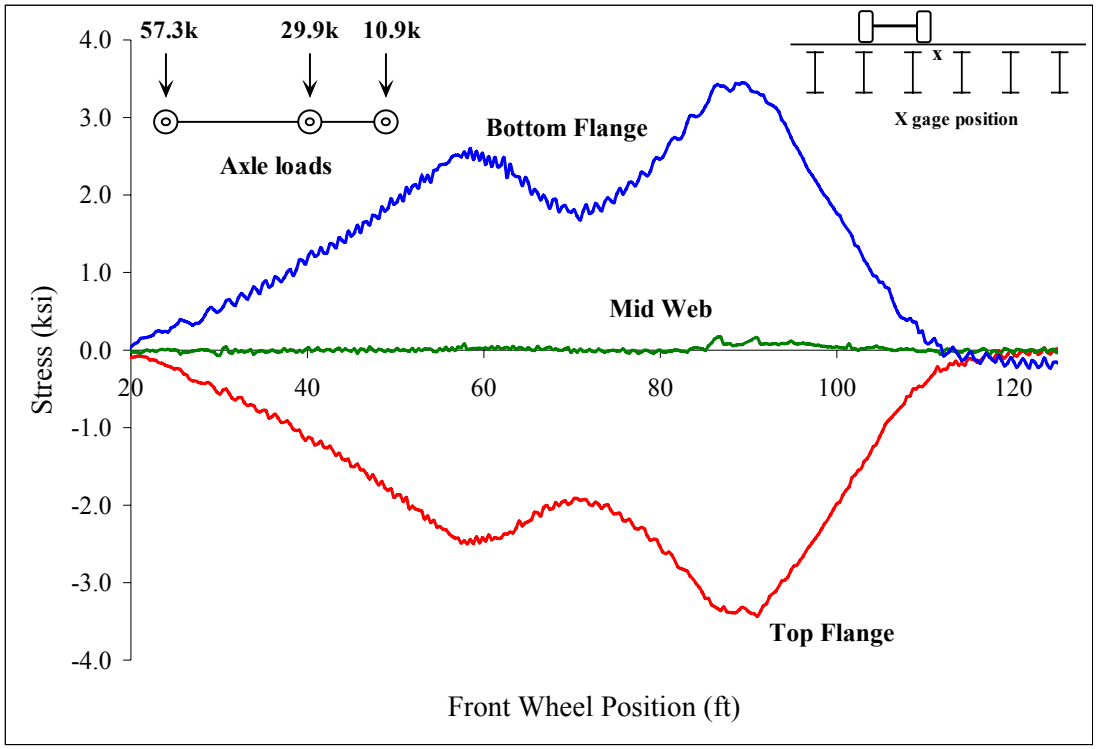

Figure C 52: Beam 4

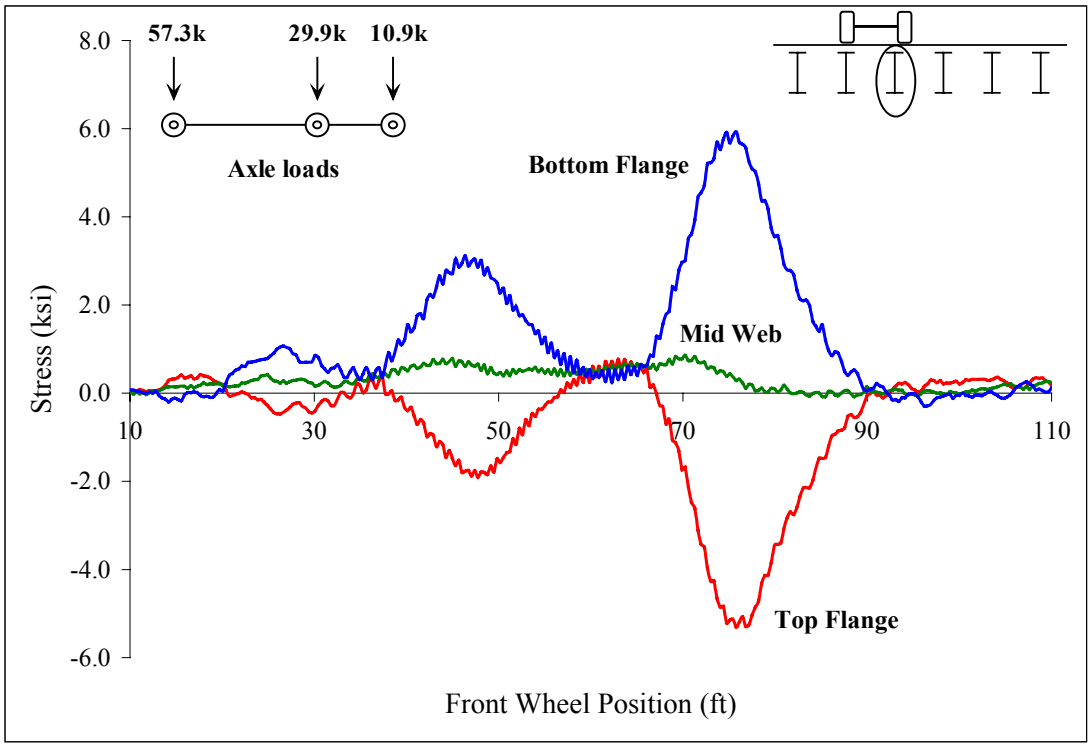

Figure C 53: South quarter point of stringer 3

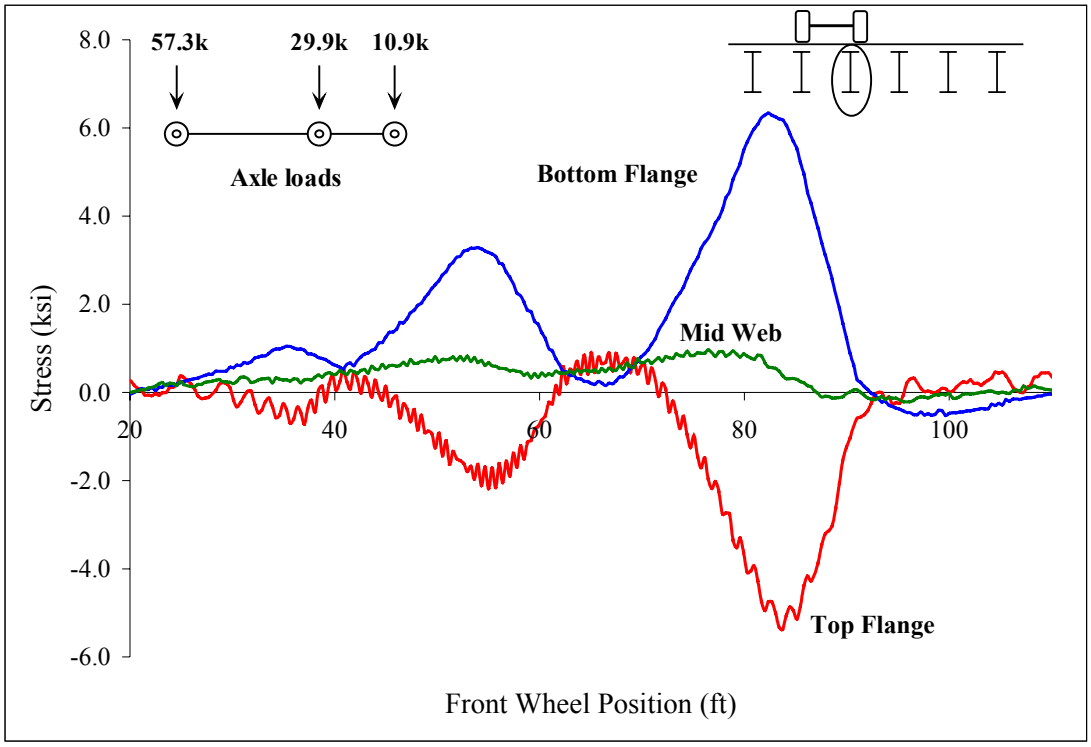

Figure C 54: North quarter point of stringer 3

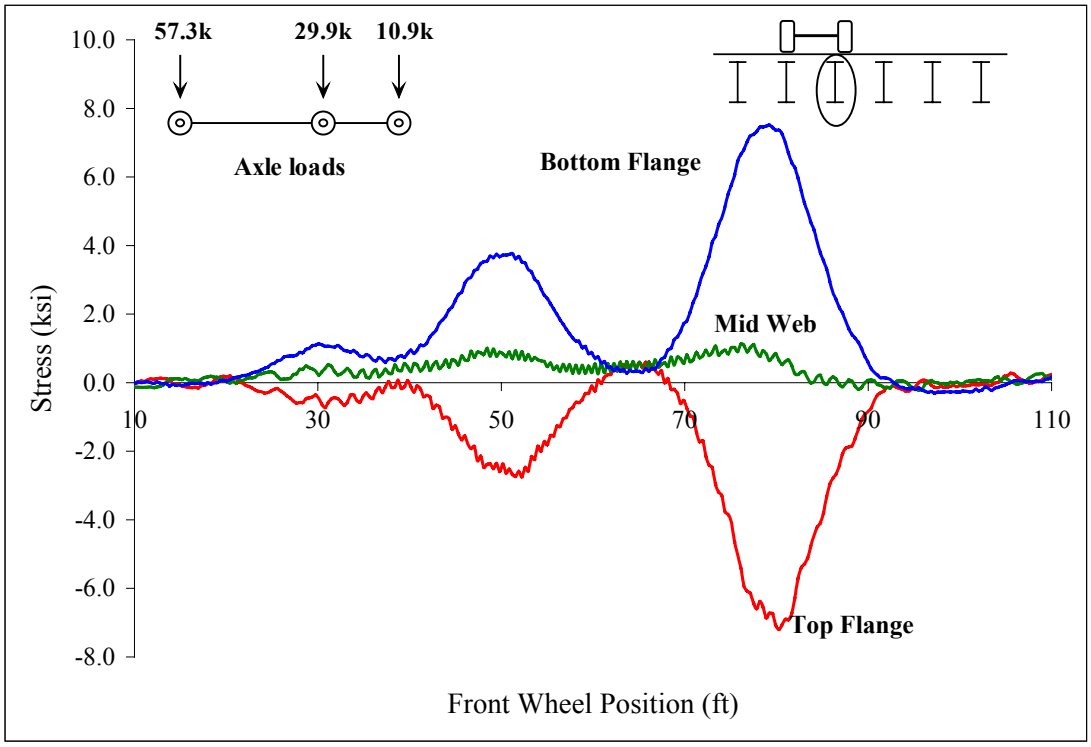

Figure C 55: Midpoint stringer 3

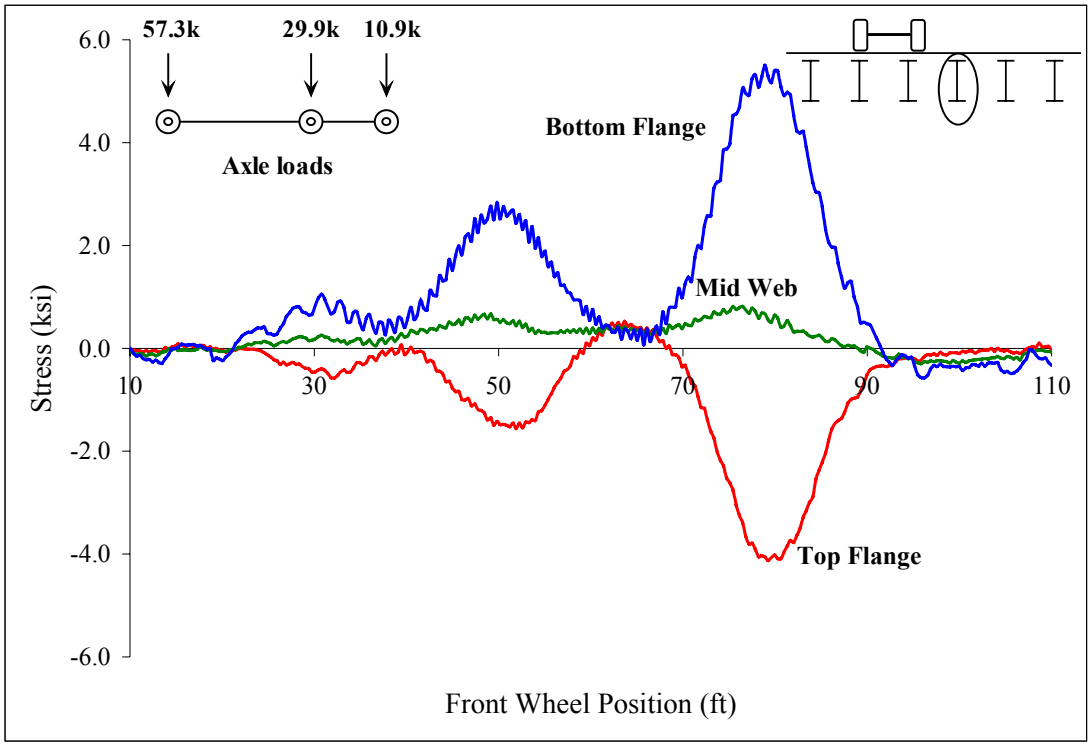

Figure C 56: Midpoint stringer 4

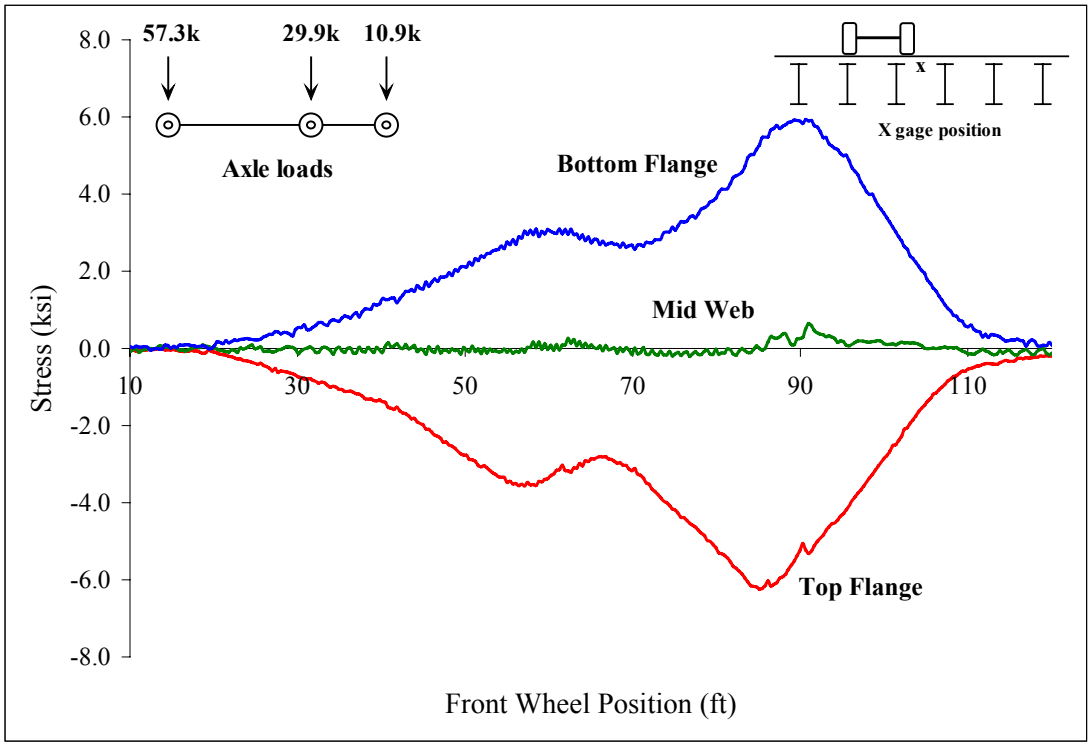

Figure C 57: Beam 5

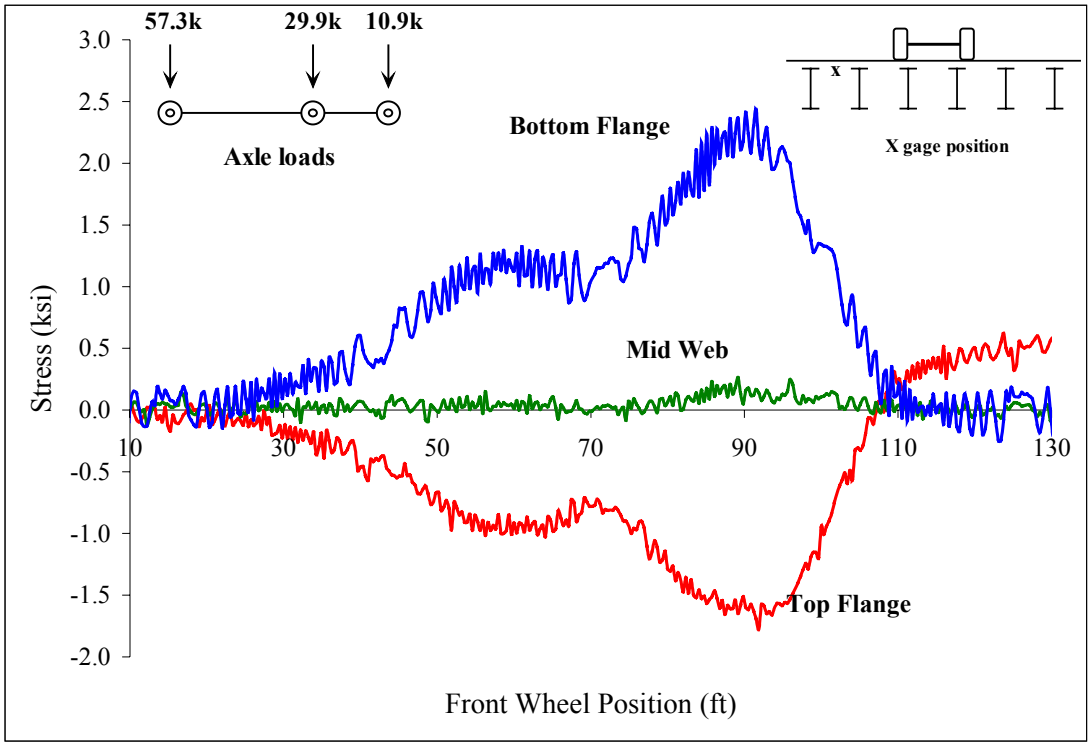

Figure C 58: Beam 4

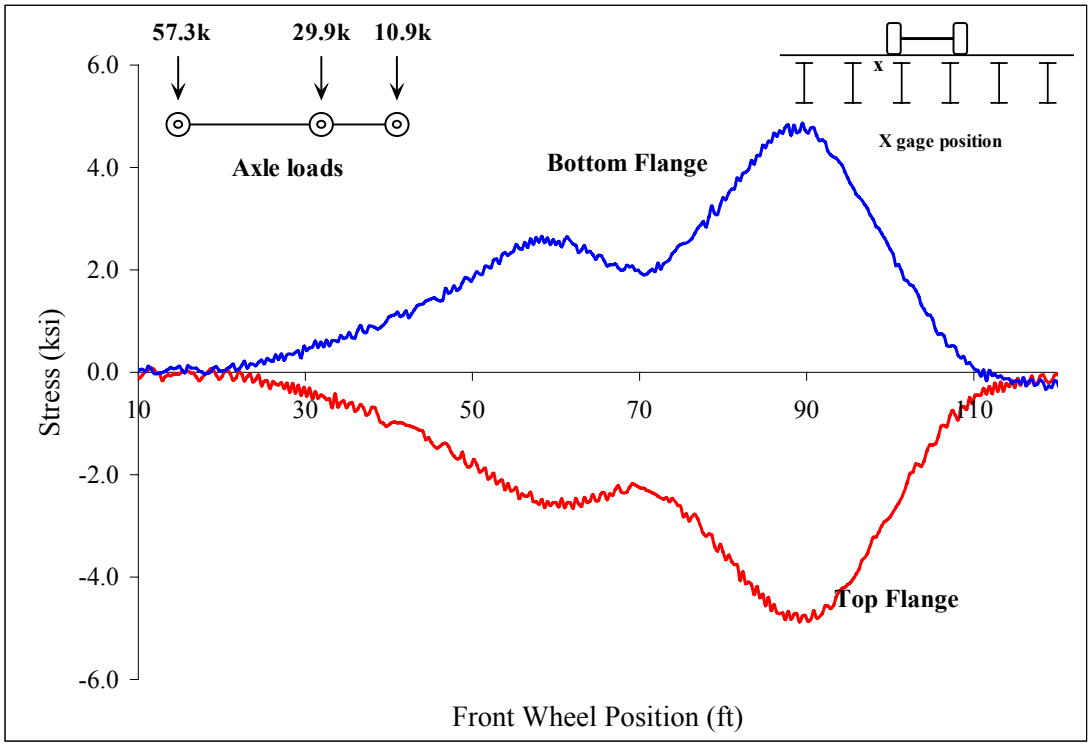

Figure C 59: Beam 4

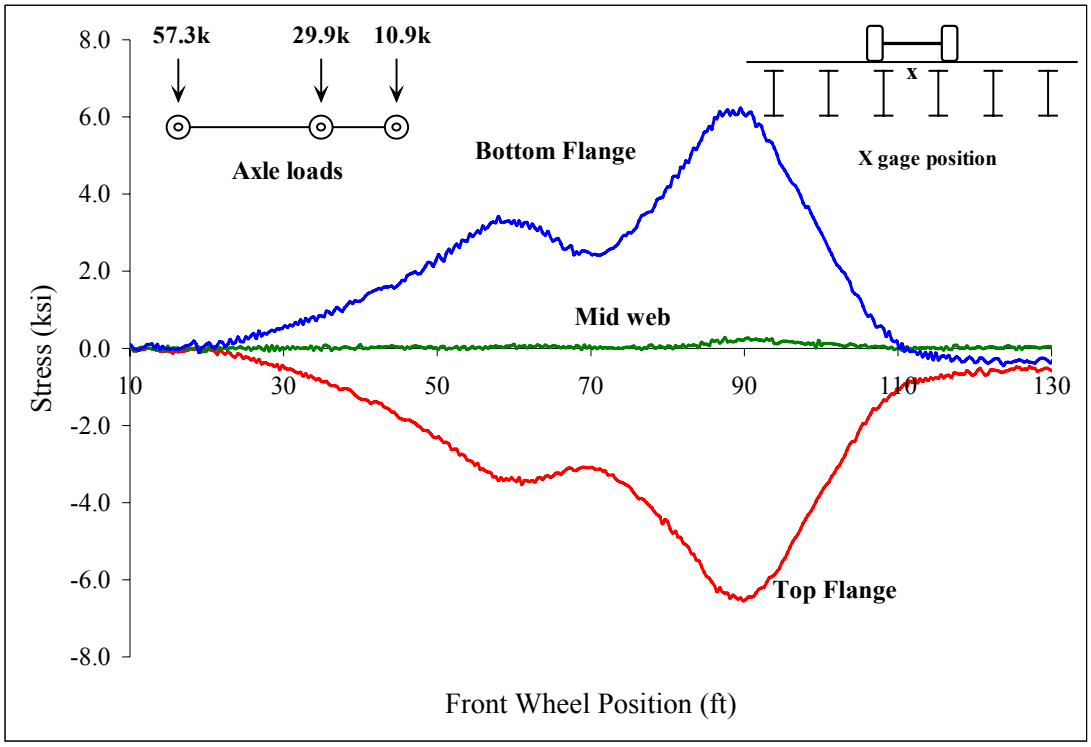

Figure C 60: Beam 4

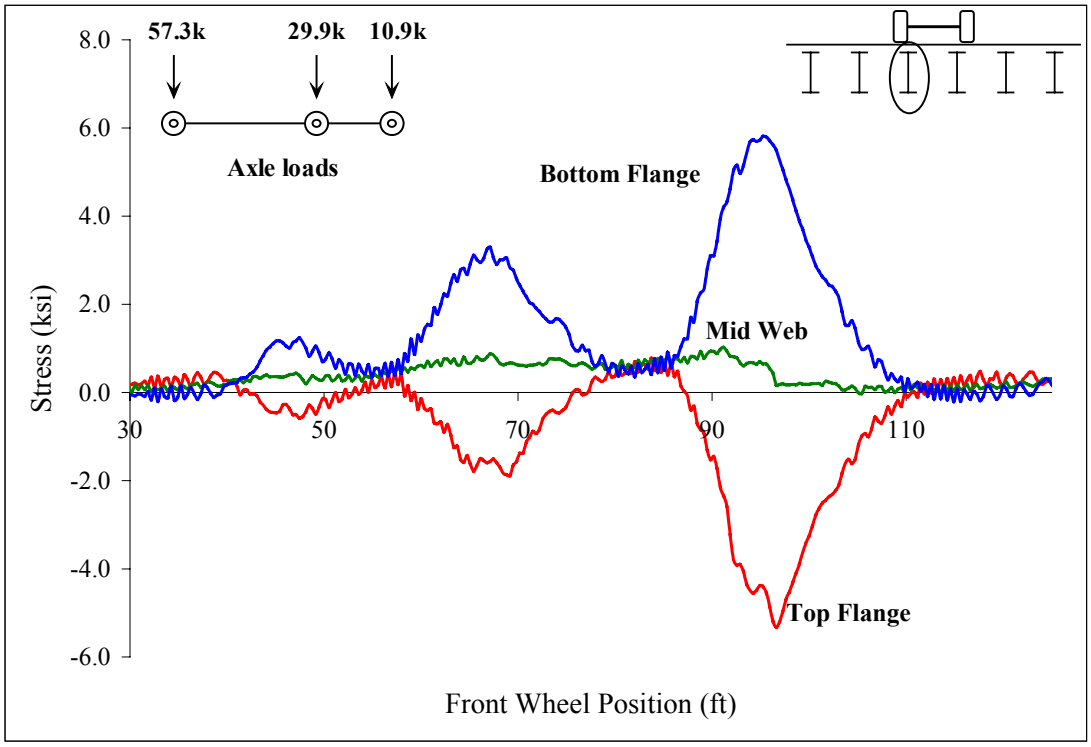

Figure C 61: South quarter point of stringer3

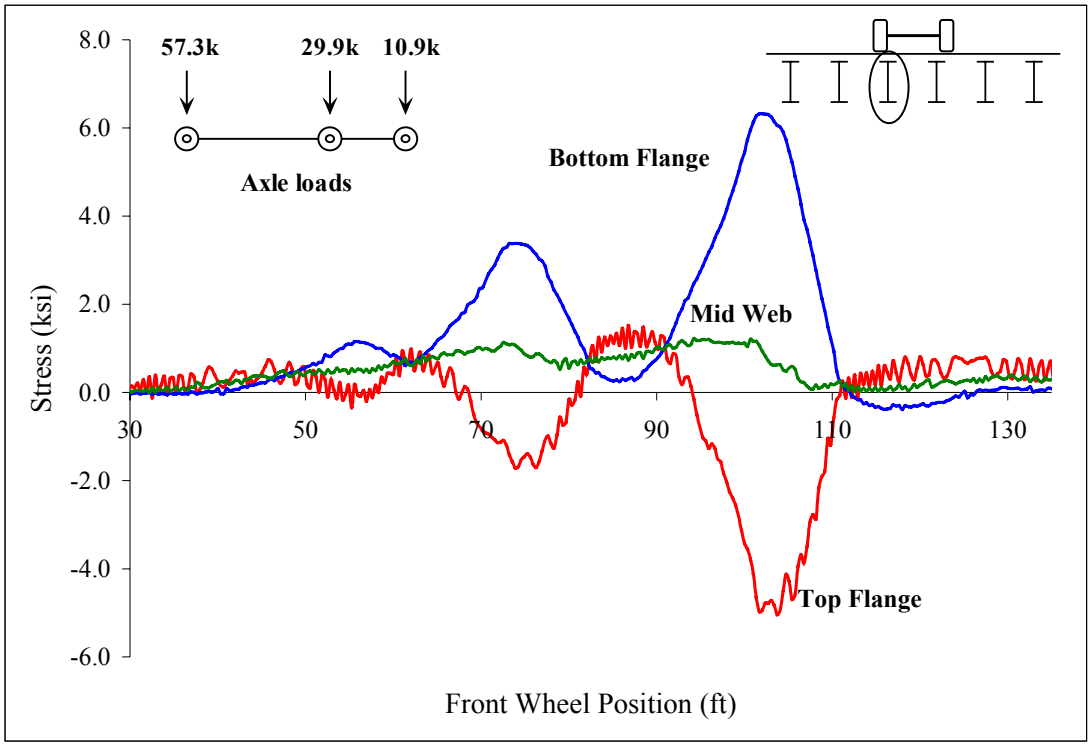

Figure C 62: North quarter point of stringer 3

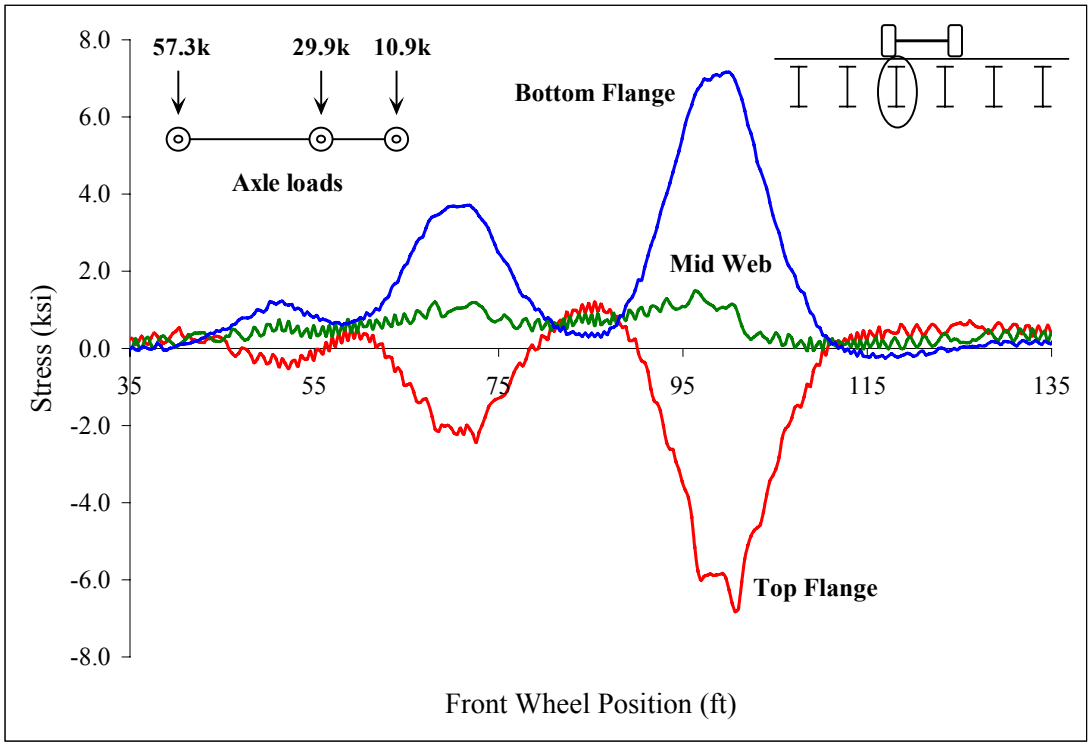

Figure C 63: Midspan stringer 3

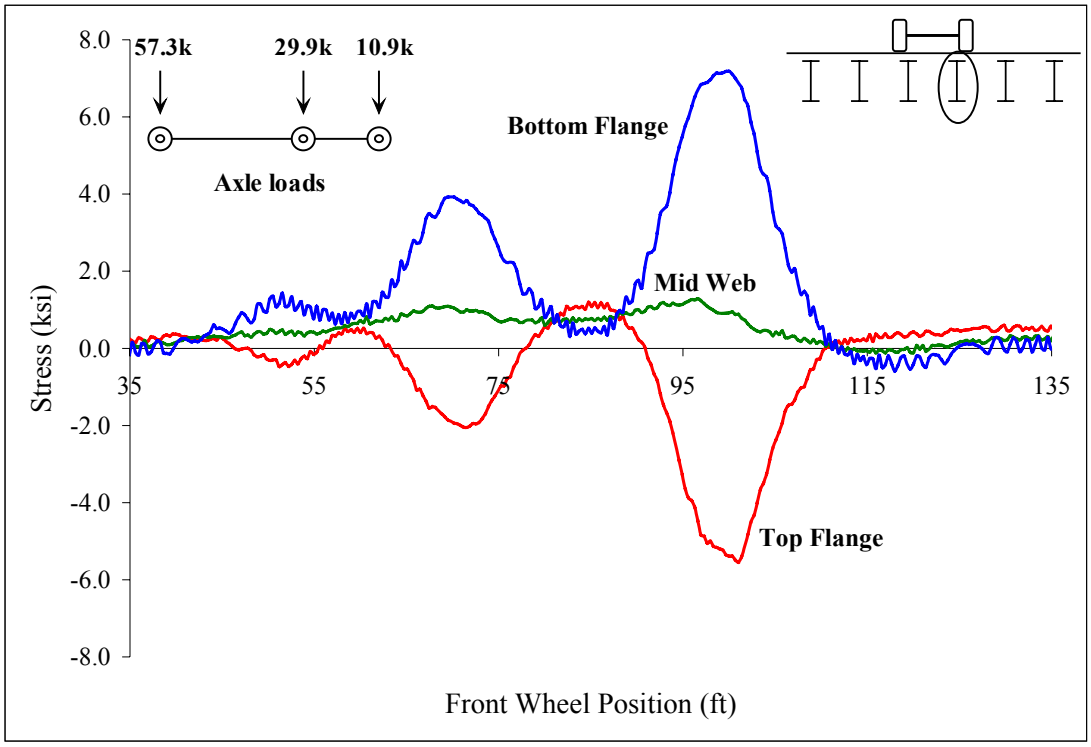

Figure C 64: Midspan stringer 4

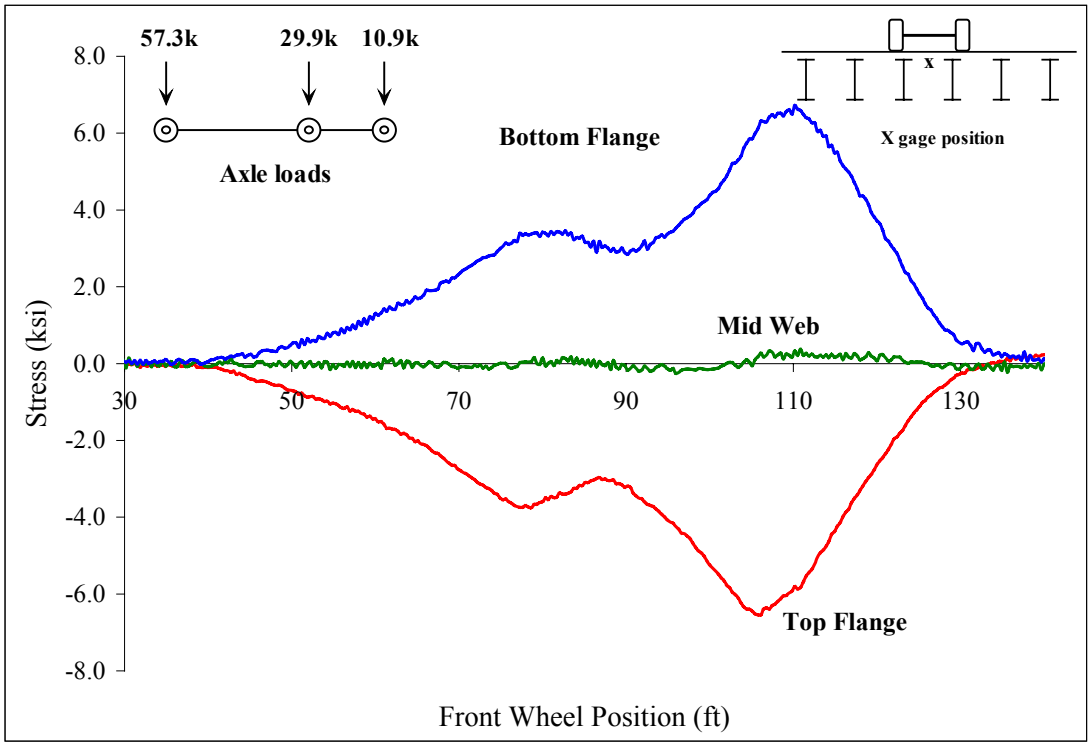

Figure C 65: Beam 5

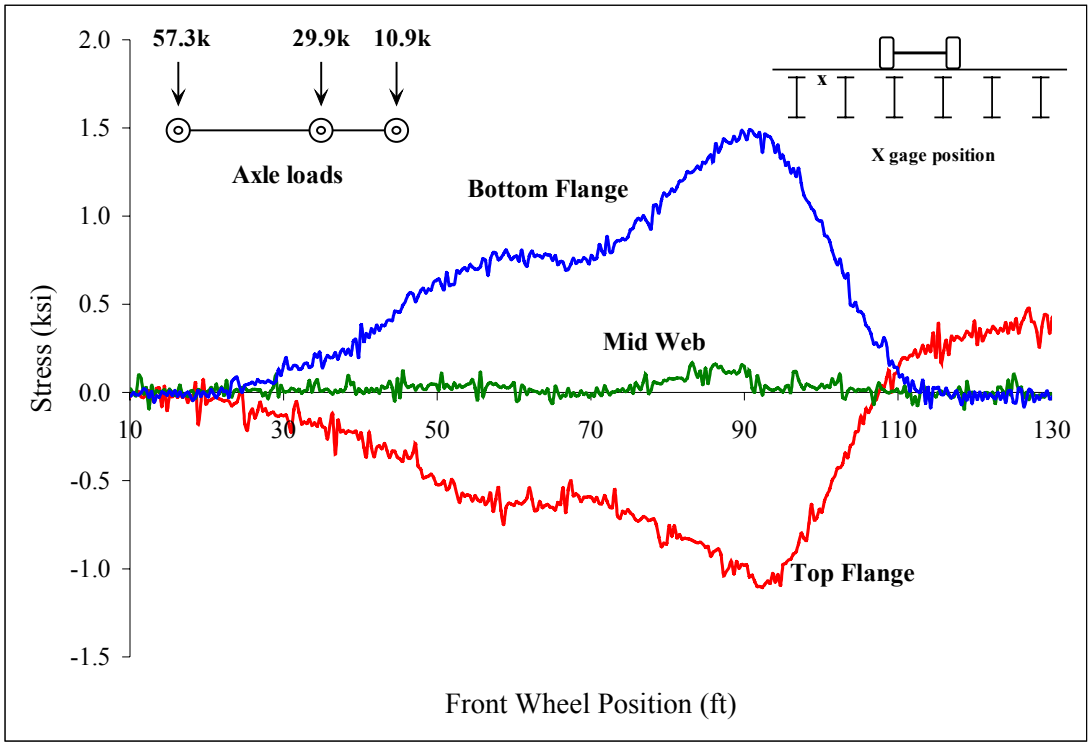

Figure C 66: Beam 4

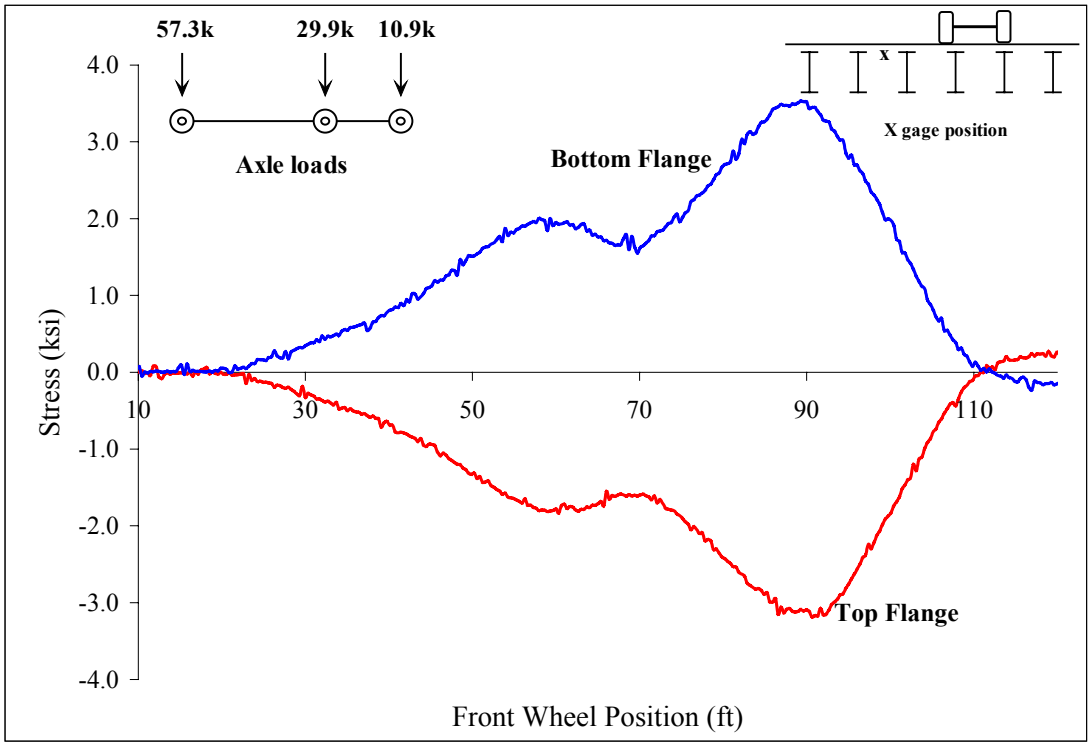

Figure C 67: Beam 4

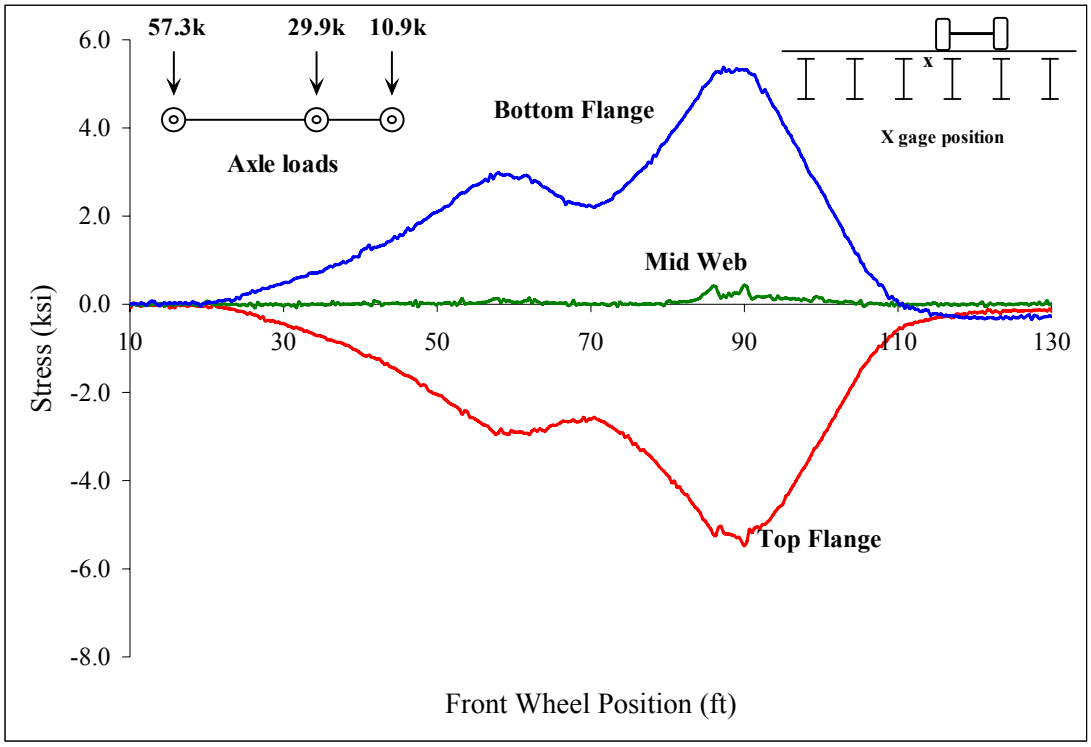

Figure C 68: Beam 4

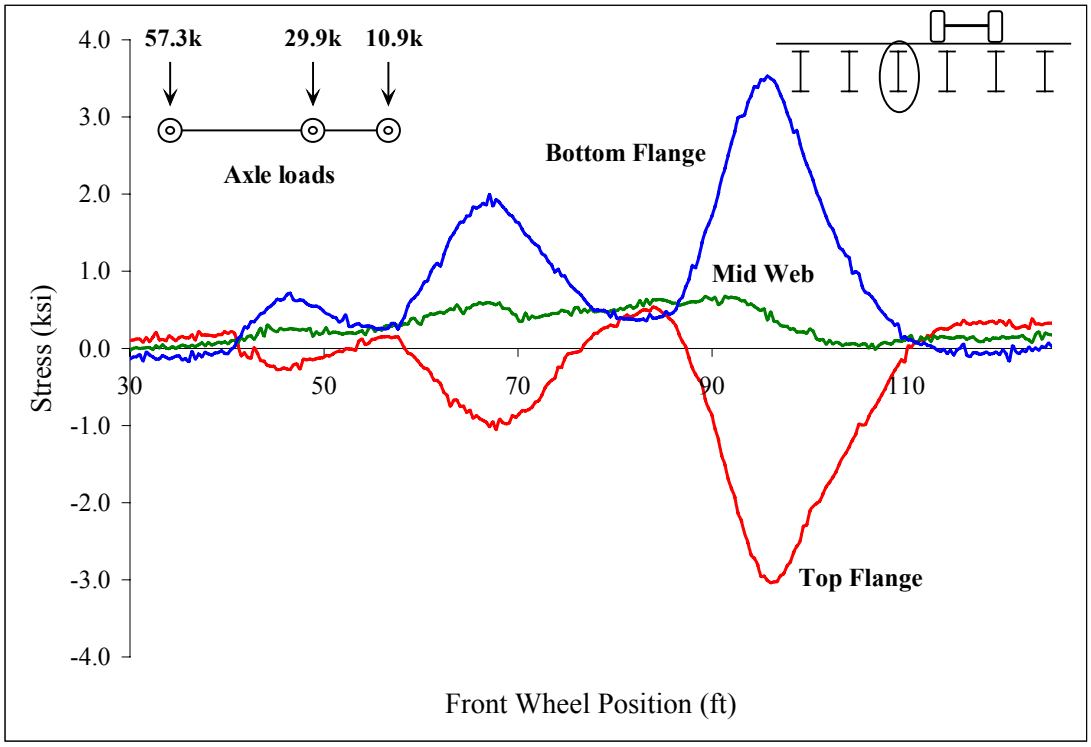

Figure C 69: South quarter point of stringer 3

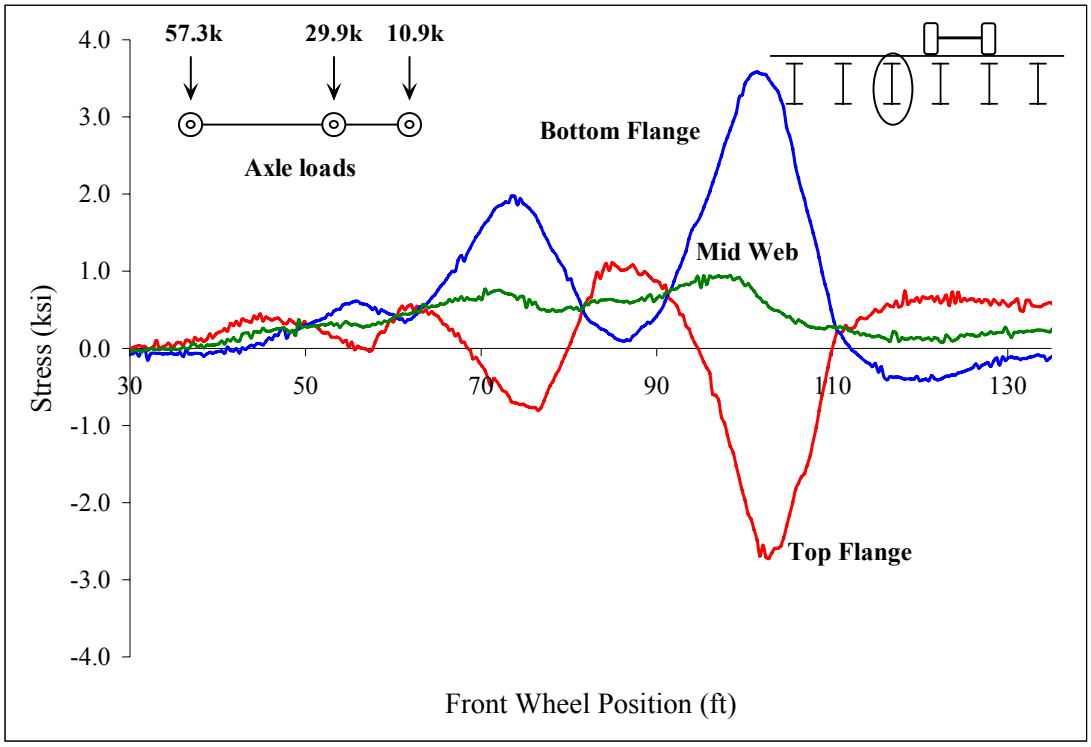

Figure C 70: North quarter point of stringer 3

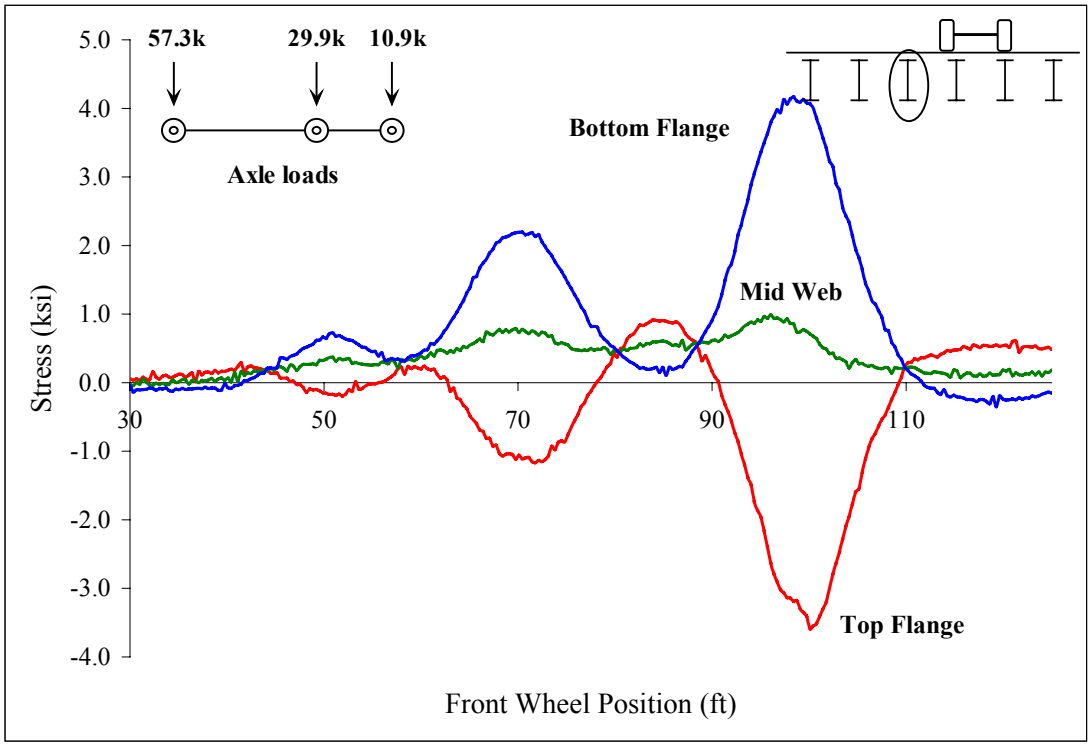

Figure C 71: Midspan stringer 3

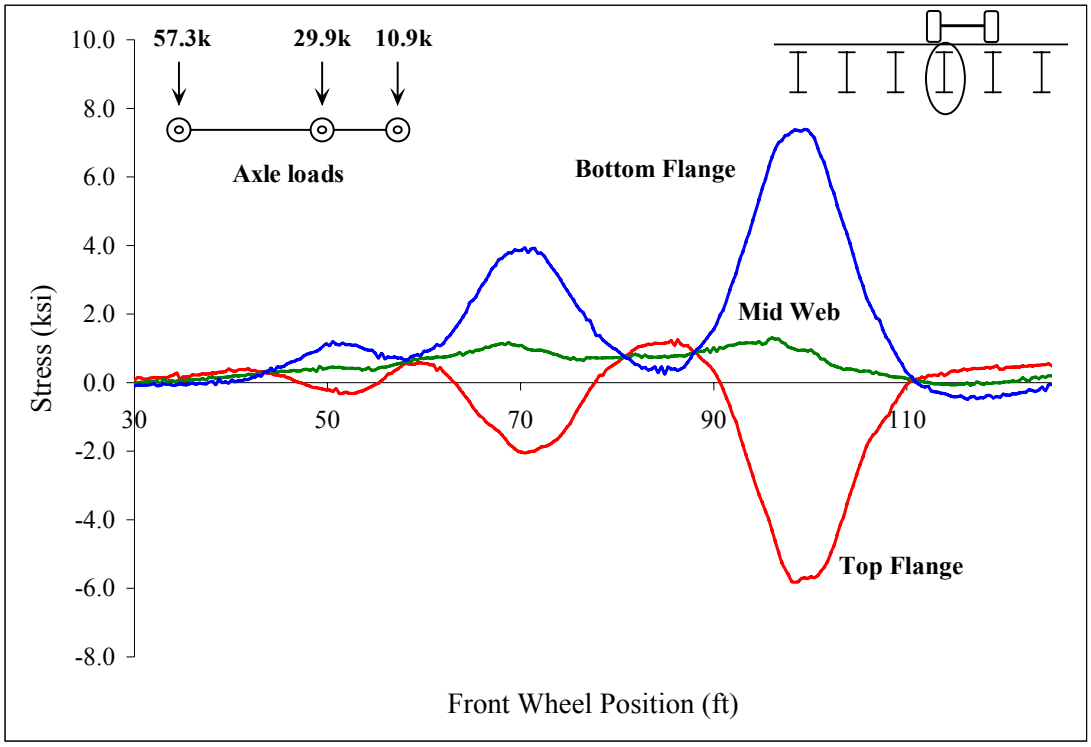

Figure C 72: Midspan stringer 4

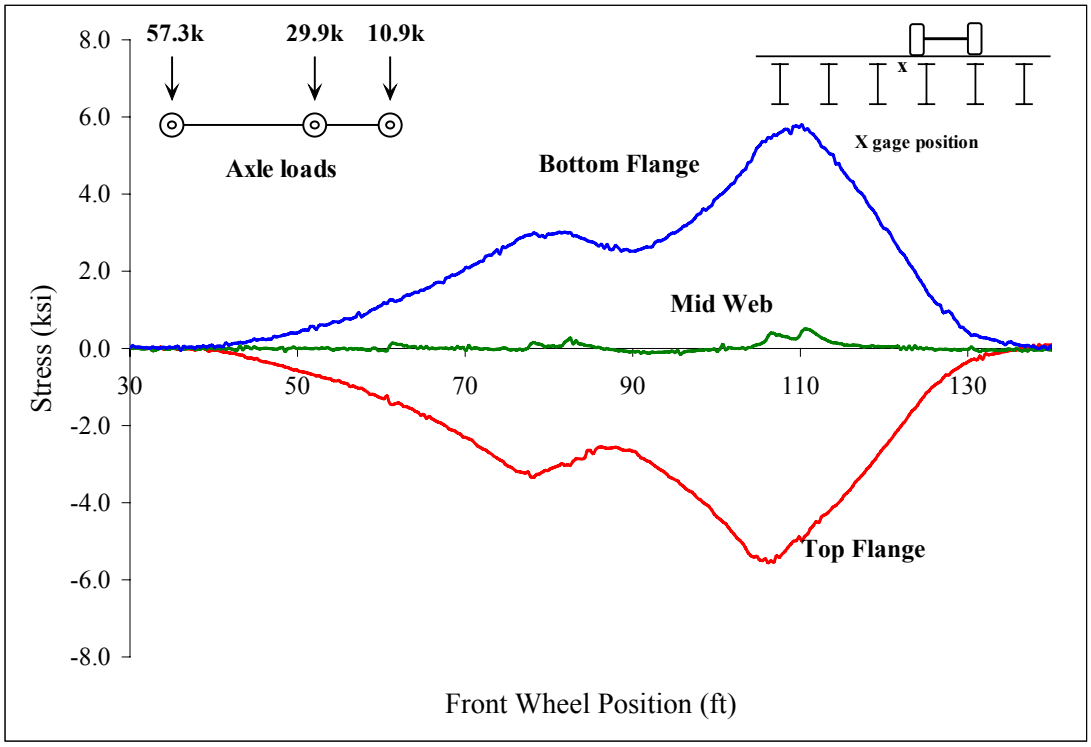

Figure C 73: Beam 5